DTIC FILE COPY

A Unified Approach to Electromagnetic Wave Propagation in Turbulence and the Evaluation of Multiparameter Integrals

R.J. Sasiela

1 July 1988

Lincoln Laboratory

MASSACHUSETTS INSTITUTE OF TECHNOLOGY

LEXINGTON, MASSACHUSETTS

DTIC
ELECTE
S AUG 1 7 198
E

88 8 15 11

This technical report has been reviewed and is approved for publication.

FOR THE COMMANDER

Hugh L. Southall

Hugh L. Southall, Lt. Col., USAF
Chief, ESD Lincoln Laboratory Project Office

MASSACHUSETTS INSTITUTE OF TECHNOLOGY
LINCOLN LABORATORY

A UNIFIED APPROACH TO ELECTROMAGNETIC WAVE PROPAGATION IN TURBULENCE AND THE EVALUATION OF MULTIPARAMETER INTEGRALS

R.J. SASIELA
Group 54

TECHNICAL REPORT 807

1 JULY 1988

Approved for public release; distribution unlimited.

LEXINGTON   MASSACHUSETTS

TABLE OF CONTENTS

LIST OF ILLUSTRATIONS

viii

LIST OF TABLES

OVERVIEW

Temperature fluctuations in the atmosphere lead to density fluctuations. The refractive index is proportional to the density; therefore, there are stochastic variations in the refractive index that affect the propagation of electromagnetic waves. These fluctuations are evident in the shimmering of images that we see above heated surfaces. These refractive index fluctuations have a profound effect on astronomical images viewed through large apertures and severely affect the propagation of laser beams propagated through the atmosphere. Turbulence causes the images seen through astronomical telescopes to be much larger than the diffraction-limited size and to jitter in position. It also causes the return image amplitude to vary — an effect referred to as "twinkling" in the popular press and scintillation in the technical literature. In the propagation of laser beams through the atmosphere, turbulence can cause the beam to break up and to be much larger than the diffraction size.

Many measurements have been made of the distribution of the turbulence in the atmosphere versus altitude. It has been found that the turbulence profile varies with geographical location, time of day, season, weather, and presence of high-altitude winds. Several turbulence models have been proposed and are used in problems. The common models generally used are the SLCSAT day and night models and a model that is generally referred to as the Hufnagel-Valley model. The last model has two free parameters so that the strength of the turbulence can be varied. That model is the one used most often in this report because of the ability to change turbulence strengths and because of its convenient analytic properties.

Adaptive-optics systems were devised to overcome turbulence effects on laser-beam propagation and imaging. In these systems, a bright source is propagated through the atmosphere, and the distortion of the beam is measured. If the conjugate of measured phase distortion is applied to a deformable mirror, the image will be corrected and a laser beam bounced off the mirror will be predistorted so that its phase front will be flat after it traverses the turbulent atmosphere. An adaptive-optics system does not, however, make a perfect

1

correction to completely overcome the effects of turbulence. There are only a finite number of actuators on the deformable mirror, so that all scales of turbulence are not corrected. There can be a time delay before the correction is applied, and the turbulence will change in that time. The beacon source to determine the correction may not be in the same direction as the object to be imaged or the direction one wants to propagate the laser. The turbulence changes in different directions, and a correction made for a certain direction will not apply along another ray path. The effects of different turbulence along different paths are called anisoplanatic effects. The angular difference between two ray paths for which the effect of turbulence is starting to be significantly different is called the isoplanatic angle.

The theory in this report was developed to aid the performance predictions and to analyze the data in the experiments that were and will be performed with a variety of systems. A variety of quantities of interest such as the Strehl ratio, the beam jitter, the beam profile, the effect of diffraction, inner and outer scale sizes and system defects will be considered. As concrete examples of the application of the theory it will be applied to several systems that are being actively considered by the adaptive-optics community. One experiment uses a 69-actuator adaptive-optics system with a 0.6-m aperture to propagate a corrected beam to a target at a range of 600 km. Another system uses an adaptive-optics system that has a deformable mirror with 241 actuators also with a 60-cm beam director. The corrected beam is directed at a cooperative target satellite and the space shuttle. The target satellite is considered to be launched into a 500-km orbit and contains a 4-m square target board with 85 sensors to sample the amplitude of the corrected beam and a lead-ahead boom whose position can be changed between passes. The boom supports a corner-cube array reflector for a beacon that will be used to provide the information to drive the adaptive-optics optics system. The proposed shuttle-based experiment will be used to measure the energy received in a bucket and the angle of arrival of a corrected laser beam. In addition, the analysis in this report is used to examine some of the problems in performing a mirror-relay experiment in which a compensated beam is bounced off an exoatmospheric mirror to a target. Also analyzed are possible experiments with larger apertures that are in the meter and several meter size range.

2

mirror to a target. Also planned and analyzed is a much larger, several-meter aperture ground system for an FEL (Free Electron Laser) experiment.

The simplest quar: ies to calculate are the phase and amplitude variance. The phase variance can be used to find the wavefront tilt, which is of primary interest for many applications. Knowing how close the image size or laser-beam intensity on axis is to the diffraction-limited value is of great interest: this quantity is referred to as the Strehl ratio. If the distortion is small, the Strehl ratio can be approximated by the extended Maréchal formula given by

$$SR = \exp\left[-\phi^2\right] \quad ,$$

where the quantity in the exponential is the phase variance in radians squared. This formula is only accurate when the phase variance is below a few tenths. Formulas that are valid over a larger range of phase distortion are developed in this report.

To analyze the performance of astronomical telescopes and adaptive-optics systems, one is interested in finding the effect of turbulence on the jitter, twinkling, Strehl ratio, and beam profile. These problems are more difficult than finding the phase and amplitude variances. In order to solve these problems one has to analyze Maxwell's equations with turbulence effects present, which results in stochastic differential equations. These equations are formidable: general solutions do not exist. Tatarski[1] has developed ways to simplify these equations; and combine them with the Rytov approximation, thus making the problem tractable. The use of the Rytov approximation makes the solution for the amplitude valid only if the amplitude fluctuations are not very large. For large amplitude fluctuations, a different, more complicated theory is needed. Fortunately, for most astronomical problems and most problems associated wi'i adaptive-optics systems, the amplitude fluctuations are small, and the simpler theory applies.

Saying that the solution is tractable does not mean that the solution is easily obtained. Unfortunately, the analysis to obtain the final form of the answer is usually quite difficult, and

some ingenuity is involved in each problem. The final answer is also not in a very convenient form — being a complicated multiple integral. This expression is usually evaluated numerically, and the answer expressed in terms of graphs for a range of parameter values. These calculations have to be redone for new turbulence or wind models, zenith angles, and parameter values. The solutions in some cases have been made more general, as in the papers of Fried[2] and Tyler[3] by defining normalized quantities; the tabular and graphical nature of the answers, however, make these results difficult to use in systems-analysis codes. For complicated problems, in which there are several independent parameters, even the representation of the results of these integrations is difficult.

For these reasons, a new approach to solving these problems was developed. In this report, a powerful method is presented to allow one to evaluate the phase and log-amplitude variance, power spectral densities, Strehl ratios, and beam profiles for an electromagnetic wave propagating in a turbulent media.

This method is based on the Rytov approximation. Therefore, it applies to most phase problems and can be used to evaluate the scintillation when it is not large. This analysis is not applicable to nonlinear effects such as those produced by thermal blooming. The effect of defects of an adaptive-optics system including various types of anisoplanatism can be included. Anisoplanatism can include displaced apertures, apertures pointing in different directions, or two beams taking different paths because of a difference in wavelengths, and time delay. The normal optical aberrations can also be found or subtracted from the results. Results can be obtained for collimated or focused beams. The effect of point and distributed sources can also be calculated. These effects can be considered simultaneously in many cases.

The approach is based on simplifying the expressions for phase variance, structure function, and power spectral density so that they can be written, regardless of the problem, in the following forms:

Phase and scintillation variance:

$$\begin{bmatrix} \phi^2 \\ \chi^2 \end{bmatrix} = 0.2073 k_o^2 \int_0^L dz \ C_n^2(z) \int d\vec{\kappa} \ f(\kappa) \begin{bmatrix} C_p \\ C_a \end{bmatrix} \prod_i F_i(\vec{\kappa}, z)$$

Phase and log-amplitude structure function:

$$\begin{bmatrix} D_\phi(\vec{\alpha}) \\ D_\chi(\vec{\alpha}) \end{bmatrix} = 0.4146 \ k_o^2 \int_0^L dz \ C_n^2(z) \int d\vec{\kappa} \ f(\kappa) \begin{bmatrix} C_p \\ C_a \end{bmatrix} [1 - \cos\{\vec{\kappa} \cdot \vec{\alpha} D\}] \prod_i F_i(\vec{\kappa}, z)$$

Power spectral density:

$$F(\omega) = 1.303 \ k_o^2 \omega \int_0^L dz \frac{C_n^2(z)}{v^2(z)} \int_0^\infty \frac{c \, dc \ U(c-1)}{\sqrt{c^2-1}} \ f\left(\frac{\omega c}{v(z)}\right) \begin{bmatrix} C_p \\ C_a \end{bmatrix} \prod_i F_i\left(\frac{\omega c}{v(z)}, z\right).$$

In these expressions, $C_n^2(z)$ is the strength of turbulence versus propagation distance, $f(\kappa)$ is the transverse turbulence spectrum, $v(z)$ is the wind velocity, C_p and C_a are functions that depend on whether the beam is collimated, focused at the source or at the target, and $\prod_i F_i(\vec{\kappa}, z)$ is the product of transverse spatial filters. The turbulence spectrum can contain inner and outer scale effects. The essential difference between various problems is the choice of filter functions. In this report, filter functions are derived to extract any Zernike mode such as piston and tilt, to account for any form of anisoplanatism, and to consider point and distributed sources for adaptive-optics systems. Using these three formulas, the solution to an individual problem can be written down very quickly in the form of a triple integral for the structure function and variance of phase and amplitude related quantities. This is a significant simplification over previous techniques; however, in addition, it is shown how to perform these integrations to generally obtain simple expressions that do not contain any integrals. The integration technique will now be briefly described.

The angle integration in the transverse-spectrum space can usually be easily performed so that these problems are reduced to the evaluation of a double integral.

5

The evaluation of the integral over the spatial-transform space becomes increasingly difficult as the number of independent parameters in the integrand increases. For single parameter problems, the integral over the transverse spatial spectrum or c can be put in the form

$$H^*(s) = \int_0^\infty dy\, H(y)\, y^{s-1}.$$

This is the Mellin transform of $H(y)$; it is simply evaluated by lookup in a Mellin transform table followed by evaluating the resultant expression for a specific value of s. The number of Mellin transforms needed to solve turbulence problems is surprisingly small, and the transforms for all problems considered to date are listed in the report. For problems with two parameters, a more complicated procedure must be used. A convolution theorem is used to convert the integral into an equivalent one in the complex plane of the form

$$H(x) = \frac{1}{2\pi i} \int ds\, x^{-s}\, L(s)$$

where $L(s)$ is the ratio of Gamma functions and the path of integration goes from $-i\infty$ to $+i\infty$ along a path determined by the specifics of a particular problem. The utility of this form stems from the property that the only singularities of the integrand are poles of numerator Gamma functions which occur when their arguments are negative integers. This property allows this integral to be evaluated very easily using pole-residue integration by closing the path of integration in the direction determined by the properties of the integrand. The result is a Taylor-series solution for the value of the integral. For large values of the parameter, this series may converge slowly, and an asymptotic series is found in those cases. The asymptotic series is the sum of the residues of the poles on the other side of the path of integration plus a contribution from the steepest descent path. This is easily evaluated. It is found that usually fewer than ten terms, and often one or two terms, give an accurate value of the integral, and there is an overlap of the range of validity of the two series, therefore, allowing one to represent the solution over the entire parameter range with a few terms.

For problems containing more than two parameters, it is shown that the integral can be transformed into one in several complex planes. The technique of pole-residue integration is generalized in this report so that power series solutions are also obtained in those cases. In the process of evaluating the integrals the natural parameters of the solution emerge, which allows one to obtain physical insight into the nature of the interactions of the various parameters.

After performing this integration, the problem has now been reduced to an integration along the propagation direction. It is shown that for the Hufnagel-Valley model of turbulence this integral can often be evaluated analytically. Therefore, by using these methods, the solutions of turbulence problems are usually expressed as the sum of a few terms that do not contain any integrals. For some problems the last integration must be performed numerically. This is just a single integration and does not have numerical difficulties associated with it.

These techniques can be augmented to find the Strehl ratio and beam profile. The extended Huygens-Fresnel approximation can be used to show that the beam profile and Strehl ratio can be written as

Beam profile:

$$I_n(\vec{r}) = \frac{1}{2\pi} \int d\vec{\alpha}\ K(\alpha) \exp\left[i\frac{k_o D\vec{r} \cdot \vec{\alpha}}{z} - \frac{D(\vec{\alpha})}{2} \right]$$

Strehl ratio:

$$SR = \frac{1}{2\pi} \int d\vec{\alpha}\ K(\alpha) \exp\left[-\frac{D(\vec{\alpha})}{2} \right]$$

where $K(\alpha)$ is the modulation transfer function of a circular aperture. The integration is over a circular aperture of unit radius. The problems of finding the beam shape and Strehl ratio are more complicated, since the structure function appears in the exponential of an integral. Simple solutions cannot be found for all values of Strehl ratio; however, they can be found in the regime that is of most interest for adaptive-optics problems. It is shown that by using the techniques that were developed to find the previous quantities plus an expansion in Gegenbauer polynomials that the expression for the Strehl ratio when it is greater than 0.3 can be written as

7

$$SR = \exp\left[-\sigma_\phi^2\right] g(E)$$

where $g(E)$ is a polynomial expression, σ_ϕ^2 is the phase variance, and E depends on the particular problem being solved. The same techniques can be used to obtain series solutions for the beam profile.

The mathematical analysis leading to the results is formidable to many, since it uses mathematical concepts that are not normally part of the education of an engineer or physicist. Once the time is spent to master these techniques, however, the application of the methods that are developed is rather straightforward. Flow diagrams of how to use this approach to solve problems are given. In fact, the method is so consistent that it should be possible to write a computer program that completes the solution after the problem is set up utilizing an algorithmic approach as is used in MACSYMA.

This report is composed of three parts. Many persons are not interested in the details of the derivations but are interested in obtaining an answer to a problem of interest. Part I is aimed at that audience and, also, is a useful summary to others with a deeper interest in the theory. A summary of the relevant formulas developed in parts 2 and 3 is given in tables. In addition, a step by step method for solving each type of straightforward problem is provided. More complicated problems are not covered in these flowcharts, since they require a deeper understanding of the theory.

In part 2, a general method of performing integrations of the same form as those encountered in solving turbulence problems is developed. This method is mathematically intensive and uses the properties of Gamma functions, Mellin transforms, pole-residue integration in several complex planes, and asymptotic series. The method of doing integrations in several complex planes is not available in the literature.

In part 3, a general method is developed to allow one to quickly set up turbulence problems. This method is a generalization of Tatarski's method of spectral expansions. Using this method, one can represent the effect of anisoplanatism, defects in the adaptive-optics

8

system, and the extraction or subtraction of Zernike modes as filter functions multiplying the turbulence spectrum. These filter functions can usually be cascaded so that any number of effects can be considered. Using general formulas, one obtains the expression for the phase or log-amplitude variance, or power spectral density as a triple integration over the transverse spatial spectrum and the axial coordinate.

These integrals can often be evaluated analytically. The integral over angle in spatial transform space can usually be easily performed. The integral over the magnitude of the transverse spectrum, which can contain many parameters due to the various effects being considered, is evaluated by the method introduced in part 2. The last integral over the axial coordinate can typically be evaluated analytically for most problems of interest using the Hufnagel-Valley model of turbulence.

The evaluation of the Strehl ratio and beam profile is performed by a modification of the integration method of part 2.

The method of integration developed in part 2 has applications in any field in which this type of integral is encountered.

This report evolved over several years and with the help of colleagues. I want to thank Lee Bradley for suggesting the usefulness of Mellin transforms and Gegenbauer polynomials, Ronald Parenti for discussions on how to handle distributed sources, John Shelton for help in resolving the issue of integration in several complex planes, Robert Kramer for carefully reading the report and making suggestions on how to modify it to make it more readable, and to Charles Primmerman for offering suggestions on how to organize the material. Finally, a special note of thanks to Carole Kelly for making numerous revisions and putting this report in its final form.

This report contains much new material with which the typical reader will not be acquainted. I have tried to explain this material or indicate references to it. I would appreciate any comments the reader has on how to make this report easier to read. My hope is that an

expanded version of this report containing more tutorial material will be published in a form that will have a broader audience.

1. FLOWCHARTS AND SUMMARY TABLES

1.1 INTRODUCTION

Problems concerning the propagation of electromagnetic waves in turbulent media are considered to be difficult for two reasons: each problem is treated as a separate entity, and there are several difficult steps in arriving at the final expression for the effect of interest. In addition, this final expression is in the form of a complicated multiple integral. The evaluation of this expression poses problems both because of numerical difficulties and also because the final answer is given in terms of tables or curves for a few parameter values — a form that is often difficult to extend to new parameter values or zenith angles without repeating the calculation and is often not very useful for systems-analysis calculations. For these reasons, calculations in this area are avoided except by a cadre of specialists. It is shown in the three parts of this report that turbulence problems in which the Rytov approximation (slowly varying turbulence parameters and low scintillation) is valid can be approached in a systematic fashion, and answers can be expressed in terms of rapidly converging series of the parameters of the problem. The forms of the answer can be derived quickly, give physical insight, and may easily be re-evaluated for new parameter values or zenith angles.

It is shown that many of the problems of interest can be expressed as a spatial filter function operating on the turbulence spectrum. The rms value is often the quantity desired. To find this quantity, the expression must be multiplied by its complex conjugate, and then the expected value must be found. This expression contains at least a six-fold integral. The reduction of the number of integrals, which consists of making substitutions and approximations, follows the same procedure from problem to problem. It is shown that the problems are reducible to integrals over the transverse spatial spectrum and along the propagation direction. This triple integration can serve as a starting point for most problems, obviating the need to perform the previous integrals. The integration over the angular coordinates in spatial-spectrum space is usually easy to perform, thus reducing the problem to

evaluating a double integral — one over the magnitude of the transverse spatial spectrum, the other over the propagation direction.

The integral over the magnitude of the turbulence spectrum can be evaluated by Mellin-transform techniques and results in rapidly converging series. The problem has now been reduced to finding various moments of the turbulence strength profile and then summing the series terms. Sometimes the parameters that determine the path of integration contain the axial coordinate. Because the parameter changes in magnitude along the propagation direction, it may be necessary to change the path of integration at some point along the path. For this reason, the final answer can contain partial moments of the turbulence that are integrals of the turbulence strength times some function of the axial coordinate over part of the path. For the Hufnagel-Valley model of turbulence, the full and partial turbulence moments of the turbulence strength multiplied by a power of the propagation direction can be evaluated analytically. Two other turbulence models that are often used called the SLCSAT day and night models can be represented by an equivalent Hufnagel-Valley model with parameters chosen so that they have the same values of coherence diameter and anisoplanatic angle. The net result is that the final answer can often be expressed as the sum of a few terms that do not contain any integrals.

The evaluation of the structure function and power spectral density are performed in the same manner. Finding the beam profile and Strehl ratio is more complicated but can be done for uncorrected turbulence. For adaptive-optics problems in which the Strehl ratio is greater than 0.3, the beam profile and Strehl ratio can also be found using the same techniques augmented by the introduction of Gegenbauer polynomials. The evaluation of the Strehl ratio using this technique is valid over a greater range than the extended Maréchal formula.

In this part of the report, detailed flowcharts are given to allow one to calculate the phase and log-amplitude variances, the power spectral density, and Strehl ratio. These flowcharts are synopsis of the results in parts 2 and 3. More complicated problems are not treated in these flowcharts; these require the use of techniques developed in parts 2 and 3.

1.2 FLOWCHARTS

In this sec'on, flowcharts are presented that allow one to solve most of the simple problems of interest in turbulence propagation. This section does not consider the case of forming new filter functions by combining complex filter functions and then taking the absolute value squared. This technique is discussed in the problems of finding the Zernike minus the Gradient tilt in Section 3.5.3, beam movement at a target in Section 3.5.5, tracked tii in Section 3.5.6, and scintillation on a corrected beam in Section 3.5.7. Combining filter functions for these problems is basically not difficult, but, it requires an understanding of the filter functions that is not easy to convey in flowcharts. The evaluation of the integrals obtained in these problems is covered in the flowcharts.

There are two basic kinds of flowcharts in this section. There are the step by step flowcharts that allow one to set up a problem. In these flowcharts, there are some boxes with asterisks. The asterisk indicates that there is another flowchart that goes into detail on how to accomplish the step in the box. Some of these additional flowcharts are of the second type that are really not flowcharts but logical ordering of cases that allow one to select a formula to be used in the solution of the problem. All the formulas that are necessary to set up problems and evaluate integrals are contained in Tables A to J at the end of the flowcharts. These formulas are derived in parts 2 and 3.

The first flowchart, in Figure 1-1, describes the general method that is applicable to the solution of all problems. After the general formula applicable to finding the quantity of interest is selected, one has to choose the filter functions to insert in the integral. If some Zernike quantity is wanted, a filter function from Table B is selected. If the source is a point or a distributed source rather than a collimated beam, a filter function is selected from Table E. If anisoplanatism effects are wanted, then the proper formulas for the effects under consideration are selected from Table E. The formulas given do not allow one to combine the anisoplanatic effects with the distributed sources, and that is why they are on separate paths in the

13

flowcharts. These effects can be combined by going back to the fundamental relations. That is not done in this report. After the problems are set up in terms of integrals, they are evaluated.

In Figure 1-2, the first box of the previous flowchart is expanded. The procedure for selecting the correct formulas to find phase or log-amplitude related quantities for the variance, power spectral density or structure functions for collimated and focused beams is described.

The steps to find the filter function with anisoplanatism with as many effects as desired included are shown in Figure 1-3. The selection of the correct formulas for Zernike components and distributed sources is shown in Figures 1-4 and 1-5, respectively. As pointed out in the section where these relations are derived, subtracting Zernike modes like tilt from the full structure function is not strictly correct because the Zernike modes are not statistically independent. The error in subtracting the tilt is less than 10% in calculating the Strehl ratio. The evaluation of gradient tilt components is considered in Figure 1-6.

At this point, the solution of the problem is written down in terms of a multiple integral. The general evaluation of this integration is shown in Figure 1-7. For phase and log-amplitude problems, there is a triple integration over kappa space and over the axial coordinate. For power spectral density, there is a double integration over c and over the axial coordinate. The integration over the angle in kappa space can usually be easily done. The performance of the other integrations is discussed in detail in other flowcharts.

The integration over kappa or c where there are single or no parameters is easy to perform as shown in Figure 1-8. By a change of variables, the integrand can be put in a form that can be evaluated by looking up a Mellin transform in the table, and possibly using a transformation formula, inserting a specific value for the variable, and evaluating the expression using the Mellin Transform pairs in Table F. For two or more parameters, the Mellin convolution integral is used to convert the integral into one in the complex plane as shown in Figure 1-9. Specifically, the steps required to evaluate an integral in a single complex plane are illustrated in Figure 1-10. The steps in evaluating the asymptotic series are shown in Figure 1-11. Integration in two complex planes is considered in Figure 1-12. Integrations in more than two

complex planes are a generalization of the last technique and are discussed in Section 2.5 of part 2.

The last integration over z is considered in Figure 1-13. When the results of the previous integrations give a power series in z and the Hufnagel-Valley model is used, then the result of this integration is an analytic expression. For that reason, it is desirable to always consider turbulence profiles that can be expressed as a Hufnagel-Valley model. In Appendix C, parameters for the Hufnagel-Valley model are given that result in the same value of coherence diameter and isoplanatic angle as the SLCSAT day and night models. These pseudo SLCSAT day and night models are used in this report rather than the original models.

In Figure 1-14 is a flowchart to obtain the Strehl ratio for anisoplanatic effects. Chromatic anisoplanatism is not considered in these flowcharts, but is considered in the main text.
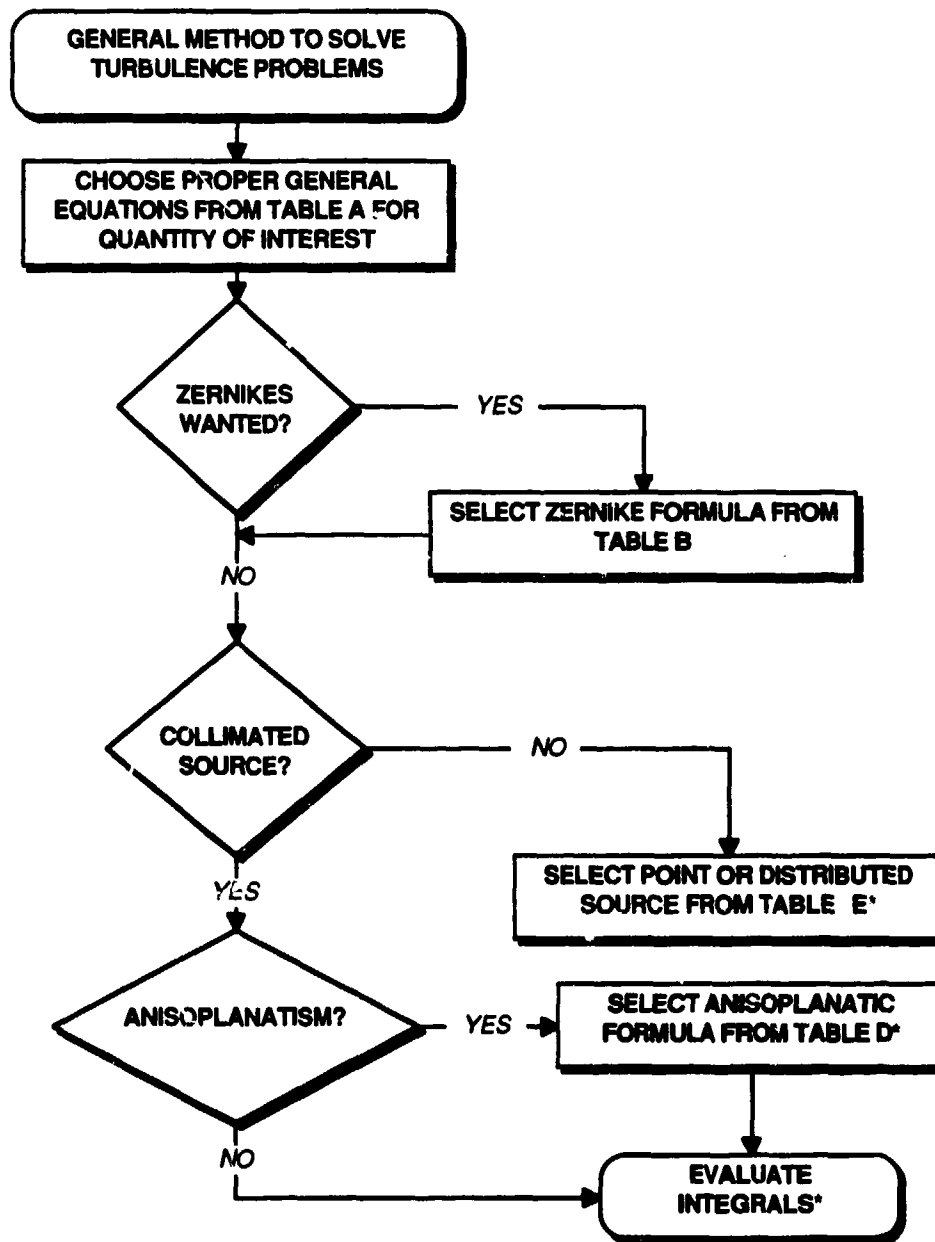
Figure 1-1. Flowchart of the overall method of solving turbulence problems..

16

```
┌─────────────────────────────────────────┐
│  CHOOSE PROPER GENERAL EQUATION FROM     │
│     TABLE A FOR QUANTITY OF INTEREST     │
└─────────────────────────────────────────┘
                    │
                    ▼
┌─────────────────────────────────────────┐
│         VARIANCE — FORMULA A.1           │
│   TEMPORAL POWER SPECTRAL DENSITY — A.3  │
│        STRUCTURE FUNCTION — A.2          │
└─────────────────────────────────────────┘
                    │
                    ▼
┌─────────────────────────────────────────┐
│        PHASE RELATED QUANTITIES          │
│   COLLIMATED SOURCE — UPPER PART OF A.4  │
│ (IF WELL WITHIN FRESNEL DISTANCE SET TO UNITY) │
│   FOCUSED AT APERTURE — MIDDLE PART OF A.4 │
│     FOCUSED AT S — LOWER PART OF A.4      │
└─────────────────────────────────────────┘
                    │
                    ▼
┌─────────────────────────────────────────┐
│       LOG–AMPLITUDE RELATED QUANTITIES   │
│ COLLIMATED SOURCE FOR PROPAGATION FROM 0 TO L — UPPER PART OF A.5 │
│ FOR PROPAGATION FROM L TO 0 — CHANGE L - z TO z IN ABOVE EQUATION │
│   FOCUSED AT APERTURE — MIDDLE PART OF A.5 │
│     FOCUSED AT S — LOWER PART OF A.5      │
└─────────────────────────────────────────┘
```

Figure 1-2. Choosing the filter function for variance, temporal power spectrum, and structure functions for collimated and focused beams.
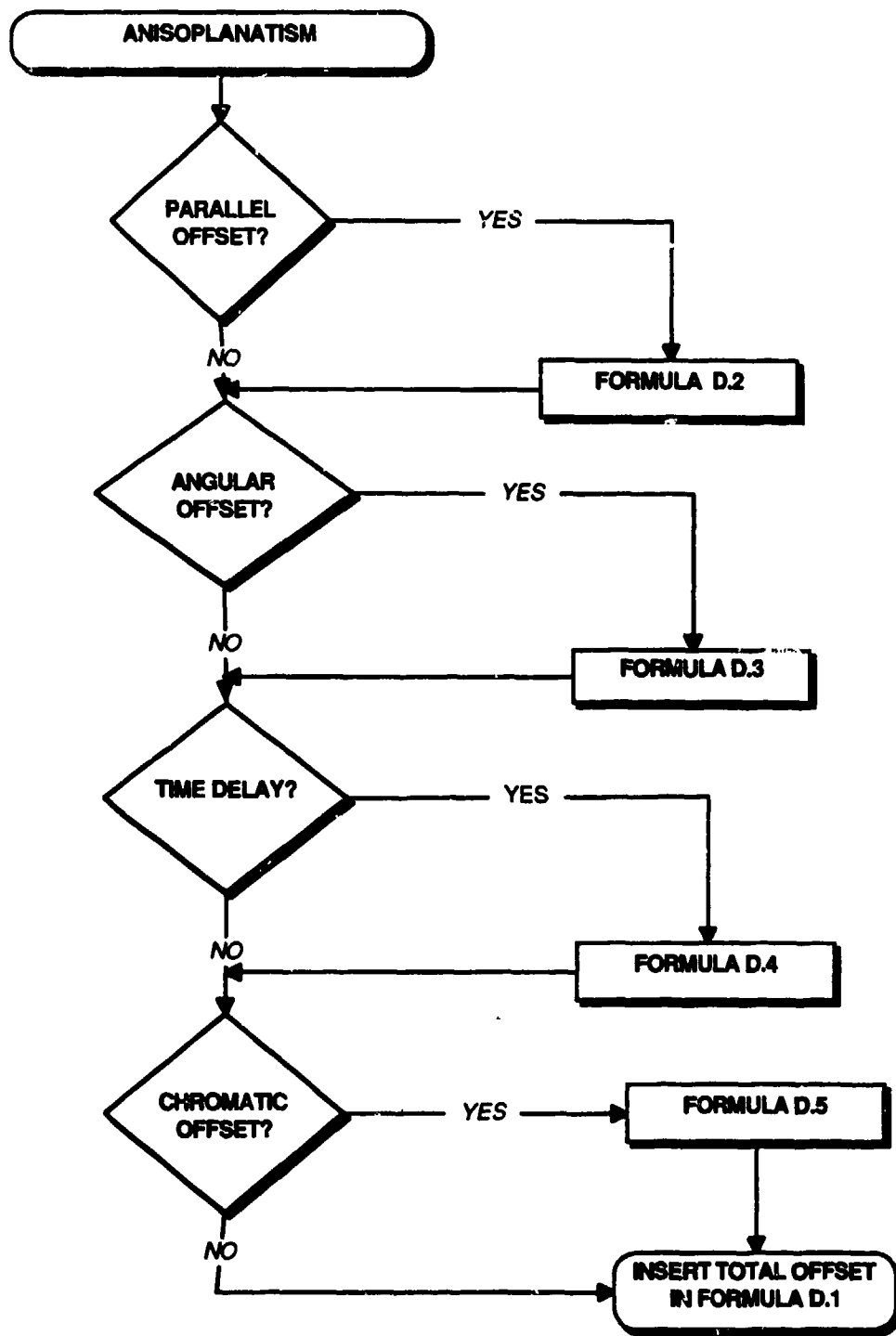
Figure 1-3. Filter functions for anisoplanatism.

18

```
                    ┌─────────────────────────────────┐
                    │      ZERNIKE COMPONENTS         │
                    └─────────────────────────────────┘
                                    │
                                    ▼
            ┌───────────────────────────────────────────┐
            │  ANY ZERNIKE COMPONENT PHASE VARIANCE       │
            │                 B.1                         │
            └───────────────────────────────────────────┘
                                    │
                                    ▼
        ┌──────────────────────────────────┐      ┌──────────────────────┐
        │   PISTON PHASE VARIANCE B.2        │─────▶│  PISTON VARIANCE B.3  │
        └──────────────────────────────────┘      └──────────────────────┘
                                    │
                                    ▼
            ┌──────────────────────────┐      ┌──────────────────────┐
            │   TILT PHASE VARIANCE     │      │   TILT VARIANCE       │
            │   EACH AXIS B.4           │─────▶│   EACH AXIS B.6       │
            │   2-AXIS B.5              │      │   2-AXIS B.7          │
            └──────────────────────────┘      └──────────────────────┘
                                    │
                                    ▼
            ┌───────────────────────────────────────────┐
            │  PISTON REMOVED PHASE VARIANCE B.8          │
            └───────────────────────────────────────────┘
                                    │
                                    ▼
            ┌───────────────────────────────────────────┐
            │   PISTON AND TILT REMOVED PHASE             │
            │           VARIANCE B.9                      │
            └───────────────────────────────────────────┘
                                    │
                                    ▼
            ┌───────────────────────────────────────────┐
            │  2-AXIS TILT VARIANCE ON AN ANNULAR         │
            │           APERTURE B.10                     │
            └───────────────────────────────────────────┘
```
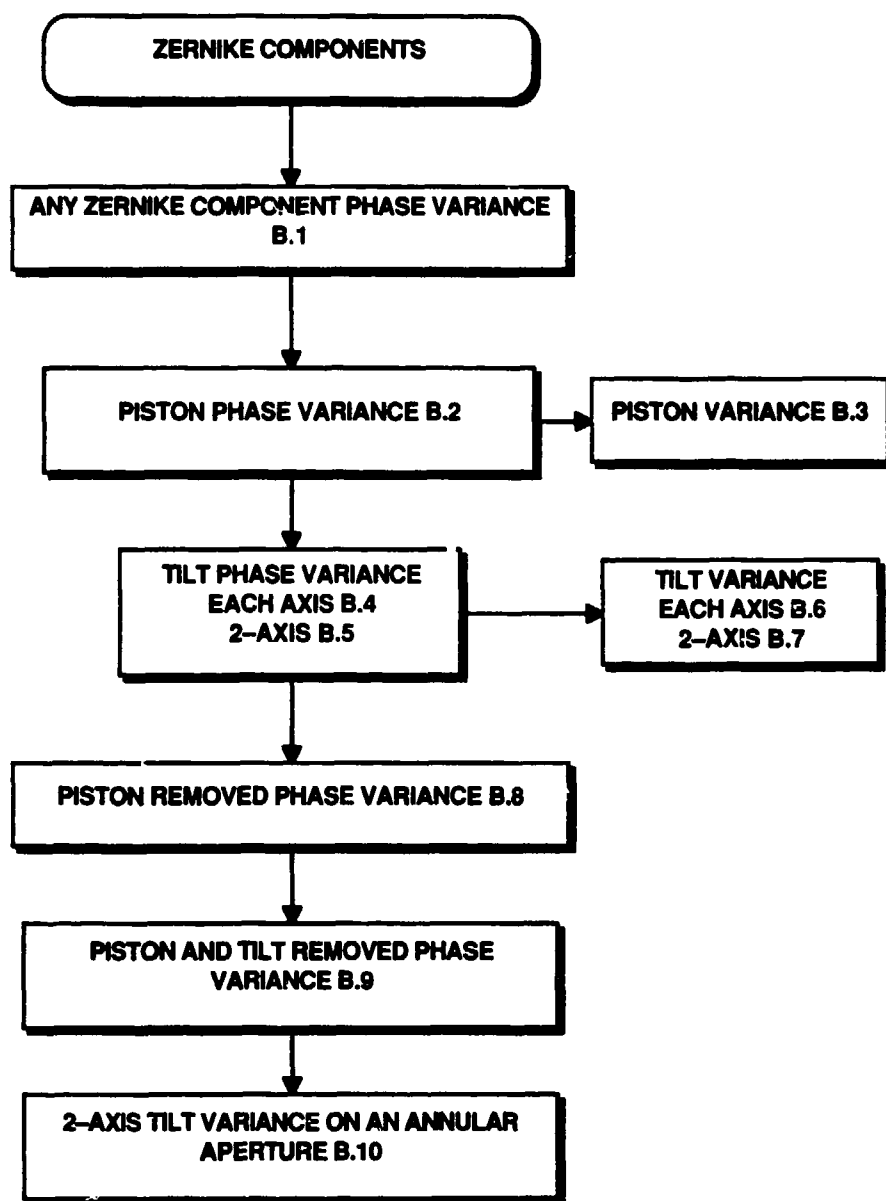
Figure 1-4. Filter functions for Zernike components.

```
┌─────────────────────────────────┐
│   POINT OR DISTRIBUTED SOURCE   │
└─────────────────────────────────┘
                 │
                 ▼
┌─────────────────────────────────┐
│      ON-AXIS UNIFORM SOURCE     │
│               E.1               │
└─────────────────────────────────┘
                 │
                 ▼
┌─────────────────────────────────┐
│      ANISOPLANATIC EFFECT       │
│   COMPARISON WITH A COLLIMATED  │
│               BEAM              │
└─────────────────────────────────┘
                 │
                 ▼
┌─────────────────────┐      ┌─────────────────────────┐
│  OFFSET POINT SOURCE│─────▶│   OFFSET POINT SOURCE   │
│         E.2         │      │   EVERYTHING SYMMETRIC  │
└─────────────────────┘      │           E.3           │
           │                 └─────────────────────────┘
           │                              │
           │                              ▼
           │                 ┌─────────────────────────┐
           │                 │  CENTERED POINT SOURCE  │
           │                 │   EVERYTHING SYMMETRIC  │
           │                 │           E.4           │
           │                 └─────────────────────────┘
           ▼
┌─────────────────────────┐      ┌─────────────────────────┐
│   OFFSET, DISTRIBUTED,   │─────▶│  CENTERED, DISTRIBUTED,  │
│ UNIFORM, CIRCULAR SOURCE │      │ UNIFORM, CIRCULAR SOURCE │
│           E.5            │      │           E.6            │
└─────────────────────────┘      └─────────────────────────┘
```
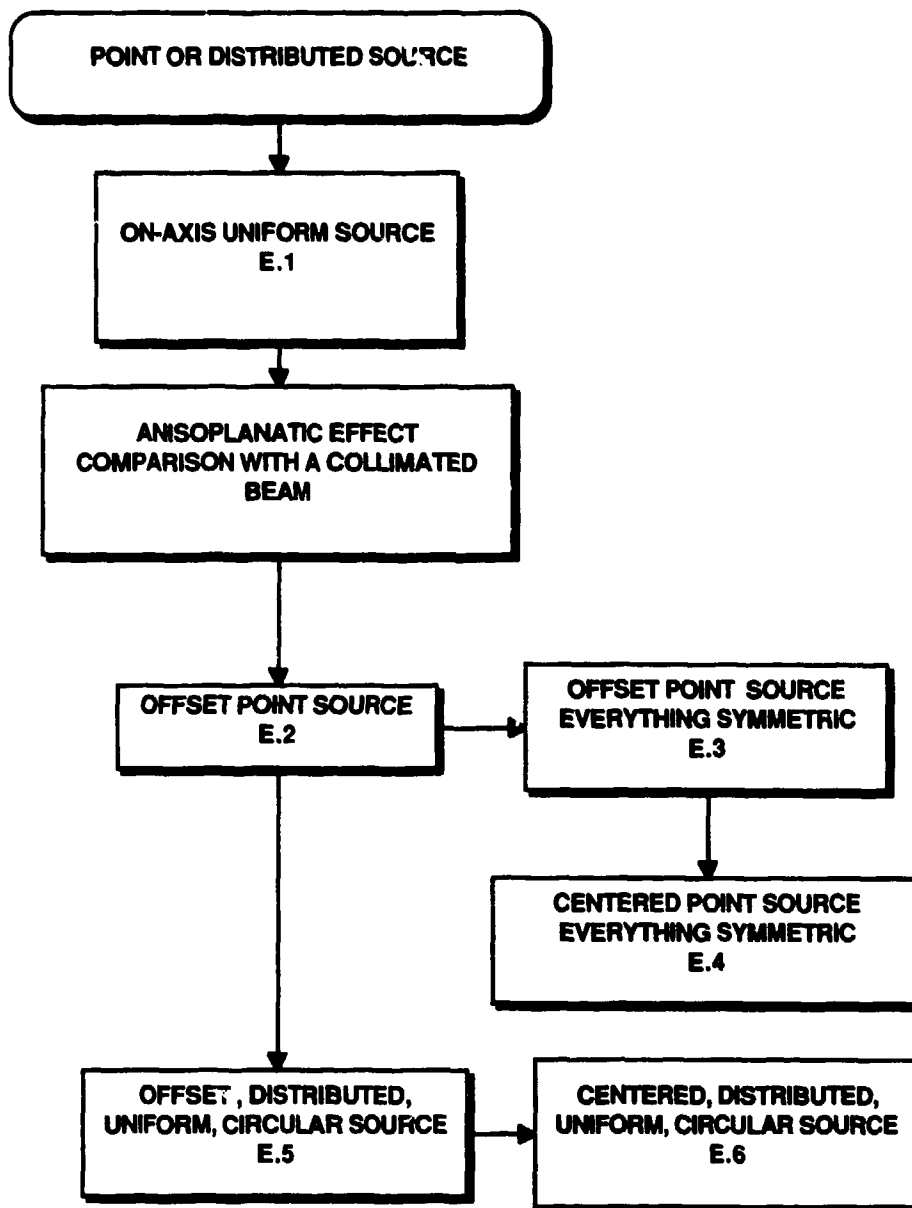
Figure 1-5. Filter functions for point or distributed sources.

20
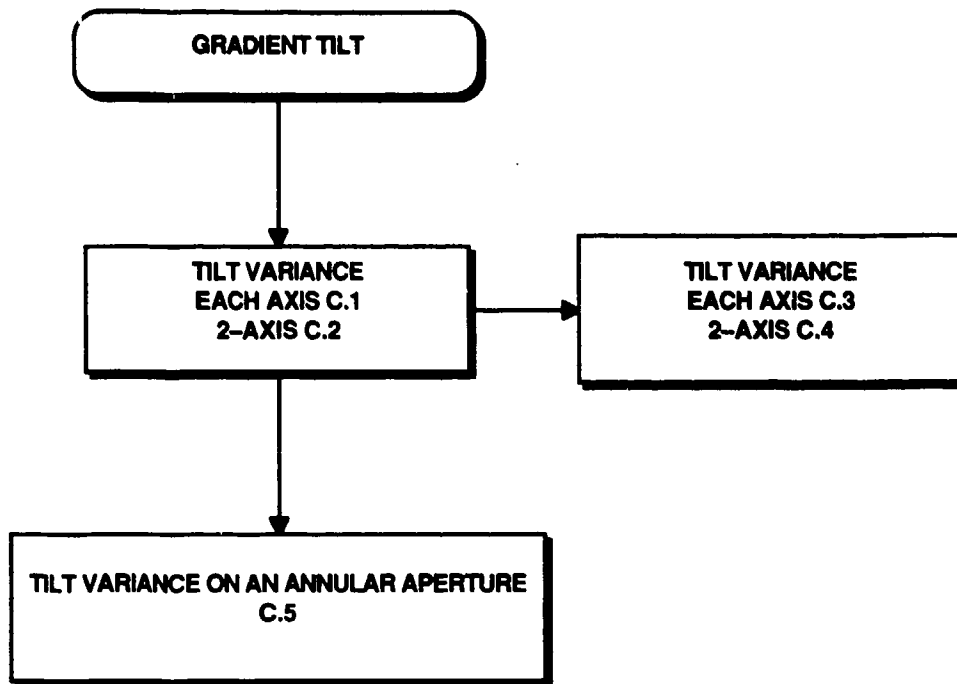
Figure 1-6. Filter functions for gradient tilt.
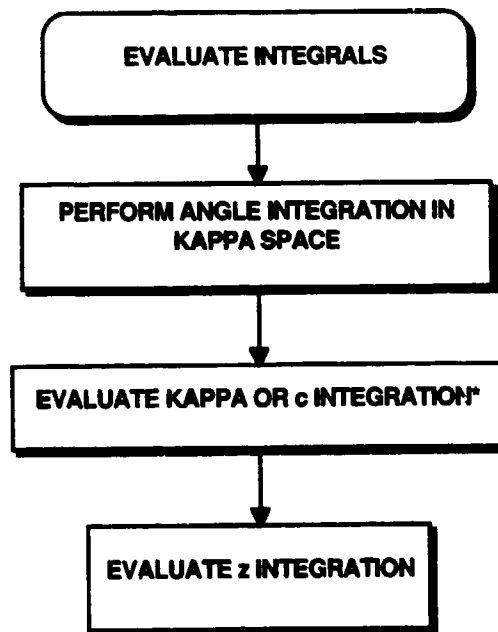
Figure 1-7. Overall method to evaluate integrals.

21
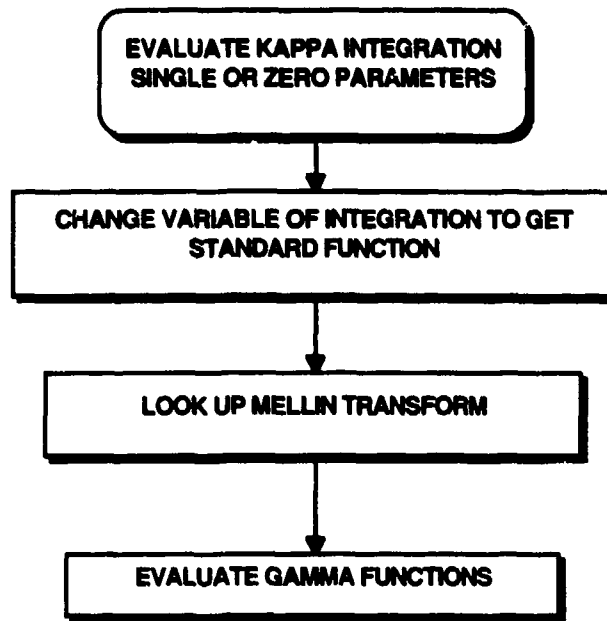
Figure 1-8. Method of evaluating integrals with single or no parameters.
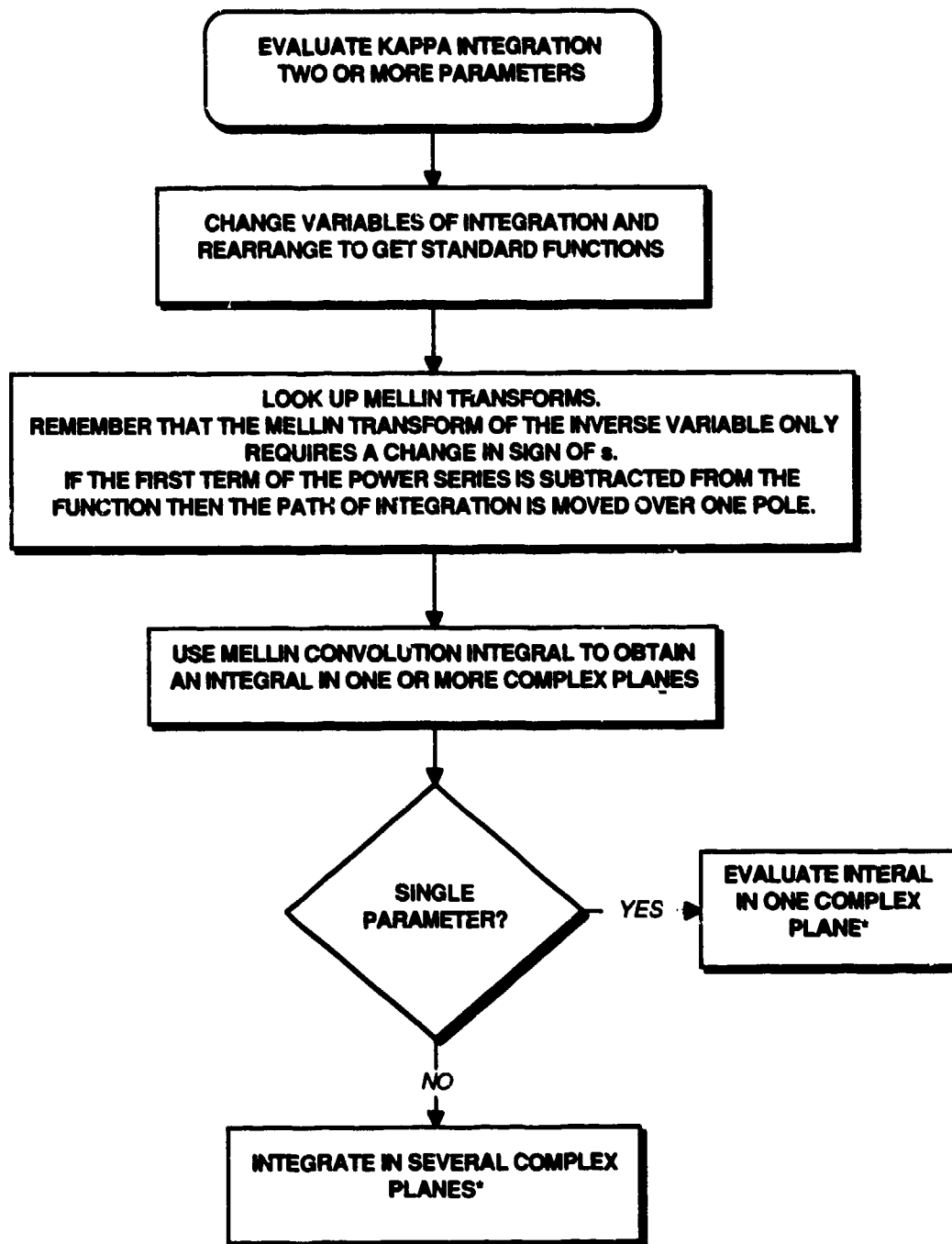
Figure 1-9. Method of evaluating integrals with two or more parameters.
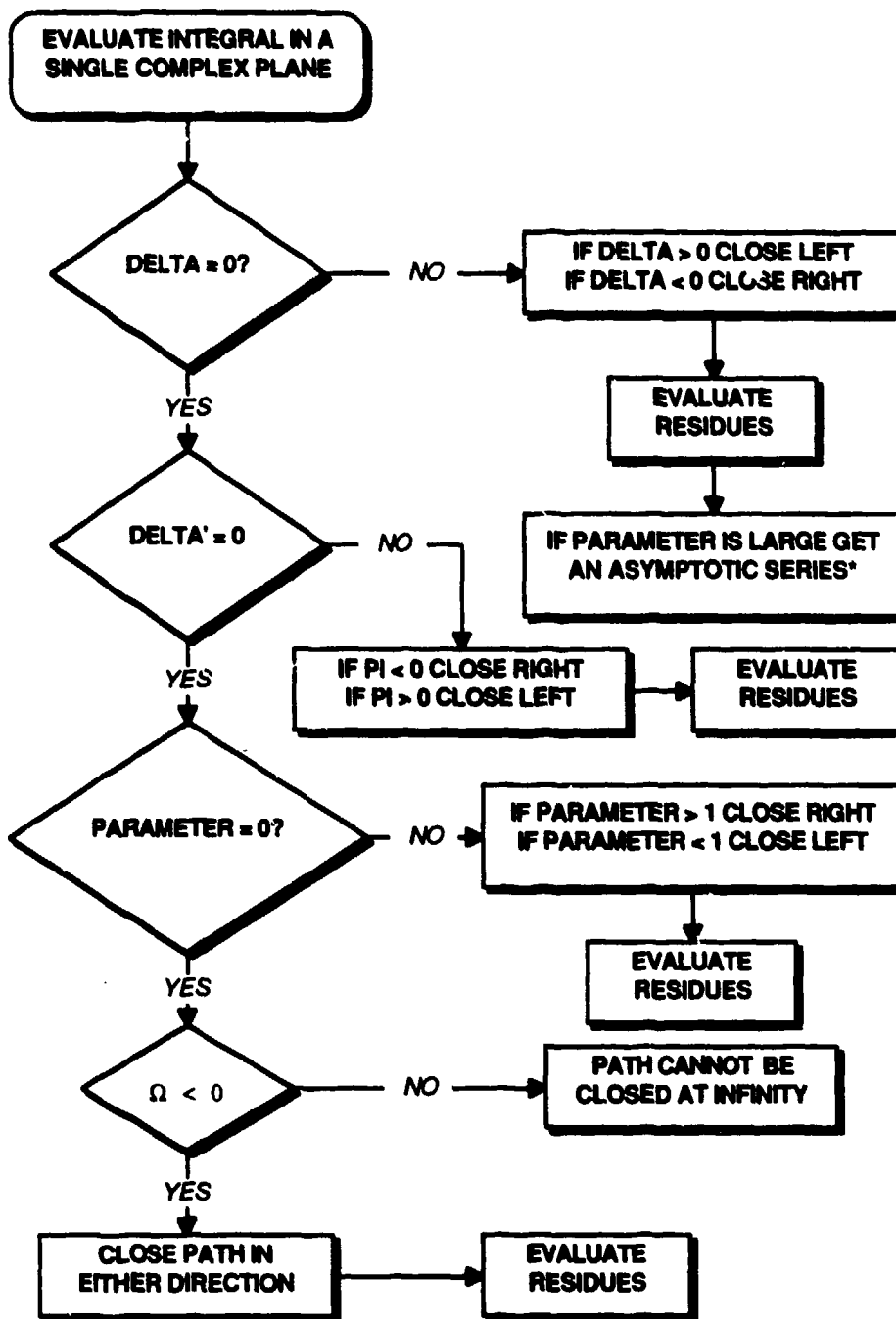
Figure 1-10. Evaluation of the integral in a single complex plane.

24
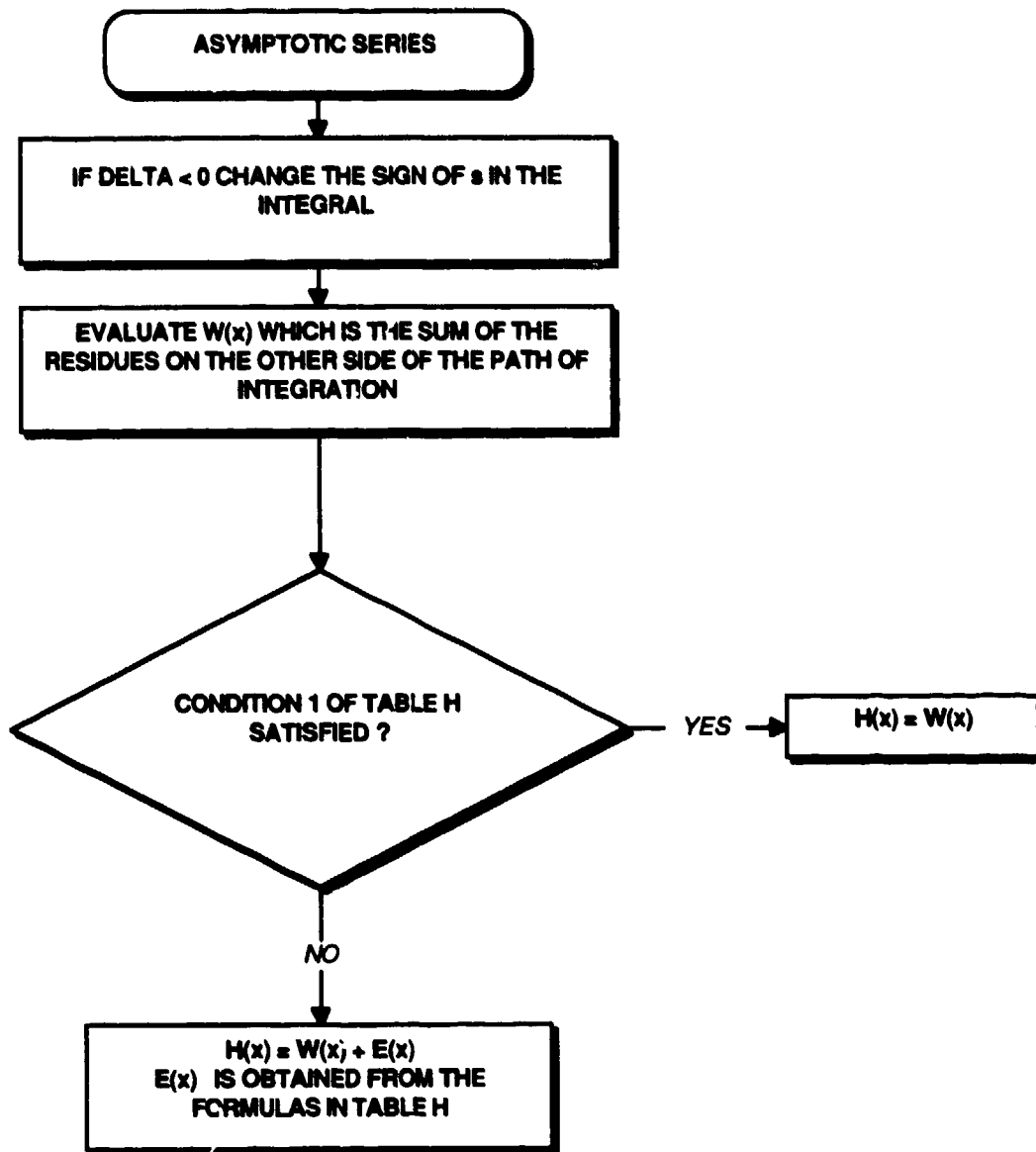
Figure 1-11. Evaluation of the asymptotic series.

25
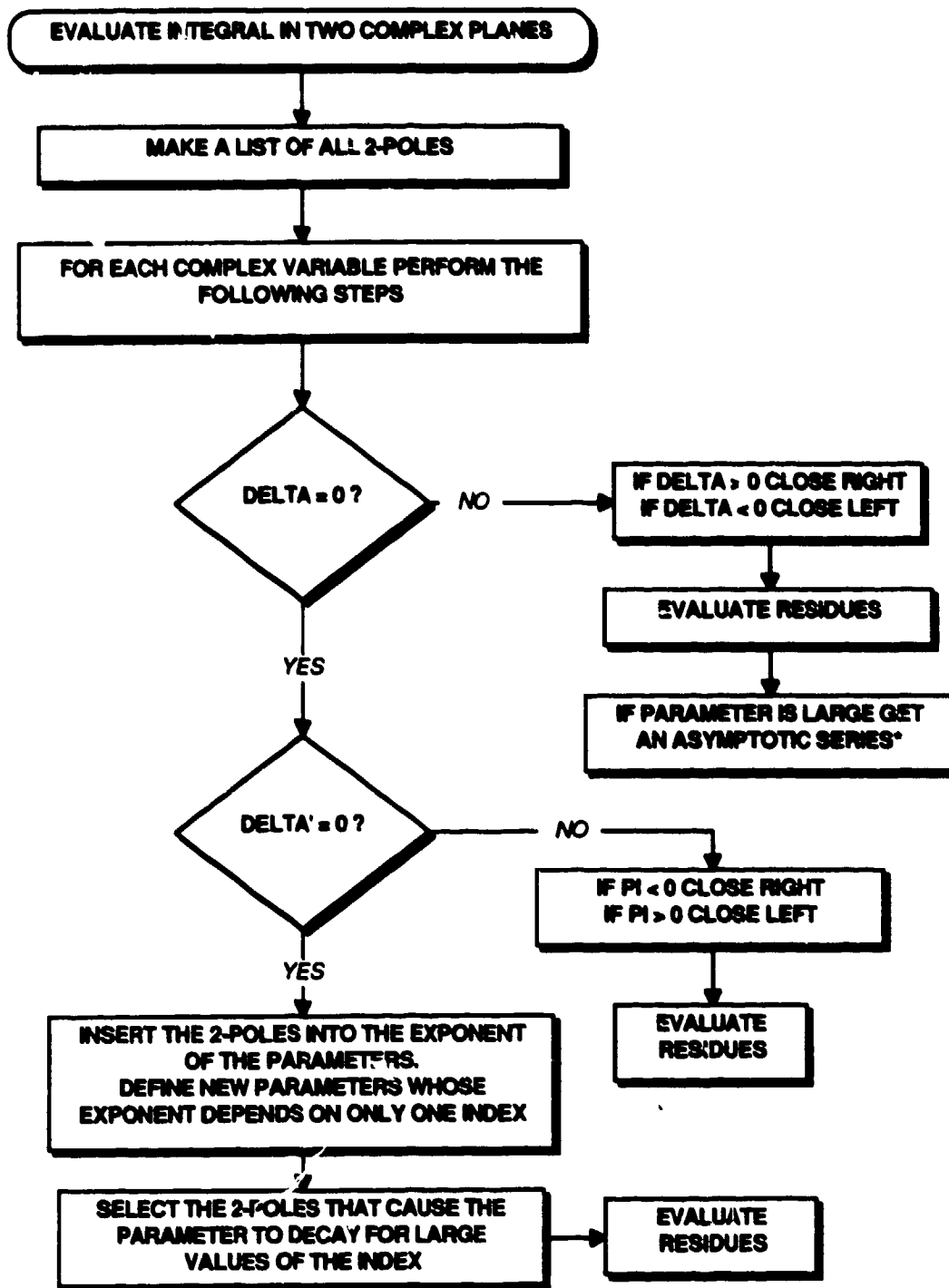
Figure 1-12. Evaluation of the integral in two complex planes.

26
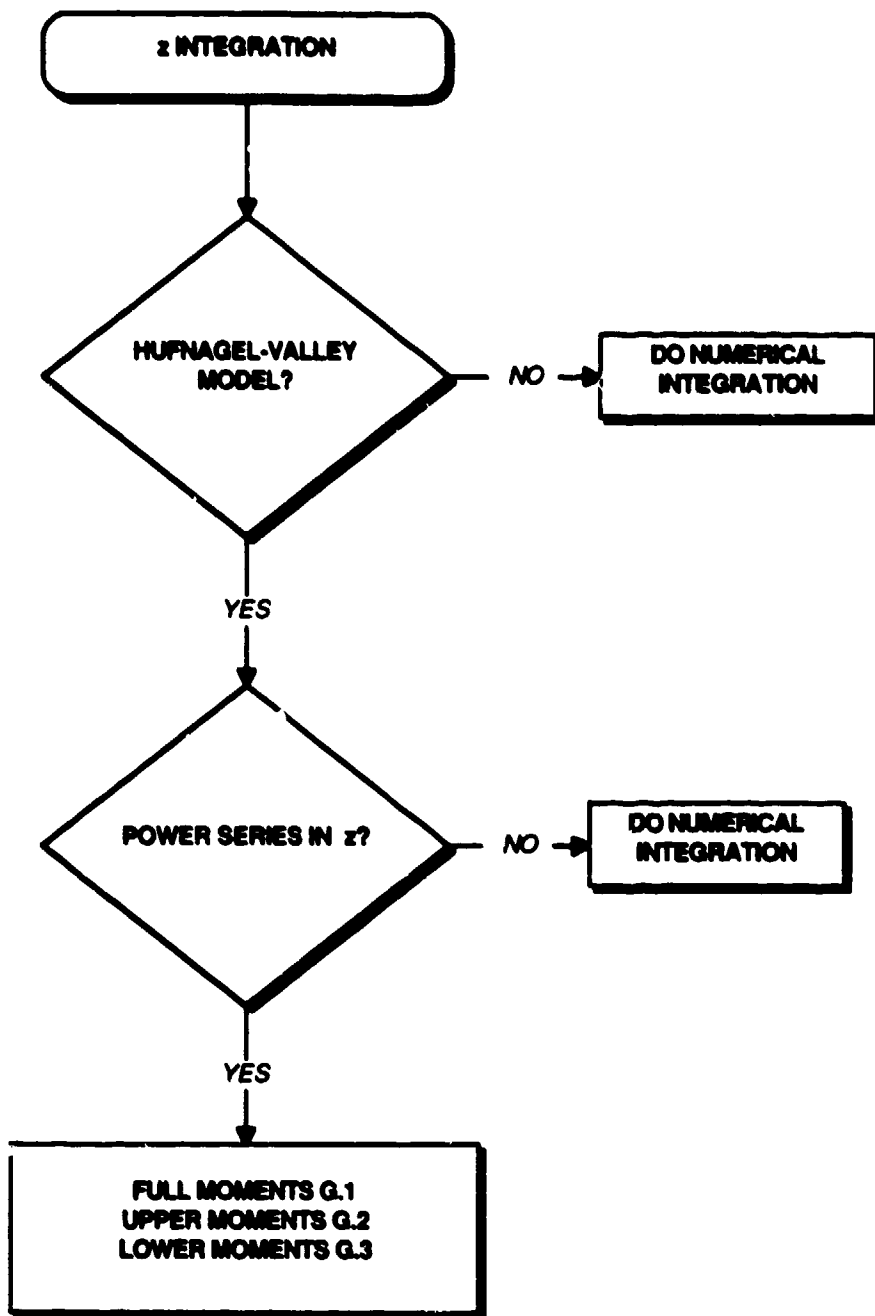
Figure 1-13. Evaluating of the z integration.

STREHL RATIO FOR ANISOPLANATISM
USE FORMULAS IN TABLE J

USE GENERAL FORMULA J.1 AND J.2

FOF DISPLACEMENT ANISOPLANATISM USE J.4 AND J.5
FOR ANGULAR ANISOPLANATISM USE J.6 AND J.7
FOR TIME DELAY USE J.9 THROUGH J.11
FOR CHROMATIC ANISOPLANATISM SEE SECTION 3.9.3.4
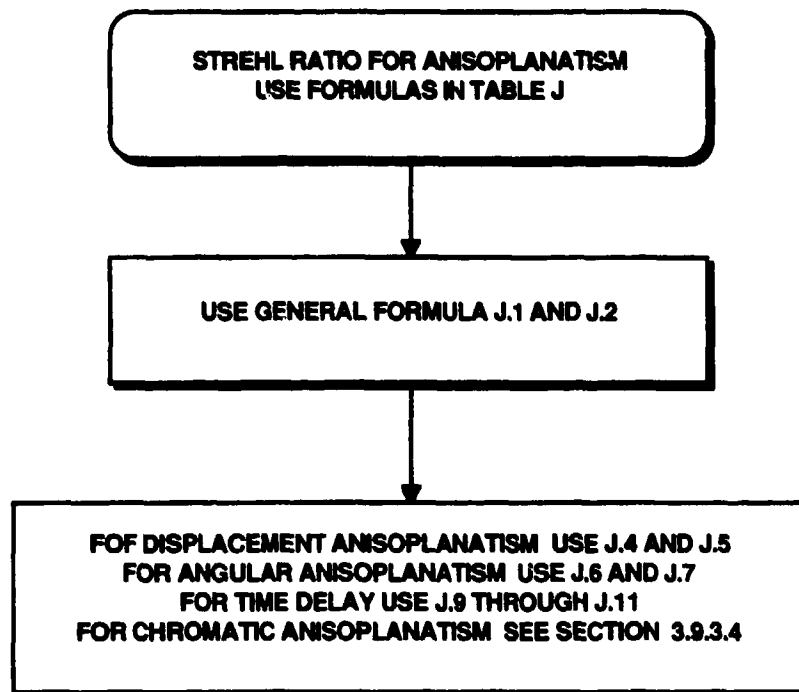
Figure 1-14. Finding the Strehl ratio with anisoplanatism.

28

TABLE A

Formulas for the Phase and Scintillation Variance, Structure Function, and PSD

Phase and Scintillation Variance

$$\begin{bmatrix} \phi^2 \\ \chi^2 \end{bmatrix} = 0.2073 \ k_o^2 \int\limits_0^L dz \ C_n^2(z) \int d\vec{\kappa} \ f(\kappa) \begin{bmatrix} C_p \\ C_a \end{bmatrix} \prod_i F_i(\vec{\kappa}, z) \tag{A.1}$$

Phase and Log-Amplitude Structure Function

$$\begin{bmatrix} D_\phi(\vec{\alpha}) \\ D_\chi(\vec{\alpha}) \end{bmatrix} = 0.4146 k_o^2 \int\limits_0^L dz \ C_n^2(z) \int d\vec{\kappa} \ f(\kappa) \begin{bmatrix} C_p \\ C_a \end{bmatrix} [1 - \cos\{\vec{\kappa} \cdot \vec{\alpha}D\}] \prod_i F_i(\vec{\kappa}, z) \tag{A.2}$$

Power Spectral Density

$$F(\omega) = 1.303 \ k_o^2 \omega \int\limits_0^L dz \ \frac{C_n^2(z)}{v^2(z)} \int\limits_0^\infty \frac{c \, dc \ U(c-1)}{\sqrt{c^2 - 1}} \ f\left(\frac{\omega c}{v(z)}\right) \begin{bmatrix} C_p \\ C_a \end{bmatrix} \prod_i F_i\left(\frac{\omega c}{v(z)}, z\right) \tag{A.3}$$

where

$$C_p = \begin{cases} \cos^2\left[\dfrac{\kappa^2(z-L)}{2k_o}\right] \\ \left(\dfrac{z}{S}\right)^{5/3} \cos^2\left[\dfrac{\kappa^2 S(S-z)}{2k_o S}\right] \\ \left(\dfrac{S-z}{S}\right)^{5/3} \cos^2\left[\dfrac{\kappa^2 z S}{2k_o(z-S)}\right] \end{cases} \text{ for a wave that is } \begin{bmatrix} \text{collimated} \\ \\ \text{focused at } 0 \\ \\ \text{focused at } S \end{bmatrix} \tag{A.4}$$

$$C_a = \begin{cases} \sin^2\left[\dfrac{\kappa^2(z-L)}{2k_o}\right] \\ \left(\dfrac{z}{S}\right)^{5/3} \sin^2\left[\dfrac{\kappa^2 S(S-z)}{2k_o S}\right] \\ \left(\dfrac{S-z}{S}\right)^{5/3} \sin^2\left[\dfrac{\kappa^2 z S}{2k_o(z-S)}\right] \end{cases} \text{ for a wave that is } \begin{bmatrix} \text{collimated} \\ \\ \text{focused at } 0 \\ \\ \text{focused at } S \end{bmatrix} \tag{A.5}$$

and $\quad f(\kappa) = \left[\kappa^2 + \kappa_o^2\right]^{-11/6} \exp\left[-\kappa^2/\kappa_i^2\right] \approx \kappa^{-11/3}$ (A.6)

For finding the PSD let $\kappa = \omega c / v(z)$ in Equations (A.4) and (A.5)

29

TABLE B

Filter Functions for Zernike Components of the Waveform

$$
\left.\begin{array}{l} F_{even\,m,\,n}(\vec{\kappa}) \\ F_{odd\,m,\,n}(\vec{\kappa}) \\ F_{m,\,n}(\vec{\kappa}) \end{array}\right\} = (n+1)\left[\frac{2\,J_{n+1}(\kappa D/2)}{\kappa D/2}\right]^2 \begin{cases} 2\cos^2(m\varphi) \\ 2\sin^2(m\varphi) \\ 1 \quad (m=0) \end{cases} \quad \text{Zernike Polynomials}
$$

(B.1)

$$
F(\vec{\kappa},\,z) = \left[\frac{2J_1(\kappa D/2)}{\kappa D/2}\right]^2 \quad \text{Piston Phase Variance} \qquad \text{(B.2)}
$$

$$
F(\vec{\kappa},\,z) = \left(\frac{1}{k_o}\right)^2\left[\frac{2J_1(\kappa D/2)}{\kappa D/2}\right]^2 \quad \text{Piston Variance} \qquad \text{(B.3)}
$$

$$
\left.\begin{array}{l} F_x(\vec{\kappa},\,z) \\ F_y(\vec{\kappa},\,z) \end{array}\right\} = \left[\frac{4\,J_2(\kappa D/2)}{\kappa D/2}\right]^2 \begin{cases} \cos^2(\varphi) \\ \sin^2(\varphi) \end{cases} \quad \text{Zernike-Tilt Phase Variance} \qquad \text{(B.4)}
$$

$$
F(\vec{\kappa},\,z) = \left[\frac{4\,J_2(\kappa D/2)}{\kappa D/2}\right]^2 \quad \text{Two-axis Phase Variance of Zernike-Tilt} \qquad \text{(B.5)}
$$

$$
\left.\begin{array}{l} F_x(\vec{\kappa},\,z) \\ F_y(\vec{\kappa},\,z) \end{array}\right\} = \left(\frac{16}{k_o D}\right)^2\left[\frac{J_2(\kappa D/2)}{\kappa D/2}\right]^2 \begin{cases} \cos^2(\varphi) \\ \sin^2(\varphi) \end{cases} \quad \text{Zernike-Tilt Variance} \qquad \text{(B.6)}
$$

TABLE B (Continued)

Filter Functions for Zernike Components of the Waveform

$$F(\vec{\kappa}, z) = \left(\frac{16}{k_o D}\right)^2 \left[\frac{J_2(\kappa D / 2)}{\kappa D / 2}\right]^2 \qquad \text{Two-Axis Zernike-Tilt Variance} \qquad \text{(B.7)}$$

$$F(\vec{\kappa}, z) = 1 - \left[\frac{2 J_1(\kappa D / 2)}{\kappa D / 2}\right]^2 \qquad \text{Piston Removed Phase Variance} \qquad \text{(B.8)}$$

$$F(\vec{\kappa}, z) = 1 - \left[\frac{2 J_1(\kappa D / 2)}{\kappa D / 2}\right]^2 - \left[\frac{4 J_2(\kappa D / 2)}{\kappa D / 2}\right]^2 \qquad \text{Piston and Tilt Removed} \qquad \text{(B.9)}$$

$$\text{Phase Variance}$$

Two-Axis Zernike-Tilt Variance on an Annular Aperture

$$F(\vec{\kappa}, z) = \left[\frac{16}{k_o D\left(1 - \beta^4\right)}\right]^2 \left[\frac{J_2(\kappa D / 2)}{\kappa D / 2} - \beta^3 \frac{J_2(\kappa \beta D / 2)}{\kappa \beta D / 2}\right]^2 \qquad \text{(B.10)}$$

where $\beta = D_i / D$ and D_i is the inner radius

TABLE C

Filter Functions for Gradient Tilt Components of the Waveform

$$\left.\begin{array}{c} F_x(\vec{\kappa}, z) \\ F_y(\vec{\kappa}, z) \end{array}\right\} = J_1^{\,2}(\kappa D / 2)\begin{cases} \cos^2(\varphi) \\ \sin^2(\varphi) \end{cases} \quad \text{Gradient Tilt Phase Variance} \qquad (C.1)$$

$$F(\vec{\kappa}, z) = J_1^{\,2}(\kappa D / 2) \quad \text{Two-Axis Phase Variance of Gradient Tilt} \qquad (C.2)$$

$$\left.\begin{array}{c} F_x(\vec{\kappa}, z) \\ F_y(\vec{\kappa}, z) \end{array}\right\} = \left(\frac{4}{k_o D}\right)^2 J_1^{\,2}(\kappa D / 2)\begin{cases} \cos^2(\varphi) \\ \sin^2(\varphi) \end{cases} \quad \text{Gradient Tilt Variance} \qquad (C.3)$$

$$F(\vec{\kappa}, z) = \left(\frac{4}{k_o D}\right)^2 J_1^{\,2}(\kappa D / 2) \quad \text{Two-Axis Gradient Tilt Variance} \qquad (C.4)$$

Two-Axis Gradient Tilt Variance for an Annular Aperture

$$F(\vec{\kappa}, z) = \left[\frac{4}{k_o D\left(1 - \beta^2\right)}\right]^2 \left[J_1(\kappa D / 2) - \beta\, J_1(\kappa \beta D / 2)\right]^2 \qquad (C.5)$$

where $\beta = D_i / D$ and D_i is the inner radius

32

TABLE D

Filter Functions for Anisoplanatic Effects in an Adaptive-Optics System

Anisoplanatism

$$F(\vec{\kappa}, z) = 2\left[1 - \cos\left\{\vec{\kappa} \cdot \vec{d}(z)\right\}\right] \qquad \text{General Formula} \qquad \text{(D.1)}$$

$$\vec{d}(z) = \vec{d} \qquad \text{Parallel Displacement} \qquad \text{(D.2)}$$

$$\vec{d}(z) = \vec{\Theta} z \qquad \text{Angular Offset} \qquad \text{(D.3)}$$

$$\vec{d}(z) = \vec{v}(z)\tau \qquad \text{Time Delay} \qquad \text{(D.4)}$$

$$\vec{d}(z) = -\frac{\zeta \sin(\zeta) \Delta n_o}{\zeta \cos^2(\zeta)} \int_0^z dx \ \alpha(x) \qquad \text{Chromatic Offset} \qquad \text{(D.5)}$$

TABLE E

Filter Functions for Point and Distributed Sources

Point and Distributed Sources

$$F(\vec{\kappa}, z) = \left[2\frac{J_1\left(\frac{\kappa D_s z}{2H}\right)}{\frac{\kappa D_s z}{2H}} \right]^2 \quad \text{On-Axis Uniform Circular Source of Diameter } D_S$$

(E.1)

Anisoplanatic Effects (Reference Is Collimated Beam)

$$F(\vec{\kappa}, z) = \frac{16}{D^2} \int_0^{D/2} r\, dr \left[1 - J_o\left(\frac{\kappa r z}{H}\right)\cos\left(\vec{\kappa} \cdot \frac{\vec{b}z}{H}\right) \right] \quad \text{Offset Point Source} \quad \text{(E.2)}$$

$$F(\vec{\kappa}, z) = 2\left[1 - \frac{2J_1\left(\frac{\kappa D z}{2H}\right)}{\frac{\kappa D z}{2H}} J_o\left(\frac{\kappa b z}{H}\right) \right] \quad \text{Offset Point Source with Symmetry} \quad \text{(E.3)}$$

$$F(\vec{\kappa}, z) = 2\left[1 - 2\frac{J_1\left(\frac{\kappa D z}{2H}\right)}{\frac{\kappa D z}{2H}} \right] \quad \text{Centered Point Source with Symmetry} \quad \text{(E.4)}$$

Distributed, Circular, Uniform, Offset Source

$$F(\vec{\kappa}, z) = 1 - \frac{4J_1(Dx)}{Dx}\frac{2J_1(D_s x)}{D_s x} \cos\left(\vec{\kappa} \cdot \frac{z\vec{b}}{H}\right) + \left[2\frac{J_1(D_s x)}{D_s x} \right]^2 \quad \text{(E.5)}$$

where $\qquad x = \frac{\kappa z}{2H}$

Distributed, Circular, Uniform, Centered Source with Symmetry

$$F(\vec{\kappa}, z) = 1 - \frac{4J_1(Dx)}{Dx}\frac{2J_1(D_s x)}{D_s x} + \left[2\frac{J_1(D_s x)}{D_s x} \right]^2 \quad \text{(E.6)}$$

34

TABLE F		
Mellin Transforms that Are Useful for Turbulence Problems		

$$\exp(-x) \quad \rightarrow \Gamma[s] \qquad\qquad \text{Re } s > 0 \qquad\qquad (\text{F.1})$$

$$\sin(x) \quad \rightarrow 2^{s-1}\sqrt{\pi}\,\Gamma\begin{bmatrix} 1/2 + s/2 \\ 1 - s/2 \end{bmatrix} \qquad |\text{Re } s| < 1 \qquad (\text{F.2})$$

$$\cos(x) \quad \rightarrow 2^{s-1}\sqrt{\pi}\,\Gamma\begin{bmatrix} s/2 \\ 1/2 - s/2 \end{bmatrix} \qquad 0 < \text{Re } s < 1 \qquad (\text{F.3})$$

$$\sin^2(x^2) \quad \rightarrow -\frac{\sqrt{\pi}}{8}\Gamma\begin{bmatrix} s/4^* \\ 1/2 - s/4 \end{bmatrix} \qquad -4 < \text{Re } s < 0 \qquad (\text{F.4})$$

$$J_\nu(x) \quad \rightarrow 2^{s-1}\Gamma\begin{bmatrix} s/2 + \nu/2 \\ \nu/2 + 1 - s/2 \end{bmatrix} \qquad -\text{Re } \nu < \text{Re } s < 3/2 \qquad (\text{F.5})$$

$$J_\nu^2(x) \quad \rightarrow \frac{1}{2\sqrt{\pi}}\Gamma\begin{bmatrix} s/2 + \nu,\, 1/2 - s/2 \\ \nu + 1 - s/2,\, 1 - s/2 \end{bmatrix} \qquad -2\text{Re } \nu < \text{Re } s < 1 \qquad (\text{F.6})$$

$$J_\nu(x)J_{\nu+1}(x) \rightarrow \frac{1}{2\sqrt{\pi}}\Gamma\begin{bmatrix} s/2 + \nu + 1/2,\, 1 - s/2 \\ \nu + 3/2 - s/2,\, 3/2 - s/2 \end{bmatrix} \quad -1 - 2\text{Re } \nu < \text{Re } s < 2$$

$$(\text{F.7})$$

$$(1 + x)^{-p} \quad \rightarrow \frac{\Gamma[s,\, p - s]}{\Gamma[p]} \qquad 0 < \text{Re } s < \text{Re } p \qquad (\text{F.8})$$

35

TABLE F (Continued)
Mellin Transforms that are Useful for Turbulence Problems

$(1 - x)^{a-1} U(1 - x) \quad \rightarrow \Gamma[a] \Gamma\begin{bmatrix} s \\ s + a \end{bmatrix}$ $\qquad$ Re $a > 0$ $\quad$ Re $s > 0$

$\hfill$ (F.9)

$(x - 1)^{a-1} U(x - 1) \quad \rightarrow \Gamma[a] \Gamma\begin{bmatrix} 1 - a - s \\ 1 - s \end{bmatrix}$ $\qquad$ Re $a > 0$ $\qquad$ Re$(a + s) < 1$

$\hfill$ (F.10)

$1 \qquad \rightarrow \lim_{\varepsilon \to 0} \left[\dfrac{1}{s + \varepsilon} - \dfrac{1}{s - \varepsilon} \right]$ $\qquad$ $-\varepsilon <$ Re $s < \varepsilon$

$\hfill$ (F.11)

$\cos^{-1}(x) U(1 - x) \rightarrow \cdots \dfrac{\sqrt{\pi}}{4} \Gamma\begin{bmatrix} s/2 + 1/2, -s/2 \\ s/2 + 1, 1 - s/2 \end{bmatrix}$ $\qquad$ Re $s > 0$

$\hfill$ (F.12)

$U(1 - x) \qquad \rightarrow \Gamma\begin{bmatrix} s \\ s + 1 \end{bmatrix}$ $\qquad$ Re $s > 0$

$\hfill$ (F.13)

$U(x) \qquad \rightarrow \Gamma\begin{bmatrix} -s \\ 1 - s \end{bmatrix}$ $\qquad$ Re $s < 0$

$\hfill$ (F.14)

$\sin^n(x^2) \rightarrow \dfrac{\sqrt{\pi}}{2^{2n+1}} \sum_{k=0}^{n-1} (-1)^{n+k-1} \dfrac{(2n)!(n-k)^{-s/2}}{k!(2n-k)!} \Gamma\begin{bmatrix} s/4* \\ \frac{1}{2} - s/4 \end{bmatrix}$ $\qquad$ | Re s| $< \frac{1}{2}$

$\hfill$ (F.15)

TABLE G

Hufnagel-Valley Moments of Turbulence

Hufnagel-Valley Full Moment

$$\mu_n = \int_0^\infty dz\, C_n^2(z)\, z^n = \sec^{n+1}(\zeta)\left[5.94 \times 10^{-20+3n}\left(\frac{W}{27}\right)^2 \Gamma(n+11) \right.$$
$$\left. + 4.05 \times 10^{-13}\Gamma(n+1)(1500)^n + A \times 100^{n+1}\Gamma(n+1) \right]$$

(G.1)

Hufnagel-Valley Upper Moment

$$\mu_n^+(L) = \int_L^\infty dz\, C_n^2(z)\, z^n = \sec^{n+1}(\zeta)\left[5.94 \times 10^{-20+3n}\left(\frac{W}{27}\right)^2 \Gamma\left(n+11, \frac{H}{1000}\right) \right.$$
$$\left. + 4.05 \times 10^{-13}\Gamma\left(n+1, \frac{H}{1500}\right)(1500)^n + A \times 100^{n+1}\Gamma\left(n+1, \frac{H}{100}\right) \right]$$

(G.2)

Hufnagel-Valley Lower Moment

$$\mu_n^-(L) = \int_0^L dz\, C_n^2(z)\, z^n = \sec^{n+1}(\zeta)\left[5.94 \times 10^{-20+3n}\left(\frac{W}{27}\right)^2 \gamma\left(n+11, \frac{H}{1000}\right) \right.$$
$$\left. + 4.05 \times 10^{-13}\gamma\left(n+1, \frac{H}{1500}\right)(1500)^n + A \times 100^{n+1}\gamma\left(n+1, \frac{H}{100}\right) \right]$$

(G.3)

TABLE H

Formulas to Find the Asymptotic Series

Integral to be Evaluated

$$H(x) = \frac{1}{2\pi i} \int ds \, x^{-s} \, \frac{\prod_{i=1}^{A} \Gamma[a_i + \alpha_i s] \prod_{j-1}^{B} \Gamma[b_j - \beta_j s]}{\prod_{k=1}^{C} \Gamma[c_k + \gamma_k s] \prod_{m=1}^{D} \Gamma[d_m - \delta_m s]}$$

(H.1)

Definitions

$$\Delta = \sum_{i=1}^{A} \alpha_i + \sum_{m=1}^{D} \delta_m - \sum_{j=1}^{B} \beta_j - \sum_{k=1}^{C} \gamma_k$$

(H.2)

$$\Pi = -\ln |x| - \Delta'$$

(H.3)

$$\Xi' = A + D - B - C$$

(H.4)

$$\Xi = A + B - C - D$$

(H.5)

$$\nu = \sum_{i=1}^{A} a_i + \sum_{j=1}^{B} b_j - \sum_{k=1}^{C} c_k - \sum_{m=1}^{D} d_m$$

(H.6)

$$\Omega = \nu + C - A - \Xi'/2 + 1$$

(H.7)

$$\Delta' = \sum_{i=1}^{A} \alpha_i \ln(\alpha_i) + \sum_{m=1}^{D} \delta_m \ln(\delta_m) - \sum_{j=1}^{B} \beta_j \ln(\beta_j) - \sum_{k=1}^{C} \gamma_k \ln(\gamma_k)$$

(H.8)

$$B' = \sum_{j=1}^{B} \beta_j$$

(H.9)

$$D' = \sum_{m=1}^{D} \delta_m$$

(H.10)

$$\Lambda = [D' - B']$$

(H.11)

Formulas to Find the Asymptotic Series

$$B'' = \sum_{j=1}^{B} b_j \tag{H.12}$$

$$D'' = \sum_{m=1}^{D} d_m \tag{H.13}$$

$$\rho = [\,v + (1 - \Xi)\,/\,2\,]\,/\,\Delta \tag{H.14}$$

$$\Delta'' = \sum_{i=1}^{A} a_i \ln \alpha_i + \sum_{j=1}^{B} b_j \ln \beta_j - \sum_{k=1}^{C} c_k \ln \gamma_k - \sum_{m=1}^{D} d_m \ln \delta_m \tag{H.15}$$

$$\Delta''' = \sum_{i=1}^{A} \ln \alpha_i + \sum_{j=1}^{B} \ln \beta_j - \sum_{k=1}^{C} \ln \gamma_k - \sum_{m=1}^{D} \ln \delta_m \tag{H.16}$$

$$E(x) = \frac{2(2\pi)^{(\Xi - 1)/2}}{\sqrt{\Delta}}$$
$$\times x^{\rho} \exp\{- \rho\Delta' - \Delta x^{1/\Delta} \exp[-\Delta'/\Delta]\cos[\pi\Lambda/\Delta] + \Delta'' - \Delta'''/2\}$$
$$\times \cos\{\Delta x^{1/\Delta} \exp[-\Delta'/\Delta]\sin[\pi\Lambda/\Delta] + \pi[-\rho\Lambda + B'' - D'' - (B - D)/2]\} \tag{H.17}$$

If $\qquad\qquad \Delta' = \Delta'' = \Delta''' = 0, \quad B = B', \quad D = D', \tag{H.18}$

then the above simplifies to

$$E(x) = \frac{2(2\pi)^{(\Xi - 1)/2}}{\sqrt{\Delta}} x^{\rho} \exp\{-\Delta x^{1/\Delta} \cos[\pi\Lambda/\Delta]\}$$
$$\times \cos\{\Delta x^{1/\Delta} \sin[\pi\Lambda/\Delta] + \pi[(1/2 - \rho)\Lambda + B'' - D'']\} \tag{H.19}$$

Condition 1: For $\Xi > 0$, $B' \geq 1$, then $H(x) = W(x)$ \tag{H.20}

TABLE I

Mellin Transforms, Convolution Integrals, and Transformation Formulas

The Mellin Transform Pair is Given by

$$H(x) \rightarrow H^*(s) \equiv M(H(x)) \equiv \int_0^\infty dx\ H(x) x^{s-1} \tag{I.1}$$

and

$$H(x) = \frac{1}{2\pi i} \int ds\ H^*(s) x^{-s} \tag{I.2}$$

Transformation Formulas

$$H(ax)\ \ a > 0\ \rightarrow a^{-s} H^*(s) \tag{I.3}$$

$$x^a H(x) \qquad \rightarrow H^*(s + a) \tag{I.4}$$

$$H(x^p) \qquad \rightarrow H^*(s/p)/|p| \qquad p \neq 0 \tag{I.5}$$

The Mellin Convolution Integral is Given by

$$H(x) = \int_0^\infty \frac{dt}{t} H_o(t) H_1\left[\frac{x}{t}\right] \rightarrow H^*(s) = H_o^*(s) H_1^*(s) \tag{I.6}$$

For More than One Parameter, the Convolution Theorem is

$$H\left(x_1\ \dots, x_N\right) = \int_0^\infty \frac{dt}{t} H_o(t) \prod_{j=1}^N H_j\left(\frac{x_j}{t}\right) \rightarrow H_o^*(s_1 + \dots s_N) \prod_{j=1}^N H_j^*(s_j)$$

$$= H^*(s_1 \dots, s_N) \tag{I.7}$$

The Inverse Transform is

$$H(x_1, \dots, x_N) = \frac{1}{(2\pi i)^N} \int \dots \int ds_1 \dots ds_N\ H^*(s_1 + \dots s_N) x_1^{-s_1} \dots x_N^{-s_N} \tag{I.8}$$

40

TABLE J

Formulas to Find Strehl Ratio with Anisoplanatism

$$SR \approx \exp[-\sigma_\varphi^2]\left[1 + 0.9736\,E + 0.5133E^2 + 0.2009\,E^3 + 0.0697\,E^4 + 0.02744\,E^5\right] \tag{J.1}$$

$$E = \frac{2.91k_o^2 d_2}{D^{1/3}} \tag{J.2}$$

$$\sigma_\varphi^2 = 2.91k_o^2 \int_0^\infty dz\ C_n^2(z)d^{5/3}(z) = 2.91k_o^2 d_{5/3} \tag{J.3}$$

Displacement Anisoplanatism

$$d_2 = \mu_0 d^2 \tag{J.4}$$

$$\sigma_\varphi^2 = 2.91k_o^2\,\mu_o d^{5/3} = 6.88\left(\frac{d}{r_o}\right)^{5/3} \tag{J.5}$$

Angular Anisoplanatism

$$d(z) = \Theta z \tag{J.6}$$

$$d_2 = \mu_2 \Theta^2 \tag{J.7}$$

$$\sigma_\varphi^2 = 2.91k_o^2\Theta^{5/3}\int_0^L dz\ C_n^2(z)\ z^{5/3} = \left(\frac{\Theta}{\Theta_o}\right)^{5/3} \tag{J.8}$$

Time Delay

$$d_2 = \int_0^L dz\ C_n^2(z)\ v^2(z)\tau^2 = v_2\tau^2 \tag{J.9}$$

$$\sigma_\varphi^2 = 2.91k_o^2\int_0^L dz\ C_n^2(z)\ v^{5/3}(z)\tau^{5/3} = (\tau/\tau_o)^{5/3} \tag{J.10}$$

where the velocity moment is defined as

$$v_n = \int_0^L dz\ C_n^2(z)v^n(z) \tag{J.11}$$

The characteristic time is defined by

$$\tau_o^{-5/3} = 2.91k_o^2\int_0^L dz\ C_n^2(z)v^{5/3}(z) \tag{J.12}$$

41

2. THE EVALUATION OF MULTIPARAMETER INTEGRALS

2.1 INTRODUCTION

In Marichev's book[4] a powerful method for evaluating integrals is developed. His method applies to all integrals whose integrand is the product of two generalized hypergeometric functions. For that case, he shows that the integral, which can be transformed into a Mellin-Barnes integral, can be expressed as a finite sum of generalized hypergeometric functions which are equivalent to a Meijer's G-function. He briefly considers the case in which the integrand is the product of more than two functions and states that this area has not been developed. In this part of the report, his method is generalized to apply to the case in which the integrand is the product of N functions, and the final answer is expressed in terms of rapidly converging series — a form that is more useful for numerical evaluation on a personal computer.

The evaluation of an integral with N parameters is shown to be equivalent to the integration of a function composed of the ratio of Gamma functions in $N - 1$ complex planes. Methods of evaluating integrals with general functions in N complex planes are not available, but, because the complex variables appear only as sums, the integrals encountered using this method can be evaluated.

Marichev puts his integrals into a standard form in which the complex variables have unity coefficients, in which case, Slater's theorem applies, and the answer is a sum of generalized hypergeometric functions. Using this technique, one can show that the Strehl ratio for uncorrected turbulence can be written as the sum of six generalized hypergeometric functions, five of the form $_5F_{10}()$ and one $_6F_{11}()$. This form is not convenient for either obtaining physical insight or in evaluating the expressions on a personal computer. Here, the step of putting the integrand into the standard form is short circuited, since the answer will be obtained in the more convenient form of infinite series. For small values of the parameter, a power series is obtained, and for large values an asymptotic series is sometimes applicable. Each of

these series are obtained in a straightforward manner, and the method is amenable to algorithmic solutions.

The properties of Mellin transforms and Gamma functions that are useful in this analysis are given here. A short table of Mellin transforms used in the examples given from turbulence theory is included. Examples of evaluating integrals with one, two, and three parameters to obtain power and asymptotic series are given. Examples of the multiple pole case are also treated.

This technique is particularly well suited to evaluating the integrals obtained in considering wave propagation in turbulence since the kernel of the Mellin transform matches the Kolmogorov spectrum. The method is also applicable to any field in which this type of integral is encountered.

2.2 GAMMA FUNCTIONS

The integrals will be shown to be expressible as the ratio of Gamma functions; in order to perform the integration, several properties of Gamma functions are necessary. The relevant properties are reviewed in this section.

The definition of the Gamma function is

$$\Gamma(s) = \int_0^\infty dx \exp(-x) x^{s-1} = \sum_{n=0}^\infty \frac{(-1)^n}{n!} \frac{1}{s+n} + \int_1^\infty dx \exp(-x) x^{s-1}. \quad (2.2.1)$$

The argument s can be complex. The last integral on the right is an entire function and it is easy to see that the only singularities of the Gamma function are simple poles at the negative integers, $-n$, with residue $(-1)^n/n!$. The reciprocal of the Gamma function can be shown to be an entire function; therefore, the only singularities of the ratio of Gamma functions come from the numerator. Plots of the Gamma function and its reciprocal are shown in Figure 2-1.

For convenience the following notation introduced by Marichev is used

$$\Gamma\begin{bmatrix} \alpha_1, \dots, \alpha_m \\ \beta_1, \dots, \beta_n \end{bmatrix} = \frac{\Gamma(\alpha_1)\Gamma(\alpha_2) \dots \Gamma(\alpha_m)}{\Gamma(\beta_1)\Gamma(\beta_2) \dots \Gamma(\beta_n)}. \quad (2.2.2)$$

44
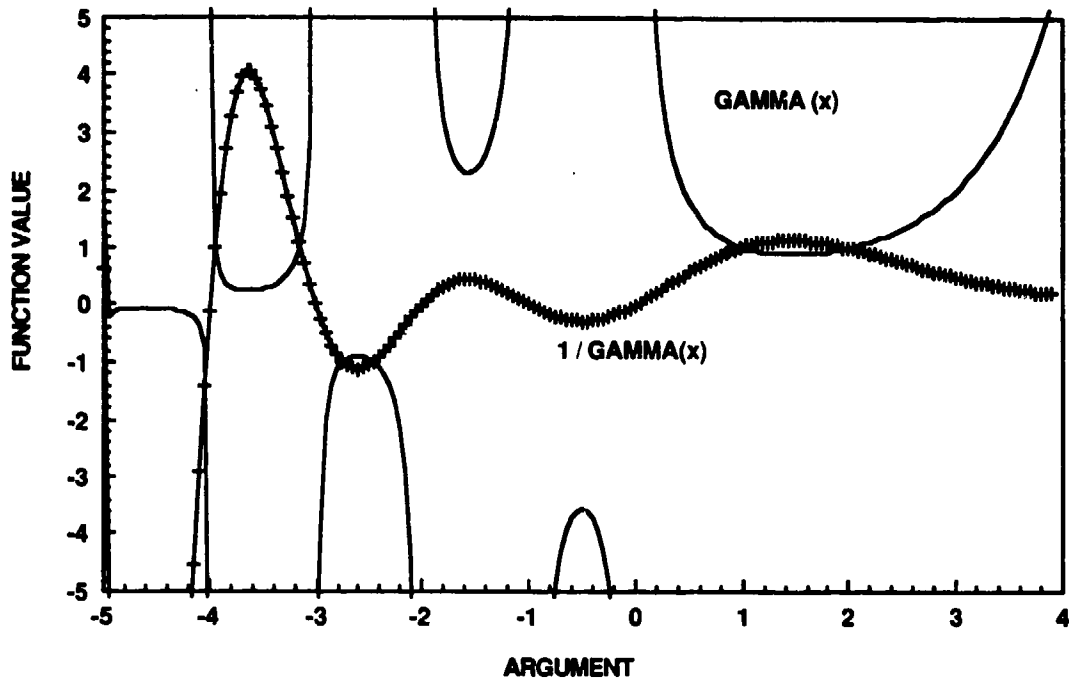
Figure 2-1. Plot of the Gamma function and its reciprocal.

From the duplication formula for Gamma functions, one finds

$$\frac{1}{\Gamma(s)} = \frac{\sin(\pi s)}{\pi} \Gamma(1 - s). \qquad (2.2.3)$$

Using integration by parts on the definition, one can show that

$$\Gamma(s + 1) = s\Gamma(s). \qquad (2.2.4)$$

For integer arguments, one finds $\Gamma(N + 1) = N\,!$. Some calculators can evaluate the factorial function at noninteger values. The above relation can be used on those calculators to evaluate the Gamma function.

Gamma functions with integer multipliers of s can be converted into Gamma functions with unity coefficients of s by the Gauss-Legendre multiplication formula

$$\Gamma(ms) = m^{ms - 1/2}(2\pi)^{(1 - ms)/2} \prod_{k=0}^{m-1} \Gamma(s + k / m). \qquad (2.2.5)$$

For large values of the argument, Stirling's formula gives the asymptotic series as

$$\Gamma(s) = \sqrt{2\pi}\ s^{s - 1/2} \exp(-s)\,[1 + s / 12 + s^2 / 288 + \dots \ |\ \arg\ s| < \pi. \qquad (2.2.6)$$

There is a branch cut along the negative real axis.

45

2.3 MELLIN TRANSFORMS AND SIMPLE INVERSE TRANSFORMS

Mellin transforms are particularly useful in problems dealing with wave propagation in turbulence. For simple problems in which the Kolmogorov spectrum is used, the kernel of the Mellin transform matches the turbulence spectrum, and the integrals can be evaluated by table lookup. For more complex problems, a convolution theorem is used to transform the integral into one in the complex plane. Because the Mellin transform of a function is the ratio of Gamma functions, this integration can be performed using the method of pole residue integration. If the path can be changed into a closed curve, the value of the integral as given by Cauchy's formula is just $2\pi i$ times the sum of the residues at the enclosed poles.

2.3.1 Mellin Transforms

The Mellin transform pair is given by

$$H(x) \rightarrow H^*(s) \equiv M(H(x)) \equiv \int_0^\infty dx\ H(x) x^{s-1}, \qquad (2.3.1)$$

and
$$H(x) = \frac{1}{2\pi i} \int ds\ H^*(s) x^{-s}. \qquad (2.3.2)$$

The path of integration in the inverse transform is determined by the convergence properties of the function being transformed. The Mellin transform of any function that can be expressed as a generalized hypergeometric function, a category that includes most of the common functions (algebraic, exponential, trigonometric, inverse trigonometric, hyperbolic, logarithmic, complete elliptic and sine and cosine integrals, error functions, Gegenbauer polynomials, Bessel and other orthogonal functions), is given as the ratio of Gamma functions. Marichev lists 1200 Mellin transforms. Oberhettinger[5] has an extensive list of Mellin transforms, but, they are not all expressed in the form of the ratio of Gamma functions as those in Marichev are. In Table F of part 1 are Mellin transforms of functions that are useful for problems dealing with wave propagation in turbulence. The values of s on the real axis for which the integral converges are also given in the table. The specification of the region of convergence is used when

choosing the path of integration in doing the inverse Mellin transform. The two-unit step functions in Equation (F.9) and (F.10) can be used to convert integrals with finite limits into ones with infinite limits that can be evaluated using the theory to be presented. The asterisk after one term in the Mellin transform of the sine squared is a notation that is adopted in this report to signify that the path of integration passes between the first and second poles of that Gamma function. In most cases, this notation is all that is necessary to define the path of integration in complicated problems in which there are an infinite number of poles on both sides of the path of integration. For simpler Mellin transforms, such as that of the Bessel function, the conditions for convergence must be stated explicitly. Table F can be augmented by using the following properties of Mellin transforms:

$$H(ax) \quad a > 0 \quad \rightarrow a^{-s} H^*(s), \tag{2.3.3}$$

$$x^a H(x) \qquad \rightarrow H^*(s + a), \tag{2.3.4}$$

$$H(x^p) \qquad \rightarrow H^*(s/p)/|p| \qquad p \neq 0. \tag{2.3.5}$$

From these relations, one can easily extend the Mellin transforms in the tables to new functions. For instance, the Mellin transform of a Gaussian function can be found from that of the exponential given in Equation (F.1) by using Equations (2.3.5) and (2.3.3) as

$$\exp(-x) \rightarrow \Gamma(s) \quad \therefore \exp\left(-[x/a]^2\right) \rightarrow 0.5 a^s \Gamma(s/2). \tag{2.3.6}$$

There is a parallel to the Fourier convolution integral, that is the Mellin convolution integral given by

$$H(x) = \int_0^\infty \frac{dt}{t} H_o(t) H_1\left[\frac{x}{t}\right] \rightarrow H^*(s) = H_o^*(s) H_1^*(s). \tag{2.3.7}$$

Notice the difference between this integral and the Fourier convolution integral. There is the term $1/t$, and the argument of the second function is the reciprocal of the variable. Obtaining the Mellin transform of a function in which the variable is the reciprocal of the usual variable as required above is trivially obtained by replacing s by $-s$ in the function's Mellin transform by

47

the use of Equation (2.3.5). The parameter in the problem is x. Notice that there are two functions and only one parameter. Each of the two functions could have had a separate parameter; however, a change of variables is used to eliminate one parameter from the integral. The second parameter only appears as a multiplication constant of the integral.

This relation can be generalized to obtain the Mellin transform of the product of $N + 1$ functions as

$$H\left(x_1 \ldots, x_N\right) = \int_0^\infty \frac{dt}{t} H_o(t) \prod_{j=1}^N H_j\left(\frac{x_j}{t}\right) \to H_o^*(s_1 + \ldots s_N) \prod_{j=1}^N H_j^*\left(s_j\right)$$

$$= H^*(s_1 \ldots, s_N) \cdot$$

$$(2.3.8)$$

In this form, the complex variables either appear alone or all summed together. The inverse transform is

$$H(x_1 \ldots, x_N) = \frac{1}{(2\pi i)^N} \int \ldots \int ds_1 \ldots ds_N \ H^*(s_1 + \ldots s_N) x_1^{-s_1} \ldots x_N^{-s_N}, \quad (2.3.9)$$

where the path of integration is determined by the conditions placed on the complex variables and the N parameters to obtain convergence of the Mellin transforms of the original functions.

In the single parameter case, to evaluate the integral in the complex plane, it will be shown that the path of integration can be closed at infinity in a clockwise or counterclockwise direction depending on the integrand. The value of the integral is the sum of the residues at the enclosed poles.

For many problems, one has to obtain the Mellin transform of a function minus the first term of its power series. It is easy to show that the Mellin transform is that of the original function, except the path of integration has moved over one pole. To illustrate this, consider the transform given in Equations (F.5) and (F.11) as

$$M(J_o(x) - 1) = \lim_{\varepsilon \to 0} \left[2^{s-1} \Gamma\left[\begin{matrix} s/2 \\ 1 - s/2 \end{matrix}\right] - \frac{1}{s + \varepsilon} + \frac{1}{s - \varepsilon}\right] \quad 0 < \text{Re } s < \varepsilon.$$

$$(2.3.10)$$

48

The path of integration and pole location are shown in Figure 2-2. The poles go to infinity in the left-half plane. The pole locations are slightly displaced from their true positions on the real axis for clarity.
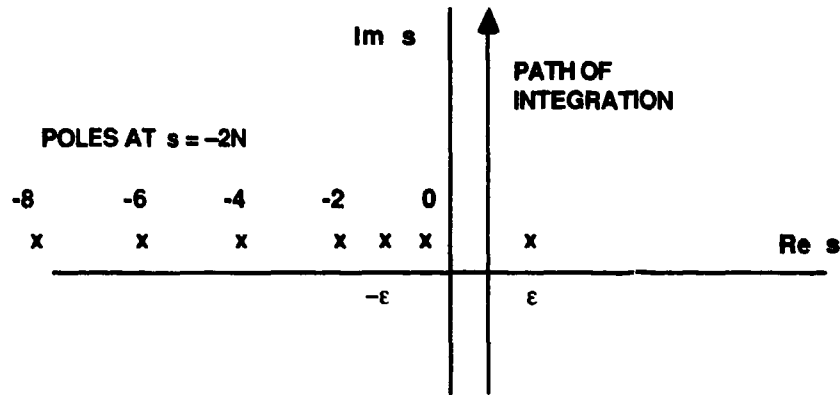
Figure 2-2. Pole location and path of integration for integral.

In the limit, the two poles at $s = 0$ and $s = -\epsilon$ cancel. The result is that the path of integration can now cross the real axis anywhere between the pole at $s = 0$ and at $s = -2$ without changing the value of the integral. Therefore, the Mellin transform is equal to

$$M (J_0(x) - 1) = 2^{s-1} \Gamma \begin{bmatrix} s/2^* \\ 1 - s/2 \end{bmatrix} \quad -2 < \text{Re } s < 0. \qquad (2.3.11)$$

where the notation of using an asterisk to signify that the path of integration passes between the first and second poles was used again. In this case, the conditions on Re s are redundant The movement of the path of integration past a pole is what is meant by the analytic continuation of the integral. It is obvious how to extend this result to that in which the first m terms of the power series are subtracted from the function. In that case, the path of integration moves past m poles of the original function.

2.3.2 Evaluation of the Integral with a Single Or One Parameter

If there is only a single parameter in the integral, a change of variables can be made to bring the parameter outside the integral. The integrand then does not contain any parameters and it can be evaluated by table lookup.

49

Many interesting turbulence problems fall into this category. After the angular integration, the integral in κ-space is evaluated by putting the integrand into a form that is evaluated by table lookup of the appropriate Mellin transform. This technique is used on all the single parameter problems of Section 3.5.

To illustrate this technique, consider the integral of a power of the radial coordinate times the modulation transfer function for a circular aperture. This integral is needed in the evaluation of many turbulence problems. This integral is given by

$$I(s) = \int_0^1 d\alpha \; \alpha^{s+1} K(\alpha) = \int_0^1 \alpha \, d\alpha \; \alpha^s \frac{16}{\pi} \left[\cos^{-1}(\alpha) - \alpha(1 - \alpha^2)^{1/2} \right]. \quad (2.3.12)$$

By using the unit step function, this can be put in the form of a Mellin transform

$$I(s) = \int_0^\infty d\alpha \frac{16}{\pi} \left[\alpha^{(s+2)-1} \cos^{-1}(\alpha) U(1 - \alpha) - \alpha^{(s+3)-1}(1 - \alpha^2)^{1/2} U(1 - \alpha) \right].$$

$$(2.3.13)$$

The Mellin transforms for the first function is given in Equation (F.12) with s replaced by $s + 2$. This changes the condition for convergence to Re $s > -2$. The Mellin transform of the second integral is in Equation (F.9) with s replaced by $s + 3$ and the use of Equation (2.3.5). The condition for convergence of that expression becomes Re $s > -3$. For convergence of the entire integral, the more restrictive condition on the first function must be used. Since $\Gamma(1/2) = \sqrt{\pi}$ the integral is equal to

$$I(s) = \frac{4}{\sqrt{\pi}} \left(\Gamma \begin{bmatrix} s/2 + \frac{3}{2}, -s/2 - 1 \\ s/2 + 2, -s/2 \end{bmatrix} - \Gamma \begin{bmatrix} s/2 + \frac{3}{2} \\ s/2 + 3 \end{bmatrix} \right) \qquad \text{Re } s > -2. \quad (2.3.14)$$

Using the property of the Gamma function given in Equation (2.2.4), this reduces to

$$I(s) = \frac{8}{\sqrt{\pi}} \frac{1}{2+s} \Gamma \begin{bmatrix} s/2 + \frac{3}{2} \\ s/2 + 3 \end{bmatrix} \qquad \text{Re } s > -2. \quad (2.3.15)$$

The single pole due to the denominator term can be expressed as the ratio of two Gamma functions; this will be done in the section on Strehl ratios.

2.4 INTEGRAL EVALUATION WITH TWO PARAMETERS

A power series is defined to be the Taylor series expansion of the function. Later, series solutions that are not Taylor series but asymptotic series will be considered. Methods of determining the value of the integral in terms of the series that converges most rapidly are developed in this section when the integrand contains two parameters. This generalization from the one parameter case allows one to evaluate more complicated problems. These problems can not be evaluated simply by table lookup. The integral is transformed into one in the complex plane and the methods of integrating in the complex plane are employed to evaluate it. The methods of doing this are developed in this section. A change of variables is made to factor out one parameter so that the remaining integral has only one parameter, x.

2.4.1 Power Series Solutions

To convert the integral into one in the complex plane, the Mellin convolution theorem is used. The resultant integral to be evaluated has an integrand that is the ratio of Gamma functions. The general form of the integral in the complex plane is a Mellin-Barnes integral given by

$$H(x) = \frac{1}{2\pi i} \int ds\, x^{-s}\ \frac{\displaystyle\prod_{i=1}^{A} \Gamma[a_i + \alpha_i s] \prod_{j-1}^{B} \Gamma[b_j - \beta_j s]}{\displaystyle\prod_{k=1}^{C} \Gamma[c_k + \gamma_k s] \prod_{m=1}^{D} \Gamma[d_m - \delta_m s]}. \tag{2.4.1}$$

The pole location and path of integration for a typical integral are shown in Figure 2-3. The path of integration can have all the poles of the Gamma function on one side of the path of integration or can split the poles of a Gamma function. In all the turbulence problems considered so far, the path of integration had all the poles or all the poles but the first on one side of the path of integration. The methods developed here are not sensitive to the pole locations.

51

PATH OF
INTEGRATION

s-PLANE

x   x   x   x   x   x | x

TYPICAL POLES OF A TERMS

x   x   x   x   x   x   x

x   x   x   x   x   x

TYPICAL POLES OF B TERMS

x   x   x   x   x   x
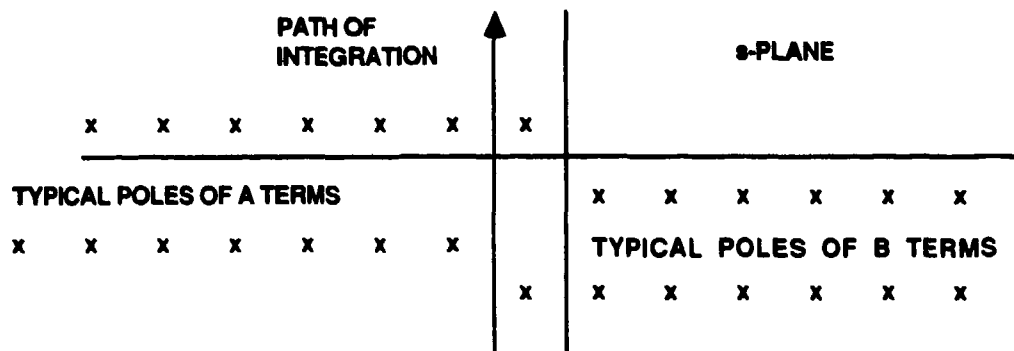
Figure 2-3. Typical path of integration and pole location for integral being considered.

The general solution to this integral can be expressed in terms of Fox's H function. If the coefficients of s are rational, then the solution can be expressed in terms of Meijer's G function. These facts are mentioned to allow the reader to look up properties of these functions if desired. We will develop all the properties of the solution that are necessary to evaluate the integral in terms of rapidly converging series, and knowledge of the properties of these functions is not necessary.

In this section, it is assumed that the poles are simple. No problems encountered so far in analyzing propagation in turbulent media have had multiple poles. Multiple poles can be treated as the limit of poles coalescing, and the results for the regular and asymptotic series are valid in this limit. The details of doing this are carried out in Appendix A.

Marichev considered the conditions on closing the path along the infinite semicircle for the case in which the coefficients of s were unity. He put them in that form in order to arrive at answers that could be expressed as the sum of generalized hypergeometric functions. One can obtain unity coefficients for the case in which all the coefficients of s are rational by making the substitution $s = ay$, where a is the least common denominator of the coefficients. This substitution makes all the coefficients of y integers, and, by using the Gauss-Legendre multiplication formula given in Equation (2.2.5), unity coefficient of y are obtained. The

52

number of Gamma functions is equal to the sum of the coefficients of y. Using that procedure, one arrives at final answers that are the sum of high order generalized hypergeometric functions. This form is not only lengthy to write down, but also, it provides little physical insight. Here, a different procedure will be used. The coefficients of s will be left as they are, and the final answer will be obtained as a rapidly converging series of the parameters. This method works even if the coefficients are irrational. Separate power series are obtained for large and small parameter values, while under certain conditions for large parameter values, an asymptotic series will be obtained.

Pole-residue integration is the method that is used to evaluate the integral. To apply this method, the path of integration must be closed in the complex plane and the value of the integral is the sum of the residues at the enclosed poles. The form of the answer that results is a series in terms of powers of the parameter. The answer can be expressed as

$$H(x) = \sum_n x^{-s_n} G(s_n) ,$$
(2.4.2)

where $G(s_n)$ is the value of the residue at the pole occurring at s_n. The summation is over all the poles enclosed in the path of integration.

In order to close the path on the infinite semicircle without affecting the value of the integral, the integrand must decrease faster than $1/s$ for large values of s. The conditions for convergence along the semicircle in the left-half plane will now be obtained. Make the following definitions

$$\Xi' = A + D - B - C .$$
(2.4.3)

$$\Xi = A + B - C - D .$$
(2.4.4)

$$\Delta = \sum_{i=1}^{A} \alpha_i + \sum_{m=1}^{D} \delta_m - \sum_{j=1}^{B} \beta_j - \sum_{k=1}^{C} \gamma_k .$$
(2.4.5)

$$\Delta' = \sum_{i=1}^{A} \alpha_i \ln(\alpha_i) + \sum_{m=1}^{D} \delta_m \ln(\delta_m) - \sum_{j=1}^{B} \beta_j \ln(\beta_j) - \sum_{k=1}^{C} \gamma_k \ln(\gamma_k) .$$
(2.4.6)

53

$$V = \sum_{i=1}^{A} a_i + \sum_{j=1}^{B} b_j - \sum_{k=1}^{C} c_k - \sum_{m=1}^{D} d_m . \tag{2.4.7}$$

$$A' = \sum_{i=1}^{A} \alpha_i ; \quad B' = \sum_{j=1}^{B} \beta_j ; \quad C' = \sum_{k=1}^{C} \gamma_k ; \text{ and } D' = \sum_{m=1}^{D} \delta_m . $$

$$\tag{2.4.8)-(2.4.11}$$

To determine whether the path of integration can be closed in the left-half plane, the asymptotic behavior of the integrand must be examined in that region. Stirling's formula is not valid when the argument of the Gamma function goes to negative infinity on the real axis. To obtain a valid expression, the duplication formula given in Equation (2.2.3) can be used to eliminate the Gamma functions with positive coefficients for s and put the integrand into the following form

$$I = z^{-s} \pi^{A-C} \frac{\displaystyle\prod_{j=1}^{B} \Gamma[b_j - \beta_j s] \prod_{k=1}^{C} \Gamma[1 - c_k - \gamma_k] s \, \sin[(c_k + \gamma_k s)\pi]}{\displaystyle\prod_{m=1}^{D} \Gamma[d_m - \delta_m s] \prod_{i=1}^{A} \Gamma[1 - a_i - \alpha_i s] \, \sin[(a_i + \alpha_i s)\pi]} . $$

$$\tag{2.4.12}$$

The parameter x is real; however, in the development that follows, this will be generalized to allow complex values, and x is replaced by z. All the other constants are assumed to be real and non-negative. Only the behavior with respect to s is of interest in determining convergence. The symbol O will be used to denote the order of magnitude of the quantity. To examine the behavior at negative infinity, the following two relations are necessary

$$\lim_{s \to \infty} \sin[(a + \alpha s) \pi] = O[\exp\{\alpha \pi \mathrm{Im}(s)\}], \tag{2.4.13}$$

and

$$\lim_{s \to \infty} \Gamma(s) = O[\exp\{(s - 1/2)\ln(s) - s\}]. \tag{2.4.14}$$

Using these relations in the integrand and using the previous definitions after the terms are rearranged, the integrand can be shown to be of the order of

$$
\begin{aligned}
I = O[\exp\{- &\operatorname{Re}(s)\ln|z| + \operatorname{Im}(s)\arg(z) \\
&+ [\operatorname{Im}(s)\arg(-s) + \operatorname{Re}(s)]\Delta\ln|s| + \operatorname{Re}(s)[\Delta - \Delta'] \\
&+ \ln|s|[v - \Xi'/2 + C - A] + |\operatorname{Im}(s)|[\Xi \arg(-s) + \pi(C' - A')]\}]. \quad (2.4.15)
\end{aligned}
$$

There is a hierarchy of terms that determine the convergence properties at infinity. The terms in decreasing order of importance are $\operatorname{Re}(s) \ln|s|$, $\operatorname{Re}(s)$, and $\ln|s|$.

The dominant term in determining convergence on the real axis is the one with $\Delta\operatorname{Re}(s)\ln|s|$. If $\Delta > 0$, the integral can be closed in the left-half plane. A similar analysis can be performed to see when the integral can be closed in the right-half plane. Doing that analysis results in the requirement that $\Delta < 0$. For both these cases, a single power series is obtained, and it converges quickly for small values of the parameter. For large values, the series converges slowly, and there can be numerical difficulties in calculating the sum that contains terms with large values that alternate in sign. In this parameter regime, an asymptotic series is appropriate, and the method to derive this series is discussed in the next subsection.

If $\Delta = 0$, the term with $\operatorname{Re}(s)[-\ln|z| - \Delta']$ is the most important. Let

$$
\Pi = -\ln|z| - \Delta'. \quad (2.4.16)
$$

For $\Pi < 0$, the path can be closed in the right-half plane. For $\Pi > 0$, the path can be closed in the left-half plane. Typically, if $\Delta = 0$ then also $\Delta' = 0$, and in that case, for $|z| > 1$, the path can be closed in the right-half plane, while for $|z| < 1$, the path can be closed in the left-half plane. Here, separate power series for large and small values of z are obtained and both converge rapidly.

If $\Delta = 0$ and $z = 1$, the integrand behaves as

$$
I = O\{s^{(v + C - A - \Xi'/2)}\}. \quad (2.4.17)
$$

For convergence on the infinite semicircle, the integrand has to decrease faster than s^{-1} and this gives the condition

$$
\Omega = v + C - A - \Xi'/2 + 1 < 0. \quad (2.4.18)
$$

55

If this condition is satisfied, the path of integration can be closed in either direction. If this condition is not satisfied then the path cannot be closed at infinity and pole-residue integration cannot be used.

2.4.2 Asymptotic Series

For large values of the parameter, when $\Delta \neq 0$, an asymptotic series is appropriate. Asymptotic series can be found for complex values of z; however, these are more complicated than those for real values of z that are represented by x. Since real values only occur in all the problems that have been encountered in turbulence, that is the only case that is considered here. The asymptotic series is found by moving the path of integration into the right-half plane. By Cauchy's residue theorem, the value of the original integral is equal to the integration along the new path plus the residue at any poles that were crossed in moving the path of integration into the right-half plane. The integral along the new path of integration is found by the method of steepest descent. In this method, the path is deformed from the original path to a path through a saddle point and in the direction that decreases most rapidly away from the saddle point. Along this new path, the value of the integrand is a maximum at the saddle point and decreases very rapidly away from it. Therefore, the value of the integrand is just due to a small section about the saddle point that can be evaluated with a power series approximation for the integrand about that point. To review this method, which is described in detail in many places[6] consider the following integral

$$I = \int_{-i\infty}^{i\infty} ds \; g(s)\exp[f(s)].$$
(2.4.19)

Express

$$f(s) = f(s_o) + f'(s_o)(s - s_o) + \frac{f''(s_o)}{2}(s - s_o)^2 + \dots.$$
(2.4.20)

It is assumed that there is a parameter that is very large so that only these terms are necessary to express the value of the integral with sufficient accuracy. In the problem discussed here it will

be seen that the parameter that causes the power series to converge slowly serves the function of the large parameter. At a saddle point, the value of the first derivative is zero. This gives equations to determine the real and imaginary parts of s_o at the saddle point. The integral along this path is that of a Gaussian function with infinite limits that is easily evaluated to give

$$I = \int_{-i\infty}^{i\infty} ds \; g(s_o) \exp\left[f(s_o) + \frac{f''(s_o)}{2}(s - s_o)^2 \right] \approx \sqrt{\frac{2\pi}{f''(s_o)}} \; g(s_o) \exp\left[f(s_o) \right].$$

(2.4.21)

This is the first term of the asymptotic expansion. Additional terms can be found if desired. For typical problems, the first term of the asymptotic series is sufficient, since it is generally found that contributions due to the poles that are crossed in moving the path of integration to the saddle point have a much larger contribution.

The asymptotic value of the integral has contributions due to poles to the right of the path of integration plus the steepest descent contribution. Under certain conditions, one of these two terms dominates the result and the other can be neglected. If there are no poles to the right of the path of integration, the steepest descent contribution must always be included. The contribution at poles decays algebraically (power of x). We will find that the behavior of the steepest descent contribution can vary sinusoidally, can have exponential decay or exponential increase with x. For the sinusoidal variation, both the pole contributions and the steepest descent contribution are important, and both must be retained. When the steepest descent contribution decays exponentially, it can be neglected if there are any pole contributions. If the steepest descent contribution increases exponentially, the pole contributions are negligible. Conditions on the coefficients that result in these various cases will be considered.

To find the asymptotic value of the integral that is being considered, make the following additional definitions

$$A = [D' - B'],$$

(2.4.22)

57

$$B'' = \sum_{j=1}^{B} b_j \, , \qquad\qquad (2.4.23)$$

$$D'' = \sum_{m=1}^{D} d_m \, , \qquad\qquad (2.4.24)$$

$$\rho = [\, v + (1 - \Xi) / 2 \,] / \Delta, \qquad\qquad (2.4.25)$$

$$\Delta'' = \sum_{i=1}^{A} a_i \ln \alpha_i + \sum_{j=1}^{B} b_j \ln \beta_j - \sum_{k=1}^{C} c_k \ln \gamma_k - \sum_{m=1}^{D} d_m \ln \delta_m \, ,$$
$$\qquad\qquad (2.4.26)$$

$$\Delta''' = \sum_{i=1}^{A} \ln \alpha_i + \sum_{j=1}^{B} \ln \beta_j - \sum_{k=1}^{C} \ln \gamma_k - \sum_{m=1}^{D} \ln \delta_m \, . \qquad (2.4.27)$$

The case $\Delta > 0$ is considered in this section. In that case, the path of integration can be closed in the left-half plane. If $\Delta < 0$, the substitution $s \rightarrow -s$ can be made in the integrand which changes signs so that now $\Delta > 0$, and the results that are derived below will apply.

For the asymptotic series, the behavior of the integrand in the right-half plane must be examined. As a simple case, the asymptotic series for $B = D = 0$ in Equation (2.4.1) with simple poles will be derived first. For this case, there is no branch cut in the right-half plane and the evaluation of the asymptotic series is straightforward. The behavior of the integrand for large s must be found. Unlike the order of magnitude calculation previously made to determine whether the integral converges on an infinite circle, a more exact value of the functions is required. The asymptotic expansion of a Gamma function is

$$\Gamma[\, a_i + \alpha_i s \,] = \sqrt{2\pi} \, \exp\left[(\, a_i + \alpha_i s - 1/2) \ln (\, a_i + \alpha_i s) - a_i - \alpha_i s \,\right] .$$
$$\qquad\qquad (2.4.28)$$

The following expansion is used

$$\ln (\, a_i + \alpha_i s) = \ln (\, \alpha_i s [1 + a_i / \alpha_i s]) \approx \ln (\, \alpha_i) + \ln (s) + a_i / \alpha_i s. \quad (2.4.29)$$

58

If this is inserted into the Equation (2.4.12) and a similar expansion is performed for the other Gamma functions in the integrand, one obtains

$$I = \frac{(2\pi)^{\Xi/2}}{2\pi i}\int ds$$
$$\times \exp\left[\,\Delta' - \Delta'''/2 + s[\,\Delta' - \Delta - \ln(x)] + \ln(s)(v - \Xi/2) + \Delta s\ln(s)\right]. \quad (2.4.30)$$

If the exponent is designated by $f(s)$, the requirement of having the derivative of the exponent equal to 0 to find the saddle point yields

$$\frac{df(s)}{ds} = 0 = [\,\Delta' - \Delta - \ln(x)] + \frac{v - \Xi/2}{s} + \Delta[1 + \ln(s)]. \quad (2.4.31)$$

Since s is large, the solution can be approximated by

$$\ln(s_o) = -\frac{1}{\Delta}[\,\Delta' - \ln(x)], \quad (2.4.32)$$

and $\qquad\qquad s_o = x^{1/\Delta}\exp[-\Delta'/\Delta]. \quad (2.4.33)$

The value of s_0 is large since x is large which agrees with the assumption that the path of integration was moved far into the right-half plane.

The second derivative is

$$\frac{d^2f(s)}{ds^2} = -\frac{v - \Xi/2}{s^2} + \frac{\Delta}{s} \approx \frac{\Delta}{s}. \quad (2.4.34)$$

Each higher order derivative has an increasingly higher value of power of s in the denominator. Therefore, the higher order derivatives are small compared to the second, and the assumption that the function can be expressed as a constant term plus a quadratic term is valid. If these values are substituted into Equation (2.4.21), one obtains for the asymptotic series

$$I(x) = \frac{(2\pi)^{(\Xi-1)/2}}{\sqrt{\Delta}}x^\rho\exp\left[-\Delta x^{1/\Delta}\exp(-\Delta'/\Delta) + \Delta'' - \Delta'''/2 - \rho\Delta'\right]. \quad (2.4.35)$$

For most problems encountered $\Delta' = \Delta'' = \Delta''' = 0$, then the expression used by Marichev is obtained which is

$$I(x) = \frac{(2\pi)^{(\Xi-1)/2}}{\sqrt{\Delta}}x^\rho\exp\left[-\Delta x^{1/\Delta}\right]. \quad (2.4.36)$$

59

This solution has an exponential decay.

The more general case with B and D not equal to zero in Equation (2.4.1) will now be considered. Since the arguments of the Gamma function are negative for the Gamma functions with B and D there is a branch cut along the positive real axis for these functions. The path of integration is now split into 2 parts, one along the upper half plane and one along the lower half plane. Since x is real, because of the symmetry of the integrand, the value of the integral is twice the real part of the upper integration. In the upper half plane, the negative of the function is obtained by rotating 180 degrees in the positive angular direction, so that

$$-s = |s| \exp(i\pi).$$ (2.4.37)

For large s, the Gamma function with negative argument can be written as

$$\Gamma(b - \beta s) = \sqrt{2\pi} \exp[(b - \beta s - 1/2)i\pi + (b - \beta s - 1/2)\ln(\beta)$$
$$+ \beta s + \ln|s|(b - \beta s - 1/2)].$$ (2.4.38)

Insert this expression and similar ones for the other Gamma functions with negative arguments and the expressions in Equations (2.4.28) and (2.4.29) for those with positive arguments into the integrand. Combine terms using the definitions given above, one finds that the value of the integral is

$$I = 2\,\mathrm{Re}\,\frac{(2\pi)^{\Xi/2}}{2\pi} \int_0^{i\infty} ds \exp\{s[-\Delta + \Delta' - \ln(x)] + \Delta s \ln(s) + \ln(s)[v - \Xi/2]$$
$$+ \Delta'' - \Delta'''/2 + i\pi[B'' - D'' + (D - B)/2 + s(D' - B')]\}.$$

(2.4.39)

To find the saddle point, again set the derivative of the exponent equal to 0. Neglecting terms that are small because s is large, one obtains for the position of the saddle point the value

$$\ln(s_o) = [\ln(x) - \Delta' - i\pi\Delta]/\Delta,$$ (2.4.40)

and

$$s_o = x^{1/\Delta} \exp[-\Delta'/\Delta] \exp[-i\pi\Delta/\Delta].$$ (2.4.41)

The value of the second derivative is the same as that given in Equation (2.4.34). If these expressions are inserted into the expression for the value of the steepest descent integral given

in Equation (2.4.21), there are terms that cancel and others that can be combined using the above definitions. If the steepest descent contribution is designated by $E(x)$ for this more general case to conform to Marichev's notation, one obtains

$$E(x) = \frac{2(2\pi)^{(\Xi-1)/2}}{\sqrt{\Delta}} \text{Re exp}\{\rho[\ln(x) - \Delta' - i\pi\Lambda]$$

$$- \Delta x^{1/\Delta} \exp[-\Delta'/\Delta]\exp[-i\pi\Lambda/\Delta] + \Delta'' - \Delta''' / 2 + i\pi[B'' - D'' + (B - D)/2]\}.$$

(2.4.42)

Using the fact that for real a and b one has

$$\text{Re exp}[a + ib] = \exp(a)\cos(b),$$ (2.4.43)

one obtains

$$E(x) = \frac{2(2\pi)^{(\Xi-1)/2}}{\sqrt{\Delta}}$$

$$\times x^\rho \exp\{-\rho\Delta' - \Delta x^{1/\Delta}\exp[-\Delta'/\Delta]\cos[\pi\Lambda/\Delta] + \Delta'' - \Delta'''/2\}$$

$$\times \cos\{\Delta x^{1/\Delta}\exp[-\Delta'/\Delta]\sin[\pi\Lambda/\Delta] + \pi[-\rho\Lambda + B'' - D'' - (B - D)/2]\}. \quad (2.4.44)$$

For the case

$$\Delta' = \Delta'' = \Delta''' = 0, \quad B = B', \quad D = D', \quad (2.4.45)$$

one obtains a result that can be shown to be equal to that obtained by Marichev

$$E(x) = \frac{2(2\pi)^{(\Xi-1)/2}}{\sqrt{\Delta}} x^\rho \exp\{-\Delta x^{1/\Delta}\cos[\pi\Lambda/\Delta]\}$$

$$\times \cos\{\Delta x^{1/\Delta}\sin[\pi\Lambda/\Delta] + \pi[(1/2 - \rho)\Lambda + B'' - D'']\}. \quad (2.4.46)$$

For the asymptotic series, the residues of all the poles on the right side of the path of integration that will be called $W(x)$ are needed. The general solution is

$$H(x) = W(x) + E(x). \quad (2.4.47)$$

The above equation is all that is needed in general to get the solution. In some cases, one of the terms is insignificant compared to the other and that will be obvious once the terms are evaluated. Marichev shows that conditions can be written down so that one term or the other is

61

the only significant one. Care must be exercised in using his conditions since he does not allow the path of integration to separate poles of a Gamma function. If the conditions in Equation (2.4.45) hold, then one of Marichev's conditions does hold and that is

Condition 1: For $\Xi > 0$, $B' \geq 1$, then $H(x) = W(x)$. (2.4.48)

The $E(x)$ term has exponential decay, as one can easily determine from Equation (2.4.46), and can be neglected.

Asymptotic series have certain properties that are useful. The asymptotic series that have been derived are all of the Poincairé type[7] which implies the following properties:

(1) the error in truncation is less than the first term neglected,

(2) the asymptotic series of the sum or difference of two functions is equal to the sum or difference of the asymptotic series of the individual functions,

(3) the asymptotic series of the integral or derivative of a function is equal to the integral or derivative of the asymptotic series of that function, and

(4) the asymptotic series is unique for a given function.

In the above derivations, it was assumed that $\Delta > 0$. If $\Delta < 0$, change s to $-s$ in the integral and then the sign changes so that $\Delta > 0$, and the above results apply.

$I(x)$ and $E(x)$ are the first terms of the series representation of the asymptotic series. Generally, for most problems this answer is accurate enough. If more terms of the series are required they can be obtained by using the approach in Luke[8]. This approach is very complicated and different expressions apply for different conditions on the parameters. The details of this approach will not be given here; however, the results of using it to calculate additional terms of the asymptotic series will be discussed in the next section.

Asymptotic series and steepest descent contributions can be found in the case where the integration is in several complex planes. For two complex planes, formulas in Born and Wolfe in the section on asymptotic series are useful as a starting point. There are two conditions to look at for the two complex plane case. In the first, one parameter is large while the other is small; in the second both parameters are large. Extending the analysis given above to these two

cases does not pose any conceptual problems. The answers obtained have the correct behavior if one parameter is negligible. Since none of the problems considered in this report needs this type of analysis, it is not given here.

2.4.3 Example and Accuracy of the Asymptotic Series

Consider the Mellin transform of the Bessel function minus unity that was found in Equation (2.3.11) as

$$M(J_o(x) - 1) = 2^{s-1} \Gamma \begin{bmatrix} s/2^* \\ 1 - s/2 \end{bmatrix} \quad -2 < \mathrm{Re}\ s < 0. \qquad (2.4.49)$$

The inverse transform is given in general in Equation (2.3.1). If the above relation is substituted into that relation, and s is changed to $2s$, the function becomes

$$J_o(x) - 1 = \frac{1}{2\pi i} \int ds\, (x/2)^{-2s} \frac{\Gamma[s^*]}{\Gamma[1-s]}. \qquad (2.4.50)$$

The value of $\Delta = 2$, which requires the path of integration to be closed in the left-half plane. There are poles at $s = -n$, for $n = 1, 2, \ldots$. Remember, the reason that $n = 0$ is not included is because of the $*$ symbol, which means that the path of integration passes between the first and second poles of the function. Evaluating the function at these poles, one obtains

$$J_o(x) - 1 = \sum_{n=1}^{\infty} \frac{(-1)^n}{[n!]^2} \left[\frac{x}{2}\right]^{2n}. \qquad (2.4.51)$$

This is just the power series of the Bessel function with the first term removed. This is what is expected, since the first term is unity and it is subtracted away by the second term on the left.

The asymptotic series has the contribution of the one pole to the right of the path of integration and the steepest descent path, which is given by the term $E(x)$. This is equal to

$$J_o(x) - 1 \approx \sqrt{\frac{2}{\pi x}} \cos[x - \pi/4] - 1. \qquad (2.4.52)$$

An asymptotic series with more terms can be found using Equations (4.11.4-4), (7.4.6-3), and (7.4.2-8) of Luke to give

$$J_o(x) - 1 \approx \sqrt{\frac{2}{\pi x}} \exp\left[-\frac{1}{16 x^2}\right] \cos\left[x - \frac{1}{8x} - \frac{25}{368 x^2} - \pi/4\right] - 1. \qquad (2.4.53)$$

The two asymptotic series are compared to the actual value of the function in Figure 2-4 and the difference between the.e approximations and the exact value is plotted in Figure 2-5. The exact value of the function is covered up by the power and asymptotic series because there is a region of overlap in which either series is a good approximation. As one can see, the simple asymptotic series in combination with five terms of the power series gives the value of the Bessel function with an accuracy of better than 1%. This is adequate for most problems. If ten terms of the power series are used in conjunction with the more accurate asymptotic series, the maximum error in representing the Bessel function is 0.01%.

2.4.4 Obtaining Asymptotic Series from Power Series

Sometimes the power series solution is known, but the parameter in the summation may be large. In that case, the power series converges slowly, and there can be numerical problems in summing large terms that alternate in sign In that case, the asymptotic series representation of the power series is wanted. The techniques that have been developed can be used to find the
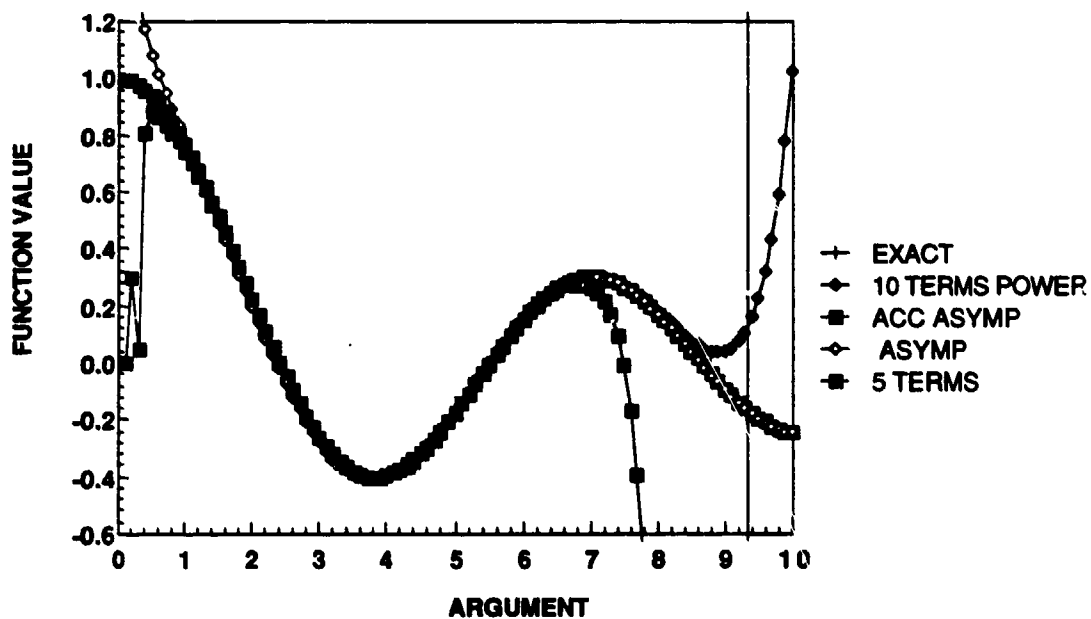
Figure 2-4. Comparison of the values of $J_0(x)$ obtained from various approximations.
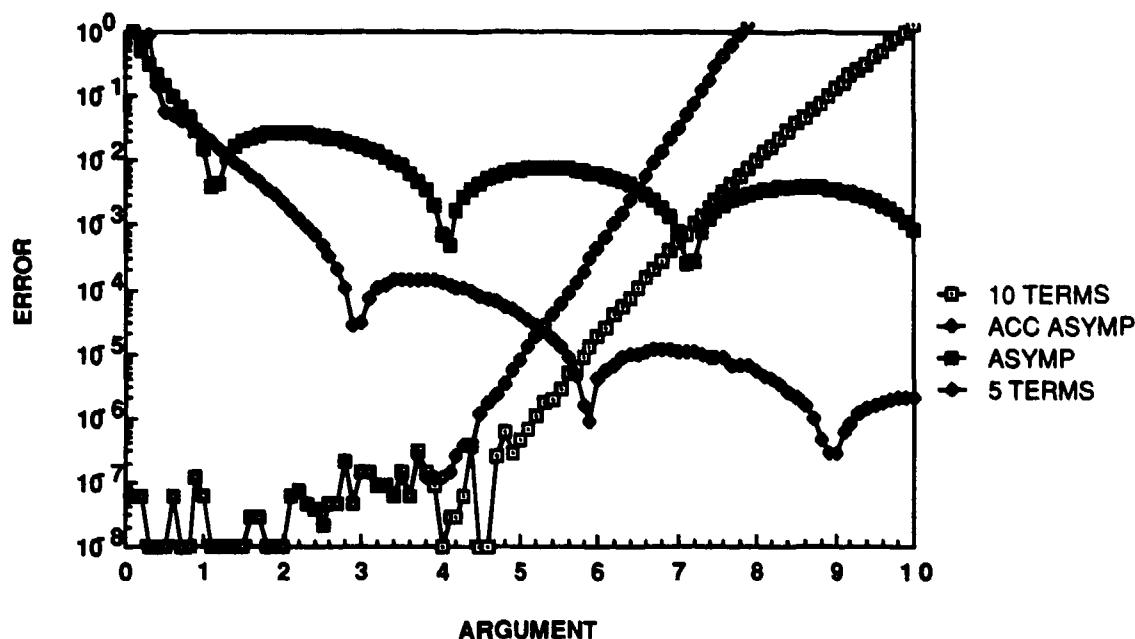
Figure 2-5. Comparison of the errors in the values of $J_0(x)$ obtained from various approximations.

asymptotic series. When the summation has coefficients that can be represented by Gamma functions in the numerator and denominator, then it can easily be represented by a Mellin-Barnes integral in the complex plane. Once this integral is obtained, an asymptotic series can be easily found using the techniques developed above.

To illustrate this technique, the double integral of an incomplete Gamma function will be considered. The power series of the incomplete Gamma function is

$$\gamma(a, x) = \sum_{n=0}^{\infty} \frac{(-1)^n}{n!} \frac{x^{a+n}}{n!(a+n)} . \qquad (2.4.54)$$

Suppose the following integral is wanted

$$P(a, x) = \int_0^x dw \int_0^w dy \, \gamma(a, y) = x^{a+2} \sum_{n=0}^{\infty} \frac{(-1)^n}{n!} \frac{x^n}{(a+n)(a+n+1)(a+n+2)} . \qquad (2.4.55)$$

65

The power series was integrated term by term, a method that is allowed as long as the resulting series converges, which it does.

For large values of x, this infinite series converges slowly and there are numerical problems in evaluating the sum of large terms that alternate in sign. It is desirable to write the asymptotic series for this function. It is not difficult to see that by using the recursion relation for Gamma functions given in Equation (2.2.4) this can be represented as

$$P(a, x) = x^{a+2} \sum_{n=0}^{\infty} \frac{(-1)^n}{n!} \frac{\Gamma[a + n] x^n}{\Gamma[a + 3 + n]} = \frac{x^{a+2}}{2\pi i} \int ds \; x^{-s} \Gamma \begin{bmatrix} s, \; a - s \\ a + 3 - s \end{bmatrix}. \quad (2.4.56)$$

The path of integration passes between the poles of the first Gamma function and the three poles of the second Gamma function that are not canceled out by the Gamma function in the denominator. Since $\Delta = 1$, the path of integration should be closed in the left-half plane and one obtains the summation given in Equation (2.4.55). To obtain the asymptotic series, since Condition 1 given in Equation (2.4.48) applies, one has only to sum the contribution of the three poles to the right of the path of integration to give

$$I \approx \frac{\Gamma(a)x^2}{2} \left[1 - \frac{2a}{x} + \frac{(a + 1)a}{x^2} \right]. \quad (2.4.57)$$

2.5 INTEGRAL EVALUATION WITH THREE OR MORE PARAMETERS

In this section, the method of evaluating integrals with three or more parameters will be illustrated by working through several examples. The method presented here is based on heuristic extensions of known techniques of integrating in several complex planes. The cases considered here in which the pole locations are functions of the sum of the complex variables have not been investigated to my knowledge. The case in which the pole locations are separable into the product of terms that only depend on one complex variable has been studied and is available in standard texts in the field.[9] For that simple case, each complex integration can be considered separately in the standard manner. The case encountered in this report is not nearly so straightforward. An example of the technique of evaluating an integral in two complex planes is discussed using the analysis in the literature. Then it is looked at a second

66

time in a slightly different way, and shown to give the same answer. This second approach is generalizable to our problem.

2.5.1 Method Of Integration

Consider the integral

$$I = \frac{1}{(2\pi i)^2} \iint ds \ dt \ \frac{F(s, t)}{st(s - a)(t + b)} \ , \qquad (2.5.1)$$

where s and t are complex variables, and a and b are positive.

The function $F(s, t)$ is assumed to have no singularities in the two complex planes s and t. Both integrations go from $-i\infty$ to $+i\infty$, and the real parts along the path are negative. Notice that the poles are only functions of a single complex variable. It has been shown in the literature that the integrals can be treated separately so that this integral can be written as

$$I = \frac{1}{(2\pi i)^2} \int \frac{ds}{(s - a)s} \int dt \ \frac{F(s, t)}{t(t + b)} \ . \qquad (2.5.2)$$

Suppose the integrand is such that the path can be closed in the right half t-plane without changing the value of the integration, then the residue at the pole at $t = 0$ is the only contribution. The remaining integral is

$$I = \frac{1}{(2\pi i)} \int ds \ \frac{F(s, 0)}{s(s - a)b} \ . \qquad (2.5.3)$$

If the path of integration can be closed in the right-half plane in doing the s integration, one obtains the contributions at the two poles at $s = 0$ and a to obtain for the value of the integral

$$I = \frac{F(a, 0)}{ab} - \frac{F(0, 0)}{ab} \ . \qquad (2.5.4)$$

Looked at a little more abstractly in the 4-space of the two complex variables, each of the poles occurs at a value for one of the complex variables. The value of the other complex variable can be anything; therefore, the locus of a single pole in 4-space is a two-dimensional sheet of points. If there were only a single pole in the integrand and it was in the first complex variable, then the second integration would be zero. There must be at least two poles in the integrand to get a contribution. Since each of these poles corresponds to a sheet of poles in

67

4-space, what one is finding is the intersection of the two sheets of points in 4-space which gives a single point if the two sheets intersect at an angle. It is easy to convince yourself that the intersection is a point since there are four parameters to describe a point in 4-space and the condition to have a single pole gives two equations. Therefore, the simultaneous occurrence of two poles gives four equations to find the four quantities that describe a point in 4-space.

With this insight, the problem can be tackled in a second way that can be generalized by finding all the singular points in 4-space that are described by the simultaneous occurrence of two poles. The properties of the integrand are used to decide which way the path can be closed to determine which of these singular 4-space points contribute to the integrand. The three possible double poles of the integral in Equation (2.5.1) are

$$
\begin{aligned}
&(1) \ s = 0, t = 0, \\
&(2) \ s = 0, t = -b, \\
&(3) \ t = 0, s = a.
\end{aligned}
\tag{2.5.5}
$$

The three points above will be called 4-space singular points or 2-poles for short.

From the conditions of closure that were stated above, the values of s and t must be greater than or equal to zero; therefore, only the 2-poles 1 and 3 contribute to the integral. If the double integral is evaluated at these poles, the previous answer is obtained. This same procedure can be used when the poles are linear combinations of the two complex variables. Consider the integral

$$
I = \frac{1}{(2\pi i)^2} \iint ds \ dt \ \frac{F(s, t)}{st(s + t - a)(t + b)}.
\tag{2.5.6}
$$

The pole that contains the sum of the two complex variables has poles in a sheet in 4-space also and will intersect the other planes. The sets of 2-poles for this integral are

$$
\begin{aligned}
&(1) \ s = 0, t = 0, \\
&(2) \ s = 0, t = -b, \\
&(3) \ s = 0, s + t - a = 0 \rightarrow s = 0, t = a, \\
&(4) \ t = 0, s + t - a = 0 \rightarrow t = 0, s = a.
\end{aligned}
\tag{2.5.7}
$$

68

The conditions on s and t that require both of their real parts to be equal to or greater than zero give valid contributions from the 2-poles 1, 3, and 4, so that the integral is equal to

$$I = \frac{F(a, 0)}{ab} - \frac{F(0, 0)}{ab} + \frac{F(0, -b)}{ab}. \tag{2.5.8}$$

The generalization of this technique to a higher number of complex planes is obvious. For instance, for three complex planes, one would have to find all combinations of three simultaneous poles to find the 3-poles in 6-space. The path of integration was closed based on the integrand. As we saw before, sometimes the integrand must be closed in the opposite manner in order to get a rapidly converging asymptotic series. In finding asymptotic series, sometimes there is an extra term $E(x)$. How to find that term in this problem is discussed at the end of Section 2.4.2. Typically, for problems of interest when the path of integration is closed in the wrong direction, one encloses poles whose contribution overwhelm the $E(x)$ term that is then neglected.

2.5.2 Two Complex Plane Example

Several examples are now worked out to illustrate the method on known problems. The first example considered is the integral of a product of exponentials that is easily evaluated by normal methods. This example is used to illustrate how to evaluate integrals in two and three complex planes. A more complicated known integral containing the product of two Bessel functions and a sinusoid is also evaluated after this. Consider

$$I = \int_0^\infty \prod_{i=1}^N e^{-a_i u} \, du. \tag{2.5.9}$$

For the sum of the a's greater than zero, this is easily integrated to give

$$I = \left[\sum_{i=1}^N a_i \right]^{-1}. \tag{2.5.10}$$

This integral can be converted into the form in which the generalized Mellin convolution theorem can be applied by making the following changes of variables

$$a_1 = x, \tag{2.5.11}$$

69

$$a_2 u = x / y \rightarrow y = q_1 / a_2, \qquad (2.5.12)$$

$$a_3 u = x / z \rightarrow z = q_1 / a_2. \qquad (2.5.13)$$

Then

$$I = \frac{1}{a_1} \int_0^\infty x \; e^{-x} e^{-x/y} e^{-x/z} \frac{dx}{x}. \qquad (2.5.14)$$

Using the Mellin convolution theorem given in Equations (1.7) to (1.8), one obtains

$$I = \frac{1}{a_1 (2\pi i)^2} \iint ds \; dt \; \Gamma[s + t + 1, - s, - t] \left(\frac{a_1}{a_2}\right)^{-s} \left(\frac{a_1}{a_3}\right)^{-t}. \qquad (2.5.15)$$

This example is more complicated than the last because of the presence of Gamma functions. Each Gamma function has poles at all negative integers, and each pole is a sheet in 4-space. One has to determine the intersection of all these sheets with those of the other poles, however; aside from the proliferation of poles, the problem is analyzed in exactly the same manner as the previous ones. The combination of all double poles is

$$- s = -n, - t = - m \rightarrow s = n, \; t = m.$$
$$s + t + 1 = - m, -s \; = - n \rightarrow s = n, \; t = -n \; - \; m - 1.$$
$$s + t + 1 = - n, -t \; = - m \rightarrow s = -n \; - \; m - 1, \; t = m. \qquad (2.5.16)$$

The indices n and m are positive integers.

Here $\Delta = 0$ for both complex variables. The way the path of integration can be closed depends on the relative sizes of the parameters. Let $a_1 > a_2$ and $a_1 > a_3$, then the path of integration should be closed so that the real parts of the parameters are greater than or equal to zero for large values of m and n. Since these indices are summed for some of the 2-poles, new parameters must be found in which they appear independently. This is easily done by substituting the above relations in the exponent of the parameters. The constant terms are neglected since they do not affect the direction of path closure. These relations are:

$$(1) \qquad \left(\frac{a_1}{a_2}\right)^{-n} \left(\frac{a_1}{a_3}\right)^{-m},$$

$$(2) \quad \left(\frac{a_1}{a_2}\right)^{-n}\left(\frac{a_1}{a_3}\right)^{n+m} \rightarrow \left(\frac{a_3}{a_1}\right)^{-m}\left(\frac{a_2}{a_3}\right)^{n},$$

$$(3) \quad \left(\frac{a_1}{a_2}\right)^{n+m}\left(\frac{a_1}{a_3}\right)^{-m} \rightarrow \left(\frac{a_2}{a_3}\right)^{-m}\left(\frac{a_1}{a_2}\right)^{n}. \qquad (2.5.17)$$

The first set of poles is the only one that converges for both indices, and the integral is equal to

$$I = \frac{1}{a_1} \sum_{n=0}^{\infty} \sum_{m=0}^{\infty} \frac{(-1)^{n+m}}{n!\ m!} \Gamma[1 + n + m]\left(\frac{a_1}{a_2}\right)^{-n}\left(\frac{a_1}{a_3}\right)^{-m}. \qquad (2.5.18)$$

To show the equivalence of the direct result with this double infinite series, note that for $a_1 > a_2$ and $a_1 > a_3$ one obtains

$$I = \frac{1}{a_1 + a_2 + a_3} = \frac{1}{a_1\left[1 + \frac{a_2}{a_1} + \frac{a_3}{a_1}\right]} = \frac{1}{a_1} \sum_{n=0}^{\infty} (-1)^n\left[\frac{a_2}{a_1} + \frac{a_3}{a_1}\right]^n. \qquad (2.5.19)$$

Using the binomial theorem when $a_3 > a_2$, one obtains

$$I = \frac{1}{a_1} \sum_{n=0}^{\infty} \sum_{m=0}^{\infty} \left(\frac{a_1}{a_2}\right)^{-n}\left(\frac{a_3}{a_2}\right)^{m} \frac{n!}{(n-m)!\ m!}. \qquad (2.5.20)$$

If one changes the variables to

$$m \rightarrow m' \quad and \quad n \rightarrow n' - m' \quad with \quad m \le n, \qquad (2.5.21)$$

then the summation reduces to the result that we obtained using Mellin transform techniques in Equation (2.5.18).

Therefore, the Mellin transform method produces the correct result although it was in terms of infinite series rather than a simple function as in the direct integration. In general, one would not recognize the double series that was obtained as the simple function that was obtained by a direct integration. The conditions on the parameters are more restrictive than the one that the sum of the parameters must be greater than zero obtained by the direct integration. The order of the inequalities of the parameters can be changed, which causes other pole pairs to be the ones enclosed in the path of integration. These other solutions can be shown to be all equal.

71

The more restrictive conditions on the parameters are necessary to express the answer as a double sum. From this example, one learns that in solving problems of this type, the conditions obtained to get an answer. even though they are correct, may be too restrictive. The fact that an answer is not in the most compact form and expressible in terms of simple functions is not a major deficiency because more complicated problems cannot in general be expressed simply in terms of elementary functions.

2.5.3 Example with Four Parameters

The method will now be extended to the case of four parameters where an integration over three complex planes is required. If a fourth exponential with parameter a_4 is added to the integral and $a_4 u = w$, then the convolution theorem gives

$$I = \frac{1}{a_1 (2\pi i)^3} \iiint ds \ dt \ du \ \Gamma[s + t + u + 1, -s, -t, -u]\left(\frac{a_1}{a_2}\right)^{-s}\left(\frac{a_1}{a_3}\right)^{-t}\left(\frac{a_1}{a_4}\right)^{-u},$$

$$(2.5.22)$$

where s, t, and u are separate complex variables.

The sets of 3-poles in 6-space are at

(1) $-s = -n, -t = -m, -u = -p \rightarrow s = n, t = m, u = p,$

(2) $s + t + u + 1 = -p, -s = -n, -t = -m \rightarrow s = n, t = m, u = -1 - n - m - p,$

(3) $-s = -n, -u = -p, s + t + u + 1 = -m \rightarrow s = n, u = p, t = -1 - n - m - p,$

(4) $-t = -m, -u = -p, s + t + u + 1 = -m, \rightarrow t = m, u = p, s = -1 - n - m - p,$

$$(2.5.23)$$

where n, m and p are positive integers.

As in the last section, these relations are substituted back into the exponents of the variables to give:

$$(1) \quad \left(\frac{a_1}{a_2}\right)^{-n}\left(\frac{a_1}{a_3}\right)^{-m}\left(\frac{a_1}{a_4}\right)^{-p},$$

$$(2) \quad \left(\frac{a_1}{a_2}\right)^{-n}\left(\frac{a_1}{a_3}\right)^{-m}\left(\frac{a_1}{a_4}\right)^{n+m+p} \rightarrow \left(\frac{a_4}{a_2}\right)^{-n}\left(\frac{a_4}{a_3}\right)^{-m}\left(\frac{a_1}{a_4}\right)^{p},$$

$$(3) \quad \left(\frac{a_1}{a_2}\right)^{-n}\left(\frac{a_1}{a_3}\right)^{n+m+p}\left(\frac{a_1}{a_4}\right)^{-p} \rightarrow \left(\frac{a_3}{a_2}\right)^{-n}\left(\frac{a_1}{a_3}\right)^{m}\left(\frac{a_3}{a_4}\right)^{-p},$$

$$(4) \quad \left(\frac{a_1}{a_2}\right)^{n+m+p}\left(\frac{a_1}{a_3}\right)^{-m}\left(\frac{a_1}{a_4}\right)^{-p} \rightarrow \left(\frac{a_2}{a_3}\right)^{-m}\left(\frac{a_1}{a_2}\right)^{n}\left(\frac{a_2}{a_4}\right)^{-p}. \qquad (2.5.24)$$

If the conditions on the parameters are such that all the fractions that are in the integral in Equation (2.5.22) are less than unity, the value of the real part of all three complex variables must be equal to or greater than zero. The only pole set that satisfies this requirement is the first one; therefore, the value of the integral is

$$I = \frac{1}{a_1}\sum_{n=0}^{\infty}\sum_{m=0}^{\infty}\sum_{p=0}^{\infty}(-1)^{n+m+p}\frac{(n+m+p)!}{n!\ m!\ p!}\left(\frac{a_1}{a_2}\right)^{-n}\left(\frac{a_1}{a_3}\right)^{-m}\left(\frac{a_1}{a_4}\right)^{-p}. \qquad (2.5.25)$$

If the fraction in Equation (2.5.10) is expanded into a triple power series, one obtains

$$I = \frac{1}{a_1}\sum_{i=0}^{\infty}\sum_{j=0}^{i}\sum_{k=0}^{j}(-1)^{j}\left(\frac{a_2}{a_1}\right)^{i}\left(\frac{a_3}{a_2}\right)^{j}\left(\frac{a_4}{a_3}\right)^{k}\frac{i!\ j!}{(i-j)!\ (j-k)!\ k!}. \qquad (2.5.26)$$

I evaluated the series numerically for a few examples and showed that the results of the series and the simple fraction were the same.

2.5.4 Example from the Integral Tables

The method will now be applied to an example that is a little more difficult. Consider the following integral from Gradshteyn and Ryzhik,[10] Equation (6.711.3)

$$I = \int_0^{\infty} u^{\nu-\mu-2} J_\mu(au) Y_\nu(bu)\sin(cu)du = \frac{2^{\nu-\mu-1}d^\mu b^{-\nu}c\ \Gamma[\nu]}{\Gamma[\mu+1]}, \qquad (2.5.27)$$

with $a > 0,\ b > 0,\ b-a > c > 0$ and $\mathrm{Re}\ \nu < \mathrm{Re}\ \mu + 3$.

This integral will be put into standard form by the following transformations

$$au = x,\ bu = x/y \rightarrow y = a/b,\ cu = x/z \rightarrow z = a/c. \qquad (2.5.28)$$

73

Then

$$I = a^{-v+\mu+1}\int_0^\infty \frac{dx}{x} \, x^{v-\mu-1} J_\mu(x) J_v\left(\frac{x}{y}\right)\sin\left(\frac{x}{z}\right).$$

(2.5.29)

This can be converted into an integral in two complex planes using the Mellin transforms in Equations (F.5) and (F.2). After the substitutions $s \to 2s$ and $t \to 2t$ one obtains

$$I = \frac{\sqrt{\pi}\, a^{-v+\mu+1} 2^{-2+v-\mu}}{(2\pi i)^2} \int ds \, dt \left(\frac{a}{b}\right)^{-2s}\left(\frac{a}{c}\right)^{-2t}$$
$$\times \Gamma\begin{bmatrix} s+t+v/2-1/2, -s+v/2, 1/2-t \\ -s-t-v/2+\mu+3/2, s+1+v/2, t+1 \end{bmatrix}.$$

(2.5.30)

The locations of the 2-poles are at

(1) $1/2-t=-m, -s+v/2=-n \to s=n+v/2, t=m+1/2,$
(2) $-s+v/2=-n, s+t+v/2=-m \to s=n+v/2, t=-m-v,$
(3) $1/2-t=-m, s+t+v/2=-n \to s=-1/2-n-m, t=m+1/2.$ (2.5.31)

Since $\Delta = 0$ for both complex variables, the size of the parameters determines the direction of path closure. Substituting the above relations back into the exponents in the integrand gives:

(1) $\left(\frac{a}{b}\right)^{-2n}\left(\frac{a}{c}\right)^{-2m},$

(2) $\left(\frac{a}{b}\right)^{-2n}\left(\frac{a}{c}\right)^{2m},$

(3) $\left(\frac{a}{b}\right)^{2n+2m}\left(\frac{a}{c}\right)^{-2m} \to \left(\frac{a}{b}\right)^{2n}\left(\frac{c}{b}\right)^{2m}.$

(2.5.32)

If the two fractions in the integral are less than unity, both exponents must be less than zero. The first set of double poles is the only one that satisfies the criteria, and the integral is equal to

$$I = \sqrt{\pi}\, a^{-v+\mu+1} 2^{-2+v-\mu} \sum_{n=0}^\infty \sum_{m=0}^\infty \frac{(-1)^{n+m}}{n!\, m!}\left(\frac{a}{b}\right)^{v-2n}$$
$$\times \left(\frac{a}{c}\right)^{-1-2m} \Gamma\begin{bmatrix} v+m+n \\ \mu+1+n, 1-m-n, 3/2+m \end{bmatrix}.$$

(2.5.33)

The term $\Gamma[1 - m - n]$ in the denominator is infinite at all n and m except $m = n = 0$. This cancels out all the poles except those at $m = n = 0$. The one remaining term gives the same result as that in Equation (2.5.27). Therefore, one obtains the same compact form for the answer as that in the tables. The particular condition on the parameters produces the simple form for the result, and the expression is more complicated for other conditions on the parameters. The method above can be used to get a series solution for these other cases by closing the path of integration in the appropriate direction.

3. A UNIFIED APPROACH TO WAVE PROPAGATION IN TURBULENT MEDIA

3.1 INTRODUCTION

In this part of the report, the derivations of the expressions for variance of phase and scintillation quantities, structure function, power spectral density, Strehl ratio and beam profile are given. The derivation and tabular listing of various filter functions that are of most interest is presented. The procedure for setting up problems is illustrated by a variety of examples some of which have not been published before. The evaluation of the integrals using Mellin transform techniques was developed in the second part of this report, and these results are used to evaluate integrals in this part.

The filter functions that are derived here allow one to find the piston, tilt, or any Zernike component of the phase; to evaluate the effect of anisoplanatism (displacement, angular, time delay, and chromatic), finite frequency response, and fitting error on focused or collimated beams. (Anisoplanatism is the effect on the correction caused by propagating along a different path than that taken by the reference beacon.) Filter functions are also given to allow one to calculate the effect of point and incoherent distributed beacons on an adaptive-optics system. The filter functions can be cascaded to allow one to set up complicated problems quickly. This procedure allows one to calculate the interaction of various effects in a straightforward manner.

In the next section, the general formulas for the beam profile and the Strehl ratio are derived. In order to evaluate these expressions, the structure function must be found. This can be found from general expressions for the phase and log-amplitude variance that are derived in Section 3.3. Approximations are made to arrive at this general expression. In Appendix B, an example is worked out without the approximation and shown to add an insignificant correction. The expressions for the variances, structure functions, and power spectral density are generalized to focused beams.

77

In Section 3.4, filter functions that are useful for turbulence problems are derived. The final answer to turbulence problems is expressed in terms of moments of the turbulence distribution. The definition of these moments is given, and analytic expressions for the moments are derived in Appendix C.

Single parameter problems to illustrate the method of evaluating integrals using Mellin transforms is given in Section 3.5. The third example shows how to combine filter functions to arrive at new ones. In Section 3.6 examples of multiparameter problems are given. The evaluation of the integrals relies heavily on the results in part 2. The evaluation of the phase variance for a distributed source is complicated and uses all the previous methods. This example is discussed in detail in Section 3.7.

Next, in Section 3.8 the power spectral density is calculated for several problems. The Strehl ratio and coherence diameter for various problems is discussed in Section 3.9. The calculation of the Strehl ratio for uncorrected turbulence is given. When the structure function is more complicated, Gegenbauer polynomials are introduced to evaluate the Strehl ratio. This technique is illustrated using defects in an adaptive-optics system. These techniques are then extended to derive the beam profile for uncorrected turbulence and for an adaptive-optics system in Section 3.10.

3.2 GENERAL EXPRESSION FOR THE BEAM SHAPE AND STREHL RATIO

In this section, expressions for the beam shape and Strehl ratio are found in terms of the phase and amplitude structure functions. The relation between these structure functions and the phase and amplitude statistics is given.

The extended Huygens-Fresnel approximation to beam propagation that applies to collimated beams results in the following formula for a component of the electric field at a distance z from the source

$$E(\vec{r}, z) = \frac{1}{i\lambda z} \int d\vec{\rho} \; E(\vec{\rho}, 0) \exp\left[\frac{i\pi}{\lambda z}(\vec{r} - \vec{\rho})^2 + \chi(\vec{r}, \vec{\rho}) + i\phi(\vec{r}, \vec{\rho})\right], \quad (3.2.1)$$

where χ and ϕ are the turbulence induced log-amplitude and phase fluctuations that are produced in propagating from the ρ-plane to the r-plane as shown in Figure 3-1. The integration is over the source distribution.
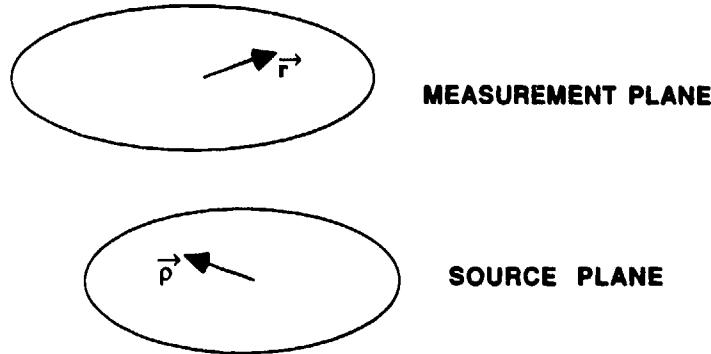
Figure 3-1. Geometry of the propagation problem.

The intensity can be found by multiplying the field by its complex conjugate. In the paraxial approximation that applies to waves that are confined to a small distance about the propagation direction, a condition that holds for laser beam propagation, second order terms in $\vec{\rho}$ and $\vec{\rho}\,'$ are negligible. With this approximation, and a source distribution $W(\vec{r}\,)$ in the aperture, the intensity is equal to

$$E(\vec{r},z)E^*(\vec{r},z) = \frac{1}{(\lambda z)^2} \int d\vec{\rho}\ d\vec{\rho}\,'\ W(\vec{\rho})W(\vec{\rho}\,')$$

$$\times \exp\left[\frac{i2\pi}{\lambda z}\{\vec{r}\cdot(\vec{\rho}-\vec{\rho}\,')\} + \chi(\vec{r},\vec{\rho}) - \chi(\vec{r},\vec{\rho}\,') + i[\phi(\vec{r},\vec{\rho}) - \phi(\vec{r},\vec{\rho}\,')]\right].$$

(3.2.2)

The average intensity can be found by taking the ensemble average of the above equation. The turbulence fluctuations are Gaussian in character and for this distribution one can show that

$$\langle\exp(\alpha A)\rangle = \exp\left[\frac{\alpha^2}{2}\langle A^2 - \langle A\rangle^2\rangle\right].$$

(3.2.3)

79

The angle brackets indicate that the ensemble average of the enclosed quantity is to be found. Therefore, the average intensity is equal to

$$\langle E(\vec{r}, z) E^*(\vec{r}, z) \rangle = \frac{1}{(\lambda z)^2} \int d\vec{\rho} \; d\vec{\rho}' \; W(\vec{\rho}) W(\vec{\rho}')$$

$$\times \exp\left[\frac{i2\pi}{\lambda z}\{\vec{r} \cdot (\vec{\rho} - \vec{\rho}')\} - D_\phi([\vec{\rho} - \vec{\rho}'] / D, \vec{r}) / 2 - D_\chi([\vec{\rho} - \vec{\rho}'] / D, \vec{r}) / 2\right].$$

$$(3.2.4)$$

The struc. re functions of phase and log-amplitude are defined to be

$$\begin{bmatrix} D_\phi(\vec{\alpha}, \vec{r}) \\ D_\chi(\vec{\alpha}, \vec{r}) \end{bmatrix} = \begin{bmatrix} \langle [\varphi(\vec{r} + \vec{\alpha}D) - \varphi(\vec{r})]^2 \rangle \\ \langle [\chi(\vec{r} + \vec{\alpha}D) - \chi(\vec{r})]^2 \rangle \end{bmatrix}.$$

$$(3.2.5)$$

To simplify this expression, change the variables of integration to normalized sum and difference coordinates as

$$\vec{\alpha}' = (\vec{\rho} + \vec{\rho}') / 2D,$$

$$(3.2.6)$$

$$\vec{\alpha} = (\vec{\rho} - \vec{\rho}') / D,$$

$$(3.2.7)$$

where D is the diameter of the circular aperture, and α is the normalized radial coordinate that goes from 0 to 1.

For cases in which the variance is independent of position, the structure function can be represented by a relation that only depends on the difference in position of the two points, and can be written as

$$\begin{bmatrix} D_\phi(\vec{\alpha}) \\ D_\chi(\vec{\alpha}) \end{bmatrix} = 2\begin{bmatrix} \langle \varphi^2(0) \rangle - \langle \varphi(\vec{\alpha}D)\varphi(0) \rangle \\ \langle \chi^2(0) \rangle - \langle \chi(\vec{\alpha}D)\chi(0) \rangle \end{bmatrix}.$$

$$(3.2.8)$$

The assumption of writing the structure function as a function only of the difference of positions is not true for many cases of interest. If tilt is subtracted from the phase over the aperture, then the phase variance is higher in the center of the aperture than at the edges. For the anisoplanatic effect of a point source over the aperture center being used as a beacon in an adaptive-optics system that is sending a collimated beam, the phase variance is again no longer stationary. In this case, the variance is higher at the aperture edge than at the center. In the

discussion of tilt removal, it will be pointed out that the error made in using the above expression is about 10% and may often be neglected. The error in assuming stationarity for the focal anisoplanatism case has not been calculated.

For a uniform field distribution over a circular aperture, the integral over the sum coordinate can be performed analytically in the following manner. Expressing the original coordinates in terms of the new ones as $\vec{p} = \vec{\alpha}' D + \vec{\partial} D / 2$, and $\vec{p}' = \vec{\alpha}' D - \vec{\partial} D / 2$. then the integral of the intensity can be expressed as

$$I = \int d\vec{p}\, d\vec{p}'\, W\,(\,\vec{p}\,)W\,(\,\vec{p}'\,)\, L(\,\vec{p},\vec{p}'\,)$$

$$= \int d\vec{\alpha}\, d\vec{\alpha}'\, W\,(\vec{\alpha}'D\, +\, \vec{\partial}D\,/\,2)W\,(\vec{\alpha}'D\, -\, \vec{\partial}D\,/\,2)L\,(\vec{\alpha}).$$

The integral in the sum coordinate is the overlap area of two circles and is evaluated in Figure 3-2. If the expression for the intensity in Equation (3.2.4) is divided by the intensity with no turbulence present, one obtains the normalized average intensity as

$$I_n(\vec{r}) = \frac{1}{2\pi}\int d\vec{\alpha}\, K(\alpha)\exp\left[\,i\frac{k_o D}{z}\vec{r}\cdot\vec{\alpha} - \frac{D(\vec{\alpha})}{2}\right], \qquad (3.2.9)$$

where the integral is over the unit circle, and the modulation transfer function for a circular aperture is given by

$$K(\alpha) = \frac{16}{\pi}\left[\cos^{-1}(\alpha) - \alpha\left(1 - \alpha^2\right)^{1/2}\right]U(1 - \alpha), \qquad (3.2.10)$$

where $U(x)$ is the unit step function. The structure function is given by

$$D(\vec{\alpha}) = D_\phi(\vec{\alpha}) + D_\chi(\vec{\alpha}). \qquad (3.2.11)$$

If the structure function is isotropic, the angle integration in the aperture can be performed using Equation (3.4.5) to give

$$I_n(r) = \int_0^1 \alpha\, d\alpha\, K(\alpha)\, J_o\!\left(\frac{k_o rD\alpha}{z}\right)\exp\left[-\frac{D(\alpha)}{2}\right]. \qquad (3.2.12)$$

The Strehl ratio, which is the value of the normalized intensity at the origin, is the most common description of the performance of an adaptive-optics system and is given by

$$SR = \frac{1}{2\pi}\int d\vec{\alpha}\, K(\alpha)\exp\left[-\frac{D(\alpha)}{2}\right]. \qquad (3.2.13)$$

81
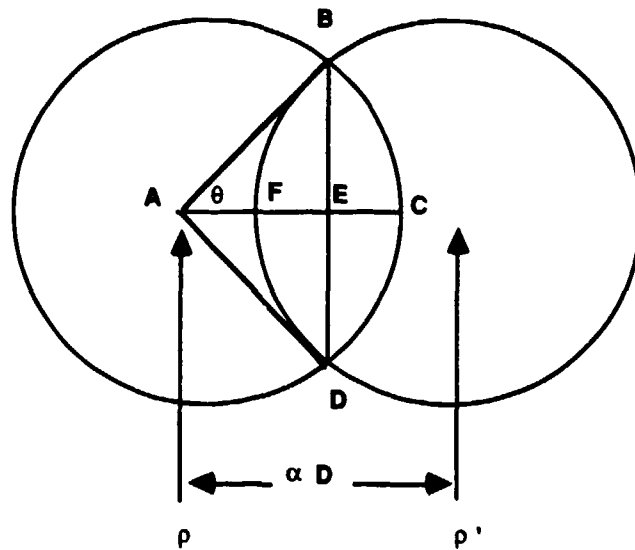
Figure 3-2. Geometry to determine overlap area of the two apertures. The integral over $\vec{a}$ is equal to the area of overlap of the two circles. The area of overlap is equal to Area(FBCD) = 2 Area(DEBC) = 2[Area(ABCD) - Area(ABED)], where Area (ABCD) = 2($D^2\theta/8$) = ($D^2/4$) $\cos^{-1}$ α and Area (ABED) = 2 Area (AEB) = 2 [($\alpha D)^2/2$] sin θ = ($\alpha D^2/4$) $\sqrt{1 - \alpha^2}$. Therefore, Overlap Area = ($D^2/2$) ($\cos^{-1}$ $\alpha - \alpha$ $\sqrt{1 - \alpha^2}$). Normalizing to give unity for the intensity on axis with no turbulence, one obtains the desired result $K(\alpha) = (16/\pi)$ ($\cos^{-1}$ $\alpha - \alpha$ $\sqrt{1 - \alpha^2}$).

82

When the structure function is isotropic, the integration over the angle in the aperture can be performed to get

$$SR = \int_0^1 \alpha \, d\alpha \, K(\alpha) \exp\left[-\frac{D(\alpha)}{2}\right].$$
(3.2.14)

The beam profile and Strehl ratio given in Equations (3.2.9), (3.2.12), (3.2.13), and (3.2.14) will be evaluated in Sections 3.9 and 3.10 after methods are developed in the intervening sections to determine the structure function for particular problems.

3.3 GENERAL EXPRESSION FOR THE PHASE AND LOG-AMPLITUDE VARIANCE, STRUCTURE FUNCTION, AND POWER SPECTRAL DENSITY

In the first part of this section, the relations for the phase and log-amplitude variance are derived using results from Tatarski for a locally stationary media. His derivation is sketched in this section, and the reader is referred to his book for a more detailed derivation of the results that are used here. The difference between Tatarski's results and those used here is that a filter function is allowed to operate on the transverse components of the spatial spectrum. This generalization allows one to tackle a great variety of problems of interest. From these expressions, the structure function and power spectral density are found. The equations developed in this section are summarized in tables in part 1, and serve as the starting point for all the turbulence problems considered later.

3.3.1 Phase and Log-Amplitude Using the Rytov Approximation

The Rytov approximation is a better approximation than the geometric-optics one. The equations of geometric-optics do not take diffraction into account and can only be used to distances that are small compared to the Fresnel distance. The Rytov approximation does account for diffraction and can be used past the Fresnel distance. The approximation breaks down for the log-amplitude when that variance is greater than about 0.3. The phase results are still valid even when the amplitude fluctuations are large. The net result is that this

83

approximation gives accurate results for the phase for all problems of interest. The results for log-amplitude are accurate as long as this variance is small. That assumption is violated for the propagation of uncorrected beams over large horizontal distances or in propagation from the ground to space; however, it is valid for a beam corrected by an adaptive-optics system. In high-scintillation cases, a multiple scattering theory is necessary to describe the log-amplitude. That will not be done in this report.

The derivation of the equations for phase and log-amplitude using the Rytov approximation are sketched below. A more detailed derivation is in Tatarski. The wave equation describing the electric field for propagation in a region with inhomogeneous refractive index, $n(\vec{r})$ is

$$\nabla_t^2 \vec{E} + k_o^2 n^2(\vec{r})\vec{E} + 2\nabla[\vec{E} \cdot \nabla \ln n(\vec{r})] = 0, \qquad (3.3.1)$$

where the free space wavenumber $k_o = 2\pi/\lambda$, and ∇_t^2 is the transverse Laplacian. If the propagation wavelength, λ, is much less than the inner scale size, the last term can be neglected. One then obtains a scalar equation for each of the electric field components. The equation for one of those components is

$$\nabla_t^2 u + k_o^2 n^2(\vec{r})u = 0. \qquad (3.3.2)$$

It will be assumed that the effect of the inhomogeneity is small, then the field and refractive index can be written in two parts as

$$n(\vec{r}) = 1 + n_1(\vec{r}), \qquad (3.3.3)$$

$$u = u_o + u_1, \qquad (3.3.4)$$

where

$$n_1(\vec{r}) << 1, \qquad (3.3.5)$$

and

$$|u_1| << |u_o|. \qquad (3.3.6)$$

The unperturbed field satisfies

$$\nabla_t^2 u_o + k_o^2 u_o = 0. \qquad (3.3.7)$$

The field affected by turbulence satisfies

$$\nabla_t^2 u_1 + k_o^2 u_1 = -2 k_o^2 n_1(\vec{r})u_o. \qquad (3.3.8)$$

The central part of the Rytov method is to represent the field in the form

$$u_1 = A \exp[iS].$$

(3.3.9)

where

$$A = A_o + A_1,$$

(3.3.10)

and

$$S - S_o = S_1 = \operatorname{Im} \frac{u_1}{u_o}.$$

(3.3.11)

Let

$$\ln \frac{A}{A_o} = \chi = \operatorname{Re} \frac{u_1}{u_o}.$$

(3.3.12)

Also define

$$\Psi = \ln u = \ln A + i\phi.$$

(3.3.13)

Express this quantity in the form of a small and large part as

$$\Psi = \Psi_o + \Psi_1,$$

(3.3.14)

where

$$\Psi_1 = \chi + i\phi_1.$$

(3.3.15)

The following assumption gives this method the alternate name of the method of smooth variations. Assume

$$|\nabla \Psi_1| << |\nabla \Psi_o|.$$

(3.3.16)

Then the following equation can be derived

$$\nabla_t^2 \Psi_1 + 2 i k_o \frac{\partial \Psi_1}{\partial z} + 2 k_o^2 n_1(\vec{r}) = 0.$$

(3.3.17)

Write the refractive index in the form of a random function with stationary increments as

$$n_1(\vec{r}_t, z) = n_1(0, z) + \int dv(\vec{\kappa}, z) \left[1 - \exp(i\vec{\kappa} \cdot \vec{r}_t)\right],$$

(3.3.18)

wi..re $\vec{r}_t$ is the transverse coordinate. The integral is over kappa space and the fact that the transverse Fourier transform is used to solve the problem gives the solution method the name "the method of spectral expansions". This is a stochastic Fourier-Stiltjes integral, and the true complexity of this relation is buried in the differential quantity in the integral. Also, write the field in the same form as

$$\Psi_1(\vec{r}_t, z) = \Psi_1(0, z) + \int d\varphi(\vec{\kappa}, z) \left[1 - \exp(i\vec{\kappa} \cdot \vec{r}_t)\right].$$

(3.3.19)

If these last two relations are substituted into Equation (3.3.17), it is found that the differential quantities must satisfy the following relation

$$2 i k_o \frac{\partial d\psi_{\ldots}, z)}{\partial z} - \kappa^2 d\varphi(\vec{\kappa}, z) + 2 k_o^2 dv(\vec{\kappa}, z) = 0. \tag{3.3.20}$$

This equation holds when the propagation distance, L, satisfies

$$L < D^4 / \lambda^3, \tag{3.3.21}$$

where D is the aperture diameter, and λ is the propagation wavelength. For diameters of interest, the range over which the assumption is valid is very large and the condition is satisfied for most problems. The solution of this equation for a wave propagating from 0 to z is

$$d\varphi(\vec{\kappa}, z) = i k_o \int_o^z dv(\vec{\kappa}, z') \exp\left[\frac{-i\kappa^2(z - z')}{2 k_o}\right] dz'. \tag{3.3.22}$$

This equation is the starting point to find the variances of the phase and the log-amplitude. If there is spatial filtering of the transverse coordinate of the refractive index spectrum, then the above derivation holds except that the refractive index spectrum is replaced by the filtered spectrum using the substitution

$$dv(\vec{\kappa}, z) \rightarrow dv(\vec{\kappa}, z)G(\vec{\kappa}, z), \tag{3.3.23}$$

where $G(\vec{\kappa}, L)$ is a composite filter function that modifies the turbulence spectrum. The justification for being able to write a filtered refractive index in this form is contained in the discussion of filter functions for Zernike polynomials in Subsection 4.1.

3.3.2 Variances, Structure Functions, and Power Spectral Densities

In spatial transform space when the Rytov approximation applies, the two-dimensional transverse spatial Fourier transform of the phase can be obtained from the imaginary part of Equation (3.3.22), which is.

$$F_t\left[d\phi_1(L)\right] = k_o \int_0^L dv(\vec{\kappa}, z') \cos\left[\frac{\kappa^2(L - z')}{2 k_o}\right] G(\vec{\kappa}, z') dz'. \tag{3.3.24}$$

The origin of the wave is at $z = 0$. The filter function for phase related quantities operates on the phase disturbance.

The Fourier transform of the log-amplitude scintillation can be obtained from the real part of Equation (3.3.?2) which is

$$F_t[d\chi(L)] = \ln\left[\frac{A(L)}{A_o}\right] = k_o \int_0^L dv(\vec{\kappa}, z')\sin\left[\frac{\kappa^2(L - z')}{2k_o}\right]G(\vec{\kappa}, z')\, dz'. \quad (3.3.25)$$

The last formula breaks down when the log-amplitude variance exceeds 0.3. For more severe scintillations, a multiple scattering theory approach is necessary. That will not be discussed in this report. Even for large scintillations, the formula for the phase is still valid. The restriction on the scintillation is important for uncorrected propagation from the ground to space and for horizontal propagation over long turbulent paths. The restriction is not important for most problems considered with adaptive-optic systems since it will be seen that the scintillation is low.

Typically, the rms values of the quantities are wanted. These are obtained by integrating the expressions over kappa-space, multiplying the resultant expressions by their complex conjugate, and taking the ensemble average. The resulting expressions for the phase, ϕ^2, and log-amplitude variances, χ^2, are

$$\begin{bmatrix}\phi^2 \\ \chi^2\end{bmatrix} = k_o^2 \iiint dz' \int_0^L dz' \left\langle dv(\vec{\kappa}, z')dv^*(\vec{\kappa}', z'')\right\rangle$$

$$\left\{\begin{matrix}\cos\left[\dfrac{\kappa'^2(L - z')}{2k_o}\right]\cos\left[\dfrac{\kappa^2(L - z')}{2k_o}\right] \\[2ex] \sin\left[\dfrac{\kappa^2(L - z'')}{2k_o}\right]\sin\left[\dfrac{\kappa^2(L - z')}{2k_o}\right]\end{matrix}\right\} G(\vec{\kappa}, z')\, G^*(\vec{\kappa}', z'). \quad (3.3.26)$$

The first two integrals are over kappa and kappa-prime space. This equation can be simplified. The ensemble average of the absolute value squared of the refractive index is given in Tatarski Equation (6.36) by

$$\left\langle dv(\vec{\kappa}, z')dv^*(\vec{\kappa}', z'')\right\rangle = E_n(\vec{\kappa}, |z' - z''|)C_n^2[(z' + z'') / 2]\delta(\vec{\kappa} - \vec{\kappa}')d\vec{\kappa}\, d\vec{\kappa}',$$

$$(3.3.27)$$

where the delta function occurs because the turbulence fluctuations at different wavenumbers are completely uncorrelated — a fact that follows from the assumption that the turbulence can be represented as a random process with stationary increments. $C_n^2(z)$ is a normalizing function that is proportional to the strength of turbulence. $E_n(\vec{\kappa}, |z' - z''|)$ is the correlation function of turbulence versus axial separation as a function of the transverse wavenumber. It is equal to the inverse Fourier transform in the axial direction of the turbulence spectrum. The inverse Fourier transform relation is given in Tatarski Equation (1.53) as

$$0.033 \, \pi \, f(\kappa, \, \kappa_-) = \int_0^\infty dz_- \, E_n(\vec{\kappa}, \, z_-)\cos(\kappa_- z_-). \tag{3.3.28}$$

This gives the special case

$$0.033 \, \pi \, f(\kappa, 0) = \int_0^\infty dz_- \, E_n(\vec{\kappa}, z_-), \tag{3.3.29}$$

where the turbulence spectrum is often represented by the following von Kármán spectrum (normalized to unity coefficient)

$$f(\kappa) = \left[\kappa^2 + \kappa_o^2 \right]^{-11/6} \exp\left[-\kappa^2/\kappa_i^2 \right], \tag{3.3.30}$$

where $\kappa_o = 2\pi/L_o$ and $\kappa_i = 2\pi/L_i$. L_o is called the outer scale of turbulence, and L_i is called the inner scale. The shape of the spectrum in the region where the inner or outer scale are important is not known in practice, and these forms are used because they are physically reasonable and mathematically convenient. Other models have been suggested and the techniques developed in this report can be used for those. Only the von Kármán spectrum is used in this report. Typically, inner and outer scale do not affect the final answer. Care should be exercised in comparing the results with outer and inner-scale effects included obtained here with those of other authors. Some define these quantities without the factor of 2π. If inner and outer scale are negligible, one obtains the commonly used result

$$f(\kappa) = \kappa^{-11/3}. \tag{3.3.31}$$

After inserting Equation (3.3.27) into Equation (3.3.26), the integration of the delta function in κ' can be immediately performed, and the expression has now been reduced to

$$\begin{bmatrix} \phi^2 \\ \chi^2 \end{bmatrix} = k_o^2 \int_0^L dz' \int_0^L dz'' \ C_n^2 \left(\frac{z'+z''}{2} \right) \int d\vec{\kappa} \ E_n(\vec{\kappa}, |z'-z''|) \begin{bmatrix} C_p \\ C_a \end{bmatrix} G(\vec{\kappa}, z') G^*(\vec{\kappa}, z''),$$

$$(3.3.32)$$

where

$$\begin{bmatrix} C_p \\ C_a \end{bmatrix} = \left\{ \begin{array}{l} \cos\left[\dfrac{\kappa^2(z'-L)}{2 k_o} \right] \cos\left[\dfrac{\kappa^2(z''-L)}{2 k_o} \right] \\[2em] \sin\left[\dfrac{\kappa^2(z'-L)}{2 k_o} \right] \sin\left[\dfrac{\kappa^2(z''-L)}{2 k_o} \right] \end{array} \right\},$$

$$(3.3.33)$$

with the region of integration in z' and z'' space shown in Figure 3-3.
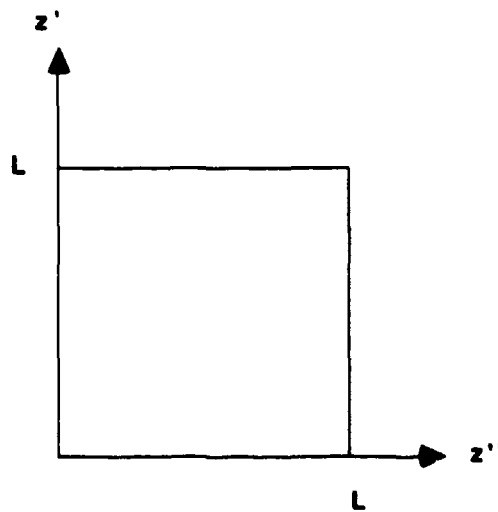
Figure 3-3. Original region of integration.

One of the axial integrations will now be eliminated. Change the variables of integration into sum and difference coordinates by the transformations

$$z_- = z' - z'',$$

$$(3.3.34)$$

89

and
$$z = \frac{1}{2}(z' + z''),$$
(3.3.35)

where the new region of integration has been transformed from the rectangular region into the diamond shaped region of Figure 3-4.
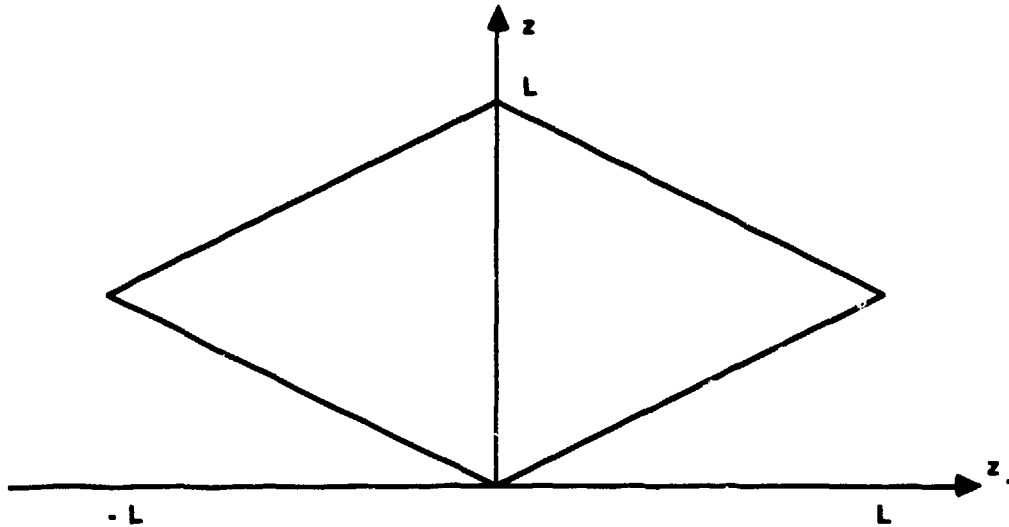
Figure 3-4. Region of integration in transformed space.

The transformed equation is

$$\begin{bmatrix} \phi^2 \\ \chi^2 \end{bmatrix} = k_o^2 \iint_{Diamond} dz_- \, dz \; C_n^2(z) \int d\vec{R} \; E_n(\vec{R}, |z_-|) \begin{bmatrix} C_p \\ C_a \end{bmatrix}$$

$$\times \; G(\vec{R}, z + z_- / 2) G^*(\vec{R}, z - z_- / 2).$$
(3.3.36)

In order to eliminate the integration over z_-, Equation (3.3.29) can be used except that the integration goes out to infinity, while the integration above has finite limits. In addition, there are other functions in the integrand that depend on that coordinate. However, the correlation function of the turbulence only has significant values over a range of tens of meters, a distance that is generally very small compared to the entire integration path; therefore, the difference coordinate can be set to zero when it is added to the sum coordinate. For the example of tracked tilt that is considered in Section 3.5.6, the results of performing this calculation without this approximation are derived in Appendix B. The magnitude of the error using the above

assumption was about 1 part in 100,000,000. Therefore, this approximation has a negligible effect on the final answer. This assumption makes the correlation function the only one that depends on z_-.

The difficulty with the finite limits of integration will now be resolved. Since the correlation function is even in z_-, the integral is twice the answer obtained using only the right-hand side of the diamond. The only part of the diamond shaped area that contributes to the integral is a thin strip close to the vertical axis since the correlation function falls off very rapidly with distance. Therefore, the diamond shaped area can be extended horizontally to infinity without significantly affecting the value of the integral. Doing this, the limit of the z_- integration goes to infinity, and the use of Equation (3.3.29) allows this integral to be evaluated. With these approximations, the integral reduces to

$$\begin{bmatrix} \phi^2 \\ \chi^2 \end{bmatrix} = 0.2073 k_o^2 \int_0^L dz \, C_n^2(z) \int d\vec{\kappa} \, f(\kappa) \begin{Bmatrix} \cos^2 \left[\dfrac{\kappa^2(z-L)}{2k_o} \right] \\ \sin^2 \left[\dfrac{\kappa^2(z-L)}{2k_o} \right] \end{Bmatrix} \prod_i F_i(\vec{\kappa}, z), \qquad (3.3.37)$$

The filter function can be a cascade of individual filters in which

$$G(\vec{\kappa}, z) G^*(\vec{\kappa}, z) = \prod_i F_i(\vec{\kappa}, z). \qquad (3.3.38)$$

For problems of laser beam propagation in the near field, an important simplifying approximation can be made. Since the argument of the trigonometric function is small, the cosine term can be replaced by unity, as

$$\cos^2 \left[\frac{\kappa^2(z-L)}{2k_o} \right] \approx 1. \qquad (3.3.39)$$

Similar expressions can be derived for a wave focused at the target and at the observation point. For the case of a wave focused at S, Tatarski shows that the phase and log-amplitude are given by

$$\begin{bmatrix} d\phi(L) \\ d\chi(L) \end{bmatrix} = k_o \int_0^L dv \Big(\frac{S\vec{R}}{S - z'}, z' \Big) \left\{ \begin{array}{c} \cos\left[\dfrac{\kappa^2 S z'}{2 k_o (S - z')} \right] \\ \sin\left[\dfrac{\kappa^2 S z'}{2 k_o (S - z')} \right] \end{array} \right\} G(\vec{R}, z')\, dz'. \qquad (3.3.40)$$

Using the following property of the refractive index average for focused beams from Tatarski

$$\left\langle dv\Big(\frac{\vec{R} L}{S - z'}, z' \Big) dv^*\Big(\frac{\vec{R}' L}{S - z''}, z'' \Big) \right\rangle = E_n(\vec{R}, |z' - z''|) C_n^2 [(z' + z'') / 2]$$

$$\times \Big(\frac{S - z'}{S} \Big)^2 \delta\Big(\vec{R}' - \frac{\vec{R}(S - z'')}{S - z'} \Big) d\vec{R}\, d\vec{R}', \qquad (3.3.41)$$

and repeating the same steps as above, one obtains for a wave propagating to the focus

$$\begin{bmatrix} \phi^2 \\ \chi^2 \end{bmatrix} = 0.2073 k_o^2 \int_0^L dz\ C_n^2(z) \int d\vec{R}\ f(\kappa) \left\{ \begin{array}{c} \left[\dfrac{z}{S} \right]^{5/3} \cos^2\left[\dfrac{\kappa^2 S (S - z)}{2 k_o S} \right] \\ \left[\dfrac{z}{S} \right]^{5/3} \sin^2\left[\dfrac{\kappa^2 S (S - z)}{2 k_o S} \right] \end{array} \right\} \prod_i F_i(\vec{R}, z).$$

$$(3.3.42)$$

To obtain the same quantities when propagating from the focus to a point S, the general form can be found from the above result by making the substitution $z \to S - z$ to get

$$\begin{bmatrix} \phi^2 \\ \chi^2 \end{bmatrix} = 0.2073\ k_o^2 \int_0^L dz\ C_n^2(z) \int d\vec{R}\ f(\kappa) \left\{ \begin{array}{c} \left(\dfrac{S - z}{S} \right)^{5/3} \cos^2\left[\dfrac{\kappa^2 z S}{2 k_o(z - S)} \right] \\ \left(\dfrac{S - z}{S} \right)^{5/3} \sin^2\left[\dfrac{\kappa^2 z S}{2 k_o(z - S)} \right] \end{array} \right\} \prod_i F_i(\vec{R}, z).$$

$$(3.3.43)$$

Similar formulas for the structure function will now be found. When the structure function depends only on the difference between the two coordinates, the displacement in real space is equivalent to a phase shift in transform space, as is seen from the following property of Fourier transforms. The transverse Fourier transform of a function is

$$F_t(f(\vec{a})) = \int d\vec{a}\ f(\vec{a}) \exp[i\vec{R} \cdot \vec{a}], \qquad (3.3.44)$$

then

$$F_t[f(\vec{a} + \vec{\partial}D)] = \int d\vec{a} \, f(\vec{a} + \vec{\partial}D)\exp[i\vec{R} \cdot \vec{a}] = \exp[-i\vec{R} \cdot \vec{\alpha}D] \, F_t[f(\vec{a})]. \quad (3.3.45)$$

Using this relation and Equation (3.3.37), the structure function is

$$D_\phi(\vec{\alpha}) = 0.2073 \, k_o^2 \int_0^L dz \, C_n^2(z) \int d\vec{R} \, f(\kappa) \cos^2\left[\frac{\kappa^2(z-L)}{2k_o}\right] \prod_i F_i(\vec{R}, z)$$

$$\times \left| 1 - \exp\{i\vec{R} \cdot \vec{\partial}D\}\right|^2$$

$$= 0.4146 \, k_o^2 \int_0^L dz \, C_n^2(z) \int d\vec{R} \, f(\kappa) \cos^2\left[\frac{\kappa^2(z-L)}{2k_o}\right] \prod_i F_i(\vec{R}, z)[1 - \cos\{\vec{R} \cdot \vec{\partial}D\}].$$

$$(3.3.46)$$

Therefore, the structure function for a collimated beam is given by

$$\begin{bmatrix} D_\phi(\vec{\alpha}) \\ D_\chi(\vec{\alpha}) \end{bmatrix} = 0.4146 \, k_o^2 \int_0^L dz \, C_n^2(z) \int d\vec{R} \, f(\kappa) \left\{ \begin{array}{c} \cos^2\left[\dfrac{\kappa^2(z-L)}{2k_o}\right] \\ \sin^2\left[\dfrac{\kappa^2(z-L)}{2k_o}\right] \end{array} \right\}$$

$$\times [1 - \cos\{\vec{R} \cdot \vec{\partial}D\}] \prod_i F_i(\vec{R}, z). \quad (3.3.47)$$

The structure function for a beam focused at S is given by

$$\begin{bmatrix} D_\phi(\vec{\alpha}) \\ D_\chi(\vec{\alpha}) \end{bmatrix} = 0.4146 \, k_o^2 \int_0^L dz \, C_n^2(z) \int d\vec{R} \, f(\kappa) \left\{ \begin{array}{c} \left(\dfrac{z}{S}\right)^{5/3} \cos^2\left[\dfrac{\kappa^2 S(S-z)}{2k_o S}\right] \\ \left(\dfrac{z}{S}\right)^{5/3} \sin^2\left[\dfrac{\kappa^2 S(S-z)}{2k_o S}\right] \end{array} \right\}$$

$$\times [1 - \cos\{\vec{R} \cdot \vec{\partial}D\}] \prod_i F_i(\vec{R}, z). \quad (3.3.48)$$

The structure function for a beam focused at $z = 0$ is given by

$$\begin{bmatrix} D_\phi(\vec{\alpha}) \\ D_\chi(\vec{\alpha}) \end{bmatrix} = 0.4146\, k_o^2 \int_0^L dz\; C_n^2(z) \int d\vec{\kappa}\; f(\kappa) \begin{Bmatrix} \left(\dfrac{S-z}{S}\right)^{5/3} \cos^2\left[\dfrac{\kappa^2 z S}{2 k_o(z-S)}\right] \\ \left(\dfrac{S-z}{S}\right)^{5/3} \sin^2\left[\dfrac{\kappa^2 z S}{2 k_o(z-S)}\right] \end{Bmatrix}$$

$$\times [1 - \cos\{\vec{\kappa} \cdot \vec{\alpha}D\}] \prod_i F_i(\vec{\kappa}, z).$$

(3.3.49)

The cause of any time changes in the turbulence are due to either wind moving the turbulence past the viewing volume or due to the slewing of the beam. Taylor's frozen turbulence assumption is used here and it assumes that the turbulence itself does not change in the typical time scales of interest. With this assumption, the power spectral density can be found by a change of variables. The transverse spatial coordinates will be changed to one over temporal frequency and another convenient coordinate. It will he recognized that everything multiplying the differential of omega (the temporal frequency variable) is the power spectral density. Assume that the wind velocity, $v(z)$, is in the x direction. Then, one can write a relation between the wavenumber in the x direction and the temporal radian frequency as

$$\kappa_x = \omega / v(z).$$

(3.3.50)

Make the additional change of variables

$$c^2 = \frac{\kappa_y^2 v^2(z)}{\omega^2} + 1,$$

(3.3.51)

from which follows

$$d\kappa_y = \frac{\omega}{v(z)} \frac{c\,dc}{\sqrt{c^2 - 1}}.$$

(3.3.52)

The last change of variables was selected since it produces an integrand for which a Mellin transform exists and is given in Equation (F.9). Express the relation for the variance given in Equation (3.3.37) in terms of these two new variables. Interchange the order of integration so that the omega integration is performed last, and express the integral from $-\infty$ to $+\infty$ as double

94

the value of an integral from 0 to $+\infty$. After these steps, the general formula for variance can be expressed as an integral over omega. The power spectral density is related to the variance as

$$\begin{bmatrix} \phi^2 \\ \chi^2 \end{bmatrix} = \frac{1}{\pi} \int_0^\infty d\omega \, F(\omega) \,. \tag{3.3.53}$$

Using this relation, the temporal power spectral density can be identified in the equation that was just derived. The one-sided power spectral density for a collimated beam is given by

$$F(\omega) = 1.303 k_o^2 \omega \int_0^L dz \, \frac{C_n^2(z)}{v^2(z)} \int_0^\infty \frac{c\,dc\; U(1-c)}{\sqrt{c^2-1}} \, f\left[\frac{\omega c}{v(z)}\right]$$

$$\times \left\{ \begin{array}{l} \cos^2\left[\dfrac{\omega^2 c^2(z-L)}{2v^2(z)k_o}\right] \\[2ex] \sin^2\left[\dfrac{\omega^2 c^2(z-L)}{2v^2(z)k_o}\right] \end{array} \right\} \prod_i F_i\left[\frac{\omega c}{v(z)}, z\right]. \tag{3.3.54}$$

Similarly, the power spectral density for a beam focused at S is given by

$$F(\omega) = 1.303 k_o^2 \omega \int_0^L dz \, \frac{C_n^2(z)}{v^2(z)} \int_0^\infty \frac{c\,dc\; U(1-c)}{\sqrt{c^2-1}} \, f\left[\frac{\omega c}{v(z)}\right]$$

$$\times \left\{ \begin{array}{l} \left[\dfrac{z}{S}\right]^{5/3} \cos^2\left[\dfrac{\omega^2 c^2 S(S-z)}{2v^2(z)k_o S}\right] \\[2ex] \left[\dfrac{z}{S}\right]^{5/3} \sin^2\left[\dfrac{\omega^2 c^2 S(S-z)}{2v^2(z)k_o S}\right] \end{array} \right\} \prod_i F_i\left[\frac{\omega c}{v(z)}, z\right]. \tag{3.3.55}$$

The power spectral density for a beam focused at $z = 0$ is given by

$$F(\omega) = 1.303 k_o^2 \omega \int_0^L dz \, \frac{C_n^2(z)}{v^2(z)} \int_0^\infty \frac{c\,dc\; U(1-c)}{\sqrt{c^2-1}} \, f\left[\frac{\omega c}{v(z)}\right]$$

$$\times \left\{ \begin{array}{l} \left(\dfrac{S-z}{S}\right)^{5/3} \cos^2\left[\dfrac{\omega^2 c^2 zS}{2v^2(z)k_o(z-S)}\right] \\[2ex] \left(\dfrac{S-z}{S}\right)^{5/3} \sin^2\left[\dfrac{\omega^2 c^2 zS}{2v^2(z)k_o(z-S)}\right] \end{array} \right\} \prod_i F_i\left[\frac{\omega c}{v(z)}, z\right]. \tag{3.3.56}$$

This technique can be used to find the error spectrum caused by a servo system that tries to correct an adaptive-optics system for turbulence. If there is a servo system with filter function given by $F_i\left[\frac{\omega x}{v(z)}, z\right]$, the residual spectrum of the system is easy to find. Cases for simple servo system filter functions are derived in Section 3.5.8.

The important equations developed in this section that are repeatedly used to solve turbulence problems are summarized in Table A in part i.

3.4 FILTER FUNCTIONS

In the last section, general expressions for the phase and log-amplitude variance, structure functions, and power spectral density were derived. To solve a specific problem, it is still necessary to insert the filter functions that modify the transverse spatial spectrum to determine the structure function. In this section, the filter functions for various operations on the phase and scintillation are derived. There is not a standard nomenclature for these filter functions. In this report, the complex filter function that operates on the field quantities will be called "the complex filter function." The absolute value squared of the complex filter function that is used to multiply the spectrum of turbulence will simply be called "the filter function."

Circular apertures are the primary focus of this report, and filter functions applicable to them are derived. Filter functions for other aperture shapes such as rectangular can be derived, but not here. Mks units are generally used throughout this report and the filter functions that are derived here will yield phase variance as radians squared and angles as radians squared. If the units are not Mks, they are stated explicitly. First, filter functions will be derived to extract any Zernike polynomial from the phase. For adaptive-optics systems, anisoplanatism is important, and filter functions for the various kinds of anisoplanatism will be derived. Finally, the filter functions for distributed and point sources will be found.

For circular apertures, the following relations for Bessel functions are repeatedly used.

The recurrence relations for Bessel functions are

$$\frac{d\left[r^{p} J_{p}(ar) \right]}{dr} = ar^{p} J_{p-1}(ar).$$ (3.4.1)

and

$$\frac{d}{dr}\left[\frac{J_{p}(ar)}{r^{p}} \right] = -\frac{a}{r^{p}} J_{p+1}(ar).$$ (3.4.2)

From this, two special cases are found as

$$\frac{d\left[rJ_{1}(ar) \right]}{dr} = arJ_{0}(ar),$$ (3.4.3)

and

$$\frac{d}{dr}\left[J_{0}(ar) \right] = -aJ_{1}(ar).$$ (3.4.4)

The following integral is also used

$$J_{0}(r) = \frac{1}{2\pi} \int_{0}^{2\pi} d\varphi \exp\left[i(r\cos\varphi) \right] = \frac{1}{2\pi} \int_{0}^{2\pi} d\varphi \cos(r\cos\varphi)$$

$$= \frac{1}{2\pi} \int_{0}^{2\pi} d\varphi \cos(r\sin\varphi).$$ (3.4.5)

3.4.1 Zernike Components of the Spectrum

Often one wants to extract or subtract a Zernike mode from the phase. The filter functions to do this are easily obtained from the spectral representation of the Zernike polynomials over a circular aperture of diameter D given in Noll.[12] The expressions in Noll are for an aperture of unit diameter and they are modified to apply to an aperture of diameter D. The definition of the Zernike polynomials are

$$Z(m, n)_{even} = \sqrt{n+1} \, R_{n}^{m}(rD/2)\sqrt{2} \cos m\theta,$$ (3.4.6)

and

$$Z(m, n)_{odd} = \sqrt{n+1} \, R_{n}^{m}(rD/2)\sqrt{2} \sin m\theta.$$ (3.4.7)

For the above two relations, $m \neq 0$. The odd and even subscripts give the x and y components of the distortion. In addition,

$$Z(0, n) = \sqrt{n+1} \, R_{n}^{0}(rD/2).$$ (3.4.8)

The radial function is given by

$$R_n^m(rD/2) = \sum_{q=0}^{(n-m)/2} \frac{(-1)^q}{q!} \frac{(n-q)!\,(rD/2)^{n-2q}}{[(n+m)/2 - q]!\,[(n-m)/2 - q]!} \cdot \qquad (3.4.9)$$

There are requirements that $\qquad\qquad m \le n, \qquad\qquad\qquad\qquad (3.4.10)$

and $\qquad\qquad\qquad\qquad |n| - m \qquad\qquad$ is even. $\qquad (3.4.11)$

The reason these polynomials are of interest is that they correspond to the common optical aberrations one encounters. $Z(0, 0)$ is the piston, $Z(1, 1)$ is the tilt, $Z(0, 2)$ is focus, $Z(2, 2)$ is astigmatism, $Z(1, 3)$ is coma, and $Z(0, 4)$ is third-order spherical distortion.

The Zernike polynomials defined above are orthogonal over the aperture. The following relation expresses that fact

$$\int d\vec{r}\; Z(m, n)Z(m', n')W(\vec{r}) = \delta_{mm'}\,\delta_{nn'} \;, \qquad (3.4.12)$$

where the aperture function has a finite value over the aperture. Expressed in terms of the unit step, it is

$$W(\vec{r}) = \frac{4U(D/2 - |\vec{r}|)}{\pi D^2} \,. \qquad (3.4.13)$$

The coefficients of the expansion of a phase function are given by

$$a(m, n) = \int d\vec{r}\; W(\vec{r})\varphi(\vec{r})Z(m, n) \,. \qquad (3.4.14)$$

For turbulence, the expansion coefficients can be considered to be Gaussian random variables, and the variance of the coefficients is given by

$$\langle a(m, n)a^*(m, n)\rangle = \iint d\vec{r}\; d\vec{r}'\; W(\vec{r})W(\vec{r}')C(\vec{r}, \vec{r}')Z'(m, n)Z^*(m, n). \qquad (3.4.15)$$

where $C(\vec{r}, \vec{r}')$ is the covariance of the phase function. The prime on the Zernike term indicates that it is a function of the primed coordinate system. In Fourier transform space this can be written as

$$\langle a(m, n)a^*(m, n)\rangle = \iint d\vec{\kappa}\; d\kappa'\; G_{m, n}(\vec{\kappa})f'(\kappa', \vec{\kappa}')\delta(\vec{\kappa} - \kappa')G^*_{m, n}(\vec{\kappa}'). \qquad (3.4.16)$$

The delta function is the result of the fact that there is no correlation of different wavenumbers in the turbulence spectrum — a fact that follows from the assumption that the turbulence can be represented as a random process with stationary increments, thereby, allowing the covariance

98

function to be written as a function solely of the difference of the coordinates. $G_{m,n}(\vec{\kappa})$ is the Fourier transform of the Zernike polynomial, $Z(m, n)$. Performing the integration over kappa prime, one obtains

$$\langle(a(m, n)\, a^*(m, n)\rangle = \int d\vec{\kappa}\; G_{m,n}(\vec{\kappa}) G^*_{m,n}(\vec{\kappa}) f'(\vec{\kappa}),\qquad (3.4.17)$$

where $f'(\vec{\kappa})$ is the spectral density of the turbulence. This expression shows that the Zernike components of the phase can be extracted by multiplying the turbulence spectrum by a filter function. Noll shows that the Fourier transforms of the Zernike polynomials are

$$\left.\begin{array}{l} G_{even\,m,\,n}(\vec{\kappa}) \\ G_{odd\,m,\,n}(\vec{\kappa}) \\ G_{m,\,n}(\vec{\kappa}) \end{array}\right\} = \sqrt{n+1}\,\frac{2 J_{n+1}(\kappa D/2)}{\kappa D/2}\left\{\begin{array}{l} (-1)^{(n-m)/2} i^n \sqrt{2}\,\cos(m\varphi), \\ (-1)^{(n-m)/2} i^n \sqrt{2}\,\sin(m\varphi), \\ (-1)^{n/2}\quad (m=0). \end{array}\right.\qquad (3.4.18)$$

These are the complex filter functions to extract the Zernike polynomials components. Therefore, in order to extract a given rms Zernike component from the phase, the Fourier spectrum of the phase must be multiplied by the absolute value squared of these complex filter functions. The absolute value squared of each Zernike component is

$$\left.\begin{array}{l} F_{even\,m,\,n}(\vec{\kappa}) \\ F_{odd\,m,\,n}(\vec{\kappa}) \\ F_{m,\,n}(\vec{\kappa}) \end{array}\right\} = (n+1)\left[\frac{2 J_{n+1}(\kappa D/2)}{\kappa D/2}\right]^2\left\{\begin{array}{l} 2\cos^2(m\varphi), \\ 2\sin^2(m\varphi), \\ 1\quad (m=0). \end{array}\right.\qquad (3.4.19)$$

Of particular interest in many problems are the piston and tilt filter functions. Two representations of these filter functions will be given. For the piston, the first representation gives the filter function that extracts the phase variance due to piston. In the second representation, the filter function extracts the physical distance due to this piston. For the tilt, the first filter function extracts the phase variance due to tilt, and the second extracts the angle in real space of this tilt. For different problems, one or the other representation is appropriate. All the filter functions will be represented by the same symbol, $F(\vec{\kappa}, z)$. The piston phase variance filter function is given by the condition $n = m = 0$ and is equal to

$$F(\vec{\kappa}, z) = \left[\frac{2 J_1(\kappa D/2)}{\kappa D/2}\right]^2.\qquad (3.4.20)$$

This filter function extracts the phase variance due to piston. To obtain the second representation that extracts the piston itself, the filter function would have to be divided by the wavenumber squared to give

$$F(\vec{\kappa}, z) = \left(\frac{1}{k_o}\right)^2 \left[\frac{2 J_1(\kappa D / 2)}{\kappa D / 2}\right]^2. \qquad (3.4.21)$$

The piston is also the average value of the quantity over the aperture; therefore, this filter function can be used to calculate effects such as aperture averaging of scintillation or the twinkling of stars and planets.

The filter function to determine the phase variance from tilt is given by the term $n = m = 1$ and is equal to

$$\left.\begin{array}{c} F_x(\vec{\kappa}, z) \\ F_y(\vec{\kappa}, z) \end{array}\right\} = \left[\frac{4 J_2(\kappa D / 2)}{\kappa D / 2}\right]^2 \left\{\begin{array}{l} \cos^2(\varphi), \\ \sin^2(\varphi). \end{array}\right. \qquad (3.4.22)$$

The two–axis tilt phase variance filter function is given by the sum of the two components and is

$$F(\vec{\kappa}, z) = \left[\frac{4 J_2(\kappa D / 2)}{\kappa D / 2}\right]^2. \qquad (3.4.23)$$

Very often, one wants the second representation that extracts the tilt variance (angle in real space). In that case, the phase variance from the tilt must be averaged over the aperture. One finds that the filter function to calculate the tilt is a factor of $(4/k_o D)^2$ times the phase variance filter function and is given by

$$F(\vec{\kappa}, z) = \left(\frac{16}{k_o D}\right)^2 \left[\frac{J_2(\kappa D / 2)}{\kappa D / 2}\right]^2. \qquad (3.4.24)$$

The x and y components in this case are

$$\left.\begin{array}{c} F_x(\vec{\kappa}, z) \\ F_y(\vec{\kappa}, z) \end{array}\right\} = \left(\frac{16}{k_o D}\right)^2 \left[\frac{J_2(\kappa D / 2)}{\kappa D / 2}\right]^2 \left\{\begin{array}{l} \cos^2(\varphi), \\ \sin^2(\varphi). \end{array}\right. \qquad (3.4.25)$$

100

In some problems, the total phase variance is calculated, and one would like the variance with some Zernike modes removed. This is easily done by subtracting the phase variance due to these components from the total variance. For instance the filter function to remove piston and tilt is

$$F(\vec{\kappa}, z) = 1 - \left[\frac{2 J_1(\kappa D / 2)}{\kappa D / 2}\right]^2 - \left[\frac{4 J_2(\kappa D / 2)}{\kappa D / 2}\right]^2 . \qquad (3.4.26)$$

Implicit in the expression above is the requirement that the cross product terms of the piston and the tilt average in some way to zero. In calculating the phase variance over an aperture, this is true because the Zernike polynomials are orthogonal over the aperture. The situation is not so simple if this is applied to the structure function. In the expression in Equation (3.2.4), the aperture average is of the exponential of the structure function. For this case one cannot use the orthogonality condition to eliminate the cross product terms. Another way of eliminating these terms is to assume that the ensemble average of these terms is zero. This assumption is true only if the Zernike polynomials are also the Karhunen-Loève polynomials of the problem. Unfortunately they are not, but for the low order Zernike modes they are very close to those polynomials. Therefore, the assumption that these terms are zero produces a small error that is less than 10% in calculating the Strehl ratio. This problem is discussed again in Section 3.4.5.

The filter functions to extract the tilt over an annular aperture with inner diameter D_i has been found by Shelton[13] to be

$$F(\vec{\kappa}, z) = \left(\frac{16}{k_o D[1 - \beta^4]}\right)^2 \left[\frac{J_2(\kappa D / 2)}{\kappa D / 2} - \beta^3 \frac{J_2(\kappa \beta D / 2)}{\kappa \beta D / 2}\right]^2, \qquad (3.4.27)$$

where $\beta = D_i / D.$ $\qquad (3.4.28)$

3.4.2 Gradient Tilt

The Zernike component of tilt is also referred to as the Z-tilt. Some tilt sensors respond to this tilt while others respond to a quantity that is closer to the Gradient tilt. For instance, if the

101

individual tilts measured in each subaperture by a wavefront sensor are averaged together, then a quantity that is close to the average transverse gradient of the wavefront across the aperture, which is called the gradient or G-tilt, is the result of the measurement. The definition of this quantity is

$$G - \text{Tilt} = \frac{4}{\pi k_o^2 D^2} \int d\vec{r} \, \nabla_t \Phi(\vec{r}),$$ (3.4.29)

where the integration is over the circular aperture. The calculation of the G-tilt is equivalent to calculating the average piston of the phase gradient. This can be calculated in transform space by multiplying the piston component of the phase by $i\kappa/k_o$ and taking the absolute value squared of the quantity to give

$$F(\vec{\kappa}, z) = \left(\frac{4}{k_o D} \right)^2 J_1^2(\kappa D / 2).$$ (3.4.30)

The x and y components of this tilt are

$$\left. \begin{array}{c} F_x(\vec{\kappa}, z) \\ F_y(\vec{\kappa}, z) \end{array} \right\} = \left(\frac{4}{k_o D} \right)^2 J_1^2(\kappa D / 2) \begin{cases} \cos^2(\varphi), \\ \sin^2(\varphi). \end{cases}$$ (3.4.31)

The filter function to calculate the phase variance due to G-tilt is obtained using the same arguments as above, to give

$$F(\vec{\kappa}, z) = J_1^2(\kappa D / 2).$$ (3.4.32)

The x and y components of this tilt variance are

$$\left. \begin{array}{c} F_x(\vec{\kappa}, z) \\ F_y(\vec{\kappa}, z) \end{array} \right\} = J_1^2(\kappa D / 2) \begin{cases} \cos^2(\varphi), \\ \sin^2(\varphi). \end{cases}$$ (3.4.33)

The G-tilt filter function for an annular aperture has also been found by Shelton to be

$$F(\vec{\kappa}, z) = \left(\frac{4}{k_o D [1 - \beta^2]} \right)^2 \left[J_1(\kappa D / 2) - \beta J_1(\kappa \beta D / 2) \right]^2.$$ (3.4.34)

If the derivations are repeated for spherical waves, then one finds that κD *has to be replaced by* $\kappa D(z)$ *in all the filter functions.*

3.4.3 Anisoplanatic Effects

Anisoplanatism is an effect encountered in an adaptive-optics system in which the beacon return propagates down a different path than the outgoing laser beam. Therefore, to derive the filter function, the difference between the Fourier transforms of the quantity of interest at each point on the path must be found. Since a displacement in real space is equivalent to a phase shift in spatial transform space as shown in Equations (3.3.45), the only difference between the quantities along the two paths is a phase shift that can vary in the propagation direction if the displacement changes. Therefore, the filter function to be applied to the phase for each realization is unity minus this phase shifted term. The filter function due to this difference in paths through the turbulence is the absolute magnitude squared of that quantity and is given by

$$F(\vec{\kappa}, z) = \left|1 - \exp\left[i\vec{\kappa} \cdot \vec{d}(z)\right]\right|^2 = 2\left[1 - \cos\left\{\vec{\kappa} \cdot \vec{d}(z)\right\}\right]. \quad (3.4.35)$$

There are several reasons why the paths can be different as shown in Figure 3.5, and this leads to different functional dependencies for d.

If the two paths are displaced a constant amount, d is a constant, and the path displacement is given by

$$\vec{d}(z) = \vec{d}. \quad (3.4.36)$$

If the two paths coincide at the origin but differ by a constant angle, Θ, the path displacement is given by

$$\vec{d}(z) = \vec{\Theta} z. \quad (3.4.37)$$

If there is a time delay, τ, that is short compared to the turbulence mixing time and the Taylor frozen turbulence assumption is valid, the displacement in this case is given by

$$\vec{d}(z) = \vec{v}(z)\tau. \quad (3.4.38)$$

If the beacon beam that senses the turbulence has a different wavelength than the laser beam that is sent out, the two-beam will take different paths through the atmosphere because of its dispersive properties. The analysis given here parallels that given by Belsher and Fried.[14] Geometric optics is used to obtain the path displacement for chromatic anisoplanatism. To
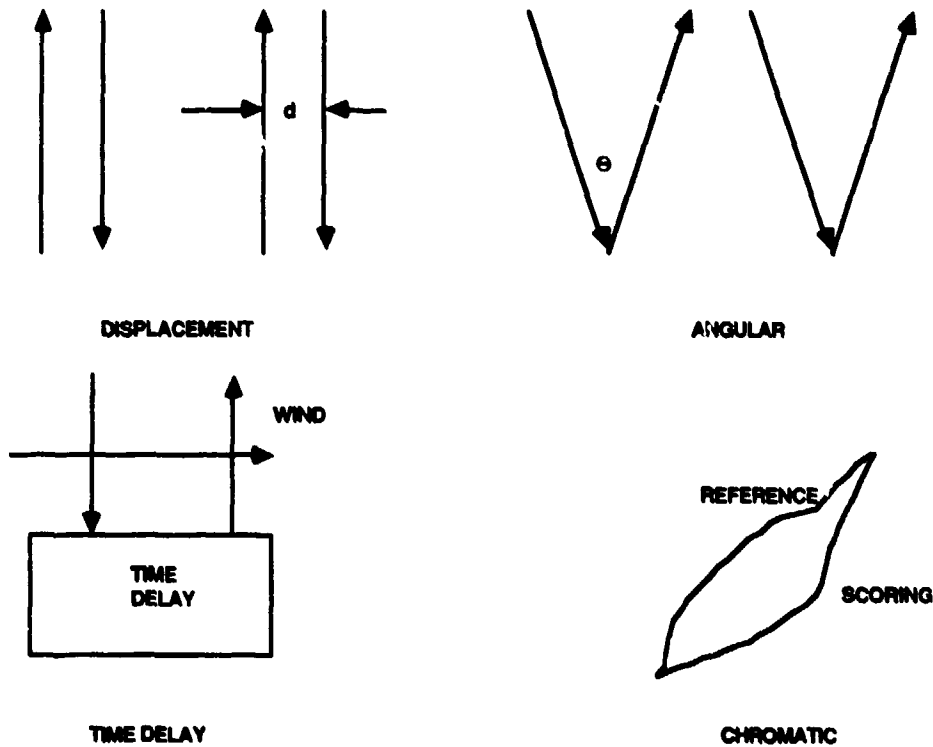
Figure 3-5. Various types of anisoplanatism.

reach an exoatmospheric target, it will be assumed that the rays at different colors are propagating at the same angle at the target. Even for near-earth targets, this is a good approximation as is shown in detail in Section 3.9.3.4. If $n(h)$ is the refractive index seen by the first wave, and $n(h) + \Delta n(h)$ is that seen by the second, and $\xi(h)$ is the zenith angle of the first, and $\xi(h) + \Delta\xi(h)$ is that of the second, Snell's law which states that $n \sin(\xi)$ is a constant gives

$$\Delta\xi(h) = -\Delta n\ (h)\tan[\xi\ (h)]. \tag{3.4.39}$$

This can be integrated along the path to yield

$$\vec{d}(z) = \int_0^z dz\ \Delta\vec{\xi}(h) = -\frac{\xi\ \sin(\xi)\ \Delta n_o}{\xi\ \cos^2(\xi)} \int_0^z dx\ \alpha(x). \tag{3.4.40}$$

where Δn_o is the difference in refractive index between the two colors at wavelengths λ_1 and λ_2 when the wavelengths are given in micrometers, and $\alpha(x)$ is the normalized air density

104

versus altitude. These functions have been approximated by Belsher as

$$\Delta n_o = \left(\lambda_1^2 - \lambda_2^2 \right) \left[\frac{29498.1}{\left(146\,\lambda_2^2 - 1 \right)\left(146\,\lambda_1^2 - 1 \right)} + \frac{255.4}{\left(41\lambda_2^2 - 1 \right)\left(41\lambda_1^2 - 1 \right)} \right] 10^{-6}. \quad (3.4.41)$$

$$\alpha(h) = \exp\left[-1.11 \times 10^{-4} h \right] \quad h < 10 \text{ km},$$

$$\alpha(h) = 1.6 \exp\left[-1.57 \times 10^{-4} h \right] \quad h > 10 \text{ km}. \quad (3.4.42)$$

A plot of the absolute value of the difference of refractive index between a wave at 0.5 micrometers and other wavelengths is shown in Figure 3-6.
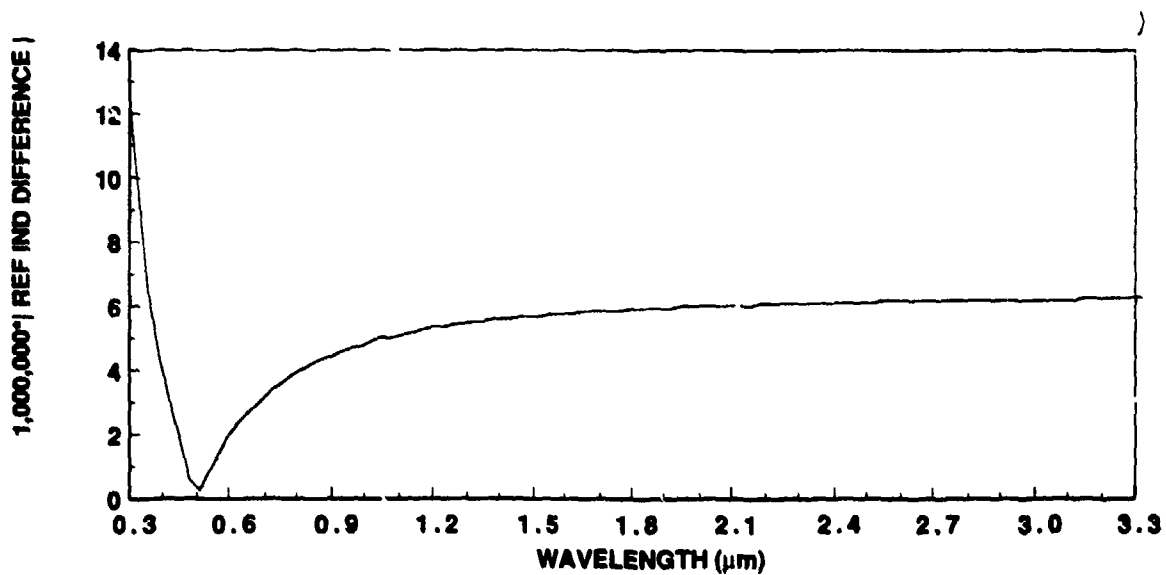
Figure 3-6. *Difference in refractive index between 0.5μm and another wavelength.*

105

The normalized air density versus height is plotted in Figure 3-7.
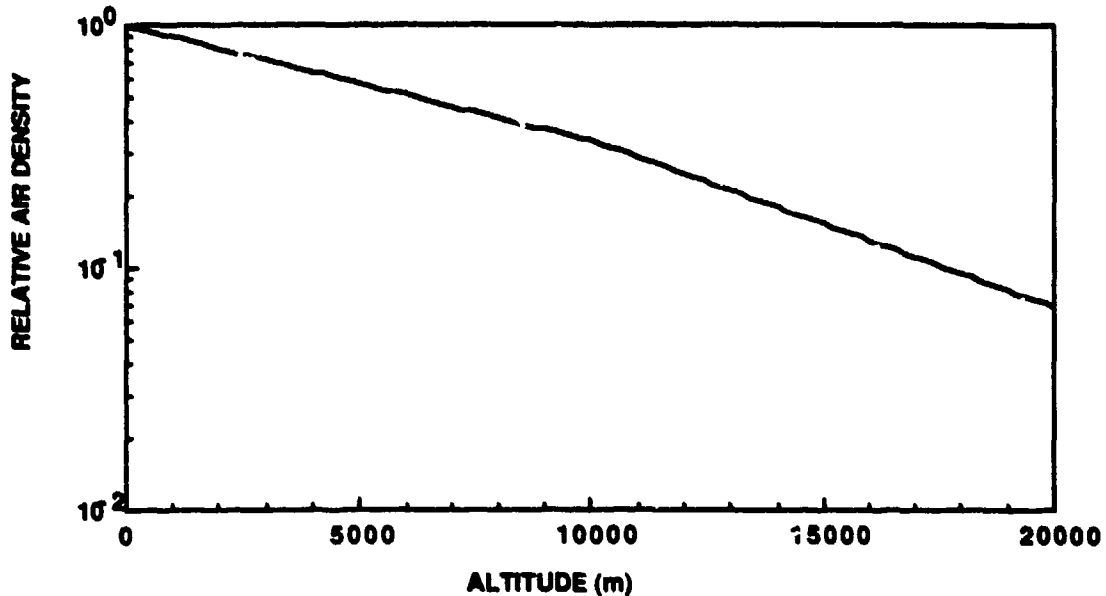
Figure 3-7. Normalized air density versus altitude.

3.4.4 Distributed Sources

Distributed sources are of interest for many problems. The light from a planet is from a source of finite size, and this has to be taken into account if one wants to calculate the phase or scintillation from that source. For many adaptive-optics systems, the beacon source or reflector is a point source or a distributed source and the corrected signal is a collimated beam. The question that arises in this case is how much does the difference in the paths of the beacon signal and the corrected beam affect the phase variance on the corrected beam. The variances due to this effect vary over the diameter of the aperture and are not spatially stationary. For that reason a structure function that depends solely on the difference in aperture positions cannot be written down for this problem. However, one can still calculate the average variances over the aperture. In adaptive-optics systems, the phase variance is small, and Maréchal's formula can be used to determine how much the Strehl ratio is degraded by this effect.

106

Consider a point source beacon at a height H displaced from the center of the aperture by a distance $\vec{b}$ as shown in Figure 3-8.
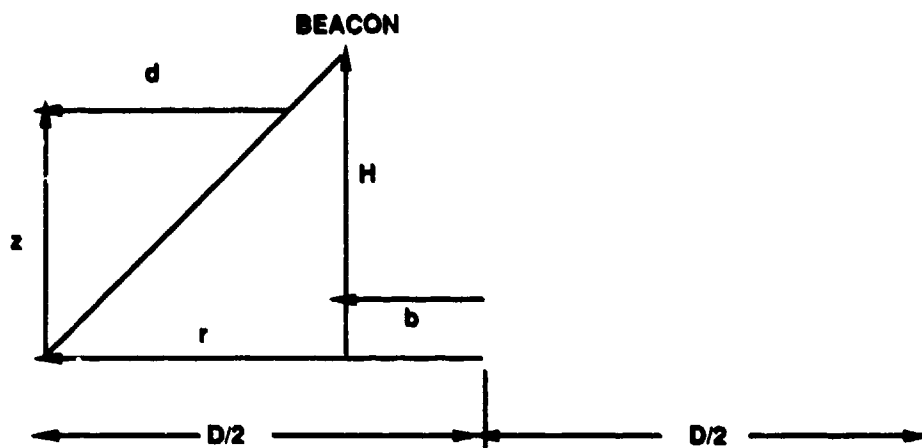
Figure 3-8. Geometry of a point source beacon.

If $\vec{r}$ is the position of a ray coming from the aperture, the anisoplanatic distance from the collimated ray coming from that point is

$$\vec{d} = \frac{z}{H}(\vec{r} - \vec{b}).$$

(3.4.43)

The above relation can be used to find the phase variance at any point in the aperture. This phase variance must be averaged over the aperture to obtain the filter function for the average variance due to a displaced point source compared to a collimated beam. The filter function is equal to

$$F(\vec{\kappa}, z) = \frac{8}{\pi D^2} \int_{\text{aperture}} d\vec{r} \left[1 - \cos\left(\vec{\kappa} \cdot \frac{z}{H}[\vec{r} - \vec{b}] \right) \right].$$

(3.4.44)

This filter function produces the phase variance with all the Zernike components included. If one wanted to obtain the phase variance with some of these modes removed, this expression would be multiplied by another filter function that removed these components in the manner described earlier.

107

The integral over angle in the aperture can be performed using Equation (3.4.5) since

$$I = \int_0^{2\pi} d\varphi \cos[a\cos(\varphi) + c] = \mathrm{Re} \int_0^{2\pi} d\varphi \exp[i\{a\cos(\varphi) + c\}] = 2\pi\cos(c)J_0(a).$$

$$(3.4.45)$$

Equation (3.4.44) becomes $\quad F(\vec{\kappa}, z) = \dfrac{16}{D^2} \displaystyle\int_0^{D/2} r\, dr \left[1 - J_0\!\left(\dfrac{\kappa z}{H}\right) \cos\!\left(\vec{\kappa} \cdot \dfrac{\vec{b}z}{H}\right)\right].$ $\quad$ (3.4.46)

If there are no other filter functions in the problem that depend on the angle in κ-space, the integral over angle can be performed using Equation (3.4.5) to give for the normalized filter function the expression

$$F(\vec{\kappa}, z) = \frac{16}{D^2} \int_0^{D/2} r\, dr \left[1 - J_0\!\left(\frac{\kappa z}{H}\right) J_0\!\left(\frac{\kappa b z}{H}\right)\right].$$

$$(3.4.47)$$

The integral over radius can be performed to give

$$F(\vec{\kappa}, z) = 2\left[1 - \frac{2 J_1\!\left(\dfrac{\kappa D z}{2H}\right)}{\dfrac{\kappa D z}{2H}} J_0\!\left(\frac{\kappa b z}{H}\right)\right].$$

$$(3.4.48)$$

For a point source over the center of the aperture with everything symmetric, the filter function is

$$F(\vec{\kappa}, z) = 2\left[1 - 2\frac{J_1\!\left(\dfrac{\kappa D z}{2H}\right)}{\dfrac{\kappa D z}{2H}}\right].$$

$$(3.4.49)$$

The effect caused by the difference in the paths between a focused and collimated beam is referred to as focal anisoplanatism. A distributed source as shown in Figure 3-9 is now considered in which the source points are incoherent with respect to each other. This case would correspond to the physically interesting cases of a reflection from a corner-cube array or a diffuse plate, or the return from a planet.

108
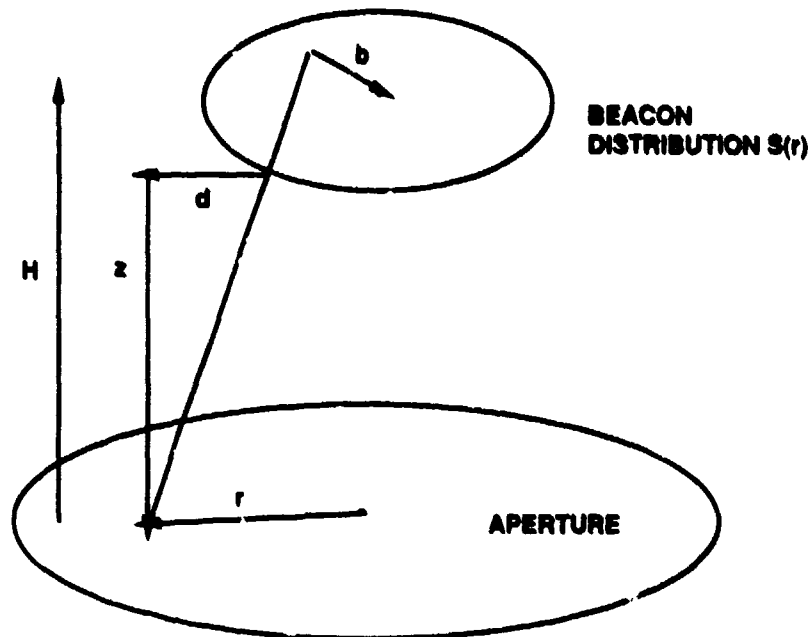
Figure 3-S. Geometry of the distributed beacon source.

To determine the filter function, consider the effect of each point in the source on a Hartmann sensor that measures the phase gradient or intensity. Each point gives a tilt or intensity, and these are added together incoherently, weighed by the source intensity. Integrating over the source intensity, normalizing, and taking the absolute value squared gives the variance at a point in the aperture. If the normalized result is subtracted from unity before taking the absolute value squared, then one obtains the variance due to the difference between a distributed source and a collimated beam. If these expressions are then averaged over the aperture, one obtains the average phase variance filter function of a circular source offset from boresight by $\vec{b}$. For the distributed source $S(\vec{r})$ the filter function is

$$F(\vec{K}, z) = \frac{4}{\pi D^2} \int d\vec{r} \left| \frac{4}{\pi D^2} \frac{\int_{source} d\vec{r}'' \, S(\vec{r}'') \exp\left[i\vec{K} \cdot \frac{z}{H}(\vec{r} - \vec{r}'' - \vec{b}) \right]}{\int_{source} d\vec{r}'' \, S(\vec{r}'')} \right|^2 . \qquad (3.4.50)$$

For a uniform circular source distribution of diameter D_s that is on boresight, the integrations can be carried out to give

$$F(\vec{\kappa}, z) = \left[2\frac{J_1(\kappa D_s z / 2H)}{\kappa D_s z / 2H}\right]^2. \qquad (3.4.51)$$

For the isoplanatic case, the filter function for the difference between a collimated beam and a distributed source is

$$F(\vec{\kappa}, z) = \frac{4}{\pi D^2}\int d\vec{r} \left|1 - \frac{4}{\pi D^2}\frac{\int_{source} d\vec{r}' \, S(\vec{r}')\exp\left[i\vec{\kappa} \cdot \frac{z}{H}(\vec{r} - \vec{r}' - \vec{b})\right]}{\int_{source} d\vec{r}' \, S(\vec{r}')}\right|^2 \cdot \qquad (3.4.52)$$

If a uniform circular source distribution is assumed, the integrations can be carried out to give

$$F(\vec{\kappa}, z) = 1 - \frac{4 J_1(Dx)}{Dx}\frac{2 J_1(D_s x)}{D_s x}\cos\left(\vec{\kappa} \cdot \frac{z\vec{b}}{H}\right) + \left[2\frac{J_1(D_s x)}{D_s x}\right]^2, \qquad (3.4.53)$$

where
$$x = \frac{\kappa z}{2H}. \qquad (3.4.54)$$

If there are no other filter functions in the problem that depend on the angle in κ-space, the integral over angle can be performed using Equation (3.4.5) to give the normalized filter function

$$F(\vec{\kappa}, z) = 1 - \frac{4 J_1(Dx)}{Dx}\frac{2 J_1(D_s x)}{D_s x} J_0\left(\frac{\kappa b z}{H}\right) + \left[2\frac{J_1(D_s x)}{D_s x}\right]^2. \qquad (3.4.55)$$

If the offset is zero, the filter function is

$$F(\vec{\kappa}, z) = 1 - \frac{4 J_1(Dx)}{Dx}\frac{2 J_1(D_s x)}{D_s x} + \left[2\frac{J_1(D_s x)}{D_s x}\right]^2. \qquad (3.4.56)$$

3.4.5 Cascading Filter Functions

In the last section, the filter functions for Zernike components, anisoplanatism, and distributed sources have been calculated. In some problems, several effects are present at

110

once, and one would like to determine the quantities of interest for that case. Certainly it would be convenient if the filter functions can be multiplied together. Unfortunately, this is not always the case. The way to build up complicated filter functions is to use the approach in calculating the spectrum of the Zernike components in Equations (3.4.15) to (3.4.16). In deriving the spectrum of the turbulence with a Zernike mode extracted as simply the product of the turbulence spectrum and the Zernike spectrum, one had to assume that the correlation function of the turbulence had stationary increments. In a similar way, one can derive the spectrum with anisoplanatic effects as the product of the turbulence spectrum and the anisoplanatic filter function. The spectrum of isoplanatism for the effects considered also has stationary increments. This new spectrum can be used as the basis to have the Zernike modes extracted by simply multiplying by the Zernike spectrum. For this type of problem, the filter functions can be simply cascaded.

After the Zernike mode is extracted, the spectrum may no longer have stationary increments. Tilt removal does not affect the phase at the center of the aperture at all but it greatly reduces the variance at the aperture edges. For this component, the residual spectrum is no longer stationary. The problem arises if one wants to multiply this spectrum by another that is also not stationary. Then the assumption that the Fourier transform of the covariance function can be written as a delta function is no longer valid. A case of practical interest is to find the phase variance for focal anisoplanatism and this is considered in Section 3.5.9.

To summarize, anisoplanatic effects, turbulence, distributed sources and piston related effects can be calculated by cascading their filter functions. Also, anisoplanatic effects, turbulence, and any Zernike effect can be calculated by cascading their filter functions. The effects of distributed sources and Zernike modes cannot be calculated exactly simply by cascading their filter functions.

The main filter functions that are used repeatedly in solving turbulence problems are listed in Tables B, C, D, and E in part 1.

111

3.4.6 Fitting Error

In an adaptive-optics system, the mirror has a finite number of actuators that results in an inability to correct for the high spatial frequency turbulence. This effect is referred to as fitting error. It is not stationary, since a perfect correction can be made at the mirror piston positions but an error is made in the intermediate mirror locations. Nevertheless, the effect of fitting error can be calculated by using an appropriate filter function. The parameters of the filter function can be chosen to give the fitting error variance obtained for various types of deformable mirrors by Belsher.[15] This filter function can be combined with other filter functions describing other defects in the adaptive-optics system to get an overall phase variance.

3.5 SINGLE PARAMETER PROBLEMS

In this section, turbulence problems that can be represented in terms of one parameter are treated. The calculation is very simple, being comprised of an integration over angle, a change of variables, and a table lookup. Some of the problems presented in these sections are much more difficult to solve by conventional techniques.

Turbulence moments are used in the calculations. Analytic expressions for the turbulence moments for the Hufnagel-Valley model are calculated in Appendix C. The definition of the complete moment is

$$\mu_n = \int_0^\infty C_n^2(z)\, z^n \; dz = \sec^{n+1}(\xi) \int_0^\infty C_n^2(h)\, h^n \; dh, \tag{3.5.1}$$

where ξ is the zenith angle. Define the upper and lower partial moments in the following way for a distance L which is at a height H where

$$L = \sec(\xi)H \quad \text{as} \tag{3.5.2}$$

$$\mu_n^+(L) = \int_L^\infty C_n^2(z)\, z^n \; dz = \sec^{n+1}(\xi) \int_H^\infty C_n^2(h)\, h^n \; dh; \tag{3.5.3}$$

112

and

$$\mu_{\Gamma_n}(L) = \int_0^L C_n^2(z) z^n dz = \sec^{n+1}(\xi) \int_0^H C_n^2(h) h^n dh. \qquad (3.5.4)$$

The zenith dependence for all problems only appears in the moments, and is incorporated in them rather than being expressed explicitly. The coherence diameter and anisoplanatic angle written in terms of moments are equal to

$$r_o^{-5/3} = 0.423 \, k_o^2 \mu_o; \qquad (3.5.5)$$

and

$$\Theta_o^{-5/3} = 0.91 \, k_o^2 \mu_{5/3}. \qquad (3.5.6)$$

The values of the coherence diameter and isoplanatic angle for a wavelength of 0.5 micrometers are plotted versus the W parameter in Figure 3-10.
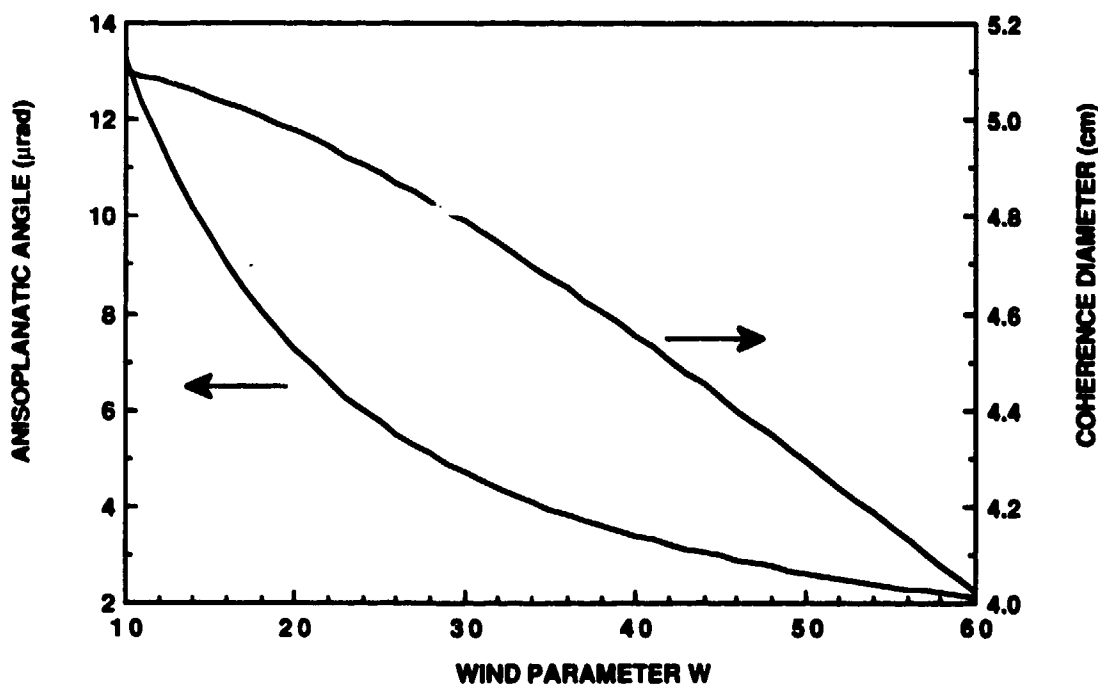
Figure 3-10. Coherence diameter and isoplanatic angle versus the Hufnagel-Valley wind parameter with $A = 1.7 \times 10^{14}$.

Useful turbulence moments at zenith for various turbulence models are given in Table 3-1. The values of the coherence diameter and anisoplanatic angle apply to a wavelength of 0.5 μm. The moment at any zenith angle can be found by multiplying by the appropriate zenith dependence given in Equation (3.5.1).

TABLE 3-1				
Turbulence Moments for Various Models				
	SLCDAY	SLCNIGHT	HV-21	HV-54
r_0 (cm)	4.98	10.1	4.96	4.18
Θ_0 (μrad)	11.8	12.9	6.9	2.40
μ_0	2.22×10^{-12}	6.84×10^{-13}	2.23×10^{-12}	2.97×10^{-12}
$\mu_{5/3}$	3.56×10^{-7}	3.07×10^{-7}	8.7×10^{7}	5.06×10^{-6}
μ_2	7.20×10^{-6}	6.13×10^{-6}	1.91×10^{-5}	1.16×10^{-4}
μ_4	1.02×10^{3}	8.32×10^{2}	3.18×10^{3}	2.08×10^{4}
$\mu_{14/3}$	6.06×10^{5}	4.91×10^{5}	1.91×10^{3}	1.25×10^{7}
$\mu_{5/6}$	3.4×10^{-10}	2.55×10^{-10}	5.45×10^{-10}	2.24×10^{-9}

3.5.1 Zernike-Tilt For Collimated And Focused Beams

First, consider the calculation of the Zernike tilt. In all the calculations of phase quantities, it will be assumed unless stated otherwise that diffraction effects are not important, and the approximation given in Equation (3.3.39) is valid. Using the filter function that is given in Equation (B.7) in Table B and the general formula for variance given in Equation (A.1) of Table A, one gets

$$T_Z^2 = 0.2073\, k_o^2 \int_0^L dz\ C_n^2(z) \int d\vec{\kappa}\ f(\kappa) \left(\frac{16}{k_o D}\right)^2 \left(\frac{J_2(\kappa D/2)}{\kappa D/2}\right)^2 . \quad (3.5.7)$$

114

Inner and outer scale effects are neglected in this section, and the turbulence spectrum is given by the approximation in Equation (A.6). The integrand in the second integral does not depend on the angle in kappa space nor on the axial coordinate. Integrating over this angle and over z using the relation for turbulence moments given in Equation (3.5.1), and making the substitution $x = \kappa D/2$ yields

$$T_Z^2 = \frac{105.1\,\mu_o}{D^{1/3}} \int_0^\infty dx\; x^{-11/3-1} J_2^2(x) = \frac{105.1\,\mu_o}{2\sqrt{\pi}\,D^{1/3}} \Gamma\left[\begin{matrix} s/2+2, \frac{1}{2}-s/2 \\ 3-s/2, 1-s/2 \end{matrix}\right]\Bigg|_{s=-\frac{11}{3}}$$

$$= \frac{105.1\,\mu_o}{2\sqrt{\pi}\,D^{1/3}} \Gamma\left[\begin{matrix} \frac{1}{6}, \frac{7}{3} \\ \frac{29}{6}, \frac{17}{6} \end{matrix}\right].$$

(3.5.8)

The integral is equal to the Mellin transform of the function given in Equation (F.6) evaluated at $s = -11/3$. The unusual notation for the Gamma function is defined in Equation (2.2.2) of part 2 and is equal to the ratio of the four individual Gamma functions. The evaluation of the Gamma function at noninteger values can be done on some hand calculators such as the Hewlett-Packard-15 by calculating the factorial of one less thar the argument. The composite Gamma function above is equal to 0.2052. Evaluating this expression, one obtains the standard result

$$T_Z^2 = \frac{6.08\,\mu_o}{D^{1/3}} = 0.3641 \left(\frac{D}{r_o}\right)^{5/3} \left(\frac{\lambda}{D}\right)^2.$$

(3.5.9)

Notice that the tilt goes to infinity as the diameter goes to zero. This singularity is removed by considering inner scale which is done in Section 3.6.5.

For a 0.6 meter diameter aperture and HV-21 turbulence, the rms tilt is 4 microradians. If the turbulence is constant along the path of length L, then the tilt variance is

$$T_Z^2 = \frac{6.08 C_n^2 L}{D^{1/3}}.$$

(3.5.10)

115

If the beam were focused at L, then the formula for focused waves in the bottom part of Equation (A.4) has to be used. Close to the focus, the argument of the cosine term is significant; however, the term multiplying it goes to zero at focus. Therefore, it is a good approximation to neglect the cosine term in calculating the tilt. Doing that the tilt variance is

$$T_Z^2 = \frac{6.08}{D^{1/3}} \int_0^L dz \ C_n^2(z) \frac{(L-z)^{5/3}}{L^{5/3}}. \tag{3.5.11}$$

If the turbulence is constant along the path, one obtains

$$T_Z^2 = \frac{6.08 C_n^2 L}{D^{1/3}} \left(\frac{3}{8}\right). \tag{3.5.12}$$

Therefore, the tilt variance is 37.5% of the collimated value and the rms tilt is 61% of the collimated value. The above results were derived by Tatarski and expressed in a different form.

3.5.2 Gradient-Tilt

In an exactly analogous fashion, the G-tilt integral can be found by putting the filter function given in Equation (C.4) into the general formula given in Equation (A.1) to obtain

$$T_G^2 = 0.2073 \ k_o^2 \int_0^L dz \ C_n^2(z) \int d\vec{\kappa} \ f(\kappa) \left(\frac{4}{k_o D}\right)^2 J_1^2(\kappa D/2). \tag{3.5.13}$$

After the same integrations, substitutions, and Mellin transforms as above, one obtains

$$T_G^2 = \frac{6.564 \ \mu_o}{D^{1/3} 2\sqrt{\pi}} \Gamma\left[\begin{matrix} \frac{1}{6}, \frac{4}{3} \\ \frac{17}{6}, \frac{11}{6} \end{matrix}\right] = \frac{5.675 \ \mu_o}{D^{1/3}} = 0.3399 \left(\frac{D}{r_o}\right)^{5/3} \left(\frac{\lambda}{D}\right)^2. \tag{3.5.14}$$

This gives a tilt that is 3.5% lower than the Z-tilt. This is the same result obtained by Ellerbroek.[16]

3.5.3 Difference Between Gradient-Tilt and Zernike-Tilt

Sometimes the position of a target is measured with a sensor that responds essentially to the G-tilt. The pointing system uses the tilt from this sensor to direct a beam at a target. The pointing of the telescope is the Zernike or Z-tilt. It is of interest to know what is the tilt jitter

116

expected at the target even if this process is performed perfectly. This problem has been analyzed by Yura and Travis[17] and they call it centroid anisoplanatism. The variance of the difference between G-tilt and Z-tilt can be found by taking the difference of their filter functions for each realization, squaring the result, and then putting this into the standard formula to give

$$T^2_{G-Z} = 0.2073 \, k_o^2 \int_0^L dz \; C_n^2(z) \int d\vec{\kappa} \; f(\kappa) \left(\frac{4}{k_o D}\right)^2 \left[\left(\frac{4 J_2(\kappa D / 2)}{\kappa D / 2}\right) - J_1(\kappa D / 2)\right]^2.$$

(3.5.15)

If the bracket is expanded, one obtains three terms, two are the sum of the Zernike and Gradient tilts. The third can be evaluated using the Mellin transforms in Equation (F.7) to obtain

$$T^2_{G-Z} = \frac{6.564 \, \mu_o}{D^{1/3} 2\sqrt{\pi}} \left\{ 16\Gamma\left[\begin{matrix} \frac{1}{6}, \frac{7}{3} \\ \frac{29}{6}, \frac{17}{6} \end{matrix}\right] + \Gamma\left[\begin{matrix} \frac{1}{6}, \frac{4}{3} \\ \frac{17}{6}, \frac{11}{6} \end{matrix}\right] - 8\Gamma\left[\begin{matrix} \frac{1}{6}, \frac{7}{3} \\ \frac{23}{6}, \frac{17}{6} \end{matrix}\right] \right\}.$$

(3.5.16)

If the Gamma functions are evaluated directly, since the terms in brackets almost cancel out, one requires five-place accuracy to achieve three-place accuracy in the final answer. Rather than doing that, the recurrence relation of Gamma functions given in Equation (2.2.4) of part 2 can be used to show that

$$T^2_{G-Z} = \frac{6.564 \, \mu_o}{D^{1/3} 2\sqrt{\pi}} \Gamma\left[\begin{matrix} \frac{1}{6}, \frac{4}{3} \\ \frac{17}{6}, \frac{11}{6} \end{matrix}\right] [1.07138 + 1 - 2.05348 \,].$$

(3.5.17)

This is equal to

$$T^2_{G-Z} = \frac{0.102 \, \mu_o}{D^{1/3}} = 0.0056 \left(\frac{D}{r_o}\right)^{5/3} \left(\frac{\lambda}{D}\right)^2.$$

(3.5.18)

The jitter will be one-third of a beamwidth when the aperture diameter is 6 times the coherence diameter. A more capable proposed adaptive-optics system with a 0.6-m aperture will be able to correct turbulence very well even if the diameter is 17 times the coherence length. If the turbulence were that severe, the Zernike minus Gradient tilt jitter would be equal to 0.66 microradians; therefore, care must be taken to assure that the tracker responds to Z-tilt.

This can be done for the wavefront sensor tracker by using the appropriate matrix to determine the tilt from the individual gradients measured in each subaperture.

3.5.4 Scintillations for Collimated and Focused Beams

To calculate the scintillation of a wave that propagates from 0 to L, use the filter function given in Equation (A.5) in the general formula in Equation (A.1) to obtain

$$\chi^2 = 0.\ 2073\ k_o^2 \int_0^L dz\ C_n^2(z)\int d\vec{\kappa}\ \kappa^{-11/3} \sin^2\left[\frac{\kappa^2(z-L)}{2\,k_o}\right]. \qquad (3.5.19)$$

Integrating over φ and making the substitution

$$x^2 = \frac{\kappa^2(z-L)}{2\,k_o}, \qquad (3.5.20)$$

one obtains

$$\chi^2 = 0.731\,k_o^{7/6}\int_0^L dz\,C_n^2(z)(L-z)^{5/6}\int_0^{\infty} dx\ x^{-5/3-1}\sin^2(x^2). \qquad (3.5.21)$$

Using the Mellin transform in Equation (F.4) evaluated at $s = -5/3$, one obtains

$$\chi^2 = 0.\ 5631\ k_o^{7/6}\int_0^L dz\ C_n^2(z)(L-z)^{5/6}. \qquad (3.5.22)$$

If the propagation were from L to 0 then $L - z$ should be replaced by z, the standard result is then obtained which is

$$\chi^2 = 0.\ 5631\ k_o^{7/6}\,\mu_{5/6}. \qquad (3.5.23)$$

This is the scintillation that one would get from a star. It is equal to 0.059 for the HV-21 model at 0.5 micrometer wavelength. Even though this number is small, there can be significant scintillation on the beam. The variance of the log intensity is four times that of the log amplitude and is equal to 0.236 Therefore, it is not too unusual to have the intensity drop by a factor of 2.

A similar calculation can be performed for a focused source. The standard Equation (A.1) is used with the filter function of a focused source given in Equation (A.5), to obtain

118

$$\chi^2 = 0.\,2073\, k_o^2 \int_0^L dz\ C_n^2(z)\int d\vec{\kappa}\ \kappa^{-11/3}\left(\frac{S-z}{S}\right)^{5/3}\sin\left[\frac{\kappa^2 z S}{2k_0(z-S)}\right]. \qquad (3.5.24)$$

Integrate over the angle and let
$$a = \kappa\sqrt{\frac{Sz}{2k_o(S-z)}}, \qquad (3.5.25)$$

then using the Mellin transform in (F.4) evaluated at $s = -5/3$ one obtains

$$\chi^2 = 0.5631\, k_o^{7/6}\int_0^S dz\ C_n^2(z)\, z^{-5/6}(1-z/S)^{5/6}. \qquad (3.5.26)$$

The above results were obtained by Tatarski in a slightly different form. If the target is much higher than the turbulence, the last term in parenthesis goes to unity and the scintillation then is equal to that of a beam propagating from space to the ground. This is much less than the scintillation of a collimated beam propagating from the earth's surface to space.

3.5.5 Beam Movement at a Target for a Collimated and Focused Beam

The next problem is another in which the complex filter function acting on the phase is calculated. This complex filter function must be squared before substituting it into the general expression. The movement of the beam due to turbulence at a target will be found. The tilt causes a beam to change position on a target as shown in Figure 3-11.
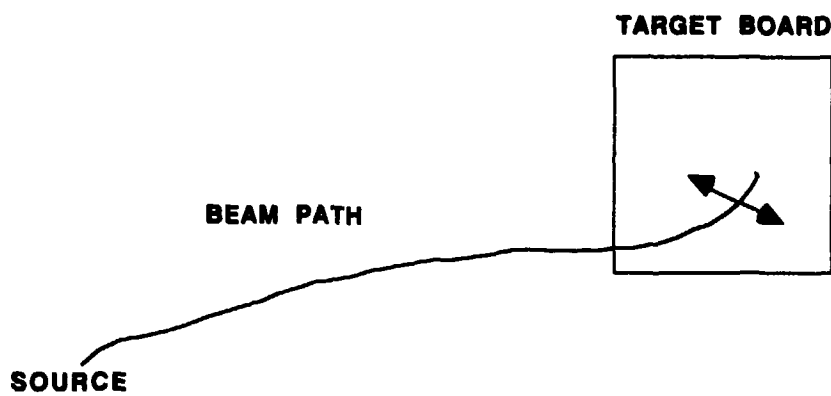

Figure 3-11. Movement jitter at a target board.

119

It is assumed that the scintillations are small so that the beam does not break up. If there are significant scintillations then that will add to the movement calculated here. With that assumption, the amount of jitter is equal to the tilt times the distance over which it acts. Therefore, the tilt filter function for this problem is

$$F(\vec{\kappa}, z) = (L - z)^2 \left(\frac{16}{k_o D}\right)^2 \left(\frac{J_2(\kappa D / 2)}{\kappa D / 2}\right)^2,$$

(3.5.27)

and the variance of the beam movement for the collimated case is

$$\chi^2 = 0.2073 \ k_o^2 \int_0^L dz \ C_n^2(z) \int d\vec{\kappa} \ f(\kappa)(L - z)^2 \left(\frac{16}{k_o D}\right)^2 \left(\frac{J_2(\kappa D / 2)}{\kappa D / 2}\right)^2.$$

(3.5.28)

This expression can be evaluated as in the example for Z-tilt to give

$$\chi^2 = \frac{6.08}{D^{1/3}} \left[L^2 \mu_o - 2L \mu_1 + \mu_2\right].$$

(3.5.29)

For distances at which the target is well above the turbulence, the first term in brackets is dominant, and the result is the physically reasonable one that the rms movement is the rms tilt times the distance. If the turbulence is constant along the path then

$$\chi^2 = \frac{2.03 L^3 C_n^2}{D^{1/3}}.$$

(3.5.30)

This functional dependence with constant turbulence along the path is the same as that reported in Fante[18] where the fourth moment of the field was used to calculate the beam displacement. The coefficient was 1.92 in that case. A Gaussian beam calculated by Prokhorov[19] gives the same dependence with the coefficient equal to 1.6. The advantage of the approach here is that the answer is arrived at in a straightforward manner and the expression given in Equation (3.5.29) applies for turbulence that can vary in space. For the focused case, the phase expression at the bottom of Equation (A.4) must be used. For the same reasons given in Section 3.5.1, the cosine term is neglected to give for the movement variance the expression

120

$$X^2 = \frac{6.08}{D^{1/3}} \int_0^L dz \; C_n^2(z) \frac{(L-z)^{11/3}}{L^{5/3}}. \qquad (3.5.31)$$

For constant turbulence along the path this can be integrated to give

$$X^2 = \frac{2.03L^3 C_n^2}{D^{1/3}} \left(\frac{9}{14}\right). \qquad (3.5.32)$$

The movement variance is 64% that of a collimated beam, and the rms movement is 80% that of a collimated beam.

3.5.6 Tracked Tilt

Suppose a tracking system is doing a perfect job of keeping a laser beam centered on a target. There will still be an angle-of-arrival jitter of the laser beam at the target because the beam had to traverse the atmosphere differently as the turbulence changed. This is illustrated in Figure 3-12. The fact that the target is being perfectly tracked means that, at each turbulence realization, the distance the beam moves due to the tilted tracking mirror is exactly canceled out by the tilt caused by traversing the atmospheric turbulence. The angle of arrival tilt will be calculated due to the turbulence at z. In the final expression, all these differential tilts are summed by integrating through the atmosphere. Therefore, if T_0 is the mirror tilt and T is the filter function of tilt, one gets

$$L dT_0 - (L - z)dT = 0, \qquad (3.5.33)$$

therefore, $\qquad\qquad dT_0 = (1 - z/L)dT. \qquad (3.5.34)$

The residual tilt at the target is the mirror tilt minus the tilt through the turbulence. This results in the following tilt at the target

$$dT_t = dT - dT_0 = z dT / L. \qquad (3.5.35)$$

The filter function for this problem is the square of the above complex filter function which is

$$F(\vec{\kappa}, z) = \left[\frac{z}{L}\right]^2 \left(\frac{16}{k_0 D}\right)^2 \left[\frac{J_2(\kappa D/2)}{\kappa D/2}\right]^2. \qquad (3.5.36)$$

121
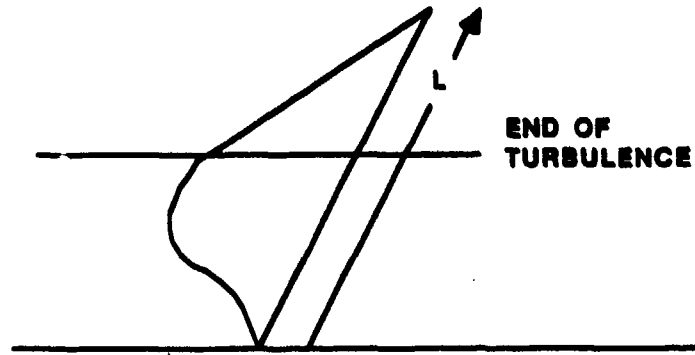
Figure 3-12. Path of rays for a perfectly tracked target.

Substituting this filter function into the general formula gives

$$T_t^2 = 0.2073 \, k_o^2 \int_0^L dz \, C_n^2(z) \int d\vec{\kappa} \; \kappa^{-11/3}\left(\frac{z}{L}\right)^2 \left(\frac{16}{k_o D}\right)^2 \left[\frac{J_2(\kappa D / 2)}{\kappa D / 2}\right]^2. \qquad (3.5.37)$$

Evaluating this in exactly the same way as the variance of Z-tilt gives

$$T_t^2 = \frac{6.08 \, \mu_2}{L^2 D^{1/3}}. \qquad (3.5.38)$$

This problem was also analyzed by Tyler.[20] His results are in the form of curves that are the result of a numerical integration of the final form of his result.

For a 0.6-m system with the target at 300 km and HV-21 turbulence, the rms tilt is 39 nanoradians.

3.5.7 Scintillation on a Corrected Beam

A perfect adaptive-optics system applies the phase shift caused by the entire atmosphere to a deformable mirror. A beam bounced off this mirror is severely distorted at first and as it propagates, the phase distortion decreases to zero at the top of the turbulence. The distorted beam will produce scintillations. The turbulence at a given altitude will cause scintillations as analyzed above; however, in this case, there is a corresponding phase shift at the mirror that tends to cancel out this scintillation. The two turbulent contributions do not act over the same

122

distance, and there will be a net scintillation for each turbulence realization. This must be squared to obtain the filter function which is

$$F(\vec{\kappa}, z) = \left(\sin\left[\frac{\kappa^2 L}{2 k_o} \right] - \sin\left[\frac{\kappa^2 (L - z)}{2 k_o} \right] \right)^2. \tag{3.5.39}$$

The scintillation is therefore equal to

$$\chi^2 = \int_0^\infty d\kappa\, 0.2073(2\,\pi)\, k_o^2 \int_0^L dz\, C_n^2(z)\, \kappa^{-8/3} \left(\sin\left[\frac{\kappa^2 L}{2 k_o} \right] - \sin\left[\frac{\kappa^2 (L - z)}{2 k_o} \right] \right)^2$$

$$= \int_0^\infty d\kappa\, \Phi(\kappa). \tag{3.5.40}$$

In the above expression, the order of integration was interchanged. Everything multiplying the differential of kappa must be the transverse spatial spectral density. For Raman scattering, this quantity is of interest since the interaction strongly depends on the spatial wavelengths of the turbulence. This expression can be integrated numerically to get the spatial spectrum at any altitude of interest. This has been done, and an example of the transverse spatial spectral density plotted versus the spatial wavelength is illustrated in Figure 3-13.

The tilt variance can be found by integrating the spectrum. Using the trigonometric identity

$$\sin\left[\frac{\kappa^2 L}{2 k_o} \right] \sin\left[\frac{\kappa^2 (L - z)}{2 k_o} \right] = \frac{1}{2}\left(\cos\left[\frac{\kappa^2 z}{2 k_o} \right] - \cos\left[\frac{\kappa^2 (2L - z)}{2 k_o} \right] \right), \tag{3.5.41}$$

one can evaluate the integral using the Mellin transforms in Equations (F.4) and (F.3) to give

$$\chi^2 = 0.563 k_o^{7/6} \int_0^L dz\, C_n^2(z) \left\{ L^{5/6} + (L - z)^{5/6} - 2^{1/6}\left[(2L - z)^{5/6} - z^{5/6} \right] \right\}. \tag{3.5.42}$$

which for altitudes well above the highest turbulence is equal to

$$\chi^2 = 0.563 k_o^{7/6} 2^{1/6} \mu_{5/6} - \frac{0.0195 k_o^{7/6} \mu_2}{L^{7/6}} + \ldots \quad . \tag{3.5.43}$$

123
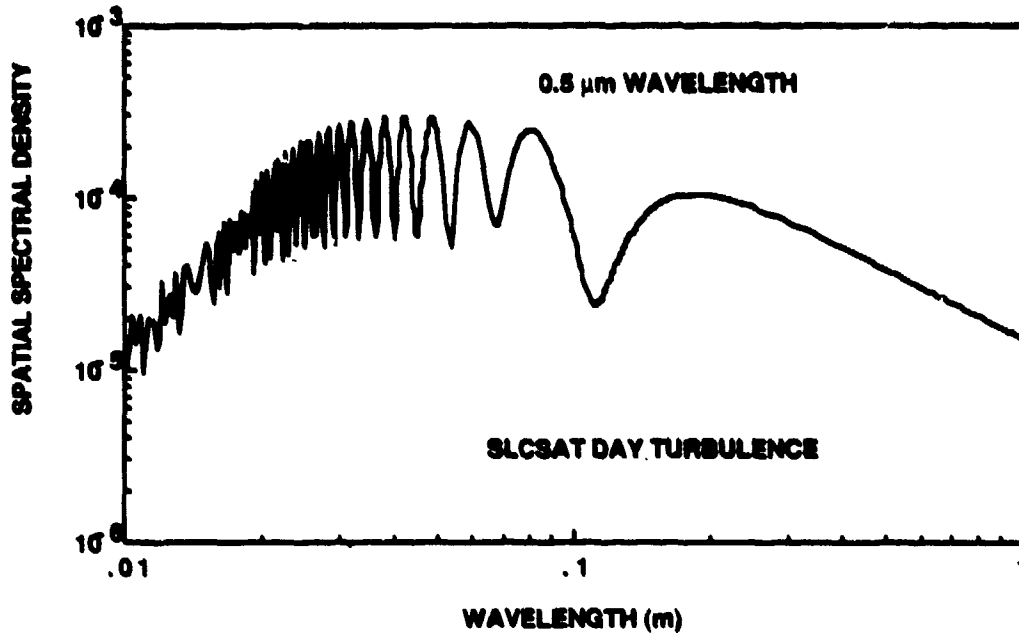
Fig 3-13. Spatial spectral density at 15 km.

The first term is a factor of 1.12 higher than the variance of the beam propagating downward through the atmosphere. The second term is small compared to the first, and it decreases with distance. As a partial verification of the accuracy of the above results, note that if the turbulence is entirely at the mirror so that the turbulence profile can be represented by a delta function, then the scintillation is zero — a result that is required.

3.5.8 Phase Variance with Finite Servo Bandwidth

Greenwood has derived the phase variance of an adaptive-optics system having finite temporal servo bandwidth with a one-pole filter and an infinitely sharp filter. The residual rms phase error due to the finite frequency response will be calculated. In this section, the same servo filter function as treated by Greenwood[21] will also be treated here. Consider the following filter function

$$F(\kappa) = \left| 1 - \frac{1}{1 + i\left(\dfrac{\omega}{\omega_{3dB}}\right)^n} \right|^2.$$

(3.5.44)

124

Greenwood's case of a single-pole filter corresponds to $n = 1$, and $n = \infty$ is the sharp cutoff case. If this is inserted into the Equation (A.3) for the power spectral density one obtains

$$\phi^2 = 0.8272 \, k_o^2 \int\limits_0^L dz \; C_n^2(z) \frac{v^{5/3}}{\omega_{3dB}^{5/3}} \int\limits_0^\infty dx \frac{x^{2n-8/3}}{1 + x^{2n}} \int\limits_0^\infty dc \frac{U(c-1)c^{-8/3}}{\sqrt{c^2-1}}. \qquad (3.5.45)$$

where
$$x = \frac{\omega}{\omega_{3dB}}. \qquad (3.5.46)$$

Using the Mellin transforms in Equations (F.8) and (F.9), one obtains for the phase variance the relation

$$\varphi^2 = \left(\frac{f_c}{f_{3dB}}\right)^{5/3} = \frac{0.051 k_o^2 v_{5/3}}{f_{3dB}^{5/3} \, n \sin\left(\frac{5\pi}{6n}\right)}. \qquad (3.5.47)$$

The velocity moment is defined by

$$v_n = \int\limits_0^L dz \; C_n^2(z) v^n(z). \qquad (3.5.48)$$

For a single pole filter $n = 1$, and using Equation (3.5.47) the characteristic frequency is equal to

$$f_c^{5/3} = 0.102 \, k_o^2 \, v_{5/3}. \qquad (3.5.49)$$

While for a sharp cutoff filter, the limit of the phase variance as n gets very large is found using L'Hospital's rule to be

$$f_c^{5/3} = 0.0196 \, k_o^2 \, v_{5/3}. \qquad (3.5.50)$$

These are the same results obtained by Greenwood.

3.5.9 Focal Anisoplanatic Tilt

It is pointed out in Section 3.4.5 that the method of cascading filter functions works as long as not more than one of the filter functions stems from an effect that depends on the radial coordinate. For the problem of finding the focal anisoplanatic tilt, this assumption is not valid.

125

The phase variance that is subtracted due to tilt is zero in the aperture center and a maximum at the aperture edge. In addition, the phase variance due to the difference between a collimated and focused beam is zero in the center and a maximum at the edge. Because there are two functions that vary radially, the problem must be solved by going back to the basic equations and rederiving the expression for the phase variance. The expression that is derived is a two-parameter integral; however, the high altitude beacon assumption reduces it to a single parameter problem which is why it is included in this section.

From Equation (3.1.22) the differential disturbance to the wave is

$$d\varphi(\vec{\kappa}, z) = ik_o \int_0^{\bar{z}} dv(\vec{\kappa}, z') \exp\left[\frac{-i\kappa^2(z - z')}{2k_o}\right] dz'. \qquad (3.5.51)$$

The phase for a collimated beam in real space can be written as the inverse Fourier transform in kappa space using the above relation as

$$d\tilde{\varphi}_c(\vec{r}, z) = \int d\vec{\kappa} \, d\varphi_c(\vec{\kappa}, z) \exp\left[i\vec{\kappa} \cdot \vec{r}\right]$$

$$= ik_o \int d\vec{\kappa} \int_0^{\bar{z}} dv(\vec{\kappa}, z') \exp\left[i\vec{\kappa} \cdot \vec{r}\right] \exp\left[\frac{-i\kappa^2(z - z')}{2k_o}\right] dz'. \qquad (3.5.52)$$

The focused beam phase is

$$d\tilde{\varphi}_f(\vec{r}, z) = ik_o \int d\vec{\kappa} \int_0^{\bar{z}} dv(\vec{\kappa}, z') \exp\left[i\vec{\kappa} \cdot \vec{r}(1 - z'/L)\right] \exp\left[\frac{-i\kappa^2(z - z')}{2k_o}\right] dz'.$$

$$(3.5.53)$$

Use was made of the fact that the separation of the rays at a radial position r in the aperture is equal to $r(1 - z/L)$ at a given distance from the source. This displacement can be represented as a phase shift in transverse spatial transform space. The tilt of the wave at the origin measured in an aperture of diameter D can be written as an operation on the phase that is the imaginary part of the above turbulence induced disturbance as

$$T = \frac{16}{k_o D^2} \int \frac{4}{\pi D^2(z)} W\left[\vec{r}/D(z)\right] \vec{r} dr \int d\vec{\kappa} \exp\left[i\vec{\kappa} \cdot \vec{r}\right] \text{Im } d\varphi(\vec{\kappa}, L). \qquad (3.5.54)$$

126

This form allows the diameter to vary with propagation distance. If the change of variables $\vec{r}' / D(z) \rightarrow \vec{y} / D$ is made, the above equation is transformed into a relation for the focused beam

$$T_f = \frac{64}{\pi D^4 k_o} \int W(\vec{y} / D) \frac{D(z)}{D} \vec{y} \, d\vec{y} \int d\vec{\kappa} \exp[\, i\vec{\kappa} \cdot \vec{r}'(1 - z / L)] \, \text{Im} \, d\varphi(\vec{\kappa}, z) \,.$$

(3.5.55)

The vector character of each of the expressions for tilt of the collimated and focused beams can be incorporated into a gradient operation in kappa space, and this will allow the integrations to be performed. Diffraction effects will be neglected, which is equivalent to setting the last exponential in Equation (3.5.53) equal to unity. Doing that, the difference of the tilts can be written as

$$T_{c-f} = \frac{64}{\pi D^4 k_o} \int_0^L dz' \int d\vec{\kappa} [\text{Im} \, d\varphi(\vec{\kappa}, z')] \nabla_{\vec{\kappa}} \int W(\vec{y} / D) \, d\vec{y}$$
$$(\cos[\vec{\kappa} \cdot \vec{y}] - \cos[\vec{\kappa} \cdot \vec{y}(1 - z'/ L)]).$$

(3.5.56)

The angular integration in the aperture can be performed by using Equation (3.4.5) with the result

$$T_{c-f} = -i \frac{128}{D^4} \int d\vec{\kappa} \int_0^L dv(\vec{\kappa}, z') dz' \nabla_{\vec{\kappa}} \int_0^{D/2} r dr [\, J_0(\kappa r) - J_0(\kappa r[1 - z'/L])\,].$$

(3.5.57)

The radial integration can be performed using the Bessel function relation in Equation (3.4.3) to give

$$T_{c-f} = -i \frac{128}{D^4} \int d\vec{\kappa} \int_0^L dv(\vec{\kappa}, z') dz' \nabla_{\vec{\kappa}} \left[\frac{J_1(\kappa D / 2) D}{2\kappa} - \frac{J_1[\kappa D(1 - z'/ L) / 2] D}{2\kappa(1 - z'/ L)} \right].$$

(3.5.58)

Performing the gradient operation using the recursion relation for Bessel functions expressed in Equation (3.4.2) gives

127

$$T_{c-f} = -i\frac{128}{D^4}\int d\vec{\kappa}\int_0^L dv(\ \vec{\kappa},\ z')dz\left[\frac{J_2(\kappa D\ /\ 2)D^2}{4\ \kappa^2} - \frac{J_2[\ \kappa D(1 - z'/\ L)\ /\ 2]D^2}{4\ \kappa^2(1 - z'/\ L)}\right]\vec{\kappa}\ .$$

$$(3.5.59)$$

To find the tilt variance, this expression must be multiplied by its complex conjugate and the ensemble average taken. Follow exactly the same steps as in Equations (3.3.26) to (3.3.37) to eliminate one integral over kappa prime and the axial coordinate. The result can be written in the standard form of the variance given by

$$T^2_{c-f} = 0.2073\ k_o^2\int_0^L dz\ C_n^2(z\ )\int d\vec{\kappa}\ f(\ \kappa)\ F(\ \vec{\kappa},\ z\ )\ .\qquad (3.5.60)$$

The filter function for focal anisoplanatic tilt in the above expression can be found using the results in Equation (3.4.2) to be

$$F(\ \vec{\kappa},\ z) = \left(\frac{16}{k_o D}\right)^2\left[\frac{J_2(\ \kappa D/2)}{\kappa D/2} - \frac{J_2[\ \kappa D(1 - z\ /\ L)/2]}{\kappa D(1 - z\ /\ L)/2}\right]^2\ .\qquad (3.5.61)$$

If this filter function is expanded and the resulting expression evaluated by Mellin transform techniques, one finds that the resulting expression is not convenient to evaluate when the altitude is well above the turbulence. Of greater use in this situation is an approximation of the filter function by a form that is appropriate for a high-altitude point source. Using the recursion relation for Bessel functions given in Equation (3.4.2) one finds for small arguments, $z\ /\ L \ll 1$, that

$$\frac{J_2(\ x + \Delta x)}{[\ x + \Delta x]} = [\ x + \Delta x]\frac{J_2(\ x + \Delta x)}{[\ x + \Delta x]^2}$$

$$\approx [\ x + \Delta x]\left\{\frac{J_2(\ x)}{x^2} + \Delta x\frac{J_2(\ x)}{x^2} - \Delta x\frac{d}{dx}\left[\frac{J_2(\ x)}{x^2}\right]\right\} \approx \frac{J_2(\ x)}{x} + \Delta x\frac{J_2(\ x)}{x^2} - \Delta x\frac{J_3(\ x)}{x}\ ,$$

$$(3.5.62)$$

which allows the filter function to be approximated by

128

$$F(\vec{\kappa}, z) \approx \frac{64 \; \kappa^2 z^2}{k_o^2 L^2 (\kappa D / 2)^2} \left[J_2(\kappa D / 2) - \frac{\kappa D}{2} J_3(\kappa D / 2) \right]^2.$$ (3.5.63)

If the above filter function is inserted into Equation (3.5.60), for the case when inner and outer scale effects are not important, one can immediately perform the angular and axial integrations to give

$$T_{c-f}^2 \approx \frac{105 \; \mu_2}{L^2 D^{1/3}} \int_0^\infty dx \; x^{-5/3-1} \left[J_2^2(x) + x^2 J_3^2(x) - 2 J_2(x) J_3(x) \right],$$ (3.5.64)

where $x = \kappa D / 2$. The tilt variance can be found using the Mellin transforms in Equations (F.6) and (F.7) and is equal to

$$T_{c-f}^2 \approx \frac{5.68 \; \mu_2}{L^2 D^{1/3}}.$$ (3.5.65)

For an HV-21 turbulence model with the source at 300 km and a diameter of 0.6 m, the rms jitter is 37.8 nrad.

The same method, as applied above, can be used to find the filter function that removes any Zernike component of the wavefront. The filter function is the magnitude squared of the difference between the complex filter function for a collimated wave and a wave focused at the observation point. These complex filter functions are given in Equation (3.4.19). For instance, for piston removal the filter function is

$$F(\vec{\kappa}, z) = \left(\frac{1}{k_o} \right)^2 \left[\frac{2 J_1(\kappa D/2)}{\kappa D/2} - \frac{2 J_1[\kappa D(1 - z/L)/2]}{\kappa D(1 - z/L)/2} \right]^2.$$ (3.5.66)

Relations for any other Zernike component can be found in a similar manner.

3.6 MULTIPARAMETER PROBLEMS

In this section, turbulence problems that can be represented in terms of two or more parameters are treated. These problems are all treated in the same fashion. Once again as in the single parameter case, one starts with integrals over kappa space and over the axial coordinate. The angle integral in kappa space is performed. A change of variables is made to a'low one parameter to be factored out of the integral. The integral over the magnitude of kappa now contains one or more parameters. The terms may have to be rearranged so that the integral can be written as the product of functions for which the Mellin transform is known. This procedure has been successfully applied to all problems encountered to date. Then, the Mellin convolution theorem can be used to convert this into an integral in one or more complex planes. Depending on the number of Gamma functions in the numerator and denominator and the size of the parameter, a power series or an asymptotic solution is found. After the integrations in the complex planes are performed, the integration over the axial coordinates is evaluated. This last integration can typically be expressed in terms of moments of the turbulence distribution. Analytic expressions for these moments are available if the Hufnagel-Valley model of turbulence is used.

Several problems of interest are evaluated in this section to showcase this method. First the tilt with outer scale of turbulence is considered. *It is found that the outer scale size can have a significant effect on the tilt.* Next, tilt anisoplanatism is considered. This is the difference in tilts of two sources that are displaced from each other. For instance, this analysis can be used to determine the differential tilt jitter of two stars. Since outer scale significantly affected the tilt, it is natural to ask if it also affects the tilt anisoplanatism. The general problem is set up in Section 3.6.2, and the integral has three parameters. First, the simpler problem with the outer scale set to infinity is solved. In addition to differential tilt due to two coincident apertures pointing in different directions, the solution also applies to sources that are displaced in a parallel direction with respect to each other. This error would apply if there were a misregistration error between the wavefront sensor and the deformable mirror in an adaptive-

130

optics system. *It is shown that if this mispointing error is kept below a tenth of the subaperture size, the tilt difference will be small.*

Next, the tilt anisoplanatism problem with outer scale included is solved. *It is found that the outer scale is not nearly as important in affecting the tilt anisoplanatism as it was the tilt.*

Then it will be shown that the inner scale limits the maximum tilt that can be measured by an aperture. Next, the effect of the central obscuration and then diffraction on the Zernike tilt is considered. Finally, several scintillation problems are considered.

For all problems the sign of the residue depends on which direction the path is closed. In calculating the residue at a pole, sometimes the path of integration must be closed to the right and sometimes to the left. One can easily show that the combination of path direction and sign of s in the Gamma function always results in a positive sign on the residue for the bulk of the poles. The single pole that may be separated by the path of integration has a negative sign when calculating the residue.

3.6.1 Tilt with Finite Outer Scale

The significant effect of the outer scale on the tilt was first pointed out by D. Murphy.[22] . To set up this problem, the general expression given in Equation (A.1) is used with the filter function for Zernike tilt given in Equation (B.7). The turbulence spectrum that is given in Equation (A.6) with the inner scale term neglected is used to give for the tilt variance with outer scale present the expression

$$T_o^2 = 0.2073 \; k_o^2 \int_0^L dz \; C_n^2(z\,) \int d\vec{\kappa} \Big[\kappa^2 + \kappa_o^2 \Big]^{-11/6} \left(\frac{16}{k_o D} \right)^2 \left[\frac{J_2(\kappa D / 2)}{\kappa D / 2} \right]^2 . \qquad (3.6.1)$$

The integrations over angle and z can be performed. Making the substitution $x = \kappa D/2$ gives

$$T_o^2 = \frac{1334 \; \mu_o \; \kappa_o^2}{D^4} \int_0^\infty \frac{dx}{x} \; J_2^2(x) \left[\left(\frac{x}{\kappa_o D / 2} \right)^2 + 1 \right]^{-11/6} . \qquad (3.6.2)$$

This can be converted into an integral in the complex plane by using the Mellin convolution integral in Equation (I.6). Define

$$H_1(x) = J_{\tfrac{1}{2}}^2(x),$$

(3.6.3)

$$H_2(a / x) = \left[(a/x)^{-2} + 1 \right]^{-11/6}.$$

(3.6.4)

and

Use the Mellin transform in Equation (F.6) for the first function. For the second, start with the relation in Equation (F.8) with $p = 11/6$ and then use Equation (I.5) with $p = -2$ to obtain the first part of the following equation. After the substitution $s \to 2s$, one obtains the second part of the equation.

$$
\begin{aligned}
T_o^2 &= \frac{1334\,\mu_o\,\kappa_o^{-11/3}}{D^4}\,\frac{1}{2\pi i}\int ds \left(\frac{\kappa_o D}{2} \right)^{-s} \\
&\quad \times \frac{1}{4\sqrt{\pi}\,\Gamma\!\left[\frac{11}{6}\right]} \Gamma\!\left[\begin{matrix} s/2 + 2,\ \tfrac{1}{2} - s/2, -s/2,\ \tfrac{11}{6} + s/2 \\ -s/2 + 3, -s/2 + 1 \end{matrix} \right] \\
&= \frac{400\,\mu_o\,\kappa_o^{-11/3}}{D^4}\,\frac{1}{2\pi i}\int ds \left(\frac{\kappa_o D}{2} \right)^{-2s} \Gamma\!\left[\begin{matrix} s + 2, -s + \tfrac{1}{2}, -s,\ s + \tfrac{11}{6} \\ -s + 3, -s + 1 \end{matrix} \right],
\end{aligned}
$$

(3.6.5)

where the path of integration does not split any of the poles of an individual Gamma function. The substitution $s \to 2s$ is often made to get most or all of the coefficients of s equal to unity. The method used to evaluate this integral is discussed in Section 2.4. Since $\Delta = 2$, the path of integration can be closed in the left-half plane, and there are contributions at the poles at $s = -11/6 - n$, and $-2 - n$ for $n = 0, 1, 2. \dots$. The resulting solution is

$$
\begin{aligned}
T_o^2 &= \frac{400\,\mu_o\,\kappa_o^{-11/3}}{D^4} \left\{ \sum_{n=0}^{\infty} \frac{(-1)^n}{n!} \left(\left(\frac{\kappa_o D}{2} \right)^{11/3 + 4n} \Gamma\!\left[\begin{matrix} -n + \tfrac{1}{6},\ n + \tfrac{7}{3}, n + \tfrac{11}{6} \\ n + \tfrac{29}{6}, n + \tfrac{17}{6} \end{matrix} \right] \right. \right. \\
&\quad \left. \left. + \left(\frac{\kappa_o D}{2} \right)^{2 + 2n} \Gamma\!\left[\begin{matrix} n + \tfrac{5}{2}, n + 2, -n - \tfrac{1}{6} \\ n + 5, n + 3 \end{matrix} \right] \right) \right\}.
\end{aligned}
$$

(3.6.6)

Using the definition of outer scale given in Equation (3.3.30), the most significant terms of these summations are

$$
T_o^2 = \frac{6.08\,\mu_o}{D^{1/3}} \left\{ 1 + 3.7\left(\frac{D}{L_o} \right)^2 + \dots - \left(\frac{D}{L_o} \right)^{1/3}\left[1.42 + 4.01\left(\frac{D}{L_o} \right)^2 \right] \right\}.
$$

(3.6.7)

132

The tilt is affected by the outer scale and the fractional decrease from the value with infinite outer scale is shown in Figure 3-14. If the outer scale size is 100 times the aperture diameter, the tilt is still decreased by 15%. This occurs because the tilt is determined mainly by the high wavelength turbulence. A finite outer scale decreases the turbulence at the long wavelengths and, thereby, decreases the tilt.
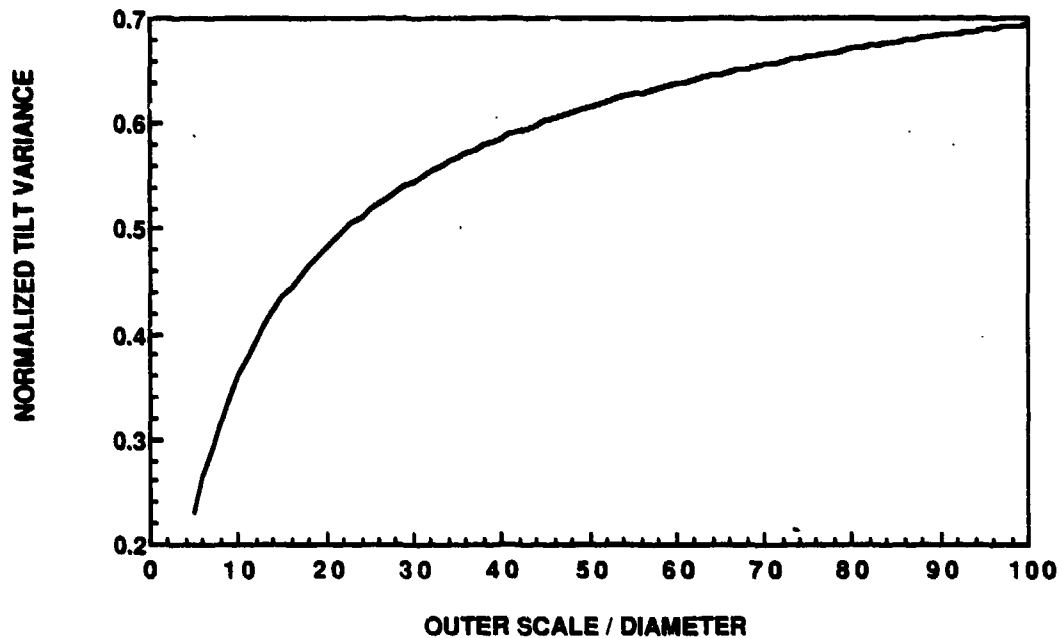

Figure 3-14   Effect of outer scale on the normalized tilt variance.

3.6.2   Setup of the General Problem for Tilt Anisoplanatism

To find the value of tilt anisoplanatism with finite outer scale, the integrand in the general formula given in Equation (A.1) is composed of three factors: the Kolmogorov spectrum with outer scale included, the Zernike or Gradient tilt in the x and y direction, and the anisoplanatic term. The effect of both displacement and angular anisoplanatism will be evaluated. The angular anisoplanatism is important in adaptive-optics systems because the beacon may not be in the correct position. The calculation also allows one to calculate the relative jitter of stars. The displacement anisoplanatism calculation allows one to determine the effect of wavefront

133

sensor and deformable mirror misalignment, and the jitter on a laser beam produced by the tracking system and the laser beam using different parts of the aperture.

The sensor for the tilt may be sensitive to either the G or Z tilt. Here the Z-tilt is calculated for the general case and the G-tilt is calculated for an angular offset with infinite outer scale. Assume that the displacement is in the x direction. It will be found that the tilt depends on whether the displacement is parallel to the displacement direction or perpendicular to it. For that reason, both the x and y components and the total Z-tilt in physical space are found using the filter functions in Equations (B.6) to (B.7). Substituting the filter functions for Z-tilt and anisoplanatism given in Equation (D.1) into Equation (A.1) and using the Kolmogorov spectrum with the inner scale neglected, one obtains for the tilt-anisoplanatism variance the expression

$$
\left\{\begin{matrix} \sigma_x^2 \\ \sigma_y^2 \\ \sigma^2 \end{matrix}\right\} = 0.4146\left(\frac{16}{D^2}\right)^2 \int\limits_0^L dz \ C_n^2(z) \int d\vec{\kappa} \left\{\begin{matrix} \cos^2(\varphi) \\ \sin^2(\varphi) \\ 1 \end{matrix}\right\}(\kappa^2 + \kappa_o^2)^{-11/6}\left(\frac{J_2\left(\frac{\kappa D}{2}\right)}{\frac{\kappa D}{2}}\right)^2
$$

$$
\times \left[1 - \cos\{\kappa d \ \cos(\varphi)\}\right] \quad . \qquad \qquad (3.6.8)
$$

The angular integration can be performed using Equation (3.892) from Gradshteyn and Ryzhik which is

$$
\int\limits_0^\pi \exp\left[i\beta\sin(x)\right]\sin^\nu(x) \ dx = \sqrt{\pi}\left(\frac{2}{\beta}\right)^\nu \Gamma(\nu + \tfrac{1}{2}) \ J_\nu(\beta); \qquad \text{Re } \nu > -\tfrac{1}{2}. \quad (3.6.9)
$$

Using the trigonometric identity

$$
\cos^2(\varphi) = 1 - \sin^2(\varphi) \qquad \qquad (3.6.10)
$$

to express the first integral in the form of Equation (3.6.9), and using the integral given in Equation (3.4.5), one can perform the phi integration to obtain

$$
\left\{\begin{matrix} \sigma_x^2 \\ \sigma_y^2 \\ \sigma^2 \end{matrix}\right\} = \frac{667}{D^2} \int\limits_0^L dz \ C_n^2(z) \int\limits_0^\infty \kappa \ d\kappa (\kappa^2 + \kappa_o^2)^{-11/6}\left(\frac{J_2\left(\frac{\kappa D}{2}\right)}{\frac{\kappa D}{2}}\right)^2 \left\{\begin{matrix} \frac{1}{2} + \frac{J_1(\kappa d)}{\kappa d} - J_0(\kappa d) \\ \frac{1}{2} - \frac{J_1(\kappa d)}{\kappa d} \\ 1 - J_0(\kappa d) \end{matrix}\right\}.
$$

$$
\qquad \qquad (3.6.11)
$$

For small values of d, the Bessel functions can be replaced by the first two terms of their power series which are

$$J_0(\kappa d) = 1 - \frac{(\kappa d)^2}{4} + \dots,$$

and

$$J_1(\kappa d) = \frac{\kappa d}{2} - \frac{(\kappa d)^3}{16} + \dots . \qquad (3.6.12)$$

If these expansions are substituted into the expressions for the tilt, one finds the tilt variance parallel to the direction of the displacement is three times that of the perpendicular component for small separations. Expanding the functions and integrating term by term cannot be done in general. The expansion above can be performed. If additional terms are used, the integrals often do not converge.

There are two integrals that, when evaluated, allow one to evaluate all three integrals in kappa-space. These are

$$I_1 = -\int_0^\infty \kappa \, d\kappa (\kappa^2 + \kappa_o^2)^{-11/6} \left(\frac{J_2\left(\frac{\kappa D}{2}\right)}{\frac{\kappa D}{2}}\right)^2 \left[\frac{J_1(\kappa d)}{\kappa d} - \frac{1}{2}\right], \qquad (3.6.13)$$

and

$$I_T = -\int_0^\infty \kappa \, d\kappa (\kappa^2 + \kappa_o^2)^{-11/6} \left(\frac{J_2\left(\frac{\kappa D}{2}\right)}{\frac{\kappa D}{2}}\right)^2 [J_0(\kappa d) - 1]. \qquad (3.6.14)$$

The previous integrals expressed in terms of these two are equal to

$$\begin{Bmatrix} \sigma_x^2 \\ \sigma_y^2 \\ \sigma^2 \end{Bmatrix} = \frac{667}{D^2} \int_0^L dz \ C_n^2(z) \begin{Bmatrix} I_T - I_1 \\ I_1 \\ I_T \end{Bmatrix}. \qquad (3.6.15)$$

These general expressions will be evaluated in Section 3.6.4. In the next section, the expression will be evaluated with outer scale neglected.

3.6.3 Tilt Anisoplanatism with Infinite Outer Scale

If the outer scale is allowed to go to infinity, the integrals contain only two parameters, and the standard Mellin convolution integral can be used to convert the integral into one in a single complex plane.

Let $t = \kappa d$ and $x = \dfrac{2d}{D}$.
$\hspace{8cm}$ (3.6.16)

The integrals are then equal to

$$\begin{Bmatrix} I_1 \\ I_T \end{Bmatrix} = \frac{-4 d^{11/3}}{D^2} \int_0^{\infty} \frac{dt}{t} \begin{Bmatrix} t^{-14/3}\left[J_1(t) - \frac{t}{2} \right] \\ t^{-11/3}\left[J_0(t) - 1 \right] \end{Bmatrix} J_2^2(t/x) \; . \hspace{1.5cm} (3.6.17)$$

Using the Mellin transforms in Equations (F.5) and (F.6) and the relation in Equation (I.6) of part 2 and the substitution $s \rightarrow 2s$, the integrals can be transformed into

$$\begin{Bmatrix} I_1 \\ I_T \end{Bmatrix} = - \frac{0.0889\, d^{11/3}}{D^2\, 2\pi i} \int ds \left(\frac{d}{D} \right)^{-2s} \cdot \begin{bmatrix} s - \frac{11}{6}*, -s + 2, & s + \frac{1}{2} \\ s + 3, & s + 1 \end{bmatrix} \begin{Bmatrix} \dfrac{1}{2\,\Gamma\left[-s + \frac{23}{6} \right]} \\ \dfrac{1}{\Gamma\left[-s + \frac{17}{6} \right]} \end{Bmatrix} ,$$
$$\hspace{12cm} (3.6.18)$$

where the asterisk means that the first pole of that term is on the other side of the path of integration. The path of integration passes between the first and second poles because of the presence of the term subtracted from the Bessel functions that cancels out the first term of the power series expansion as explained in Equations (2.3.10) and (2.3.11). The path of integration and pole location are the same for both integrals, and are shown in Figure 3-15.
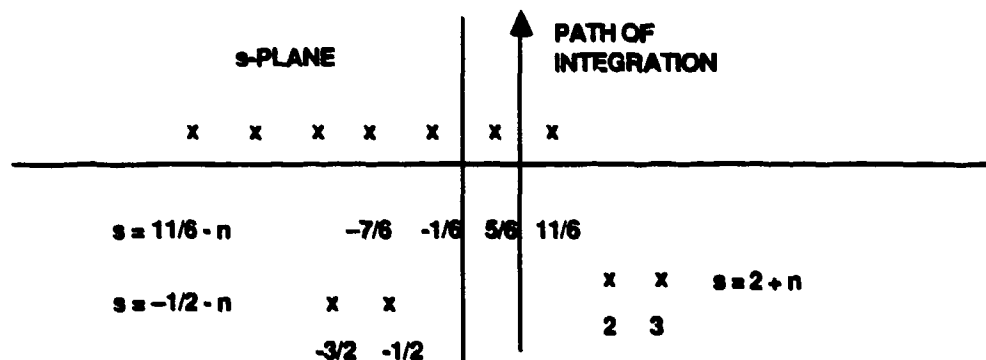

Figure 3-15. Pole location and path of integration for tilt anisoplanatism.

136

Since $\Delta = \Delta' = 0$, the direction of path closure is determined by the parameter in the integral. The point in the atmosphere at which the character of the solution changes is when the two beams do not overlap at all. For $d/D < 1$, the path of integration is closed to the left, and one obtains the residues of the poles at $s = -1/2 - n$ for $n = 0, 1, 2, \ldots$, and $s = 11/6 - n$, for $n = 1, 2, 3, \ldots$. For $d/D > 1$, the path is closed to the right, and one obtains the residues of the poles at $s = 2 + n$ for $n = 0, 1, 2, \ldots$, and the single pole at $s = 11/6$. The resultant value of the integral for small displacements, $d/D < 1$, is

$$
\left\{ \begin{matrix} I_1 \\ I_T \end{matrix} \right\}_L = \frac{-0.0889}{D^2 d^{-11/3}} \left[\sum_{n=1}^{\infty} \frac{(-1)^n}{n!} \left(\frac{d}{D} \right)^{-11/3+2n} \Gamma \left[\begin{matrix} n + \frac{1}{6}, \ -n + \frac{7}{3} \\ n + 1, \ -n + \frac{29}{6}, \ -n + \frac{17}{6} \end{matrix} \right] \left\{ \begin{matrix} \frac{0.5}{n+1} \\ 1 \end{matrix} \right\} \right.
$$
$$
\left. + \sum_{n=0}^{\infty} \frac{(-1)^n}{n!} \left(\frac{d}{D} \right)^{1+2n} \Gamma \left[\begin{matrix} -n - \frac{7}{3}, \ n + \frac{5}{2} \\ n + \frac{10}{3}, \ -n + \frac{5}{2}, \ -n + \frac{1}{2} \end{matrix} \right] \left\{ \begin{matrix} \frac{0.5}{n + \frac{10}{3}} \\ 1 \end{matrix} \right\} \right].
$$

$$(3.6.19)$$

For large displacement, $d/D > 1$, the integrals are equal to

$$
\left\{ \begin{matrix} I_1 \\ I_T \end{matrix} \right\}_U = \frac{0.0889 \, d^{11/3}}{D^2} \left[\left(\frac{d}{D} \right)^{-11/3} \Gamma \left[\begin{matrix} \frac{1}{6}, \ \frac{7}{3} \\ \frac{29}{6}, \ \frac{17}{6} \end{matrix} \right] \left\{ \begin{matrix} 0.5 \\ 1 \end{matrix} \right\} \right.
$$
$$
\left. - \sum_{n=0}^{\infty} \frac{(-1)}{n!} \left(\frac{d}{D} \right)^{-4-2n} \Gamma \left[\begin{matrix} n + \frac{1}{6}, \ n + \frac{5}{2} \\ -n + \frac{5}{6}, \ n + 5, \ n + 3 \end{matrix} \right] \left\{ \begin{matrix} \frac{0.5}{-n + \frac{5}{6}} \\ 1 \end{matrix} \right\} \right]. \qquad (3.6.20)
$$

Substituting these results into Equation (3.6.15) and realizing that the displacement can vary with the propagation distance, one finds that the tilt variances for small displacements when $d/D < 1$ are

137

$$\left\{\begin{matrix} \sigma_x^2 \\ \sigma_y^2 \end{matrix}\right\}_L = -\frac{29.6}{D^{1/3}} \int_0^{\frac{d}{D}=1} dz\, C_n^2(z)$$

$$\times \left[\sum_{n=1}^{\infty} \frac{(-1)^n}{(n)!}\left(\frac{d}{D}\right)^{2n} \Gamma\left[\begin{matrix} n+\frac{1}{6},\, -n+\frac{7}{3} \\ n+2,\, -n+\frac{29}{6},\, -n+\frac{17}{6} \end{matrix}\right] \times \left\{\begin{matrix} 2n+1 \\ 1 \end{matrix}\right\} \right.$$

$$\left. + \sum_{n=0}^{\infty} \frac{(-1)^n}{n!}\left(\frac{d}{D}\right)^{14/3+2n} \Gamma\left[\begin{matrix} -n-\frac{7}{3},\, n+\frac{5}{2} \\ n+\frac{10}{3},\, -n+\frac{5}{2},\, -n+\frac{1}{2} \end{matrix}\right]\left\{\begin{matrix} \dfrac{2n+\frac{17}{3}}{n+\frac{10}{3}} \\ \dfrac{1}{n+\frac{10}{3}} \end{matrix}\right\} \right]. \quad (3.6.21)$$

For large displacements, $d/D > 1$, the tilt variances are

$$\left\{\begin{matrix} \sigma_x^2 \\ \sigma_y^2 \end{matrix}\right\}_U = \frac{1}{D^{1/3}} \int_{\frac{d}{D}=1}^{\infty} dz\, C_n^2(z) \left[6.08\left\{\begin{matrix} 1 \\ 1 \end{matrix}\right\} \right.$$

$$\left. -29.6 \sum_{n=0}^{\infty} \frac{(-1)^n}{n!}\left(\frac{d}{D}\right)^{-1/3-2n} \Gamma\left[\begin{matrix} n+\frac{1}{6},\, n+\frac{5}{2} \\ -n+\frac{5}{6},\, n+5,\, n+3 \end{matrix}\right]\left\{\begin{matrix} \dfrac{\frac{2}{3}-2n}{-n+\frac{5}{6}} \\ \dfrac{1}{-n+\frac{5}{6}} \end{matrix}\right\} \right].$$

$$(3.6.22)$$

There is a sign difference between the two terms because the residue at the isolated pole has a negative sign associated with it as explained before. From the form of the solution, one can immediately see that for very large displacements the first term in the last equation is the only significant one. The tilt variance for each component is equal to the total tilt variance given in Equation (3.5.9). This is what one would expect since two uncorrelated tilts are being subtracted. For small displacements, the first term in the first sum in Equation (3.6.21) is the only significant term, and one can readily see that the x component is three times the y component of tilt variance as was found earlier.

Consider the case where the two apertures are pointing in the same direction but one is displaced from the other by a distance d. If the aperture displacement is small compared to the aperture diameter, then Equation (3.6.21) applies. The z integration can be performed and with the use of the recursion relation for Gamma functions the tilt can be written as

$$\begin{Bmatrix} \sigma_x^2 \\ \sigma_y^2 \end{Bmatrix} = -\frac{29.6}{D^{1/3}}\mu_0\left[\sum_{n=1}^{\infty}\frac{(-1)^n}{(n)!}\left(\frac{d}{D}\right)^{2n}\Gamma\begin{bmatrix} n+\frac{1}{6}, -n+\frac{7}{3} \\ n+2, -n+\frac{29}{6}, -n+\frac{17}{6} \end{bmatrix}\begin{Bmatrix} 2n+1 \\ 1 \end{Bmatrix}\right.$$

$$\left. + \sum_{n=0}^{\infty}\frac{(-1)^n}{n!}\left(\frac{d}{D}\right)^{2n+14/3}\Gamma\begin{bmatrix} -n-\frac{7}{3}, n+\frac{5}{2} \\ n+\frac{13}{3}, -n+\frac{5}{2}, -n+\frac{1}{2} \end{bmatrix}\begin{Bmatrix} 2n+\frac{17}{3} \\ 1 \end{Bmatrix}\right].$$

(3.6.23)

The only significant term for small displacements is the first of the first summation. Using only that term, the tilt variance can be written as

$$\begin{Bmatrix} \sigma_x^2 \\ \sigma_y^2 \end{Bmatrix} = \frac{2.67\,\mu_o}{D^{1/3}}\left(\frac{d}{D}\right)^2\begin{Bmatrix} 3 \\ 1 \end{Bmatrix}.$$

(3.6.24)

The value of total rms tilt is

$$T = 0.8\frac{\lambda}{D}\left(\frac{D}{r_0}\right)^{5/6}\left(\frac{d}{D}\right).$$

(3.6.25)

The tilt in waves is given by

$$T(\text{waves}) = 0.8\left(\frac{D}{r_0}\right)^{5/6}\left(\frac{d}{D}\right).$$

(3.6.26)

The tilt noise in a subaperture of side s will now be found. In a typical adaptive-optics system the subaperture size is equal to the expected coherence diameter. For this case, the tilt noise in a subaperture is

$$T(\text{waves})_{1-\text{axis}} = 0.566\left(\frac{d}{s}\right).$$

(3.6.27)

This tilt is due to the low spatial wavelengths of turbulence and is essentially uncorrelated between apertures. When the phase is reconstructed from the gradient measurements, the factor that relates the tilt noise to the phase variance on the full aperture is called the error

139

propagator. *For typical reconstructors this factor is about unity. Therefore, to keep the phase noise below 1/20 of a wave requires the registration error between the wavefront sensor and the deformable mirror to be kept below 1/10 of the subaperture size.*

In systems that propagate laser beams, the tracking system looks out of a certain part of the main aperture, and the laser beam is propagated out of a different part of the aperture. The full aperture is not used for each because of vignetting problems as the beam is tilted by fast steering mirrors. This misregistration can cause a relative jitter on the laser beam if the tracked signal is used to direct it. To get an idea of how large this effect is, consider the simplified problem of two beams of the same diameter that are displaced with respect to each other. For that case, Equation (3.6.25) applies. For a 0.6-m system D/r_o can be as large as 17, and for a 3.5-m system D/r_o can be as large as 100. *For these cases, in order to keep the jitter under 1/20 wave, the registration of the laser and tracking systems on the 0.6-m system has to be better than 5 mm, and that on a 3.5-m system has to be better than 6.7 mm.*

To find the anisoplanatism due to the two beams pointing in different directions, one must replace d by the angular separation times the axial distance. The upper limit in the integrations become

$$h = H_c = z \cos(\xi) = D\cos(\xi)/\Theta \quad . \tag{3.6.28}$$

The integral must now be broken into a lower term and an upper term. The total variance is the sum of these two contributions. The altitude at which the solution changes character is at the transition between having the two beams partially overlapped to that where there is no overlap. Using the definitions of the partial moments given in Equations (3.5.3) and (3.5.4), one obtains for the lower integration

$$\left\{ \begin{matrix} \sigma_x^2 \\ \sigma_y^2 \end{matrix} \right\}_L = -\frac{29.6}{D^{1/3}} \left[\sum_{n=1}^{\infty} \frac{(-1)^n \mu_{2n}^-(H_c)}{(n+1)!} \left(\frac{\Theta}{D}\right)^{2n} \Gamma \left[\begin{matrix} n+\frac{1}{6}, -n+\frac{7}{3} \\ n+1, -n+\frac{29}{6}, -n+\frac{17}{6} \end{matrix} \right] \left\{ \begin{matrix} 2n+1 \\ 1 \end{matrix} \right\} \right.$$

$$\left. + \sum_{n=0}^{\infty} \frac{(-1)^n \mu_{14/3+2n}^-(H_c)}{n!} \left(\frac{\Theta}{D}\right)^{14/3+2n} \Gamma \left[\begin{matrix} -n-\frac{7}{3}, n+\frac{5}{2} \\ n+\frac{13}{3}, -n+\frac{5}{2}, -n+\frac{1}{2} \end{matrix} \right] \left\{ \begin{matrix} 2n+\frac{17}{3} \\ 1 \end{matrix} \right\} \right] .$$

$$\tag{3.6.29}$$

140

The upper contribution is

$$
\left\{ \begin{matrix} \sigma_x^2 \\ \sigma_y^2 \end{matrix} \right\}_H = \frac{1}{D^{1/3}} \left[6.08 \; \mu_o^+(H_c) \left\{ \begin{matrix} 1 \\ 1 \end{matrix} \right\} \right.
$$

$$
\left. -29.6 \sum_{n=0}^{\infty} \frac{(-1)^n \mu_{-1/3-2n}^+(H_c)}{n!} \left(\frac{\Theta}{D} \right)^{-1/3-2n} \Gamma \left[\begin{matrix} n+\frac{1}{6}, \; n+\frac{5}{2} \\ -n+\frac{11}{6}, \; n+5, \; n+3 \end{matrix} \right] \left\{ \begin{matrix} \frac{2}{3}-2n \\ 1 \end{matrix} \right\} \right].
$$

(3.6.30)

The total phase variance is

$$
\left\{ \begin{matrix} \sigma_x^2 \\ \sigma_y^2 \end{matrix} \right\} = \left\{ \begin{matrix} \sigma_x^2 \\ \sigma_y^2 \end{matrix} \right\}_L + \left\{ \begin{matrix} \sigma_x^2 \\ \sigma_y^2 \end{matrix} \right\}_H .
$$

(3.6.31)

The most significant terms for small angular displacements are

$$
\left\{ \begin{matrix} \sigma_x^2 \\ \sigma_y^2 \end{matrix} \right\} = D^{-1/3} \left[2.67 \; \mu_2^-(H_c) \left(\frac{\Theta}{D} \right)^2 \left\{ \begin{matrix} 3 \\ 1 \end{matrix} \right\} - 3.68 \; \mu_4^-(H_c) \left(\frac{\Theta}{D} \right)^4 \left\{ \begin{matrix} 5 \\ 1 \end{matrix} \right\} \right.
$$

$$
\left. - 7.75 \; \mu_{14/3}^-(H_c) \left(\frac{\Theta}{D} \right)^{14/3} \left\{ \begin{matrix} 1.7 \\ 0.3 \end{matrix} \right\} + ... \right].
$$

(3.6.32)

Notice that the most significant term for small angles varies as the cube of the secant of the zenith angle from the relation in Equation (3.5.4), and the x-tilt variance is three times the y-tilt variance as was found previously. *The leading term gives a tilt that varies as the −7/6 power of diameter. If a system operates at one-half the wavelength of another while keeping the same diffraction-limited beam size, then the tilt jitter due to this effect will be 2.25 times worse for small separation angles.* The most significant terms for large angular displacements are

$$
\left\{ \begin{matrix} \sigma_x^2 \\ \sigma_y^2 \end{matrix} \right\} = D^{-1/3} \left[6.08 \; \mu_o^+(H_c) \left\{ \begin{matrix} 1 \\ 1 \end{matrix} \right\} - 4.04 \; \mu_{-1/3}(H_c) \left(\frac{D}{\Theta} \right)^{1/3} \left\{ \begin{matrix} 0.8 \\ 1.2 \end{matrix} \right\} + ... \right].
$$

(3.6.33)

141

The first term is twice the tilt variance for one beam. This is the expected behavior for large angles. Notice that the second term has the displacement angle to the 1/3 power causing it to decrease very slowly as the separation angle gets larger. Therefore, the asymptotic limit given in the first term is not approached until the separation angle is very large.

The only difference in the calculation for G-tilt is that the tilt-filter function is different. For that case, Equation (3.6.17) becomes

$$
\left\{ \begin{array}{c} I_1 \\ I_T \end{array} \right\} = \frac{-d^{5/3}}{16} \int_0^\infty \frac{dt}{t} \left\{ \begin{array}{c} t^{-8/3}\left[J_1(t) - \frac{t}{2} \right] \\ t^{-5/3}\left[J_0(t) - 1 \right] \end{array} \right\} J_1^2\left(\frac{t}{x} \right) .
\tag{3.6.34}
$$

This can be transformed to give the equivalent of Equation (3.6.18) as

$$
\left\{ \begin{array}{c} I_1 \\ I_T \end{array} \right\} = \frac{-5.55 \times 10^{-3} d^{5/3}}{2\pi i} \int ds \left(\frac{\Theta z}{D} \right)^{-2s} \Gamma \left[\begin{array}{c} s - \frac{5}{6}*, \; -s + 1, \; s + \frac{1}{2} \\ s + 2, \; s + 1, \; -s + \frac{11}{6} \end{array} \right] \left\{ \begin{array}{c} \frac{1}{2\left[-s + \frac{11}{6} \right]} \\ 1 \end{array} \right\} .
\tag{3.6.35}
$$

This can be integrated in the same manner as the previous case to give for the lower atmosphere contribution to the tilt anisoplanatism the value

$$
\left\{ \begin{array}{c} \sigma_x^2 \\ \sigma_y^2 \end{array} \right\}_L = - \frac{1.85}{D^{1/3}} \left[\sum_{n=1}^\infty \frac{(-1)^n \mu_{2n}^-(H_c)}{(n+1)!} \left(\frac{\Theta}{D} \right)^{2n} \Gamma \left[\begin{array}{c} n + \frac{1}{6}, \; -n + \frac{4}{3} \\ n + 2, \; -n + \frac{11}{6}, \; -n + \frac{17}{6} \end{array} \right] \left\{ \begin{array}{c} 2n + 1 \\ 1 \end{array} \right\} \right.
$$

$$
\left. + \sum_{n=0}^\infty \frac{(-1)^n \mu_{5/3+2n}^-(H_c)}{n!} \left(\frac{\Theta}{D} \right)^{8/3+2n} \Gamma \left[\begin{array}{c} -n - \frac{4}{3}, \; n + \frac{3}{2} \\ n + \frac{10}{3}, \; -n + \frac{3}{2}, \; -n + \frac{1}{2} \end{array} \right] \left\{ \begin{array}{c} 2n + \frac{11}{3} \\ 1 \end{array} \right\} \right] .
\tag{3.6.36}
$$

The upper atmosphere contribution is

$$
\left\{ \begin{array}{c} \sigma_x^2 \\ \sigma_y^2 \end{array} \right\}_H = D^{-1/3} \left[5.68 \; \mu_\alpha^+(H_c) \left\{ \begin{array}{c} 1 \\ 1 \end{array} \right\} \right.
$$

$$
\left. -1.85 \sum_{n=0}^\infty \frac{(-1)^n \mu_{-1/3-2n}^+(H_c)}{n!} \left(\frac{\Theta}{D} \right)^{-1/3-2n} \Gamma \left[\begin{array}{c} n + \frac{1}{6}, \; n + \frac{3}{2} \\ -n + \frac{11}{6}, \; n + 3, \; n + 2 \end{array} \right] \left\{ \begin{array}{c} \frac{2}{3} - 2n \\ 1 \end{array} \right\} \right] .
\tag{3.6.37}
$$

Plots for the G-tilt of the longitudinal, lateral, and total tilts for a 0.6-meter system for the HV-21 turbulence model are given in Figure 3-16. The ratio of the lateral to longitudinal tilt is given in Figure 3-17 for the same conditions.
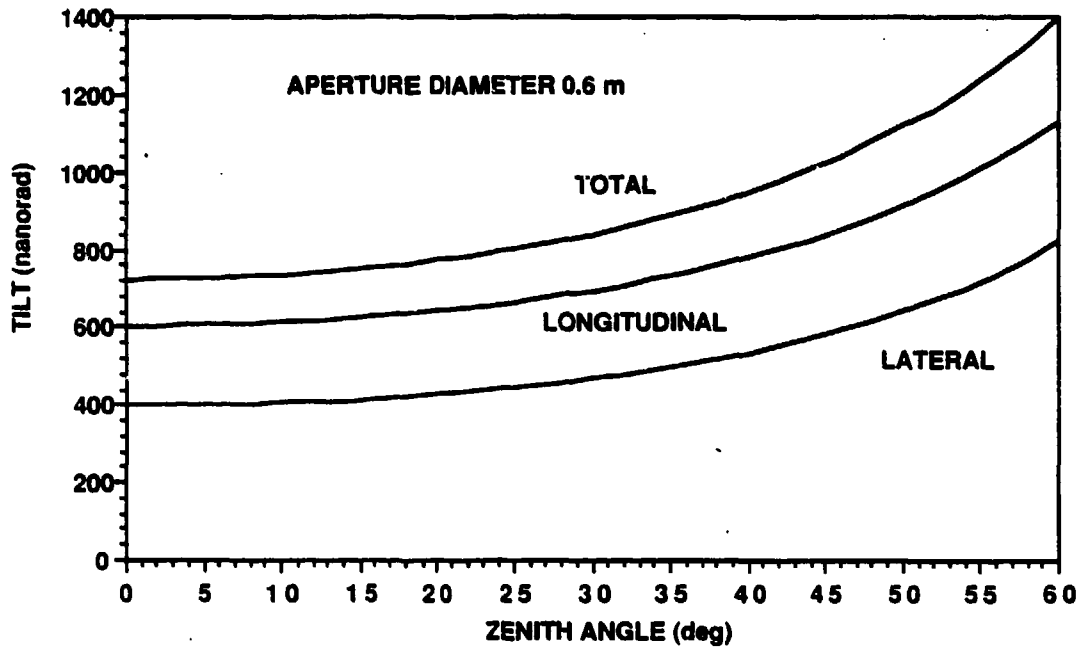

Figure 3-16. G-tilt anisoplanatism for 50-μrad separation with HV-21 turbulence.

A plot of the ratio of the longitudinal to lateral tilt is given in Figure 3-17.
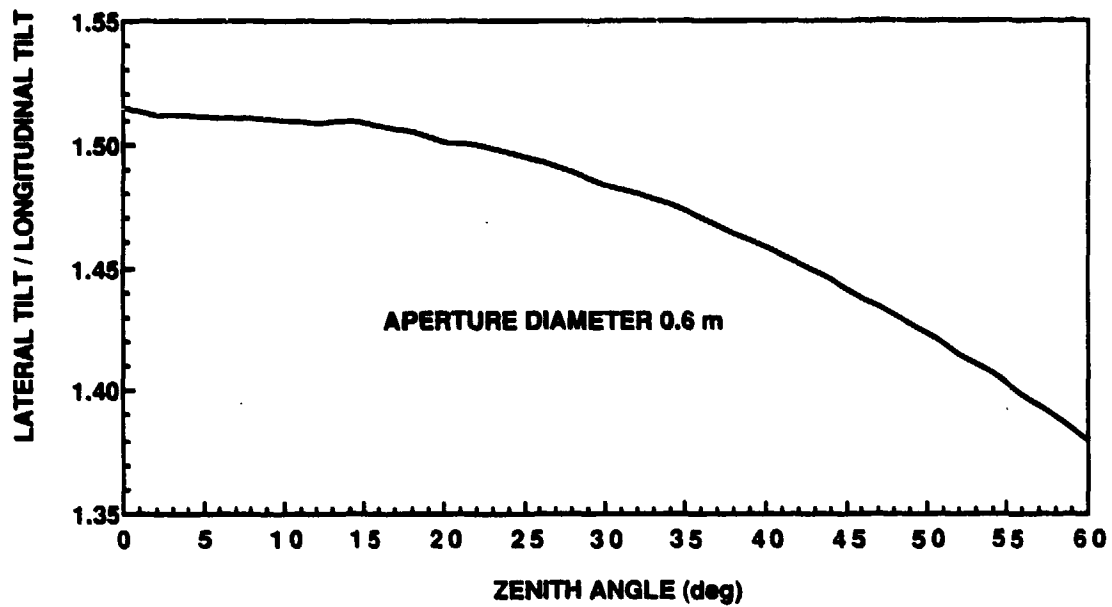
Figure 3-17. G-tilt ratios for 50-µrad separation with HV-21 turbulence versus zenith angle.

A comparison of the G and Z-tilts for a 1.2-m system are given in Figure 3-18.
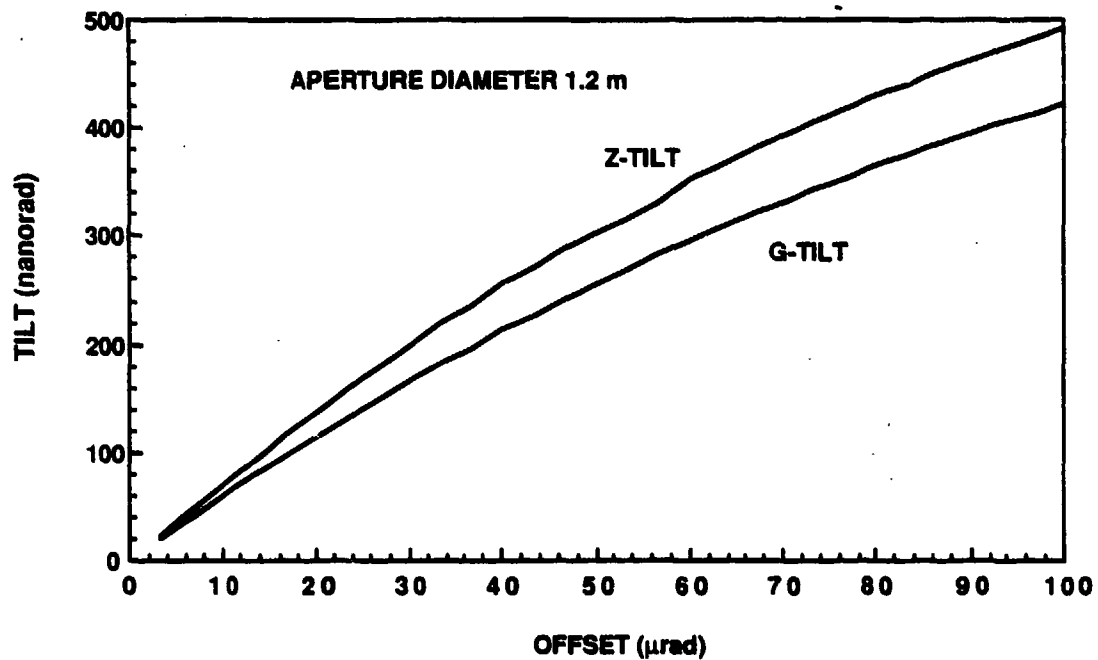
Figure 3-18. Comparison of the G- and Z-tilt anisoplanatism for a 1.2-m system with SLCSAT day turbulence.

144

These results agree with those calculated by Ellerbroek and Roberts.[23]

3.6.4 Outer Scale Effects on the Tilt Anisoplanatism

In this section, the outer scale will be included. Start from Equation (3.6.11).

$$\text{Let } \kappa d = t, \quad x = \frac{2\pi d}{L_o}, \text{ and } y = \frac{2d}{D} \qquad (3.6.38)$$

then Equations (3.6.13) and (3.6.14) are transformed into

$$\left\{ \begin{matrix} I_1 \\ I_T \end{matrix} \right\} = \frac{-4d^{11/3}}{D^2} \int_0^\infty \frac{dt}{t} \left\{ \begin{matrix} t^{-14/3}\left[J_1(t) - \frac{t}{2} \right] \\ t^{-11/3}\left[J_0(t) - 1 \right] \end{matrix} \right\} J_2^2\left(\frac{t}{y} \right)\left(1 + \left[\frac{x}{t} \right]^2 \right)^{11/6} . \qquad (3.6.39)$$

Using the generalized Mellin transform relation given in Equation (I.7) with the Mellin transforms used in the last section, plus that given in Equation (F.8), this can be converted into an integral in 2 complex planes that is

$$\left\{ \begin{matrix} I_1 \\ I_T \end{matrix} \right\} = \frac{-0.0945 \, d^{11/3}}{D^2 \, (2\pi i)^2} \iint ds \; dt \left(\frac{\pi d}{L_o} \right)^{-2s} \left(\frac{d}{D} \right)^{-2t}$$

$$\times \Gamma\left[\begin{matrix} s + t - \frac{11}{6}*, -t + 2, \frac{1}{2} + t, s, \frac{11}{6} - s \\ 3 + t, 1 + t \end{matrix} \right] \left\{ \begin{matrix} \dfrac{1}{2\,\Gamma\left[-s - t + \frac{23}{6} \right]} \\ \dfrac{1}{\Gamma\left[-s - t + \frac{17}{6} \right]} \end{matrix} \right\} . \qquad (3.6.40)$$

The two complex variables are s and t. Since $\Delta = \Delta' = 0$ for the t integration, the direction of closure depends on the size of the parameter. Since $\Delta = 2$ for the s integration, the path should be closed in the left-half plane. As explained in part 2, the only contributions are those at the simultaneous occurrence of poles in the s and t plane. The list of 2-poles are

(1) $\frac{11}{6} - s = -m, \; \frac{1}{2} + t = -n \rightarrow \; s = m + \frac{11}{6}, t = -n - \frac{1}{2}$,

(2) $\frac{11}{6} - s = -m, \; -t + 2 = -n \rightarrow \; s = m + \frac{11}{6}, \; t = 2 + n$,

(3) $\frac{11}{6} - s = -m, \; s + t - \frac{11}{6} = -n^* \rightarrow \; s = m + \frac{11}{6}, \; t = -n^* - m$,

(4) $s = -m, \; \frac{1}{2} + t = -n \rightarrow s = -m, \; t = -n - \frac{1}{2}$,

(5) $s = -m, \; -t + 2 = -n \rightarrow s = -m, \; t = 2 + n$,

(6) $s = -m, \quad s + t - \frac{11}{6} = -n^* \rightarrow s = -m, \quad t = -n^* + m + \frac{11}{6},$

(7) $\frac{1}{2} + t = -n, \quad s + t - \frac{11}{6} = -m^* \rightarrow s = -m^* + n + \frac{7}{3}, \quad t = -n - \frac{1}{2},$

(8) $-t + 2 = -n, \quad s + t - \frac{11}{6} = -m^* \rightarrow s = -m^* - n - \frac{1}{6}, \quad t = 2 + n.$ (3.6.41)

The values of m and n are integers that vary between 0 and ∞. The asterisk after a term means that the variable varies between 1 and ∞ on one side of the path of integration, and is equal to 0 on the other.

To determine the direction of path closure, the above relations are used to find the power law dependence of the variables for large values of m and n. The constant terms in the exponent do not affect the direction of path closure, and are not displayed explicitly. If the exponents have m and n terms in the same exponent, the terms must be separated by defining new variables. This statement is made clearer by performing this process for the eight sets of two-poles to give

(1) $\left(\frac{\pi d}{L_o}\right)^{-2m} \left(\frac{d}{D}\right)^{2n},$

(2) $\left(\frac{\pi d}{L_o}\right)^{-2m} \left(\frac{d}{D}\right)^{2n},$

(3) $\left(\frac{\pi d}{L_o}\right)^{-2m} \left(\frac{d}{D}\right)^{2n^*+2m} \rightarrow \left(\frac{\pi D}{L_o}\right)^{-2m} \left(\frac{d}{D}\right)^{2n^*},$

(4) $\left(\frac{\pi d}{L_o}\right)^{2m} \left(\frac{d}{D}\right)^{2n},$

(5) $\left(\frac{\pi d}{L_o}\right)^{2m} \left(\frac{d}{D}\right)^{-2n},$

(6) $\left(\frac{\pi d}{L_o}\right)^{2m} \left(\frac{d}{D}\right)^{2n^*-2m} \rightarrow \left(\frac{\pi D}{L_o}\right)^{2m} \left(\frac{d}{D}\right)^{2n^*},$

(7) $\left(\frac{\pi d}{L_o}\right)^{2m^*-2n} \left(\frac{d}{D}\right)^{2n} \rightarrow \left(\frac{\pi d}{L_o}\right)^{2m^*} \left(\frac{\pi D}{L_o}\right)^{-2n},$

(8) $\left(\frac{\pi d}{L_o}\right)^{2m^*+2n} \left(\frac{d}{D}\right)^{-2n} \rightarrow \left(\frac{\pi d}{L_o}\right)^{2m^*} \left(\frac{\pi D}{L_o}\right)^{2n}.$ (3.6.42)

This process produces the parameters that are relevant to the problem. The new parameter introduced above is the ratio of the diameter to the outer scale size. In this analysis, that ratio and the ratio of the displacement to the outer scale size will be considered to be less than 1. One could also solve the problem for these quantities greater than 1, and a different power series would be obtained.

To determine which pole residues must be included, conditions on each of the two parameters for each of the eight potential terms must be examined. Only those poles that satisfy both sets of conditions are to be included. Since the first parameter, $\pi d/L_o$, is less than 1, the exponent for large values of m must be greater than 0. In the first three sets of 2-poles above, this is not true and the path of integration is closed in the direction that does not include those poles, thereby, these terms do not contribute to the value of the integral. The last five terms have the proper sign of the exponent and contribute. In the last two terms, because of the presence of the asterisk, the value of m goes from 1 to ∞ rather than from 0 to ∞.

Examine the effect of the second parameter. For $d/D < 1$, the exponent has to be positive for large values of n. Pole sets 4 and 6 satisfy this criteria. In pole set 6, the value of n goes from 1 to ∞. For $d/D > 1$, one requires that the exponent is negative for large values of n. The correct pole sets for this case are 5 for all n, and also 6 for $n = 0$. The last term comes about because the path of integration split the poles so that one was on this side of path closure. The third parameter, $\pi D/L_o$, is less than 1, which requires positive values of the exponent for large values of n. Pole set 8 satisfies this criteria for all n.

To recapitulate these arguments, the conditions are:

(1) Pole sets 1, 2, 3, and 7 do not contribute.

(2) For $d/D < 1$, pole set 4 contributes for all n and m, and pole set 6 contributes for $n > 0$ and all m.

(3) For $d/D > 1$, pole set 5 contributes for all n and m, and pole set 6 contributes for $n = 0$, and all m.

(4) Pole set 8 contributes for all n, and for $m > 0$.

147

The value of the integral for small displacements, $d/D < 1$, can then be expressed as

$$\left\{ \begin{matrix} I_1 \\ I_T \end{matrix} \right\} = \frac{-0.0945\, d^{11/3}}{D^2} \left[\sum_{\substack{n=0 \\ m=0}}^{\infty} \frac{(-1)^{n+m}}{n!\; m!} \left(\frac{\pi d}{L_o} \right)^{2m} \left(\frac{d}{D} \right)^{2n+1} \right.$$

$$\times \Gamma \left[\begin{matrix} -m - n - \frac{7}{3},\, n + \frac{5}{2},\, \frac{11}{6} + m \\ \frac{5}{2} - n,\, \frac{1}{2} - n,\, n + m + \frac{10}{3} \end{matrix} \right] \left\{ \begin{matrix} \frac{0.5}{n+m+\frac{10}{3}} \\ 1 \end{matrix} \right\}$$

$$+ \sum_{\substack{n=1 \\ m=0}}^{\infty} \frac{(-1)^{n+m}}{n!\; m!} \left(\frac{\pi D}{L_o} \right)^{2m} \left(\frac{d}{D} \right)^{-11/3+2n}$$

$$\times \Gamma \left[\begin{matrix} n - m + \frac{1}{6},\, m - n + \frac{7}{3},\, m + \frac{11}{6} \\ -n + m + \frac{29}{6},\, -n + m + \frac{17}{6},\, n + 1 \end{matrix} \right] \left\{ \begin{matrix} \frac{0.5}{n+1} \\ 1 \end{matrix} \right\}$$

$$+ \left(\frac{D}{d} \right)^4 \sum_{\substack{n=0 \\ m=1}}^{\infty} \frac{(-1)^{n+m}}{n!\; m!} \left(\frac{\pi d}{L_o} \right)^{2m+1/3} \left(\frac{\pi D}{L_o} \right)^{2n}$$

$$\left. \times \Gamma \left[\begin{matrix} n + \frac{5}{2},\, -m - n - \frac{1}{6},\, m + n + 2 \\ n + 5,\, n + 3,\, m + 1 \end{matrix} \right] \left\{ \begin{matrix} \frac{0.5}{m+1} \\ 1 \end{matrix} \right\} \right].$$

(3.6.43)

For large displacements, $d/D > 1$, the integral is equal to

$$\left\{ \begin{matrix} I_1 \\ I_T \end{matrix} \right\} = \frac{-0.0945\, d^{11/3}}{D^2} \left[\sum_{\substack{n=0 \\ m=0}}^{\infty} \frac{(-1)^{n+m}}{n!\; m!} \left(\frac{\pi d}{L_o} \right)^{2m} \left(\frac{d}{D} \right)^{-4-2n} \right.$$

$$\times \Gamma \left[\begin{matrix} -m - n + \frac{1}{6},\, n + \frac{5}{2},\, \frac{11}{6} + m \\ 5 + n,\, 3 + n,\, m - n + \frac{5}{6} \end{matrix} \right] \left\{ \begin{matrix} \frac{0.5}{m-n+\frac{5}{6}} \\ 1 \end{matrix} \right\}$$

$$- \left(\frac{D}{d} \right)^4 \sum_{m=0}^{\infty} \frac{(-1)^m}{m!} \left(\frac{\pi D}{L_o} \right)^{1/3+2m} \Gamma \left[\begin{matrix} -m + \frac{1}{6},\, m + \frac{7}{3},\, m + \frac{11}{6} \\ m + \frac{29}{6},\, m + \frac{17}{6},\, n + 1 \end{matrix} \right] \left\{ \begin{matrix} \frac{0.5}{n+1} \\ 1 \end{matrix} \right\}$$

$$+\left(\frac{D}{d}\right)^4 \sum_{\substack{n=0 \\ m=1}}^{\infty} \frac{(-1)^{n+m}}{n!\ m!} \left(\frac{\pi d}{L_o}\right)^{2m+1/3} \left(\frac{\pi D}{L_o}\right)^{2n}$$

$$\times \Gamma \begin{bmatrix} n+\frac{5}{2},-m-n-\frac{1}{6},\ m+n+2 \\ n+5, n+3,\ m+1 \end{bmatrix} \begin{Bmatrix} \frac{0.5}{m+1} \\ 1 \end{Bmatrix} \Biggr].$$

$$(3.6.44)$$

If the outer scale goes to infinity, only the terms with $m = 0$ contribute, and these expressions reduce to the ones in the last section in which the outer scale was neglected.

For no angular difference between the two beams and small displacements of the aperture, $d/D < 1$, the tilt variance can be written as

$$\begin{Bmatrix} \sigma_x^2 \\ \sigma_y^2 \end{Bmatrix} = \frac{-31.5\ \mu_o}{d^{1/3}} \left[\sum_{\substack{n=0 \\ m=0}}^{\infty} \frac{(-1)^{n+m}}{n!\ m!} \left(\frac{\pi d}{L_o}\right)^{2m} \left(\frac{d}{D}\right)^{2n+5} \right.$$

$$\times \Gamma \begin{bmatrix} -m-n-\frac{7}{3},\ n+\frac{5}{2},\frac{11}{6}+m \\ \frac{5}{2}-n,\frac{1}{2}-n,n+m+\frac{13}{3} \end{bmatrix} \begin{Bmatrix} 2n+2m+\frac{17}{3} \\ 1 \end{Bmatrix}$$

$$+ \sum_{\substack{n=1 \\ m=0}}^{\infty} \frac{(-1)^{n+m}}{n!\ m!} \left(\frac{\pi D}{L_o}\right)^{2m} \left(\frac{d}{D}\right)^{2n+1/3} \Gamma \begin{bmatrix} n-m+\frac{1}{6},m\ -n+\frac{7}{3},m\ +\frac{11}{6} \\ -n+m+\frac{29}{6},-n\ +m+\frac{17}{6},n\ +2 \end{bmatrix} \begin{Bmatrix} 2n+1 \\ 1 \end{Bmatrix}$$

$$+ \sum_{\substack{n=0 \\ m=1}}^{\infty} \frac{(-1)^{n+m}}{n!\ m!} \left(\frac{\pi d}{L_o}\right)^{2m+1/3} \left(\frac{\pi D}{L_o}\right)^{2n} \Gamma \begin{bmatrix} n+\frac{5}{2},-m-n-\frac{1}{6},\ m+n+2 \\ n+5,\ n+3,\ m+2 \end{bmatrix} \begin{Bmatrix} 2m+1 \\ 1 \end{Bmatrix} \left. \right].$$

$$(3.6.45)$$

The most significant terms for small displacements are the $n = 1$, $m = 0$, and the $n = 1$, $m = 1$ terms of the second summation, which give

$$\begin{Bmatrix} \sigma_x^2 \\ \sigma_y^2 \end{Bmatrix} = \frac{2.67\ \mu_o}{D^{1/3}} \left(\frac{d}{D}\right)^2 \begin{Bmatrix} 3 \\ 1 \end{Bmatrix} \left[1 - 20.6 \left(\frac{D}{L_o}\right)^2 + ... \right] \qquad (3.6.46)$$

149

The first term is the same as that in Equation (3.6.24) in which outer scale was neglected. In Section 3.6.1 when tilt with outer scale was considered, the outer scale had a significant effect on the tilt because the leading term with the outer scale was to the inverse one-third power. Here the effect is small if the outer scale size is significantly greater than the diameter because the leading term is the inverse second power of the ratio. The physical reason this occurs is that for small relative aperture displacements, the two beams see the same tilt from long wavelength turbulence which cancels when the tilts are subtracted from each other. Mathematically, this subtraction had the result of having the third summation start at $m = 1$ rather than 0. The term that was eliminated has the one-third power law dependence on outer scale.

For an angular displacement of the beam, the tilt anisoplanatism can be written for small angles and low altitudes, $\Theta z/D > 1$, as

$$
\left\{ \begin{matrix} \sigma_x^2 \\ \sigma_y^2 \end{matrix} \right\} = \frac{-31.5}{D^{1/3}} \left[\sum_{\substack{n=0 \\ m=0}}^{\infty} \frac{(-1)^{n+m} \mu_{2n+2m+14/3}^-(H_c)}{n!\, m!} \left(\frac{\pi\Theta}{L_o} \right)^{2m} \left(\frac{\Theta}{D} \right)^{2n+14/3} \right.
$$

$$
\times \Gamma \left[\begin{matrix} -m - n - \frac{7}{3}, n + \frac{5}{2}, \frac{11}{6} + m \\ \frac{5}{2} - n, \frac{1}{2} - n, n + m + \frac{13}{3} \end{matrix} \right] \left\{ \begin{matrix} 2n + 2m + \frac{17}{3} \\ 1 \end{matrix} \right\}
$$

$$
+ \sum_{\substack{n=1 \\ m=0}}^{\infty} \frac{(-1)^{n+m} \mu_{2n}^-(H_c)}{n!\, m!} \left(\frac{\pi D}{L_o} \right)^{2m} \left(\frac{\Theta}{D} \right)^{2n}
$$

$$
\times \Gamma \left[\begin{matrix} n - m + \frac{1}{6}, m - n + \frac{7}{3}, m + \frac{11}{6} \\ -n + m + \frac{29}{6}, -n + m + \frac{17}{6}, n + 2 \end{matrix} \right] \left\{ \begin{matrix} 2n + 1 \\ 1 \end{matrix} \right\}
$$

$$
+ \sum_{\substack{n=0 \\ m=1}}^{\infty} \frac{(-1)^{n+m} \mu_{2m}^-(H_c)}{n!\, m!} \left(\frac{\pi\Theta}{L_o} \right)^{2m+1/3} \left(\frac{\pi D}{L_o} \right)^{2n} \Theta^{-1/3}
$$

150

$$\times \Gamma \left[\begin{array}{c} n + \frac{5}{2}, -m - n - \frac{1}{6}, m + n + 2 \\ n + 5, n + 3, m + 2 \end{array} \middle| \left\{ \begin{array}{c} 2m + 1 \\ 1 \end{array} \right\} \right].$$

<div align="right">(3.6.47)</div>

At larger angles and higher altitudes, $\Theta z/D > 1$, the tilt variance is equal to

$$\left\{ \begin{array}{c} \sigma_x^2 \\ \sigma_y^2 \end{array} \right\} = \frac{-31.5}{\Theta^{1/3}} \left[\sum_{\substack{n=0 \\ m=0}}^{\infty} \frac{(-1)^{n+m}}{n! \, m!} \left(\frac{\pi \Theta}{L_o} \right)^{2m} \mu_{2m-2n-1/3} \right.$$

$$\times \Gamma \left[\begin{array}{c} -m - n + \frac{1}{6}, n + \frac{5}{2}, \frac{11}{6} + m \\ 5 + n, 3 + n, m - n + \frac{11}{6} \end{array} \middle| \left\{ \begin{array}{c} 2m - 2n + 5/3 \\ 1 \end{array} \right\} \right.$$

$$- \sum_{m=0}^{\infty} \frac{(-1)^m}{m!} \left(\frac{\pi D}{L_o} \right)^{1/3+2m} \mu_{-1/3} \Gamma \left[\begin{array}{c} -m + \frac{1}{6}, m + \frac{7}{3}, m + \frac{11}{6} \\ m + \frac{29}{6}, m + \frac{17}{6}, n + 2 \end{array} \middle| \left\{ \begin{array}{c} 2n + 1 \\ 1 \end{array} \right\} \right.$$

$$+ \sum_{\substack{n=0 \\ m=1}}^{\infty} \frac{(-1)^{n+m}}{n! \, m!} \left(\frac{\pi \Theta}{L_o} \right)^{2m+1/3} \left(\frac{\pi D}{L_o} \right)^{2n} \mu_{2m}$$

$$\times \Gamma \left[\begin{array}{c} n + \frac{5}{2}, -m - n - \frac{1}{6}, m + n + 2 \\ n + 5, n + 3, m + 2 \end{array} \middle| \left\{ \begin{array}{c} 2m + 1 \\ 1 \end{array} \right\} \right].$$

<div align="right">(3.6.48)</div>

For small angular displacements, the most significant terms with outer scale included are the $m = 0, n = 1$ term and the $m = 1, n = 1$ term of the second summation of Equation (3.6.47) which give

$$\left\{ \begin{array}{c} \sigma_x^2 \\ \sigma_y^2 \end{array} \right\} = \frac{2.67 \, \mu_2(H_c)}{D^{1/3}} \left(\frac{\Theta}{D} \right)^2 \left\{ \begin{array}{c} 3 \\ 1 \end{array} \right\} \left[1 - 20.6 \left(\frac{D}{L_o} \right)^2 + \ldots \right] \qquad \text{(3.6.49)}$$

Here the outer scale has the same relative effect as that due to displacement anisoplanatism in Equation (3.6.46).

<div align="center">151</div>

3.6.5 Tilt with Inner Scale

The expression for tilt given in Equation (3.5.9) goes to infinity when the diameter goes to zero. This obviously is an incorrect physical limit, and to determine the tilt for very small apertures the inner scale must be included. To find the tilt with inner scale, the turbulence spectrum with inner scale must be used in Equation (3.5.7) to obtain

$$T_i^2 = \frac{105.1\,\mu_o}{D^{1/3}} \int_0^\infty dx\ x^{-11/3-1} J_2^2(x) \exp\left[-(x/a)^2\right], \tag{3.6.50}$$

where
$$a = \kappa_i D / 2. \tag{3.6.51}$$

The Mellin transforms in Equations (F.6) and (F.1) can be used in the convolution integral. After the substitution $s \to 2s$ to get unity coefficients in the Gamma functions, one obtains

$$T_i^2 = \frac{29.64\,\mu_o}{D^{1/3}} \frac{1}{2\pi i} \int ds\ \Gamma\left[\begin{matrix} s+\frac{1}{6},\ -s+\frac{7}{3},\ -s \\ -s+\frac{29}{6},\ -s+\frac{17}{6} \end{matrix}\right] a^{-2s}. \tag{3.6.52}$$

Since $\Delta = 1$, the path of integration can be closed in the left-half plane. If the inner scale is larger than the diameter, then the leading term is

$$T_i^2 = \frac{6.67\mu_o}{L_i^{1/3}} + \dots . \tag{3.6.53}$$

The tilt calculated with inner scale neglected equals that above when the diameter is twice the inner scale size. If the inner scale size is 1 millimeter, the maximum tilt one could measure would be 12 microradians with the HV-21 turbulence distribution.

3.6.6 Zernike Tilt on an Annular Aperture

Most telescopes have a central obscuration so that a detailed calculation should take into account this annular geometry. Mostly the effect of the central obscuration is ignored because it does not produce a significant difference from the results over the full aperture. In this section, the effect of the central obscuration on the Zernike tilt will be calculated and shown to produce a small change in the tilt from the unobscured aperture.

152

The approach taken is the same that has been used. The expression for the phase variance given in Equation (A.1) is used in conjunction with the filter function for Zernike tilt on an annular aperture given in Equation (B.10). The tilt variance in this case is

$$T_a^2 = 0.2073 k_o^2 \int_0^L dz\, C_n^2(z) \int d\vec{\kappa} \left(\frac{16}{k_o D[1-\beta^4]}\right)^2 \left[\frac{J_2(\kappa D / 2)}{\kappa D / 2} - \beta^3 \frac{J_2(\kappa \beta D / 2)}{\kappa \beta D / 2}\right]^2.$$

(3.6.54)

The obscuration ratio, β, is equal to the ratio of the diameter of the central obscuration to the full diameter. The angular and axial integrations can be performed, and if the term in brackets is squared, the first term is just the Zernike tilt of a full aperture and the second term squared is the same multiplied by a constant. Making the substitution $x = \kappa D/2$, the tilt can then be written as

$$T_a^2 = \frac{6.08\mu_o}{D^{1/3}[1-\beta^4]^2}\left[1 + \beta^{23/3} - 210\beta^2 \int_0^\infty \frac{dx}{x}\cdot x^{-11/3} J_2(x) J_2(\beta x)\right].$$

(3.6.55)

Using the Mellin convolution theorem and the Mellin transform in Equation (F.5), and making the substitution $s \rightarrow 2s$, one obtains for the last integral

$$I = \frac{2^{-14/3}}{2\pi i} \int ds\, \beta^s \Gamma\left[\begin{matrix} s - \frac{5}{6}, -s + 1 \\ -s + \frac{23}{6}, s + 2 \end{matrix}\right].$$

(3.6.56)

Since $\Delta = \Delta' = 0$, and the obscuration ratio is always less than 1 the path of integration is closed in the right-half plane and the integral is equal to the residues at $s = 1 + n$, $n = 0, 1, 2,$ .... The tilt variance is equal to

$$T_a^2 = \frac{6.08\mu_o}{D^{1/3}[1-\beta^4]^2}\left(1 + \beta^{23/3} - 1.36\sum_{n=0}^\infty \frac{(-1)^n}{n!} \beta^{4+2n} \Gamma\left[\begin{matrix} n + \frac{1}{6} \\ -n + \frac{17}{6}, n + 3 \end{matrix}\right]\right).$$

(3.6.57)

The first few terms of the solution which give an answer accurate to better than 1% for all

153

obscuration ratios are

$$T_a^2 \approx 6.08 \; \mu_o \frac{\left[1 + \beta^{23/3} - 2.196 \; \beta^4 + 0.2236 \; \beta^6 - 0.02717 \; \beta^8 - 0.0004808 \; \beta^{10}\right]}{D^{1/3}\left[1 - \beta^4\right]^2}.$$

(3.6.58)

The curve of this function is shown in Figure 3-19.
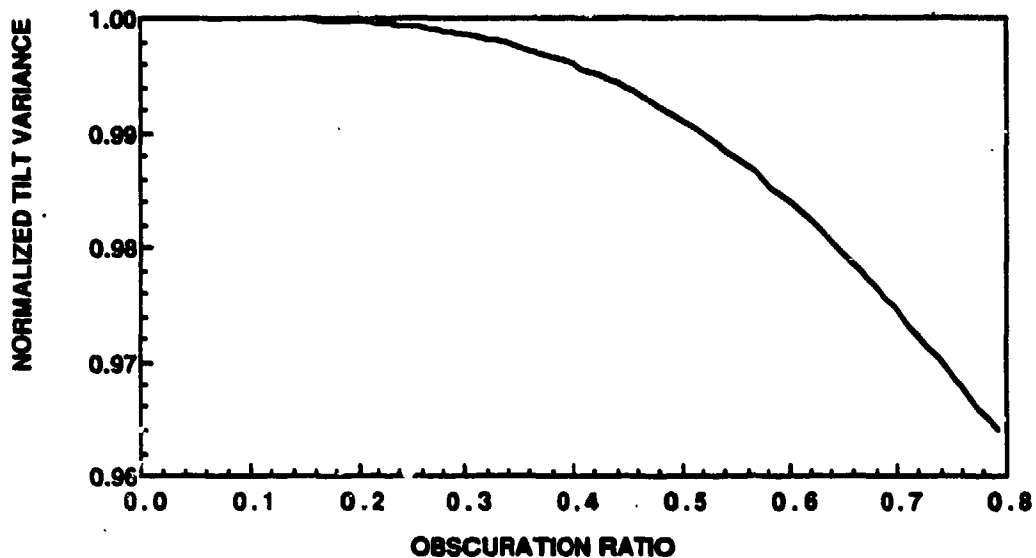
Figure 3-19. Normalized Zernike tilt for an annular aperture.

Notice that there is very little change in the measured tilt even for sizable central obscurations. This agrees with the conclusions of Greenwood.[24]

3.6.7 Diffraction with Zernike Tilt

As the beam propagates, it eventually spreads due to diffraction and the tilt can be affected. In this section, the effect of diffraction on the Zernike tilt is considered by using the standard formula for phase variance given in Equation (A.1) with the tilt term given in Equation (B.7) and the collimated term given in Equation (A.4). By not setting the cosine term equal to 1 as was done in the past, diffraction effects can be calculated. The formula for the tilt is

154

$$T_d^2 = 0.2073 \, k_o^2 \int_0^L dz \; C_n^2(z) \int d\vec{\kappa} \; \kappa^{-11/3} \left(\frac{16}{k_o D}\right)^2 \left[\frac{J_2(\kappa D/2)}{\kappa D/2}\right]^2 \cos^2\left[\frac{\kappa^2(z-L)}{2k_o}\right].$$

$$(3.6.59)$$

Integrate over angle and let

$$x = \kappa D / 2, \qquad\qquad (3.6.60)$$

and

$$t = D\sqrt{\frac{k_o}{2(L-z)}} \; . \qquad\qquad (3.6.61)$$

The integral becomes

$$T_d^2 = \frac{105}{D^{1/3}} \int_0^L dz \; C_n^2(z) \int_0^\infty \frac{dx}{x} \; x^{-11/3} J_2^2(x)\left[1 - \sin^2(x/t)^2\right]. \; (3.6.62)$$

The first term is the Zernike tilt that was found previously. Using the Mellin convolution theorem with the Mellin transforms given in Equations (F.6) and (F.4), and the use substitution $s \to 2s$, one obtains

$$T_d^2 = \frac{6.08 \, \mu_o}{D^{1/3}} \left(1 + \frac{2.159}{\mu_o} \int_0^L dz \, C_n^2(z) \int ds \, t^{-2s} \Gamma\left[\begin{array}{c} s + \frac{1}{6}, -s + \frac{7}{3}, -s / 2* \\ -s + \frac{29}{6}, -s + \frac{17}{6}, \frac{1}{2} + s / 2 \end{array}\right]\right).$$

$$(3.6.63)$$

Since $\Delta = 1$, the path of integration should be closed in the left-half plane. Because t is large, an asymptotic series is appropriate, and the simple poles in the right-half plane that are located at $s = -7/3 + n$, $n = 0, 1, 2, \ldots$, and at $s = 2n$, $n = 1, 2, 3, \ldots$ gives an asymptotic series that is the sum of these terms plus the $E(x)$ term. The case of tilt measured exoatmospherically at ranges that are about the Fresnel distance is considered here. In that case, the most significant term of the solution is retained. For the case where $L \gg z$ for values of z for which the turbulence is significant, the tilt is

$$T_d^2 \approx \frac{6.08 \, \mu_o}{D^{1/3}}\left[1 - 0.49\left(\frac{\lambda L}{D^2}\right)\right]. \qquad\qquad (3.6.64)$$

155

The variance has been reduced by 50% at the Fresnel range, and the tilt is reduced by about 25%. This tilt reduction will more significantly affect the high temporal frequencies which are typically caused by shorter spatial wavelengths.

3.6.8 Scintillation with Inner Scale

Scintillation of a space object as seen from the ground is mainly due to high altitude turbulence that results in a corrugation of the wavefront which causes rays to converge at some places on the ground and to move away from other regions. Since the higher spatial frequency turbulence components have a smaller distance to move before they affect the turbulence at that wavelength, one suspects that the scintillation is largely due to turbulence at short wavelengths. If this is so, then viscosity which limits the highest spatial frequencies may significantly affect the scintillation. This cutoff in the turbulence spectrum is represented by the inner scale. In this section, the inner scale will be considered to be constant with altitude in order to see if the effect might be significant for reasonable values of the inner scale size. It is found that if the inner scale size is less than a millimeter, inner scale effects do not affect the scintillation; however, if the inner scale is a centimeter or greater the scintillation is greatly reduced.

Using the standard formula for scintillations given in Equation (A.1) with the turbulence spectrum given in Equation (A.6) with inner scale retained, one obtains

$$\chi^2 = 0.2073 \, k_o^2 \int_0^L dz \; C_n^2(z) \int d\vec{\kappa} \; \kappa^{-11/3} \exp\left[-\left(\frac{\kappa^2}{\kappa_i^2}\right)\right] \sin^2\left(\frac{\kappa^2 z}{2 k_o}\right). \tag{3.6.65}$$

The wave is propagated from z equal to 0 to z equal to L. For a wave propagated from the ground to space z is replaced with $L - z$. Integrating this over the angle in kappa-space and making the substitutions

$$t = \kappa\left(\frac{z}{2 k_o}\right)^{1/2}, \tag{3.6.66}$$

and

$$x = \kappa_i\left(\frac{z}{2 k_o}\right)^{1/2}, \tag{3.6.67}$$

156

one obtains

$$\chi^2 = 1.303\, k_o^2 \int_0^L dz\; C_n^2(z) \left(\frac{z}{2k_o}\right)^{5/6} \int dt\, \frac{t^{5/3}}{t} \sin^2(t^2) \exp\left[-\left(\frac{t}{x}\right)^2\right]. \quad (3.6.68)$$

The Mellin convolution integral is used to evaluate the last integral using the transforms in Equations (F.4) and (F.5). If s is replaced by $2s$ in the integral, it is equal to

$$I = \frac{\sqrt{\pi}}{8(2\pi i)} \int ds\; x^{-2s}\; \Gamma\left[\begin{array}{c} s/2 - \frac{5}{12}*, -s \\ \frac{11}{12} - s/2 \end{array}\right]. \quad (3.6.69)$$

Since $\Delta = 0$, the direction of path closure is determined by the size of the parameter. Except at very low altitudes ($z < 4$ m), the parameter is greater than unity. The contribution below this low altitude will be neglected since it is insignificant in determining scintillation. There are poles at $s = 5/6$, and $s = n$ for $n = 0, 1, 2 \ldots$. Evaluating the residues at these poles gives

$$\chi^2 = -0.162\, k_o^{7/6} \int_0^\infty dz C_n^2(z) z^{5/6} \left[\sum_{n=0}^{\infty} \frac{(-1)^n}{n!} \Gamma\left[\begin{array}{c} n/2 - \frac{5}{12} \\ -n/2 + \frac{11}{12} \end{array}\right] \left(\frac{z\kappa_i^2}{2k_o}\right)^{-n} - 13.43\left(\frac{k_o}{z\kappa_i^2}\right)^{5/6}\right]. \quad (3.6.70)$$

The first few terms of this solution are

$$\chi^2 = 0.563\, k_o^{7/6} \mu_{5/6} - 2.175\, \mu_o k_o^{7/6} \left(\frac{\lambda_i^2}{\lambda_o}\right)^{5/6} + 1.75\frac{\lambda_i^2}{\lambda_o} k_o^{7/6} \mu_{-1/6} + \cdots . \quad (3.6.71)$$

The first term is the formula for scintillation without outer scale effects that was obtained in Section 3.5.4. The ratio of the second term to the first term is

$$\text{Ratio} = 3.86\frac{\mu_o}{\mu_{5/6}}\left(\frac{\lambda_i^2}{\lambda_o}\right)^{5/6}. \quad (3.6.72)$$

For a wavelength of 0.5 micrometers and the HV-21 turbulence model, this ratio is 0.028 for an inner scale size of 1 mm and 1.31 for inner scale size of 1 cm. Since the inner scale size is typically in this size regime, it may affect the observed scintillation.

3.6.9 Scintillation Anisoplanatism for Corrected Beams

The corrected beam in an adaptive-optics system can have scintillation due to several causes. In Section 3.5.7 the scintillation on a perfectly corrected beam was considered. Here the scintillation produced on a system that has an anisoplanatic error is considered.

For each realization, scintillation is produced by the effects of the distorted wavefront that originates at the mirror. The phase disturbance at the mirror produced by a section of turbulence at an altitude z propagates up to the turbulence section before the phase disturbance is canceled. While it propagates over this distance, amplitude scintillations build up. In the present analysis, the propagating beam has an additional phase offset due to the different paths of the collimated beam and the focused beam through the turbulence. In transform space, this offset produces a phase offset of one beam with respect to the other. It does not matter which beam this offset is applied to since the filter function is the absolute value squared of the complex filter function. The filter function for this effect is obtained by modifying the filter function in Equation (3.5.39) by including the phase term to give

$$
F(\vec{\kappa}, z) = \left| \sin\left[\frac{\kappa^2 L}{2 k_o}\right] - \exp[\, i\vec{\kappa} \cdot \vec{d}\,]\sin\left[\frac{\kappa^2(L-z)}{2 k_o}\right] \right|^2
$$

$$
= \sin^2\left[\frac{\kappa^2 L}{2 k_o}\right] + \sin^2\left[\frac{\kappa^2(L-z)}{2 k_o}\right] - 2\cos(\vec{\kappa} \cdot \vec{d})\sin\left[\frac{\kappa^2 L}{2 k_o}\right]\sin\left[\frac{\kappa^2(L-z)}{2 k_o}\right].
$$

$$(3.6.73)$$

Use the standard expression in Equation (A.1) for the amplitude variance with outer and inner scale effects neglected which is

$$
\chi^2 = 0.2073 \, k_o^2 \int_0^L dz \ C_n^2(z) \int d\vec{\kappa} \ F(\vec{\kappa}, z) \ \kappa^{-11/3}.
$$

$$(3.6.74)$$

Use the same analysis as in Section 3.5.7 to evaluate the integral of the first two terms of the filter function to obtain

$$
\chi^2 = 0.563 k_o^{7/6} \int_0^L dz \, C_n^2(z) \left[L^{5/6} + (L-z)^{5/6} \right] + I.
$$

$$(3.6.75)$$

158

The last expression is due to the last term of the filter function which can be integrated over angle and modified using the trigonometric identity for the product of sinusoids to obtain

$$I = - 1.303 \, k_o^2 \int_0^L dz \, C_n^2(z) \int d\kappa \, \kappa^{-8/3} \, J_o(\kappa d) \left(\cos\left[\frac{\kappa^2 L}{2 k_o} \right] - \cos\left[\frac{\kappa^2 (2L - z)}{2 k_o} \right] \right). \quad (3.6.76)$$

Change variables so that

$$t^2 = \frac{\kappa^2 z}{2 k_o}, \quad (3.6.77)$$

in the first term, and

$$t^2 = \frac{\kappa^2 (2L - z)}{2 k_o}, \quad (3.6.78)$$

in the second. Also let

$$x_1^2 = \frac{z}{2 k_o d^2}, \quad (3.6.79)$$

and

$$x_2^2 = \frac{2L - z}{2 k_o d^2}. \quad (3.6.80)$$

The expression then becomes

$$I = - 0.731 \, k_o^{7/6} \int_0^L dz \, C_n^2(z)$$

$$\times \left[z^{5/6} \int_0^\infty \frac{dt}{t} \, t^{-5/3} J_o\left(\frac{t}{x_1} \right) \cos \, t^2 - (2L - z)^{5/6} \int_0^\infty \frac{dt}{t} \, t^{-5/3} J_o\left(\frac{t}{x_2} \right) \cos \, t^2 \right].$$

$$(3.6.81)$$

Each of the last two integrals can be treated in the same manner using Equations (F.5) and (F.3) in the Mellin convolution integral to give

$$I_1 = \frac{1}{2 \pi i} \frac{\sqrt{\pi}}{2^{17/6}} \int ds \, (2 x^2)^{-s} \, \Gamma\left[\begin{matrix} s/2 - \frac{5}{12}, \, -s \\ \frac{11}{12} - s/2, \, 1 + s \end{matrix} \right]. \quad (3.6.82)$$

159

The only difference between the two original integrals is that the parameter is different in the above integral. Since $\Delta = -1$, the path of integration is closed in the right-half plane and there are poles located at $s = n$, $n = 0, 1, 2, \ldots$. The value of the integral is

$$I = -0.1818\, k_o^{7/6} \int_0^L dz\, C_n^2(z)$$

$$\times \sum_{n=0}^{\infty} \frac{(-1)^n}{n!} \Gamma\left[\begin{array}{c} n/2 - \frac{5}{12} \\ \frac{11}{12} - n/2, 1+n \end{array}\right]\left[z^{5/6}\left(\frac{k_o d^2}{z}\right)^n - (2L-z)^{5/6}\left(\frac{k_o d^2}{2L-z}\right)^n \right]. \quad (3.6.83)$$

If just the first term of the series is retained, the scintillation is the same as the one with no anisoplanatism given in Equation (3.5.42).

If the beacon is a point source located at H, and one wants the scintillation at a distance r off the axis, then the displacement between the collimated and focused ray is $d = \frac{zr}{H}$. For beacon heights outside the atmosphere, the parameters in the solution are large and one has to retain only the first two terms of the infinite series to get accurate results. The scintillation in this case is

$$\chi^2 \approx 0.563\, k_o^{7/6} \int_0^L dz\, C_n^2(z)\left\{ L^{5/6} + (L-z)^{5/6} - 2^{1/6}\left[(2L-z)^{5/6} - z^{5/6} \right] \right\}$$

$$+ 0.492\frac{k_o^{13/6} r^2}{H^2} \int_0^L dz\, C_n^2(z)\left[z^{11/6} - \frac{z^2}{(2L-z)^{1/6}} \right]. $$

$$(3.6.84)$$

For long ranges, the second term in brackets in the second integral is smaller than the first term and the expression reduces to

$$\chi^2 \approx 0.563\, k_o^{7/6} 2^{1/6} \mu_{5/6} + 0.492\frac{k_o^{13/6} r^2 \mu_{11/6}}{H^2}. \quad (3.6.85)$$

For the HV-21 model, if the beacon is a point source, the scoring beam is collimated, and the target is at 300 km, then the last term is equal to 0.0008 at the outer radius of the beam located at 0.3 m. This is insignificant compared to the first term which has a value of about 0.05.

Therefore, the use of a point beacon does not increase the scintillation. The expression does depend on the inverse square of the beacon height, and if the beacon were very low, one would observe a significant increase in the scintillation.

3.6.10 Scintillation Anisoplanatism

Here, the differential scintillation between two uncorrected beams that originate exoatmospherically and are displaced from each other is calculated. This analysis is applicable to the measured scintillation difference between the two components of a double star system. To solve this problem, the filter function is formed from that for anisoplanatism multiplied by the term that gives one the scintillation of a down-propagating wave which is

$$F(\vec{\kappa}, z) = 2 \sin^2\left[\frac{\kappa^2 z}{2 k_o}\right][1 - \cos(\vec{\kappa} \cdot \vec{d})]. \qquad (3.6.86)$$

Inserting this into the standard formula and performing the angular integration gives

$$\chi^2 = -2.606 \, k_o^2 \int_0^\infty dz \; C_n^2(z) \int d\kappa \; \kappa^{-8/3}[\, J_o(\kappa d) - 1]\sin^2\left[\frac{\kappa^2 z}{2 k_o}\right]. \qquad (3.6.87)$$

Let $t = \kappa d$, and $x^2 = \dfrac{2 k_o d^2}{z}$, then

$$\chi^2 = -2.606 \, k_o^2 \int_0^\infty dz \; C_n^2(z) d^{5/3} \int_0^\infty \frac{dt}{t} \; t^{-5/3}[\, J_o(t) - 1]\sin^2\left[\left(\frac{t}{x}\right)^2\right]. \qquad (3.6.88)$$

The last integral can be converted into one in the complex plane using the Mellin transforms in Equations (F.4) and (F.5) to give

$$I = \frac{\sqrt{\pi}}{2^{14/3}} \frac{1}{2\pi i} \int ds \; \left(\frac{x}{2}\right)^{-2s} \Gamma\left[\begin{array}{c} s - \frac{5}{6}*, \; -s/2* \\ \frac{11}{6} - s, \; \frac{1}{2} + s/2 \end{array}\right]. \qquad (3.6.89)$$

Since $\Delta = 1$, close the path of integration in the left-half plane and pick up the pole contributions at $s = 0$, and $5/6 - n$ for $n = 1, 2, 3, \ldots$. Therefore, the scintillation can be written as

$$\chi^2 = 1.455 \, k_o^2 \int_0^\infty dz \; C_n^2(z) d^{5/3}$$

161

$$-0.1818\, k_o^2 \int_0^\infty dz\; C_n^2(z) d^{5/3} \sum_{n=1}^\infty \frac{(-1)^n}{n!} \left(\frac{k_o d^2}{2z}\right)^{n-5/6} \Gamma \begin{bmatrix} n/2 - \frac{5}{12} \\ n+1,\, n/2 + \frac{11}{12} \end{bmatrix}.$$

(3.6.90)

For very large separations, the first pole on the other side of the path of integration that occurs at $s = 5/6$ is the main contributor. Evaluating the residue at this pole, one obtains for large path separations

$$\chi^2 \approx 2 \times 0.563\, k_o^{7/6}\, \mu_{5/6}.$$

(3.6.91)

This is twice the scintillation for a point source, and it is what is expected since the scintillations from the two sources are uncorrelated for large path separations. For two paths that are separated by a small angle, the first two terms of the general solution are retained to give

$$\chi^2 \approx 0.50 \left(\frac{\Theta}{\Theta_o}\right)^{5/3} + 2.1 k_o^{13/6} \Theta^2 \mu_{11/6}.$$

(3.6.92)

The above expression, which only includes two terms of the series solution. is only valid for angles considerably smaller than the isoplanatic angle. The scintillation increases rapidly with angle and is substantial when the separation is equal to the isoplanatic angle. This is to be contrasted with tilt anisoplanatism in which the tilt difference is very small compared to the tilt from a single object even for angles many times the isoplanatic angle. The reason for this difference in scale factors is that the tilt is caused by turbulence with long wavelengths and there has to be a substantial difference in path separations to get a different effect from these long wavelength disturbances. In contrast, the small wavelength disturbances contribute most strongly to scintillation effects and a smaller separation between paths produces significant effects. One cannot use the relative scintillation difference between stars to get a direct measurement of the turbulence distributions since, for reasonable star separations, several terms of the series solution are needed to get the correct value of scintillation and each term contains a different turbulence moment.

3.7 PHASE VARIANCE FOR A POINT AND DISTRIBUTED SOURCE

In this section, the phase variance for point and distributed sources will be found. The technique to find the variance is the same one that has been used on previous problems. The filter function for a distributed, circular, uniform source on axis given in Equation (E.6) is inserted in the formula for phase variance given in Equation (A.1). It is assumed that one is operating in the near field so that the cosine term can be replaced by 1. Doing the angle integration one obtains

$$\sigma_D^2 = 0.4146\ \pi k_o^2 \int_0^H dz\ C_n^2(z) \int_0^\infty d\kappa\ \kappa^{-8/3} \left\{ 1 - \frac{4 J_1\left(\frac{\kappa Dz}{2H}\right)}{\frac{\kappa Dz}{2H}} \frac{2 J_1\left(\frac{\kappa D_s}{2H}\right)}{\frac{\kappa D_s}{2H}} + \left[\frac{2 J_1\left(\frac{\kappa D_s}{2H}\right)}{\frac{\kappa D_s}{2H}}\right]^2 \right\}.$$

(3.7.1)

The subscript on the variance means that it refers to a distributed source . If the D subscript is missing, it means that a point source is being considered. Piston is present in the expression. If one wants the phase variance with piston and/or tilt removed, then one has to subtract the contribution to the phase variance due to these terms. The appropriate filter functions to do this are discussed in Section 3.5.9. That calculation will not be given in this report

This equation is the starting point for the evaluation of the phase variance for all the cases considered in this section. The problem will be solved in steps since the results of both a point source and a distributed source are of interest for different situations.

3.7.1 Phase Variance for a Point-Source Beacon

The expression for the phase variance for a point source with piston and tilt present can be found from Equation (3.7.1) by setting the source diameter equal to zero to obtain

$$\sigma^2 = 0.8292\ \pi k_o^2 \int_0^H dz\ C_n^2(z) \int_0^\infty d\kappa\ \kappa^{-8/3} \left[1 - \frac{2 J_1\left(\frac{\kappa Dz}{2H}\right)}{\frac{\kappa Dz}{2H}} \right].$$

(3.7.2)

Let $\quad t = \frac{\kappa Dz}{2H}$, then

163

$$\sigma^2 = -5.21 k_o^2 \int_0^H dz \, C_n^2(z) \left(\frac{Dz}{2H}\right)^{5/3} \int_0^\infty dt \, t^{-8/3-1} \left[J_1(t) - \frac{t}{2} \right]. \qquad (3.7.3)$$

The last integral converges as discussed in the section around Equations (2.3.10) and (2.3.11), and its value is just the Mellin transform of the Bessel function given in Equation (F.5) evaluated at $s = -8/3$ which is equal to 0.305. The phase variance is equal to

$$\sigma^2 = 0.5 \, k_o^2 \mu_{5/3} \left(\frac{D}{H}\right)^{5/3} = \left(\frac{0.348 \, D}{H\Theta_o}\right)^{5/3}. \qquad (3.7.4)$$

The value of the isoplanatic angle given in Equation (3.5.6) was inserted in the last expression. The phase variance is due to the angular offset of the collimated and focused rays. The phase variance varies; however, one can consider the average phase variance to be due to an angular offset equal to that of the ray that emanates from the point that is about 0.7 of the radius from the center. This angle is $0.348/H$.

The above value of the phase variance with piston included is finite unlike the result for unfiltered turbulence, which is infinite. The infinite result comes from the zero spatial wavelength term. This infinity cancels out in the subtraction of the phase of the collimated beam from that of a focused beam. Even though the above result is finite, it might be possible that the major component of this variance is due to the piston, which is no practical interest. It can be shown for satellite altitudes that the piston contribution is only 25% of the above expression. Therefore, the above simple expression is a reasonable zero order approximation to the phase variance. A 60-cm aperture looking at a point source at 300 km would have a phase variance due to an angular offset of 0.7 microradians. For typical isoplanatic angles, this will produce a very small variance.

3.7.2 Phase Variance for a Distributed Beacon

The expression for the phase variance for a distributed source with piston present can be found from Equation (3.7.1). This integral has to be put in a form for which Mellin transforms exist. To do this the integral is written as the sum of two integrals.

Let $\quad t = \dfrac{\kappa D z}{2H}$, $\quad y = \dfrac{\kappa D_s z}{2H}$ $\quad$ and $\quad x = \dfrac{D}{D_s}$, $\quad$ then

$$\sigma_D^2 = 1.1279 \left(\frac{D}{\Theta_o H} \right)^{5/3} (-I + J),$$

(3.7.5)

where the first integral is

$$I = \int_0^\infty \frac{dt}{t} \, t^{-8/3} \left(\frac{x}{t} \right) \left[J_1(t) J_1\left(\frac{t}{x} \right) - \frac{t}{2} \frac{t}{2x} \right].$$

(3.7.5)

The J term is easily evaluated using Equation (F.6) to give

$$J = \frac{1}{2} \left(\frac{D_s}{D} \right)^{5/3} \int_0^\infty dy \, y^{-11/3-1} \left[J_1^2(y) - \left(\frac{y}{2} \right)^2 \right] = -0.1331 \left(\frac{D_s}{D} \right)^{5/3}.$$

(3.7.7)

The value of I depends on x, which is not a function of z. J is also not a function of z. Therefore, the final answer just has the 5/3 moments of turbulence, which has been expressed as the isoplanatic angle in Equation (3.7.5). The form of the expression in the first integral is not one we have encountered before. It is the product of two functions minus the product of the first terms of their series expansion. If A and B are the two functions and a and b are the first terms of the series expansions, then the following identity will express the integral in a form that can be evaluated using the techniques that have been developed

$$AB - ab = (A - a)(B - b) + a(B - b) + b(A - a).$$

(3.7.8)

The original integral, I, can now be broken up into the sum of three separate integrals that are equal to

$$I_1 = x \int_0^\infty \frac{dt}{t} \, t^{-11/3} \left[J_1(t) - \frac{t}{2} \right]\left[J_1\left(\frac{t}{x} \right) - \frac{t}{2x} \right].$$

(3.7.9)

$$I_2 = 0.5 \, x^{-5/3} \int_0^\infty dy \, y^{-8/3-1} \left[J_1(y) - \frac{y}{2} \right],$$

(3.7.10)

and $\qquad\qquad I_3 = 0.5 \int_0^\infty dy \, y^{-8/3-1} \left[J_1(y) - \frac{y}{2} \right].$

(3.7.11)

The integrands in the last two expressions are the same, and their value is equal to the Mellin transform of the Bessel function evaluated at $s = -8/3$. The value of these integrals is

$$I_2 = -0.1525 \left(\frac{D_s}{D}\right)^{5/3} \quad \text{and} \quad I_3 = -0.1525. \tag{3.7.12}$$

Use the convolution theorem to evaluate the first integral. Using Equation (F.5) and letting $s \rightarrow 2s$, the first integral can be transformed into the following integral in the complex plane

$$I_1 = \frac{2^{-14/3} x}{2\pi i} \int_{-i\infty}^{i\infty} ds \left(\frac{D_s}{D}\right)^{2s} \Gamma \begin{bmatrix} s - \frac{4}{3}*, & -s + \frac{1}{2}* \\ -s + \frac{10}{3}, & s + \frac{3}{2} \end{bmatrix}, \tag{3.7.13}$$

where the asterisk indicates that the path of integration passes between the first and second poles of the Gamma function. The subtraction of the first term of the series expansion of each function has moved the path to the other side of the first pole for both Gamma functions in the numerator.

Since $\Delta = \Delta' = 0$, the path of integration is closed to the right when the source diameter is less than the aperture diameter, and it is closed to the left for the opposite case. For $D_s/D < 1$, the contribution at the poles at $s = 4/3$ and $s = 1/2 + n$ for $n = 1, 2, \ldots$ and the contribution of the other integrals gives

$$\sigma_D^2 = \left(\frac{0.348 D}{\Theta_o H}\right)^{5/3}$$

$$\times \left[1 + 0.258 \sum_{n=1}^{\infty} \frac{(-1)^{n+1}}{n!} \left(\frac{D_s}{D}\right)^{2n} \Gamma \begin{bmatrix} n - \frac{5}{6} \\ -n + \frac{17}{6}, & n + 2 \end{bmatrix} - 0.873 \left(\frac{D_s}{D}\right)^{5/3} \right]. \tag{3.7.14}$$

The first few terms of this solution are

$$\sigma_D^2 \approx \left(\frac{0.348 D}{\Theta_o H}\right)^{5/3}$$

$$\times \left[1 - 0.872 \left(\frac{D_s}{D}\right)^{5/3} + 0.763 \left(\frac{D_s}{D}\right)^2 - 0.0177 \left(\frac{D_s}{D}\right)^4 - 0.000286 \left(\frac{D_s}{D}\right)^6 \right]. \tag{3.7.15}$$

When $D_s/D > 1$, the contribution at the poles at $s = 1/2$ and $s = 4/3 - n$ for index values $n = 1, 2, \ldots$ and the other integrals gives

$$\sigma_D^2 = \left(\frac{0.348\,D_s}{\Theta_o H}\right)^{5/3} \left\{ 0.128 + 0.258 \sum_{n=1}^{\infty} \frac{(-1)^{n+1}}{n!} \left(\frac{D}{D_s}\right)^{2n} \Gamma\left[\begin{matrix} n - \frac{5}{6} \\ -n + \frac{17}{6}, \, n + 2 \end{matrix}\right] \right\}. \quad (3.7.16)$$

The first few terms of this solution are

$$\sigma_D^2 \approx \left(\frac{0.348\,D_s}{\Theta_o H}\right)^{5/3} \left[0.128 + 0.763 \left(\frac{D}{D_s}\right)^2 - 0.0177 \left(\frac{D}{D_s}\right)^4 - 0.000286 \left(\frac{D}{D_s}\right)^6 \right].$$

$$(3.7.17)$$

The normalized variance is plotted in Figure 3-20. The phase variance actually decreases as the source size increases initially and then it starts to increase.
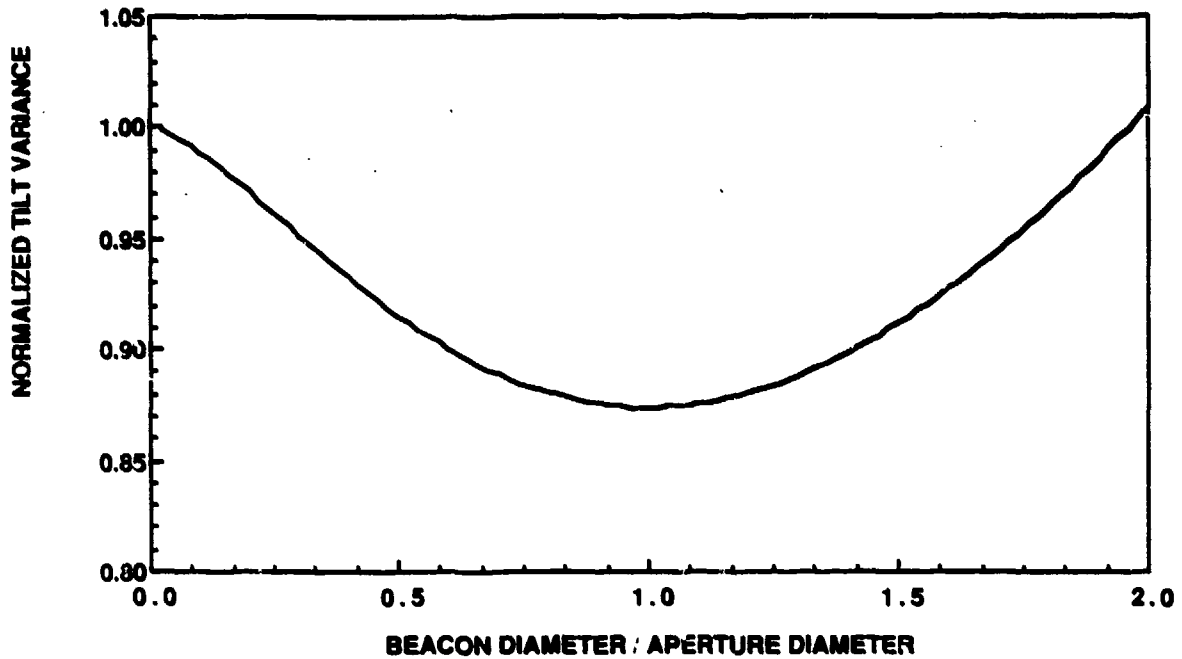
Figure. 3-20. Effect of beacon diameter on the normalized phase variance with piston and tilt present.

157

3.8 POWER SPECTRAL DENSITY

In this section, the power spectral densities for several problems of interest are derived. Many problems can be treated in a similar manner. For instance, in the first problem the beam movement at a target and the tilt spectra are derived from the same integration. Power and asymptotic series are found and shown to give a good match at the stitching point of these two solutions. Spectral analysis of turbulence induced tilt has been investigated for both plane and spherical wave cases. This section, however, concentrates on plane wave results. Plane wave results are discussed briefly in Tatarski[25] and presented in more detail in Greenwood and Fried.[26] Greenwood and Fried made a simplifying assumption in order to obtain simple, analytic results. Fields[27] has coined the term "parallel approximation" for this simplification. One consequence of the parallel approximation is that the rate at which the spectra decay at high frequencies is underestimated. Tyler[28] subsequently analyzed plane wave tilt spectra without making this approximation. However, his results remain in integral form, containing an integral over a dummy variable related to spatial frequency and an integral over altitude. In a subsequent report, Vaughn[29] provided numerical techniques to solve the integrals presented by Tyler, but no solutions have been published which do not rely heavily on numerical integration. A similar approach has been used in tilt spectra associated with a point source (spherical wave analysis). These analysis lead to integral expressions which must also be evaluated numerically (Hogge and Butts[30] and Butts[31]).

3.8.1 Power Spectral Density of Beam Movement and Tilt

The power spectral density of the beam movement at a target is found using the general expression for the power spectral density for a collimated wave given in Equations (A.3) and (A.4) with the filter function of beam movement given in Equation (3.5.26). It is assumed that one is in the near field so that the cosine term can be replaced by unity. This assumption breaks down at sufficiently high frequencies and the exact equation must be used. The effect of including the cosine term is to lower the high-frequency spectrum. The spectral density is

$$F(\omega) = 1.303 \, k_o^2 \omega \int_0^L dz \; \frac{C_n^2(z)}{v^2(z)} \int_0^\infty \frac{c \, dc \; U(c-1)}{\sqrt{c^2-1}} \left(\frac{\omega c}{v(z)}\right)^{-11/3}$$

$$\times \left(\frac{16}{k_o D}\right)^2 \left[\frac{J_2(\omega c \, D / 2v(z))}{\omega c D / 2v(z)}\right]^2 [L^2 - 2Lz + z^2]. \qquad (3.8.1)$$

The expression for the spectra of tilt is just the expression above with the last bracketed term eliminated. Let

$$x = \frac{2v(z)}{\omega D}, \qquad (3.8.2)$$

then

$$F(\omega) = \frac{1334}{D^4 \omega^{14/3}} \int_0^L dz \; C_n^2(z) v^{11/3}(z) [L^2 - 2Lz + z^2] \int_0^\infty \frac{dc}{c} \frac{U(c-1)}{\sqrt{c^2-1}} J_2^2\left(\frac{c}{x}\right) c^{-11/3}.$$

$$(3.8.3)$$

The last integral is the same for the problem of calculating the spectra of the beam movement or tilt. To evaluate the integral over c, define the functions

$$H_1\left(\frac{x}{c}\right) = J_2^2\left(\frac{c}{x}\right), \qquad (3.8.4)$$

and

$$H_2(c) = \frac{U(c-1)}{\sqrt{c^2-1}} c^{-11/3}, \qquad (3.8.5)$$

then the last integral over c can be expressed as a Meilin convolution integral using the transforms in Equations (F.6) and (F.10). If s is changed to $-2s$, one obtains

$$I = \frac{1}{2(2\pi i)} \int ds \; \Gamma\begin{bmatrix} -s + \frac{1}{2}, \; s + 2, \; s + \frac{7}{3} \\ -s + 1, \; -s + 3, \; s + \frac{17}{6} \end{bmatrix} \left(\frac{\omega D}{2v}\right)^{-2s}. \qquad (3.8.6)$$

Since $\Delta = 2$, the path of integration is closed in the left-half plane and the contributions at the two sets of poles at $s = -2 - n$ and $s = -7/3 - n$ for $n = 0, 1, 2, \ldots$ give

$$2I = -\sum_{n=0}^\infty \frac{(-1)^n}{n!} \left\{ \Gamma\begin{bmatrix} n + \frac{5}{2}, -n + \frac{1}{3} \\ n + 3, \; n + 5, -n + \frac{5}{6} \end{bmatrix} \left(\frac{\omega D}{2v(z)}\right)^{4+2n} \right.$$

$$\left. + \Gamma\begin{bmatrix} n + \frac{17}{6}, -n - \frac{1}{3} \\ n + \frac{0}{6}, \; n + \frac{16}{3}, -n + \frac{1}{2} \end{bmatrix} \left(\frac{\omega D}{2v(z)}\right)^{-\frac{14}{3}+2n} \right\}. \qquad (3.8.7)$$

169

To obtain the spectral density, the velocity profile must be inserted into the above series, and the integrations along the path performed. The final result is a series solution for the power spectral density.

For large frequencies, an asymptotic series can be found by closing the path of integration in the right-half plane and getting the pole contributions at $s = 1/2 + n$ for $n = 0, 1, 2, \ldots$. The $E(x)$ term is significant in this case and the asymptotic series is

$$2I = \frac{1}{\sqrt{\pi}}\left(\frac{2v}{\omega D}\right)^{3/2}\cos\left[\left(\frac{\omega D}{v}\right) - \frac{\pi}{4}\right]$$
$$+ \sum_{n=0}^{\infty}\frac{(-1)^n}{n!}\left\{\Gamma\left[\begin{array}{c}n + \frac{5}{2}, n + \frac{17}{6}\\ n + \frac{10}{3}, -n + \frac{1}{2}, -n + \frac{5}{2}\end{array}\right]\left(\frac{2v}{\omega D}\right)^{1+2n}\right\}. \qquad (3.8.8)$$

Notice, that in order to evaluate the coefficients of the series representation of the power spectral density, various velocity moments have to be calculated in Equation (3.8.3). If the total velocity and turbulence are constant along the path of integration, the power spectral density for low frequencies is equal to

$$F(\omega) = \frac{0.09256\ C_n^2 L^3 D^{2/3}}{v}\left(\frac{v}{\omega D}\right)^{2/3}\left\{1 - 0.3398\left(\frac{\omega D}{v}\right)^{2/3} - 0.01042\left(\frac{\omega D}{v}\right)^2\right.$$
$$+ 0.005077\left(\frac{\omega D}{v}\right)^{8/3} + 1.329 \times 10^{-4}\left(\frac{\omega D}{v}\right)^4 - 5.7 \times 10^{-5}\left(\frac{\omega D}{v}\right)^{14/3}$$
$$\left. - 1.157 \times 10^{-6}\left(\frac{\omega D}{v}\right)^6 + 4.4 \times 10^{-7}\left(\frac{\omega D}{v}\right)^{20/3}\right\}.$$

$$(3.8.9)$$

For high frequencies

$$F(\omega) \approx \frac{18.08 C_n^2 L^3 D^{2/3}}{v}\left(\frac{v}{\omega D}\right)^{17/3}$$
$$\times\left\{1 + 6.375\left(\frac{v}{\omega D}\right)^2 + 29.61\left(\frac{v}{\omega D}\right)^4 + 2.278\left(\frac{v}{\omega D}\right)^{1/2}\cos\left[\left(\frac{\omega D}{v}\right) - \frac{\pi}{4}\right]\right\}.$$

$$(3.8.10)$$

170

The term $[L^2 - 2z - z^2]$ contributes a factor of $L^3/3$. To find the tilt spectra, the analysis is the same except that this factor is not present. Therefore, the tilt spectra is the above spectra multiplied by $3/L^3$. The spectrum for low frequencies is

$$F_t(\omega) \approx \frac{0.2776\, C_n^2 D^{2/3}}{v}\left(\frac{v}{\omega D}\right)^{2/3}\left[1 - 0.3398\left(\frac{\omega D}{v}\right)^{2/3} - 0.01042\left(\frac{\omega D}{v}\right)^2\right.$$

$$+ 0.005077\left(\frac{\omega D}{v}\right)^{8/3} + 1.329 \times 10^{-4}\left(\frac{\omega D}{v}\right)^4 - 5.7 \times 10^{-5}\left(\frac{\omega D}{v}\right)^{14/3}$$

$$\left. - 1.157 \times 10^{-6}\left(\frac{\omega D}{v}\right)^6 + 4.4 \times 10^{-7}\left(\frac{\omega D}{v}\right)^{20/3}\right].$$

$$(3.8.11)$$

For high frequencies it is

$$F_t(\omega) \approx \frac{54.24\, C_n^2 D^{2/3}}{v}\left(\frac{v}{\omega D}\right)^{17/3}$$

$$\times \left[\left\{1 + 6.375\left(\frac{v}{\omega D}\right)^2 + 29.61\left(\frac{v}{\omega D}\right)^4 + 2.278\left(\frac{v}{\omega D}\right)^{1/2}\cos\left[\left(\frac{\omega D}{v}\right) - \frac{\pi}{4}\right]\right\}\right].$$

$$(3.8.12)$$

Notice that the first term of the expansion for low frequencies does not depend on diameter, and the first term of the asymptotic series has the strong dependence to the inverse fifth power of diameter. Therefore, as the diameter gets smaller, the high frequency components of beam motion increase rapidly. For low frequencies, the spectrum decreases as the inverse 2/3 power of frequency. For very high frequencies, the power decreases as the inverse 17/3 power of frequency.

At high frequencies, there is a ripple in the spectrum due to the cosine term in the asymptotic expansion. This ripple appears because of the assumption that the velocity was a constant. If the velocity varies with height, then at any frequency one obtains the sum of many cosine terms with different arguments. These terms tend to cancel out, and in that case one can neglect the cosine term.

The spectral density is plotted on a linear and logarithmic frequency scale in Figures 3-21a and 3-21b. Notice the ripple at higher frequencies due to the cosine term in the asymptotic series. Each plot contains the series solution and the asymptotic solution. As the spectral density gets smaller, in order to obtain valid answers with the series solution, one must be concerned with the numerical accuracy of each of the terms of the series since it is the cancellation of large terms that produces the resultant small spectral value. There is a good match of the curves using the eight terms of the power series and four terms of the asymptotic series.
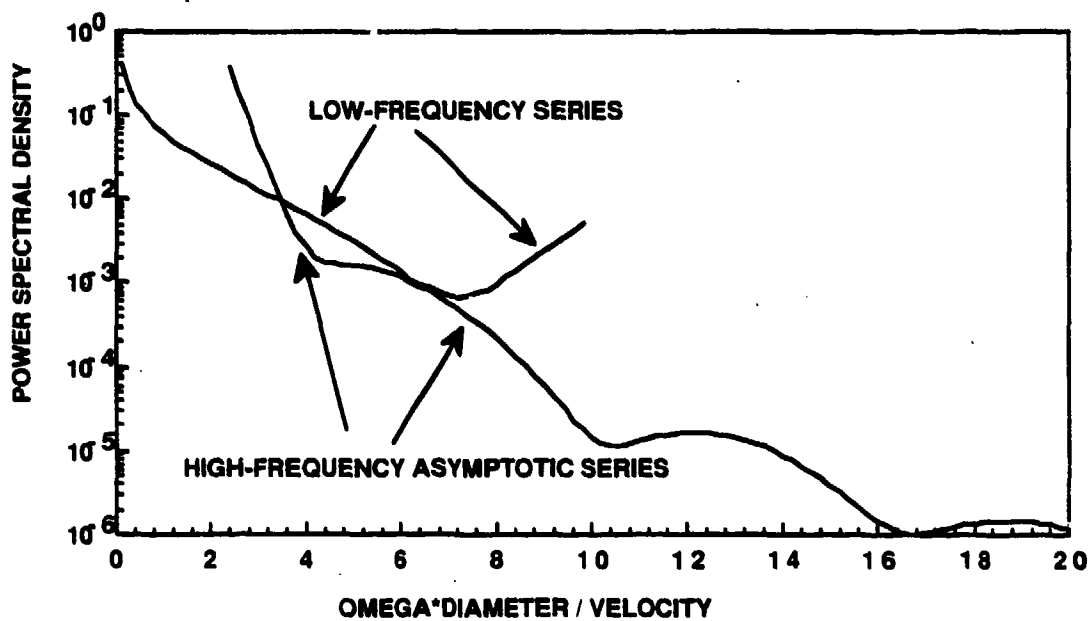
Figure 3-21a. Log-linear plot of the power spectral density of tilt using power and asymptotic series. The velocity and turbulence are constant along the path.

172
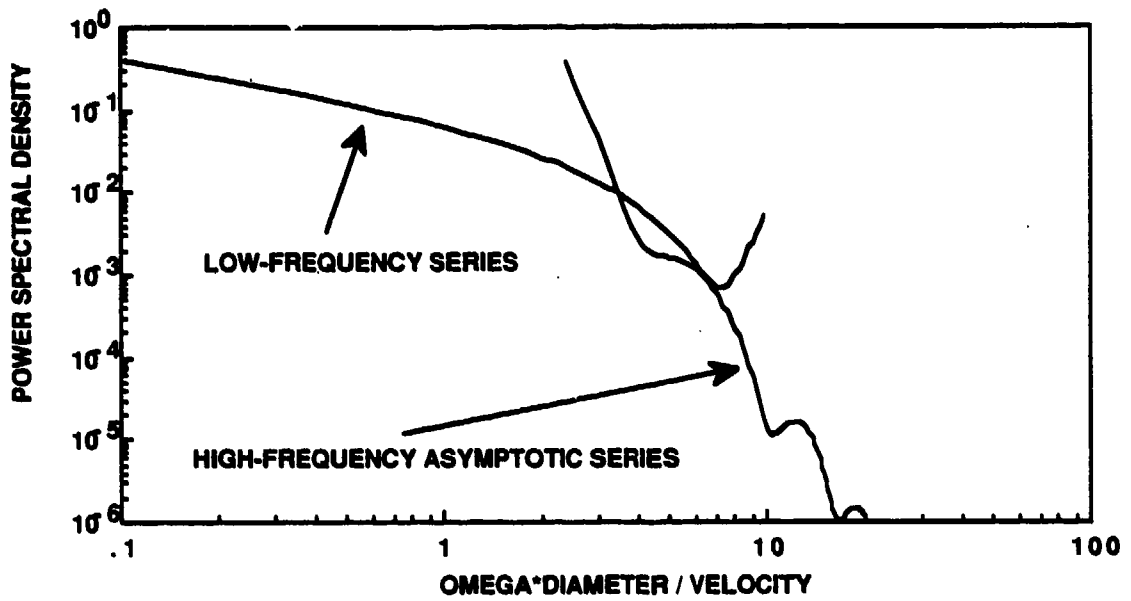
Figure 3-21b. Log-log plot of the power spectral density of tilt using power and asymptotic series. The velocity and turbulence are constant along the path.

The two series are merging together in Figures 3-22a and 3-22b.
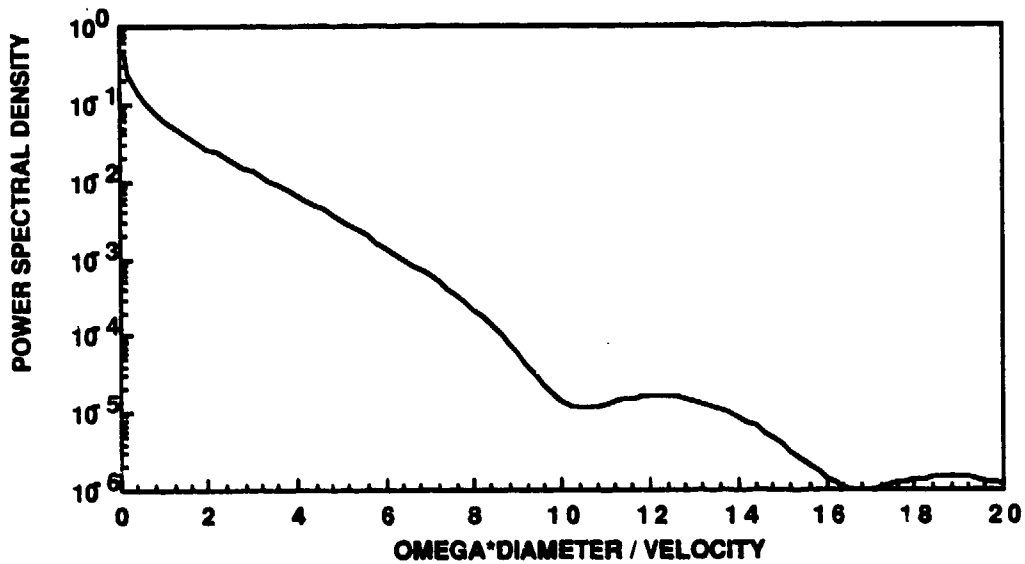
Figure 3-22a. Log-linear plot of the power spectral density of tilt with merging of the power and asymptotic series. The velocity and turbulence are constant along the path.

173
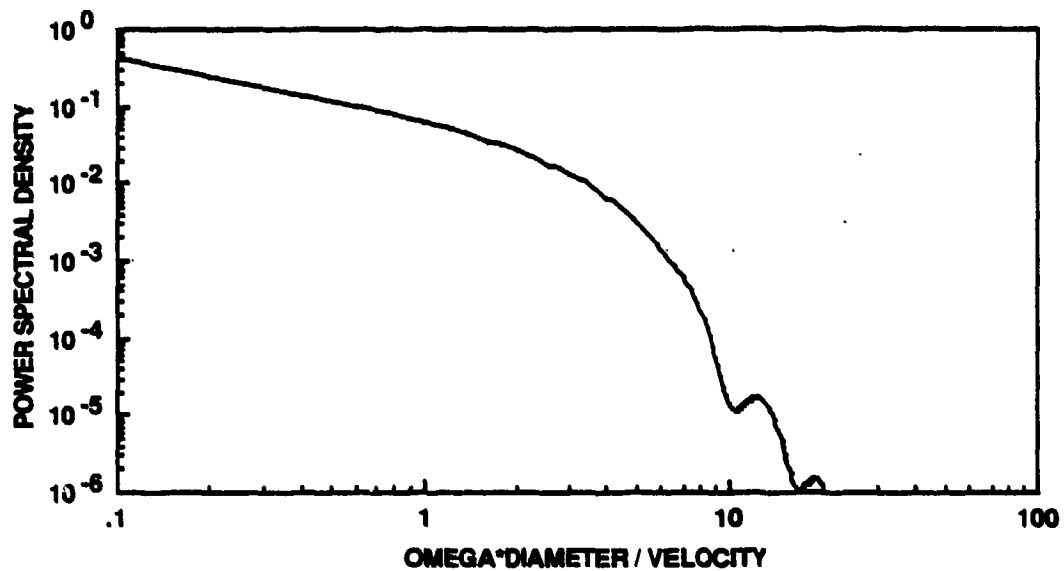
Figure 3-22b. Log-log plot of the power spectral density of tilt with merging of the power and asymptotic series. The velocity and turbulence are constant along the path.

If the velocity is allowed to vary along the path, then one must obtain the velocity moments in order to determine the spectra. Define the velocity moments as

$$v_n = \int_0^L dz \ C_n^2(z)v^n(z) = \sec(\xi) \int_0^H dh \ C_n^2(h)v^n(h).$$ (3.8.13)

The velocity in this expression is the magnitude of the velocity that is equal to the vector sum of the wind velocity and slew velocity at any altitude. The last relation assumes that both the turbulence and the wind velocity vary only with height. Using this relation, the tilt spectra can be written as

$$F_t(\omega) \approx \frac{0.2776}{\omega^{2/3}} \Big[v_{-1/3} - 0.3398(\omega D)^{2/3}v_{-1} - 0.01042(\omega D)^2 v_{-7/3}$$

$$+ 0.005077(\omega D)^{8/3}v_{-3} + 1.329 \times 10^{-4}(\omega D)^4 v_{-13/3} - 5.7 \times 10^{-5}(\omega D)^{14/3}v_{-5}$$

$$- 1.157 \times 10^{-6}(\omega D)^6 v_{-19/3} + 4.4 \times 10^{-7}(\omega D)^{20/3}v_{-7} \Big].$$

(3.8.14)

174

For high frequencies with the cosine term neglected, one obtains

$$F_t(\omega) \approx \frac{54.24}{\omega^{2/3} D^5} \left[v_{14/3} + 6.375 v_{20/3} (\omega D)^{-2} + 29.61 v_{26/3} (\omega D)^{-4} \right]. \qquad (3.8.15)$$

The velocity moments that are needed in the above series have to be calculated using the wind velocity and slew rates for the particular situation. For the slew dominated case, these moments can be expressed in terms of the turbulence moments that were previously found in an analytic form. The general case requires a numerical evaluation of these moments.

3.9 STREHL RATIO AND COHERENCE DIAMETER

3.9.1 Strehl Ratio of Uncorrected Turbulence

The problem of finding the Strehl ratio with uncorrected turbulence was analyzed by Fried.[32] He solved the problem by performing a numerical integration. He also analyzed the problem of tilt removed Strehl ratios. Because of the problem of the Zernike modes not being statistically independent, he had to make certain approximations to get physically meaningful results. This tilt removed problem has been looked at by Lutomirski, et al.,[33] Travis and Yura,[34] Wang and Marky,[35] and Wang.[36, 37]

One can obtain an exact series solution for the Strehl ratio when the turbulence is uncorrected. This technique can be used to find an equivalent coherence diameter for more complicated cases; however, a different method will be developed to find the Strehl ratio. Since turbulence is isotropic, the Strehl ratio is given by Equation (3.2.14) as

$$SR = \int_0^1 \alpha \, d\alpha \, K(\alpha) \exp[-D(\alpha)/2], \qquad (3.9.1)$$

Since

$$D(\alpha) = D_\chi(\alpha) + D_\phi(\alpha), \qquad (3.9.2)$$

the total structure function is found from Equation (A.2) with unity filter function and inner and outer scale neglected so that $f(\kappa) = \kappa^{-11/3}$ as

$$D(\alpha) = 0.4146 k_o^2 \int_0^\infty dz \, C_n^2(z) \int d\vec{\kappa} \, \kappa^{-11/3} [1 - \cos\{\vec{\kappa} \cdot \vec{\alpha}\}]. \qquad (3.9.3)$$

175

The angular and axial integrations can be performed to give

$$D(\alpha) = 2.605 \ \mu_o \ k_o^2 \int_0^\infty d\kappa \ \kappa^{-5/3-1}[1 - J_o(\kappa\alpha D)]$$

$$= 2.605 \ \mu_o k_o^2 (\alpha D)^{5/3} \ M(1 - J_o(x))\Big|_{s = -5/3}. \qquad (3.9.4)$$

The Mellin transform of the term in parenthesis is just the Mellin transform of the Bessel function given in Equation (F.5) as explained in Equations (2.3.10) and (2.3.11). Using the definition of the coherence diameter given in Equation (3.5.5), the structure function can be written as

$$D(\alpha) = 6.88 \ (\alpha D \ / \ r_o)^{5/3}. \qquad (3.9.5)$$

The integral for the Strehl ratio has been reduced to

$$SR = \int_0^1 \alpha \ d\alpha \ K(\alpha)\exp\left[-3.44\left(\frac{\alpha D}{r_o}\right)^{5/3}\right]. \qquad (3.9.6)$$

To evaluate this integral, it is convenient to express the exponential as a Mellin-Barnes integral. Marichev (Equation 5.31) expresses the exponential in terms of a confluent Gauss hypergeometric function as

$$\exp(z) = \lim_{u \to \infty} F(1, \ u; \ 1; \ z \ / \ u). \qquad (3.9.7)$$

The hypergeometric function can be written as a Mellin-Barnes integral (Gradshteyn and Ryzhik Equation (9.113)) in the following way

$$F(a, \ b; \ c; \ z) = \frac{\Gamma(c)}{\Gamma(a)\Gamma(b)} \frac{1}{2\pi i} \int ds \ (-z)^s \frac{\Gamma(a+s)\Gamma(b+s)\Gamma(-s)}{\Gamma(c+s)}. \qquad (3.9.8)$$

The path of integration has all the poles of a Gamma function on one side of the path of integration. Therefore, the exponential can be written as

$$\exp(z) = \lim_{u \to \infty} \frac{1}{2\pi i \ \Gamma(u)} \int ds \ \Gamma(u+s)\Gamma(-s)\left(\frac{-z}{u}\right)^s, \qquad (3.9.9)$$

where the path of integration is just to the left of the imaginary axis. For this case $\Delta = \Delta' = 0$, and the parameter in the integral is very small. Therefore, the path of integration can be closed

176

in the right-half plane with poles at $s = n$, and using the following limit

$$\lim_{u \to \infty} \frac{\Gamma(u + s)}{\Gamma(u)u^s} = 1, \tag{3.9.10}$$

the normal power series for the exponential is the result

$$\exp(z) = \sum_{n=0}^{\infty} \frac{z^n}{n!}. \tag{3.9.11}$$

Using the Mellin-Barnes expression for the exponential in the equation for the Strehl ratio produces

$$SR = \lim_{u \to \infty} \int \frac{d\alpha}{\Gamma(u)} \frac{K(\alpha)}{2\pi i} \int ds \, \Gamma(u + s)\Gamma(-s) \left(\frac{3.44}{u}\left(\frac{D}{r_o}\right)^{5/3}\right)^s \alpha^{5s/3 + 1}. \tag{3.9.12}$$

Interchanging the order of integration yields

$$SR = \lim_{u \to \infty} \frac{1}{2\pi i} \int ds \, \frac{\Gamma(u + s)}{\Gamma(u)}\Gamma(-s)\left(\frac{3.44}{u}\left(\frac{D}{r_o}\right)^{5/3}\right)^s \int_0^1 d\alpha \, \alpha^{1 + 5s/3}K(\alpha)$$

$$= \lim_{u \to \infty} \frac{1}{2\pi i} \int ds \, \frac{\Gamma(u + s)}{\Gamma(u)}\Gamma(-s)\left(\frac{3.44}{u}\left(\frac{D}{r_o}\right)^{5/3}\right)^s I(5s/3). \tag{3.9.13}$$

The definition in Equation (2.3.12) was used above. Take the limit, and use the value of the integration of a power of the aperture times the MTF of a circular aperture given in Equation (2.3.15). This expression for the integral is valid as long as Re $s > -9/5$ which is satisfied for the path of integration. Change s to $-s$ to put it in the standard form, and obtain

$$SR = \frac{24}{5\sqrt{\pi}} \frac{1}{2\pi i} \int ds \, \Gamma\begin{bmatrix} s, \frac{3}{2} - 5s/6, -s + \frac{5}{6} \\ 3 - 5s/6, -s + \frac{11}{6} \end{bmatrix} \left[3.44\left(\frac{D}{r_o}\right)^{5/3}\right]^{-s}. \tag{3.9.14}$$

For this case $\Delta = 1$, and the integral can be closed in the right-plane. These poles are located at $s = n$, $n = 0, 1, 2, \dots$. The power series for the Strehl ratio that is the sum of the residues at the enclosed poles is equal to

$$SR = \frac{24}{5\sqrt{\pi}} \sum_{n=0}^{\infty} \frac{(-1)^n}{n!} \Gamma\begin{bmatrix} \frac{3}{2} + 5n/6, n + \frac{6}{5} \\ 3 + 5n/6, n + \frac{11}{6} \end{bmatrix} \left[3.44\left(\frac{D}{r_o}\right)^{5/3}\right]^n. \tag{3.9.15}$$

177

The first few terms of this series are

$$SR = 1 - 1.032\left(\frac{D}{r_0}\right)^{5/3} + 0.7082\left(\frac{D}{r_0}\right)^{10/3} - 0.5015\left(\frac{D}{r_0}\right)^{5} + \dots \quad (3.9.16)$$

For large values of the parameter, this series converges slowly and an asymptotic series is needed to get a rapidly converging series. Since Condition 1 given as Equation (H.20) is true, the asymptotic series is equal to the residue of the poles on the other side of the integration path. The poles are at $s = -5/6$, and $s = -6n/5 - 9/5$ for $n = 0, 1, 2, \dots$. (Remember to multiply the second set of residues by 5/6 because the coefficient of s in the Gamma function is not unity.) The Gamma function that produces the first pole only has a single pole because the others are canceled out by the denominator. The asymptotic series is

$$SR = \left(\frac{r_0}{D}\right)^{2} - \frac{4}{\sqrt{\pi}}3.44^{-9/5}\sum_{n=0}^{\infty}\frac{(-1)^{n}}{n!}\Gamma\left[\begin{matrix}6n/5 + \frac{9}{5}, n + \frac{1}{2} \\ \frac{3}{2} - n, n + \frac{3}{2}\end{matrix}\right](3.44)^{-6n/5}\left(\frac{r_0}{D}\right)^{3+2n}.$$

$$(3.9.17)$$

The first few terms of this series are

$$SR = \left(\frac{r_0}{D}\right)^{2} - 0.6159\left(\frac{r_0}{D}\right)^{3} + 0.05\left(\frac{r_0}{D}\right)^{5} + 0.00661\left(\frac{r_0}{D}\right)^{7} + \dots \quad (3.9.18)$$

In Figure 3-23 is a plot of the Strehl ratio versus the ratio of the aperture diameter to the coherence diameter. The regular series and the asymptotic series meet with a difference of 1% by using ten terms of the power series and six terms of the asymptotic series.

In order to find the Strehl ratio with tilt removed, one would have to remove the tilt from the structure function. As was pointed out in Section 3.2, since the Zernike modes are not statistically independent, subtracting the tilt from the structure function results in an error. Since this error is not very large one can still use it to get an approximate expression. If this is done and a power series solution is obtained, one finds that the power and asymptotic series converge poorly in the transition region when the diameter is about the coherence diameter. Away from this region, the solution is close to that with the tilt present. For that reason the solution using this method is not presented here.
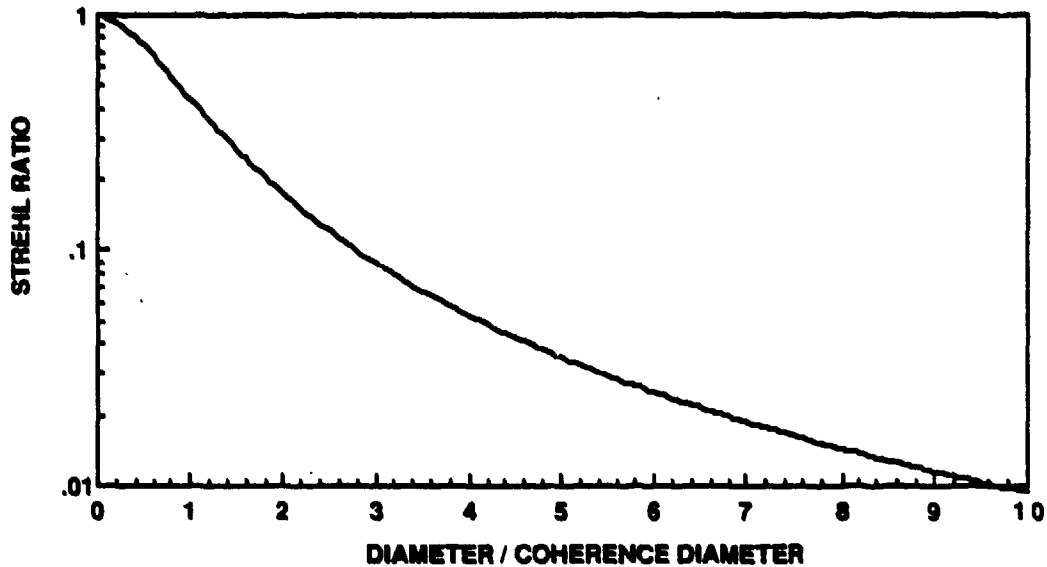
Figure 3-23. Strehl ratio for uncorrected turbulence.

3.9.2 Coherence Diameter with Inner Scale

There are several ways to define the coherence diameter. The definition that is used here is a physically intuitive one and is that value of r which divided by the aperture diameter and then squared gives the normalized intensity in the far field. This definition is consistent with Fried's definition of coherence diameter for zero inner-scale size. The coherence diameter will be evaluated by first finding the structure function, inserting this into the expression for the Strehl ratio, and then taking the limit as the aperture gets very large. The structure constant with inner-scale size included is obtained by using Equations (A.2) and (A.6) to obtain after integrating over angle

$$D(r) = 2.606 \, k_o^2 \int_0^\infty dz \, C_n^2(z) \int_0^\infty d\kappa \, \kappa^{-8/3} [1 - J_o(\kappa r)] \exp\left[-\left(\frac{\kappa}{\kappa_i}\right)^2\right]. \quad (3.9.19)$$

The last integral in kappa space can be expressed as the following Mellin integral

$$I = \frac{r^{5/3}}{2^{8/3} 2\pi i} \int ds \left(\frac{\kappa_i r}{2}\right)^{-2s} \Gamma\left[\begin{array}{c} s - \frac{5}{6}, -s \\ -s + \frac{11}{6} \end{array}\right]. \quad (3.9.20)$$

179

Since $\Delta = 1$, the integral should be closed left; however, since the parameter in the integral is large, the asymptotic series is desired. In this case, the asymptotic series is just the contribution of the poles to the right of the path of integration. Retaining the contribution only at the first two poles at $s = 0$ and $5/6$, and using the definition of inner-scale size given after Equation (3.3.30) one obtains for the structure function

$$D(r) \approx 2.91 k_o^2 \mu_o \, r^{5/3} \left[1 - 0.095 \left(\frac{L_i}{r} \right)^{5/3} \right], \qquad (3.9.21)$$

which can be written as

$$D(\alpha D) = \frac{6.88}{r_o^{5/3}} \left[(\alpha D)^{5/3} - 0.095 \, L_i^{5/3} \right]. \qquad (3.9.22)$$

The Strehl ratio which is the normalized intensity on axis can be found by inserting this structure function into Equation (3.2.14) and then using Equation (3.9.9) to obtain

$$SR = \lim_{m \to \infty} \int_0^1 d\alpha \, \frac{K(\alpha)}{\Gamma(m) 2\pi i} \int ds \, \Gamma(m+s) \Gamma(-s) \left\{ \frac{3.44}{m r_o^{5/3}} \left[(\alpha D)^{5/3} - 0.095 \, L_i^{5/3} \right] \right\}^s.$$

$$(3.9.23)$$

The second term in brackets is small compared to the first term except close to the origin which is a region that contributes very little to the value of the integration, and that expression can be approximated by the first two terms of the binomial expansion. After interchanging the order of integration and evaluating the aperture integration using Equation (2.3.15), the expression becomes

$$SR = \left(\frac{r_o}{D} \right)^2$$

$$- 0.095 \left(\frac{L_i}{D} \right)^{5/3} \int ds \, \frac{24}{5\sqrt{\pi} \, 2\pi i} \frac{\Gamma(-s) \Gamma\left[5s/6 + \frac{4}{9} \right] \Gamma\left[s + \frac{1}{5} \right]}{\Gamma\left[5s/6 + \frac{13}{6} \right] \Gamma\left[s + \frac{6}{5} \right]} \left[3.44 \left(\frac{D}{r_o} \right)^{5/3} \right]^s.$$

$$(3.9.24)$$

180

The asymptotic value of this integral is found by evaluating the residue at the first pole to the left of the path of integration that occurs at $s = -1/5$, to obtain

$$SR = \left(\frac{r_o}{D}\right)^2 \left[1 + 0.6\left(\frac{L_i}{r_o}\right)^{5/3}\right].$$

(3.9.25)

Therefore, the coherence diameter with inner scale included is

$$r_o(L_i) = r_o\sqrt{1 + 0.6\left(\frac{L_i}{r_o}\right)^{5/3}}.$$

(3.9.26)

For the inner-scale size to increase the coherence diameter by less than 1%, it must be less than 13% of the size of the coherence diameter.

3.9.3   Strehl Ratio with Anisoplanatism

As we saw in deriving the filter functions for anisoplanatism, the effect of displacement, angular mispointing, time delay, and two beacon colors can be treated as an anisoplanatic effect. In fact, if all the effects are present simultaneously, they can be added together to get a total displacement. In this section, the effect of that displacement on the Strehl ratio will be determined. To find the Strehl ratio, the structure function must first be determined. Use the expression for the structure function in Equation (A.2) with the anisoplanatic filter function given in Equation (D.1) to get

$$D(\alpha) = 0.4146 k_o^2 \int_0^\infty dz \ C_n^2(z) \int d\vec{\kappa} \ \kappa^{-11/3}[1 - \cos\{\vec{\kappa} \cdot \vec{\alpha}D\}]2[1 - \cos\{\vec{\kappa} \cdot \vec{d}(z)\}].$$

(3.9.27)

The use of this formula assumes that the structure function can be written as a function solely of the difference of the aperture coordinates. Therefore this formulation does not apply to focal anisoplanatism whose phase variance was derived in Section 3.7. Since that effect is small, the Maréchal formula can be used to find the Strehl ratio in that case. The expression in the last integral is proportional to the spatial power spectral density. In Figure 3-24 is plotted this density for pure turbulence and turbulence filtered by the aperture function. In these plots, there is no isoplanatic offset. The aperture reduced the low spatial frequency components.

181
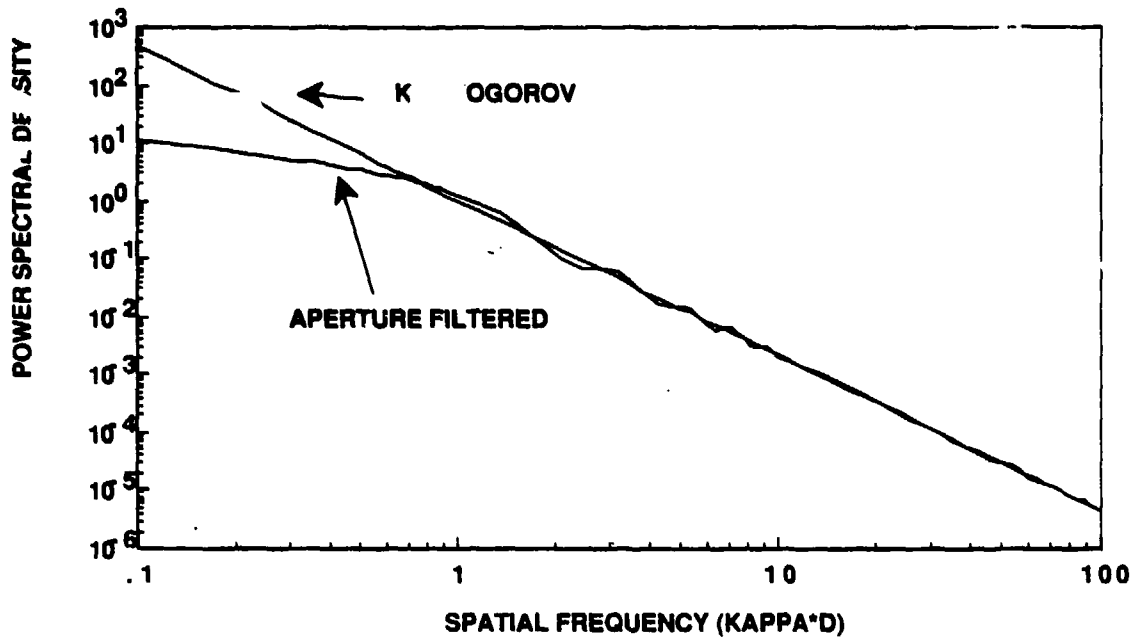
*Figure 3-24. Unfiltered and aperture filtered Kolmogorov turbulence spectrums.*
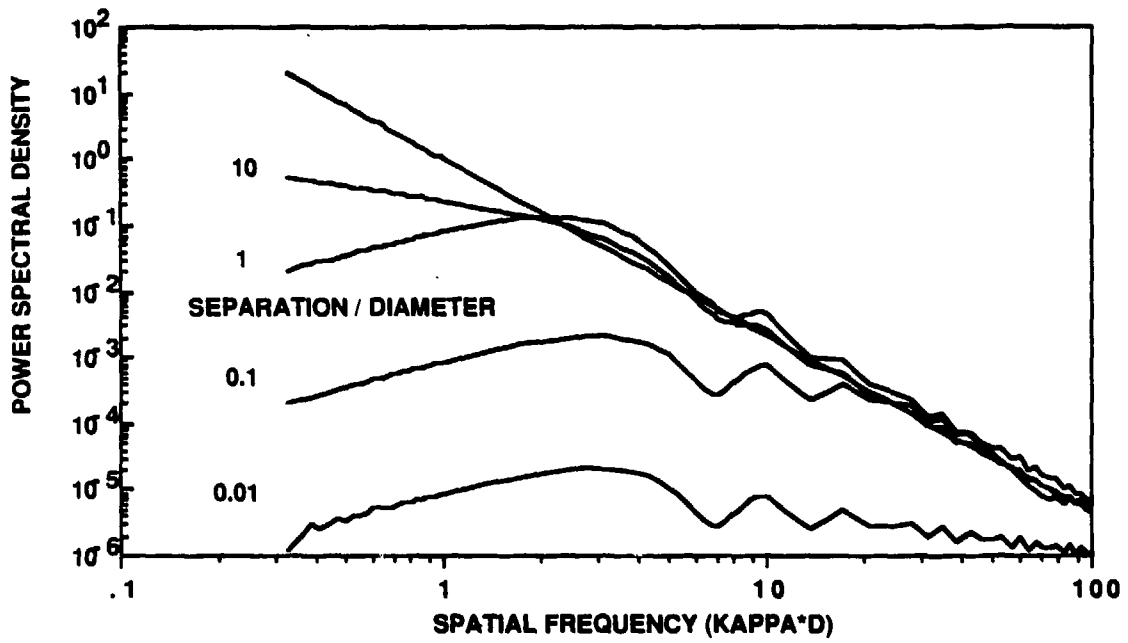
Figure 3-25. Spatial frequency spectrum for various levels of anisoplanatism.

182

The effect of anisoplanatism on the spectrum is plotted in Figure 3-25. One sees that for very little anisoplanatism there is very little power, and it is fairly independent f spatial frequency.

The expression in the last integral can be expanded and the trigonometric identity for the product of cosines used to get

$$I = 2\int d\vec{\kappa}\ \kappa^{-11/3}[1 - \cos\{\vec{\kappa}\cdot\vec{\alpha}D\} - \cos\{\vec{\kappa}\quad \vec{d}(z)\}$$
$$+ \cos\{\vec{\kappa}\cdot[\vec{\alpha}D + \vec{d}(z)]\}/2 + \cos\{\vec{\kappa}\cdot[\vec{\alpha}D - \vec{d}(z)]\}/2]. \quad (3.9.28)$$

This can be integrated over angle, and after rearranging terms, one gets

$$I = 4\pi\int d\kappa\ \kappa^{-8/3}[\{1 - J_o(\kappa\alpha D)\} + \{1 - J_o(\kappa d(z))\}$$
$$- \{1 - J_o(\kappa|\vec{\alpha}D + \vec{d}(z)|)\}/2 - \{1 - J_o(\kappa|\vec{\alpha}D - \vec{d}(z)|)\}/2]. \quad (3.9.29)$$

Using Equation (2.3.11) for each of the four terms, one obtains for the structure function

$$D(\alpha) = 2(2.91)\ k_o^2 \int_0^\infty dz\ C_n^2(z)$$

$$\times\left[(\alpha D)^{5/3} + d^{5/3}(z) - \tfrac{1}{2}|\vec{\alpha}D + \vec{d}(z)|^{5/3} - \tfrac{1}{2}|\vec{\alpha}D - \vec{d}(z)|^{5/3}\right]. \quad (3.9.30)$$

The terms in the absolute value sign are equal to

$$|\vec{\alpha}D \pm \vec{d}(z)|^{5/3} = [(\alpha D)^2 \pm 2\alpha D d(z) + d^2(z)]^{5/6}. \quad (3.9.31)$$

This expression can be simplified and numerical difficulties eliminated with the use of Gegenbauer polynomials. Their generating function is

$$(1 - 2at + a^2)^{-\lambda} = \sum_{n=0}^\infty C_n^\lambda(t)a^n. \quad (3.9.32)$$

It can be shown that the Gegenbauer polynomials can be represented as

$$C_n^\lambda(\cos\ \varphi) = \sum_{m=0}^n \frac{\Gamma(\lambda + m)\Gamma(\lambda + n - m)\cos[(n - 2m)\varphi]}{m!(n - m)![\Gamma(\lambda)]^2}. \quad (3.9.33)$$

A term that is useful is

$$C_2^{-5/6}(\cos\ \varphi) = \tfrac{5}{6}\left[1 - \tfrac{1}{3}\cos^2\ \varphi\right]. \quad (3.9.34)$$

183

For $aD > d(z)$, the terms in the structure function can be expanded in Gegenbauer polynomials. The zeroth and all odd order terms cancel and if $m \to 2m$ the result is

$$D(\alpha) = 2(2.91) k_o^2 \int_0^\infty dz \ C_n^2(z) \left[d^{5/3}(z) - (\alpha D)^{5/3} \sum_{m=1}^\infty C_{2m}^{-5/6}(\cos \varphi) \left(\frac{d(z)}{\alpha D} \right)^{2m} \right].$$

(3.9.35)

It is this canceling of the first two terms of the power series that causes numerical difficulties if the integral is evaluated numerically without the above expansion. Define

$$\sigma_\varphi^2 = 2.91 k_o^2 \int_0^\infty dz \ C_n^2(z) d^{5/3}(z) = 2.91 k_o^2 d_{5/3}.$$

(3.9.36)

For adaptive-optic systems, the Strehl ratio is fairly high, which requires the structure function to be small. This assumption allows one to retain only the first term of the Gegenbauer expansion to give

$$D(\alpha) = 2\sigma_\varphi^2 - 2x,$$

(3.9.37)

where

$$x = 2.91 k_o^2 d_2 \left[1 - \frac{1}{3} \cos^2 \varphi \right] \frac{5}{16} (\alpha D)^{-1/3},$$

(3.9.38)

and

$$d_2 = \int_0^L dz \ C_n^2(z) d^2(z).$$

(3.9.39)

The assumption that $aD > d(z)$ is not true in the center of the aperture, but, is typically true over most of the aperture. There will be a small error made by integrating this approximate expression over the entire aperture. In fact, if the exponential is expanded in a power series only the integral of the first six terms converges because of this assumption. If only the first six terms are retained, the Strehl ratio can be written as

$$SR \approx \frac{\exp[-\sigma_\varphi^2]}{2\pi} \int d\vec{\alpha} \ K(\alpha) \left[1 + x + \frac{x^2}{2} + \frac{x^3}{6} + \frac{x^4}{24} + \frac{x^5}{120} \right].$$

(3.9.40)

If just the first term in the last bracket is retained, the result is equivalent to the Maréchal assumption. The assumption used here is valid to a lower Strehl ratio than that one. The integrals over angle and the aperture coordinate can be performed analytically. The angle

184

integral, after use of the binomial theorem, is equal to

$$\Phi(n) = \frac{1}{2\pi} \int_0^{2\pi} d\varphi \left[1 - \frac{1}{3} \cos^2 \varphi \right]^n = \frac{1}{2\pi} \sum_{m=0}^n \binom{n}{n-m} 3^{-m} \int_0^{2\pi} d\varphi \cos^{2m} \varphi. \quad (3.9.41)$$

Equation (3.641-4) in Gradshteyn and Ryzhik is

$$\int_0^{\pi/2} d\varphi \cos^{2m} \varphi = \frac{\pi(2m-1)!!}{2(2m)!!}, \quad (3.9.42)$$

where

$$(2m-1)!! = (2m-1)(2m-3) \ldots (3)(1), \quad (3.9.43)$$

and

$$(2m)!! = (2m)(2m-2) \ldots (4)(2). \quad (3.9.44)$$

With these relations, the angle integral is equal to

$$\Phi(n) = 1 - \sum_{m=1}^n \binom{n}{n-m} 3^{-m} \frac{(2m-1)!!}{(2m)!!}. \quad (3.9.45)$$

The values of interest are $\Phi(0) = 1$, $\Phi(1) = 0.8333$, $\Phi(2) = 0.7083$, $\Phi(3) = 0.6134$, $\Phi(4) = 0.5404$; and $\Phi(5) = 0.4836$. The aperture integration is

$$Y(n) = \int_0^1 d\alpha \, \alpha^{1 - n/3} K(\alpha). \quad (3.9.46)$$

Using the results in Equation (2.3.15), the values of interest to us are $Y(0) = 1$, $Y(1) = 1.402$, $Y(2) = 2.087$, $Y(3) = 3.396$, $Y(4) = 6.419$, $Y(5) = 16.94$. If these values are used, the approximation to the Strehl ratio is

$$SR \approx \exp[-\sigma_\varphi^2][1 + 0.9736\, E + 0.5133 E^2 + 0.2009\, E^3 + 0.0697\, E^4 + 0.02744\, E^5],$$

$$(3.9.47)$$

where

$$E = \frac{2.91 k_o^2 d_2}{D^{1/3}}. \quad (3.9.48)$$

This result was compared to that obtained by numerical integration and shown to be in good agreement as long as the Strehl ratio was above 0.3. This expression will now be applied to various types of anisoplanatism.

185

3.9.3.1 Displacement Anisoplanatism

The terms to use to find the Strehl ratio are

$$d_2 = \mu_o d^2,$$

(3.9.49)

and

$$\sigma_\varphi^2 = 2.91 k_o^2 \mu_o d^{5/3} = 6.88 \left(\frac{d}{r_o} \right)^{5/3}.$$

(3.9.50)

Use was made of the definition of the coherence diameter given in Equation (3.5.5). If these expressions are inserted into Equation (3.9.40), then one obtains the Strehl ratio versus displacement plotted for two different scales in Figures 3-26 and 3-27. The Strehl ratio for the HV-21 model is not plotted since its Strehl ratio is virtually identical to SLCSAT day values.
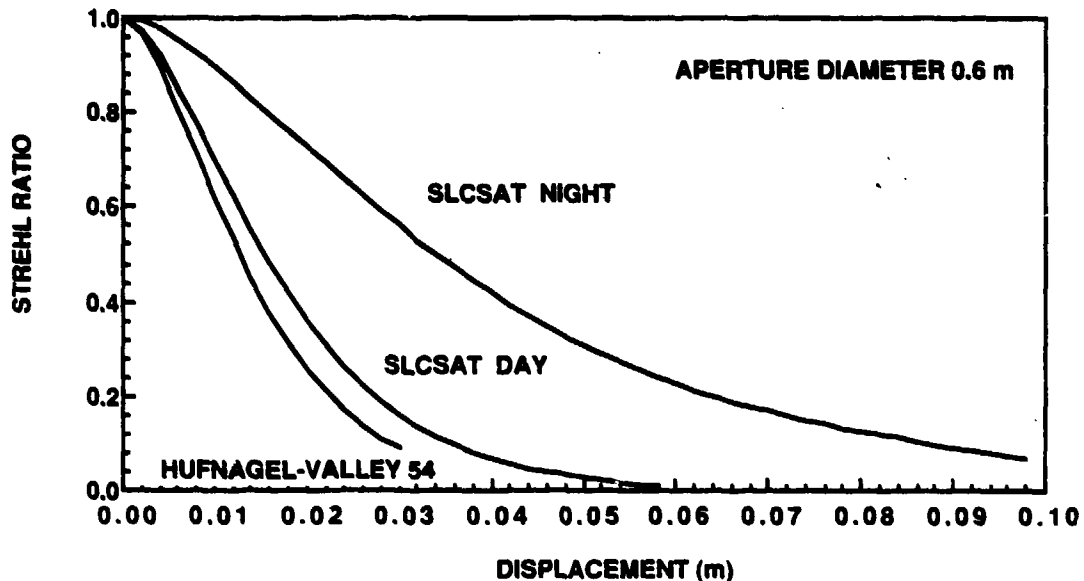
Figure 3-26. Strehl ratio versus parallel displacement for a 0.6-m diameter system with various turbulence models.

186
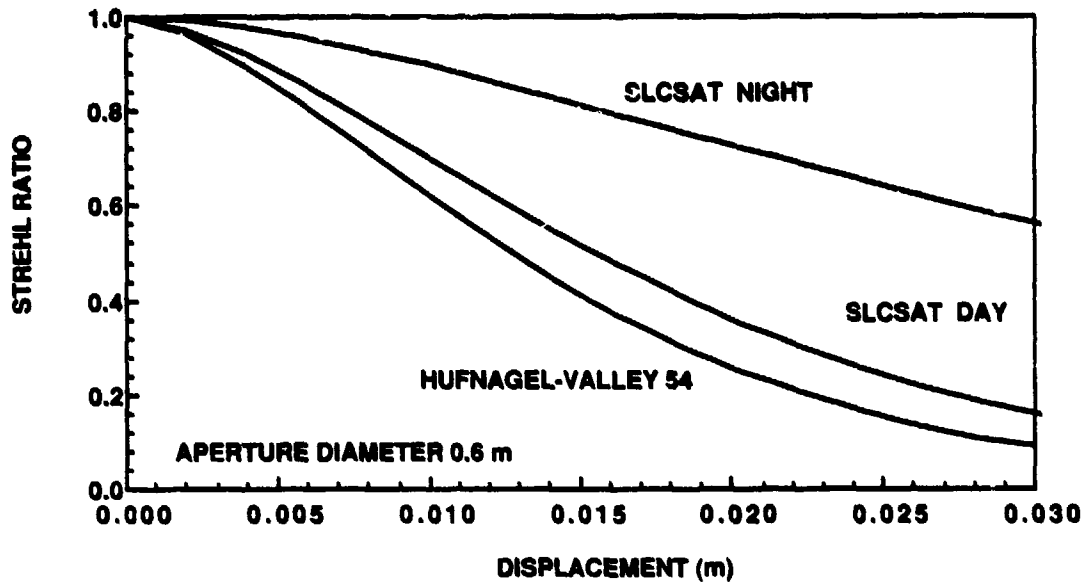
Figure 3-27. Strehl ratio versus parallel displacement for a 0.6-m diameter system with various turbulence models for small displacements.

3.9.3.2 Angular Anisoplanatism

If the beam is offset by a constant angle, then

$$d(z) = \Theta z, \tag{3.9.51}$$

and

$$d_2 = \mu_2 \Theta^2, \tag{3.9.52}$$

and

$$\sigma_\varphi^2 = 2.91 k_o^2 \Theta^{5/3} \int_0^L dz \; C_n^2(z) \; z^{5/3} = \left(\frac{\Theta}{\Theta_o} \right)^{5/3}. \tag{3.9.53}$$

Use was made of the definition of the isoplanatic patch size given in Equation (3.5.6). The Strehl ratio at zenith for various turbulence models is plotted in Figure 3-28 and at 30 degrees from zenith in Figure 3-29.

187
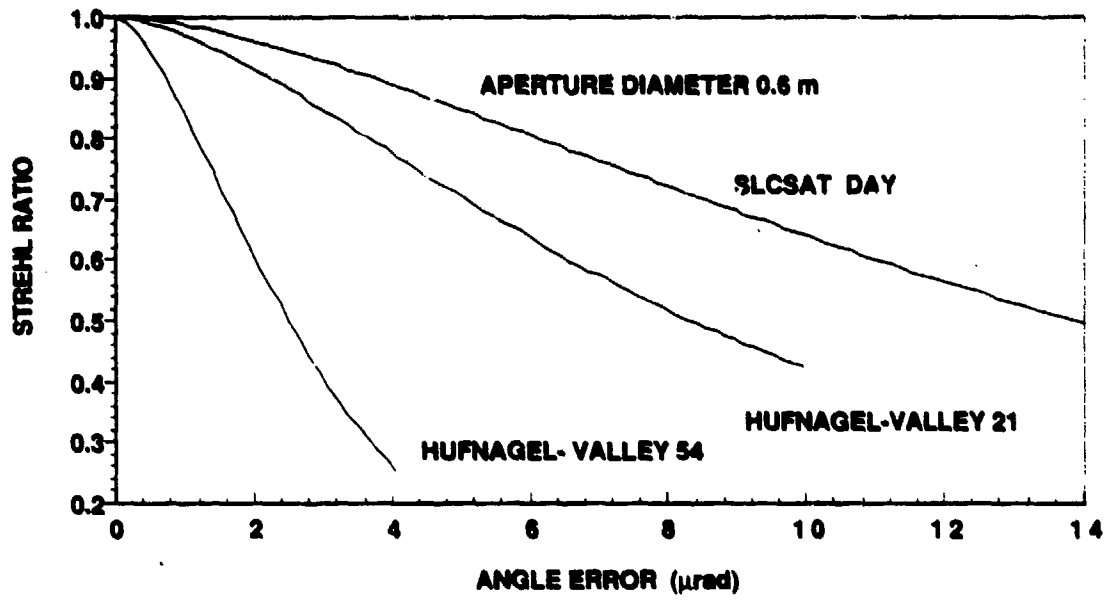
Figure 3-28. Strehl ratio for angular anisoplanatic error at zenith for various turbulence models versus separation angle for a 0.6-m system.
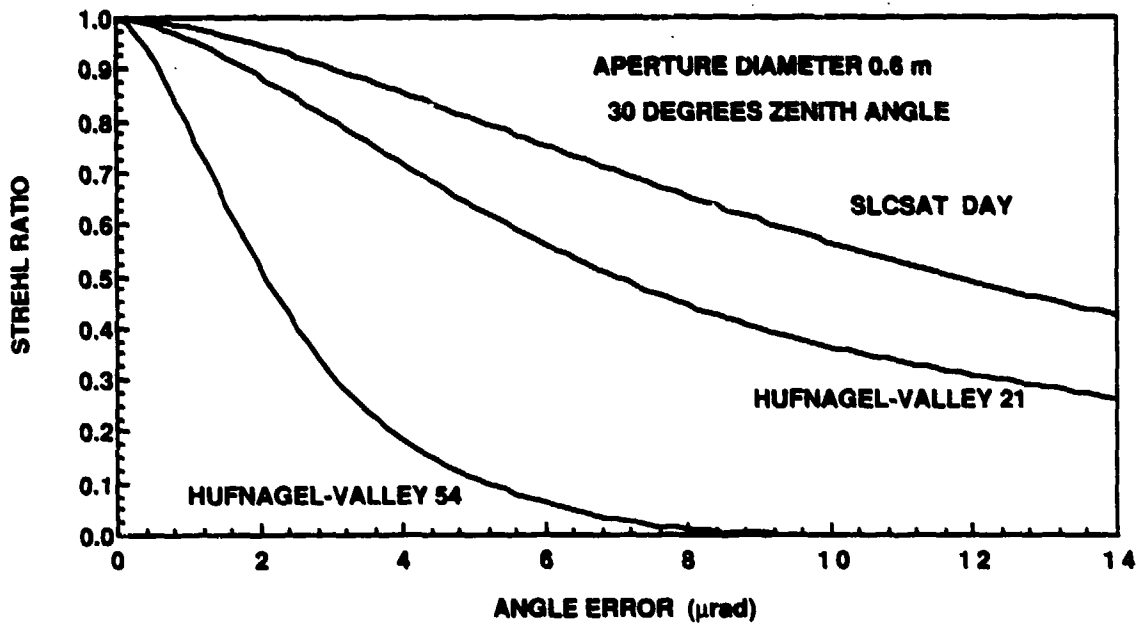
Figure 3-29. Strehl ratio for angular anisoplanatism at 30 degrees from zenith for a 0.6-m system.

3.9.3.3   Time Delay

For this case

$$d_2 = \int_0^L dz \; C_n^2(z) \; v^2(z) \tau^2 = v_2 \tau^2,$$ (3.9.54)

and

$$\sigma_\varphi^2 = 2.91 k_o^2 \int_0^L dz \; C_n^2(z) \; v^{5/3}(z) \tau^{5/3} = (\tau / \tau_o)^{5/3}.$$ (3.9.55)

where the velocity moment is defined as

$$v_n = \int_0^L dz \; C_n^2(z) v^n(z).$$ (3.9.56)

The characteristic time is defined by

$$\tau_o^{-5/3} = 2.91 k_o^2 v_{5/3}.$$ (3.9.57)

The Strehl ratio is plotted for various turbulence models at zenith for a Bufton wind model with a ground wind speed of 5 m/s in Figure 3-30 and at 30 degrees off zenith in Figure 3-31.
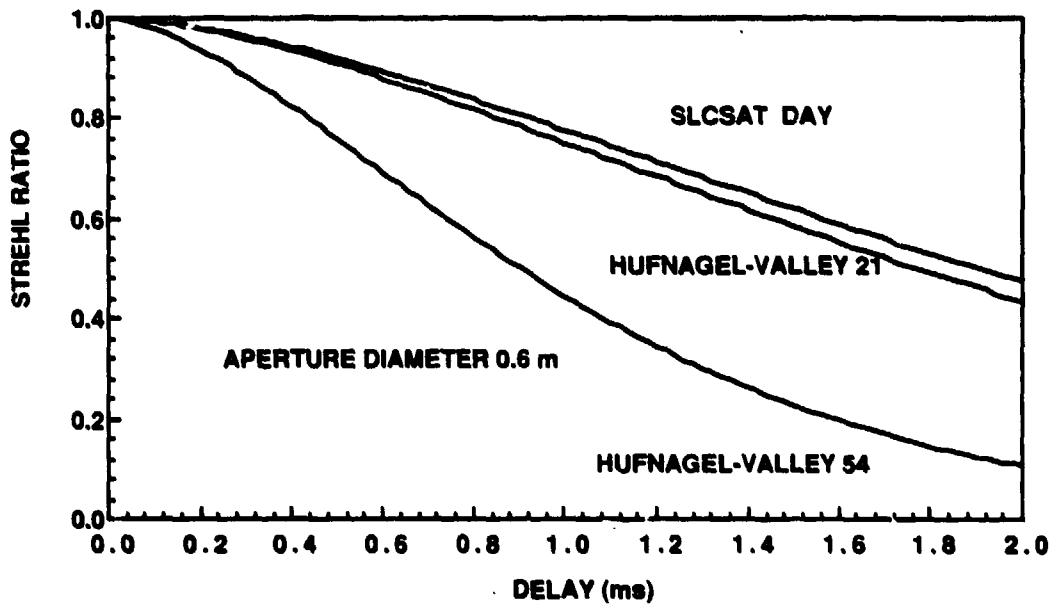
Figure 3-30.   Strehl ratio versus time delay at zenith for 0.6-m system.
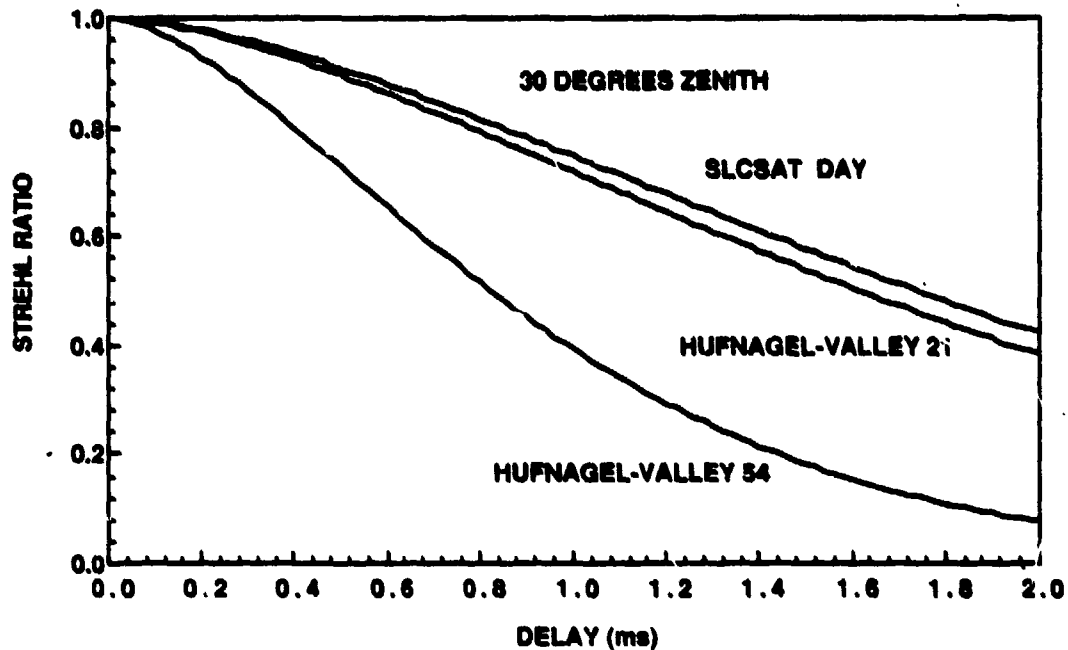
Figure 3-31. Strehl ratio versus time delay at zenith for 0.6-m system at 30 degrees zenith angle.

The Bufton wind model gives the wind versus altitude as

$$v(h) = v_g + 30 \exp\left[-\left(\frac{h - 9400}{4800}\right)^2\right].$$

(3.9.58)

3.9.3.4 Chromatic Anisoplanatism

In Section 3.4.3, the basic formulas for chromatic anisoplanatism were presented. The formulas there assumed that the rays were parallel at the target. In actuality, they converge on the target and it will be shown that the error in assuming parallel beams exoatmospherically rather than beams that converge on the target is very small. The displacement as a function of range is given in Equation (3.4.40). At the target at range R, the displacement is $d(R)$, and to hit the target squarely one must change the launching angle by $d(R)/R$. Therefore, the accurate formula for the displacement of a beam that converges on the target is

$$\vec{d}(z) = \frac{\xi \sin(\xi) \Delta n_o}{\xi \cos^2(\xi)}\left[\int_0^z dx \ \alpha(x) - \frac{z}{R} \int_0^R dx \ \alpha(x)\right].$$

(3.9.59)

The difference in refractive index between the two wavelengths can be calculated from

190

Equation (3.4.41). The last equation can be written as

$$\vec{d}(z) = -\frac{\xi \sin(\xi)\, \Delta n_0}{\xi \cos^2(\xi)} \left[I(z) - \frac{z}{R} I(R) \right]$$

(3.9.60)

The integral of the air density is easily evaluated to give

$$I(z) = 9010 \left\{ 1 - \exp\left[-1.11 \times 10^{-4} z\right] \right\} \qquad z < 10 \text{ km}$$

$$I(z) = 8161 - 10190 \exp\left[-1.57 \times 10^{-4} z\right] \qquad z > 10 \text{ km}.$$

(3.9.61)

The moments of this displacement are found to be

$$d_n = \left[\frac{\sin(\xi)\, \Delta n_0}{\cos^2(\xi)} \right]^n T_n,$$

(3.9.62)

where

$$T_n = 2.91 k_0^2 \sec(\xi) \int_0^L dh \; C_n^2(h) \left[I(h) - \frac{h \sec(\xi)}{R} I(R) \right]^n.$$

(3.9.63)

L is the height of the target. The last term in brackets goes to zero as the range becomes infinite. In Figure 3-32 is plotted a comparison of the Strehl ratio of a target at 300 km and one at infinity.
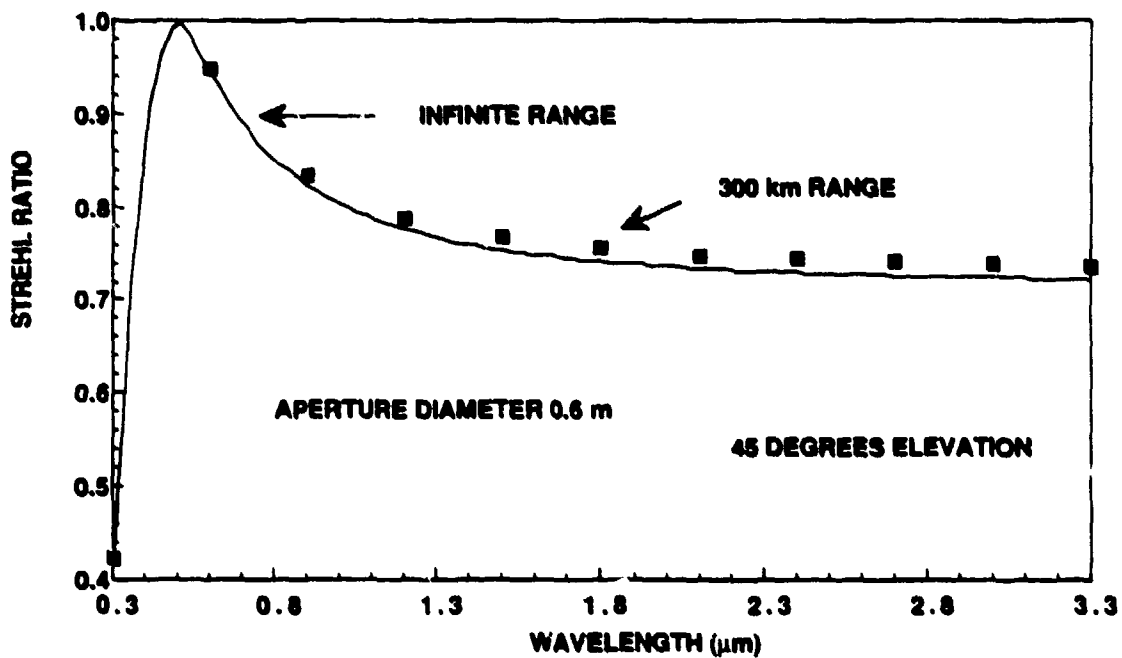

Figure 3-32. Comparison of the Strehl ratio at infinite and 300 km range.

191

There is very little difference in the two results which justifies the assumption that the rays can be considered parallel. For infinite range, the above equation reduces to

$$T_n = 2.91 k_o^2 \sec(\xi) \int_0^L dh \; C_n^2(h) \, l^n(h).$$ (3.9.64)

The results for the finite range case entails a numerical calculation for each range. The infinite range results can be calculated once for each turbulence model and used for different zenith angles. Table 3-2 contains the values of T_2 and $T_{5/3}$ for various turbulence models.

| TABLE 3-2 |
| Values of T_2 and $T_{5/3}$ for Various Turbulence Models |

MODEL	T_2	$T_{5/3}$
SLCDAY	2.706×10^{-6}	2.004×10^{-7}
SLCNIGHT	2.256×10^{-6}	1.512×10^{-7}
HV-21	0.16×10^{-6}	3.596×10^{-7}
HV-54	3.399×10^{-5}	1.867×10^{-6}
HV-72	5.949×10^{-5}	3.247×10^{-6}

Figure 3-33 contains plots of Strehl ratio for the SLCSAT day model for various elevation angles when one beam is at 0.5-micrometers wavelength.
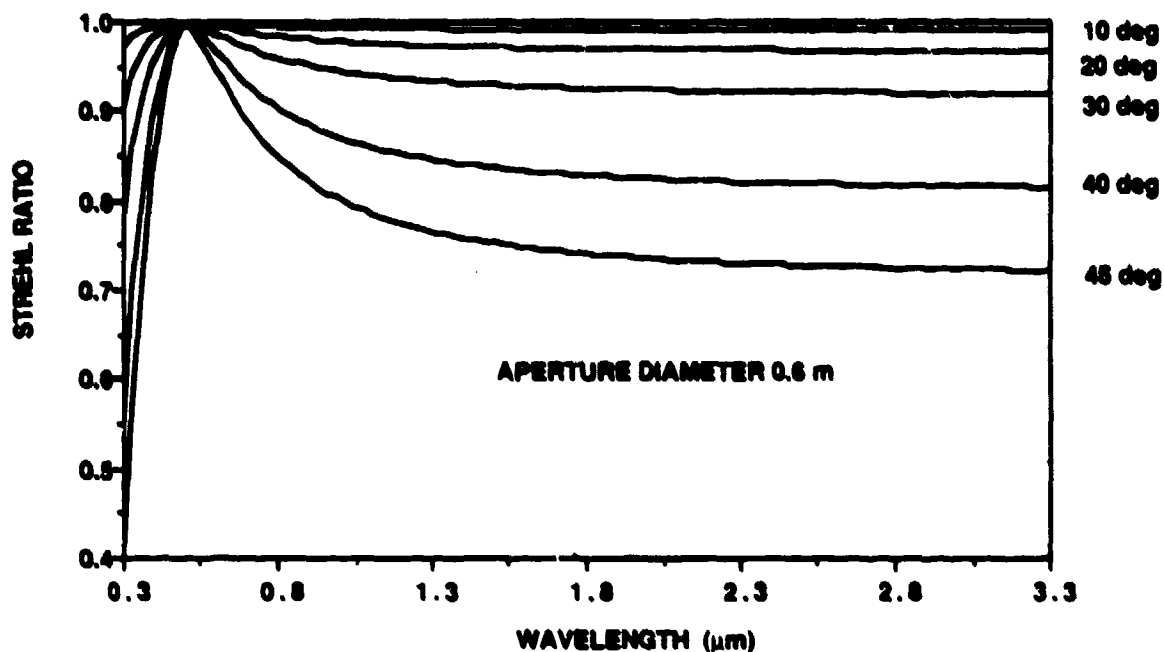
Figure 3-33. Strehl ratio for SLCSAT day turbulence with the scoring beam at 0.5 µm for a 0.6-m system.

3.9.4 Strehl Ratio in an Adaptive-Optics System

The filter function with all the defects included can be written down. The beam from the adaptive-optics system has anisoplanatic errors, errors due to fitting error, and errors due the finite system bandwidth. The composite filter function is the product of the filter function for fitting error, F_{FE}, times the filter function for finite servo response, F_S, and the phase shift due to the anisoplanatic displacement minus unity. This filter function is

$$F_{AO} = \left| F_{FE}(\kappa) F_S(\kappa_v) \exp[i\vec{R} \cdot \vec{d}(z)] - 1 \right|^2. \tag{3.9.65}$$

3.10 BEAM PROFILE

In this section, the beam profile for uncorrected turbulence and for an adaptive-optics system with anisoplanatism will be found. The method of solution uses the same tools that were used before, but, because these problems are more difficult than the calculation of the Strehl ratio, the expressions are longer. The solutions manipulate asymptotic series that have been found. This manipulation is possible because of the properties of asymptotic series of the Poincairé type that were stated at the end of Section 2.4.2.

193

3.10.1 Beam Profile for Uncorrected Turbulence

A framework for finding the beam profile for any ratio of the coherence diameter to the aperture diameter is developed. This approach expresses the beam profile as the sum of an infinite series of radial functions. A different series of functions is obtained for large coherence diameters and small coherence diameters. For weak turbulence, it is shown that the first term of the series gives the Airy function profile. Typically, one is interested in the case in which the coherence diameter is small compared to the aperture diameter. In that case, only the first term of the asymptotic series profiles is necessary to find the profile. The profile is expressed as an integral and the techniques that have been developed are used to find the profile for small and large diameters. It is shown that these two series match well at intermediate diameters and therefore give a profile that is valid for all diameters. It is interesting to note that the behavior at large radii is obtained by taking an asymptotic series of an expression obtained from an asymptotic series.

The starting point for obtaining the beam profile is the expression in Equation (3.2.12) with the structure function for uncorrected turbulence given in Equation (3.9.15). This gives the expression

$$I_n(r) = \int_0^1 \alpha \; d\alpha J_o\left(\frac{k_o rD\alpha}{z}\right) K(\alpha)\exp\left[-3.44\left(\frac{\alpha D}{r_o}\right)^{5/3}\right]. \qquad (3.10.1)$$

This integral will be evaluated by Mellin transform techniques. Let

$$x = \frac{z}{k_o rD}. \qquad (3.10.2)$$

Separate the integrand into the two functions

$$H_1(x / \alpha) = J_o(\alpha / x), \qquad (3.10.3)$$

and

$$H_2(x) = \alpha^2 K(\alpha)\exp\left[-3.44\left(\frac{\alpha D}{r_o}\right)^{5/3}\right]U(1-\alpha). \qquad (3.10.4)$$

With these definitions the beam profile is

$$I_n(r) = \int_0^\infty \frac{d\alpha}{\alpha} H_1(x / \alpha) H_2(\alpha) = \frac{1}{2\pi i} \int ds \; H_1^*(s) H_2^*(s) x^{-s}. \qquad (3.10.5)$$

194

The Mellin transform of the first term is found from Equation (F.5) as

$$H_1^*(s) = 2^{-s-1}\Gamma\begin{bmatrix}-s/2\\1+s/2\end{bmatrix}.$$

(3.10.6)

The Mellin transform of the second function can be found from the expression for the Strehl ratio that was previously found. Examining Equation (3.9.6), it is easy to see that the equivalent of Equation (3.9.13) is

$$H_2^*(s) = \lim_{u \to \infty} \frac{1}{2\pi i}\int_{-i\infty}^{i\infty} ds \frac{\Gamma(u+v)}{\Gamma(u)}\Gamma(-v)\left[\frac{3.44}{u}\left(\frac{D}{r_o}\right)^{5/3}\right]^{\nu} \int_0^1 d\alpha\, \alpha^{1+5\nu/3+s}\, K(\alpha).$$

(3.10.7)

Following the same steps as the previous analysis, one finds

$$H_2^*(s) = \frac{24}{5\sqrt{\pi}}\frac{1}{2\pi i}\int_{-i\infty}^{i\infty} dv\, \Gamma\begin{bmatrix}v, \frac{3}{2}+s/2-5v/6, -v+3s/5+\frac{6}{5}\\3+s/2-5v/6, -v+3s/5+\frac{11}{5}\end{bmatrix}\left[3.44\left(\frac{D}{r_o}\right)^{5/3}\right]^{-\nu}.$$

(3.10.8)

Since $\Delta = 5/6$, the path of integration can be closed in the left-half plane and the integral is equal to the residues at $v = -n$ for $n = 0, 1, 2, \ldots$. Therefore, the Mellin transform of this function is

$$H_2^*(s) = \frac{4}{\sqrt{\pi}}\sum_{n=0}^{\infty}\frac{(-1)^n}{n!}\Gamma\begin{bmatrix}s/2+5n/6+3/2, s/2+5n/6+1\\s/2+5n/6+3, s/2+5n/6+2\end{bmatrix}\left[3.44\left(\frac{D}{r_o}\right)^{5/3}\right]^{n}.$$

(3.10.9)

The above series converges rapidly for large coherence diameters. If the turbulence is severe, then an asymptotic series is wanted. It is easily shown that the steepest descent contribution has exponential decay and is insignificant compared to the residue of the poles to the right of the path of integration. There are poles at $v = 6n/5 + 3s/5 + 9/5$ for $v = 0, 1, 2, \ldots$, and a single pole at $v = 3s/5 + 6/5$. There is only a single pole because the singularities in the denominator cancel the other terms. Evaluating the residues at these poles gives for the asymptotic solution

195

$$H_2^*(s) = \frac{24}{5\sqrt{\pi}}\left\{\frac{\sqrt{\pi}}{3.44^{6/5}}\Gamma(3s/3 + 6/5)(3.44)^{-2s/5}\left(\frac{r_o}{D}\right)^{2+s}\right.$$

$$\left. - \sum_{n=0}^{\infty}\frac{(-1)^n}{n!}\frac{(3.44)^{-9/5-3s/5-6n/5}}{n+1/2}\left(\frac{r_o}{D}\right)^{3+s+2n}\Gamma\left[\frac{\frac{9}{5}+3s/5+6n/5}{\frac{3}{2}-n}\right]\right\}.$$

<div align="right">(3.10.10)</div>

There was an extra factor of 5/6 multiplying the last summation because the coefficient of v was 5/6.

To obtain the beam profile for large and small values of coherence diameter, these expressions must be inserted into Equation (3.10.5) and that integral evaluated by the techniques we have been using. That will not be done here but rather the beam profile will be examined in two limits. First, let us look at the profile when the turbulence is low. Only the first term of the series will be examined. To find this, insert the first term of Equation (3.10.9) and the expression in Equation (3.10.6) into Equation (3.10.5). The result is

$$I_n(r) = \frac{1}{2\pi i}\int ds \frac{2}{\sqrt{\pi}}\Gamma\left[\frac{s/2, \frac{3}{2}-s/2}{2-s/2, 3-s/2}\right]\left(\frac{k_o r D}{2z}\right)^s. \qquad (3.10.11)$$

From Equations (F.6) and(I.4), one recognizes this integral as the Airy function given by

$$I_n(r) = \left[\frac{J_1\left(\frac{k_o r D}{2z}\right)}{\left(\frac{k_o r D}{4z}\right)}\right]^2. \qquad (3.10.12)$$

Higher order terms will modify this distribution by subtracting from it. The fact that this term exists even as the turbulence gets stronger shows that the beamwidth does not increase significantly as the turbulence gets worse as long as it is not so strong that the asymptotic series is required. The characteristic of the solution is to have a strong central peak with a broader tail. This distribution is referred to as the fried-egg effect. For strong turbulence, the first term of the asymptotic approximation in Equation (3.10.10) is a good approximation and if that is inserted along with Equation (3.10.6) into Equation (3.10.5) one obtains

<div align="center">196</div>

$$I_n(r) = \frac{12}{5(3.44)^{1.2}}\left(\frac{r_o}{D}\right)^2 \frac{1}{2\pi i}\int ds\,\Gamma\left[\begin{matrix} s/2, \frac{6}{5} - 3s/5 \\ 1 - s/2 \end{matrix}\right] x^s, \qquad (3.10.13)$$

where

$$x = 0.238\,\frac{k_o r\, r_o}{z}. \qquad (3.10.14)$$

Since $\Delta = 2/5$, the path of integration can be closed in the left-half plane with the result

$$I_n(r) = 1.09\left(\frac{r_o}{D}\right)^2 \sum_{n=0}^{\infty} \frac{(-1)^n}{(n!)^2}\Gamma\left[\frac{6n}{5} + \frac{6}{5}\right] x^{2n}. \qquad (3.10.15)$$

For large distances from the origin, an asymptotic series is wanted. It can be shown that the steepest descent contribution has exponential decay; therefore, the asymptotic series is the residue at the poles to the right of the path of integration. These poles are at $s = 5n/3 + 2$, $n = 1, 2, 3, \ldots$. The $n = 0$ term cancels because of the pole in the denominator at that value and the beam profile is

$$I_n(r) = 16\left(\frac{z}{Dk_o r}\right)^2 \sum_{n=1}^{\infty} \frac{(-1)^n}{n!}\,\Gamma\left[\begin{matrix} 5n/6 + 1 \\ -5n/6 \end{matrix}\right]\left(\frac{4.197\,z}{k_o r\, r_o}\right)^{5n/3}. \qquad (3.10.16)$$

The beam shape is plotted in Figure 3-34. In the same figure is also plotted the beam shape for a wave with no turbulence but which has an aperture diameter equal to the coherence diameter. Notice that the shapes of the two profiles are close to each other when the intensity is above 0.2 of the value on axis.
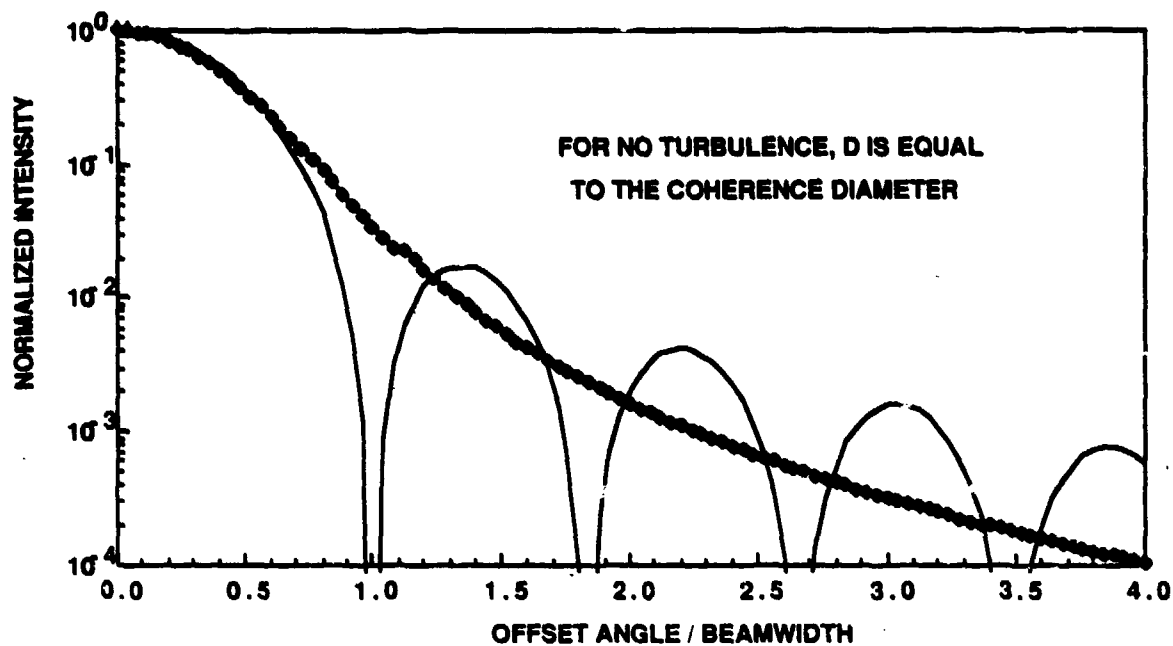
Figure 3-34. Beam shape with and without turbulence.

3.10.2 Beam Shape with Anisoplanatism

Next, the more complicated problems of finding the beam shape with anisoplanatism will be solved. The method of solution will use the method of expanding the exponential into a series of Gegenbauer polynomials as was done in the calculation of the Strehl ratio. For this reason, the beam profile will only be valid when the Strehl ratio is greater than 0.3, which is the region of most interest. The starting point will be the expression for the beam profile given in Equation (3.2.9), which is repeated here

$$I_n(\vec{r}) = \frac{1}{2\pi}\int d\vec{\alpha}\, K(\alpha)\exp\left[\, ik_o D\vec{r} \cdot \vec{\alpha} / z - D(\vec{\alpha}) / 2\right]. \qquad (3.2.9)$$

The structure function is the same as when the Strehl ratio was calculated. It is again expanded into Gegenbauer polynomials and only the first term is retained. If the exponential is expanded into a power series as was done before, the equivalent expression given in Equation (9.3.14) is

$$I_n(r) \approx \frac{\exp[-\sigma_\varphi^2]}{2\pi}\int d\vec{\alpha}\exp\left[\, ik_o D\vec{r} \cdot \vec{\alpha} / z\right] K(\alpha)\left[1 + x + \frac{x^2}{2} + \frac{x^3}{6} + \frac{x^4}{24} + \frac{x^5}{120}\right].$$

$$(3.10.17)$$

198

The integration over angle is not as straightforward as before since there is an additional term in the exponential. At this point an approximation is made. The angle dependence in the x term is small and we will replace the angular expression in x by the values that were calculated for the Strehl ratio. The angular integration can then be performed to get a Bessel function for the exponential term. Define

$$Q(v) = \frac{1}{I(v)} \int_0^1 d\alpha \; \alpha^{v+1} K(\alpha) J_o(\alpha / y) = \frac{1}{I(v)} \int_0^\infty \frac{d\alpha}{\alpha} \; \alpha^{v+2} K(\alpha) J_o(\alpha / y),$$

(3.10.18)

where

$$y = \frac{z}{k_o r D},$$

(3.10.19)

and $I(v)$ is chosen to normalize the function on axis. It is easy to see that $I(v)$ is the function that we have evaluated in Equation (2.3.15). With these definitions, the beam profile can be written as

$$I_n(r) \approx \exp\left[-\sigma_\varphi^2\right]\left[Q(0) + 0.9736 \, E Q\left(-\tfrac{1}{3}\right) + 0.5133 E^2 Q\left(-\tfrac{2}{3}\right) \right.$$
$$\left. + 0.2009 \, E^3 Q(-1) + 0.0697 \, E^4 Q\left(-\tfrac{4}{3}\right) + 0.02744 \, E^5 Q\left(-\tfrac{5}{3}\right)\right].$$

(3.10.20)

To complete the analysis, the function $Q(v)$ must be evaluated. The same method as that used in the last section will be used again. Define the first function the same as in Equation (3.10.3) and the second function as

$$H_2(\alpha) = \alpha^{2+v} K(\alpha).$$

(3.10.21)

It is easy to see that

$$H_2^*(s) = I(s + v).$$

(3.10.22)

The function we are seeking is then equal to

$$Q(v) = (1 + v/2) \Gamma\left[\begin{matrix}3 + v/2\\ \tfrac{3}{2} + v/2\end{matrix}\right] \frac{1}{2\pi i} \int ds \Gamma\left[\begin{matrix}s, \tfrac{3}{2} + v/2 - s, 1 + v/2 - s\\ 1 - s, 3 + v/2 - s, 2 + v/2 - s\end{matrix}\right]\left(\frac{1}{2y}\right)^{-2s}.$$

(3.10.23)

199

For $v = 0$, it can be shown that the integral is equal to an Airy function. For other values of v, the solution cannot be expressed in terms of simple functions. Therefore, the integral will be evaluated in terms of an infinite series. Since $\Delta = 2$, the path of integration can be closed to the left, and one obtains for the residues at $s = -n$, $n = 1, 2, 3, \ldots$ the value

$$Q(v) = (1 + v/2)\Gamma\begin{bmatrix} 3 + v/2 \\ \frac{3}{2} + v/2 \end{bmatrix} \sum_{n=0}^{\infty} \frac{(-1)^n}{(n!)^2 (n+1+v/2)} \Gamma\begin{bmatrix} n + \frac{3}{2} + v/2 \\ n + 3 + v/2 \end{bmatrix} \left(\frac{k_o rD}{2z}\right)^{2n}.$$

(3.10.24)

For large radii, an asymptotic series is wanted. This series has contributions due to both the steepest descent contribution and the poles to the right of the path of integration at $s = 1 + v/2$ and $v/2 + 3/2 + n$ for $n = 0, 1, 2, \ldots$. This asymptotic solution is equal to

$$Q(v) = (1 + \frac{v}{2})\Gamma\begin{bmatrix} 3 + v/2 \\ \frac{3}{2} + v/2 \end{bmatrix} \left\{ \sum_{n=0}^{\infty} \frac{(-1)^{n+1}}{n!(n+1/2)} \Gamma\begin{bmatrix} n + \frac{3}{2} + v/2 \\ -\frac{1}{2} - n - v/2, -n + \frac{3}{2} \end{bmatrix} \left(\frac{2z}{k_o rD}\right)^{2n+3+v} \right.$$

$$\left. + \sqrt{\pi}\,\Gamma\begin{bmatrix} v/2 + 1 \\ -v/2 \end{bmatrix} \left(\frac{2z}{k_o rD}\right)^{2+v} + \frac{1}{\sqrt{\pi}} \left(\frac{2z}{k_o rD}\right)^{3/2} \cos\left[\left(\frac{2 k_o rD}{z}\right)^{1/2} - \frac{3\pi}{2}\right] \right\}.$$

(3.10.25)

The beam pattern can be plotted for various types of anisoplanatism by putting in the appropriate values of E and σ_ϕ^2 in the above expressions. The beam pattern is plotted for angular anisoplanatism in Figures 3-35 and 3-36 for various values of offset angles. Notice how the dips in the Airy pattern fill in, and the power gets distributed at larger radial distances.

200
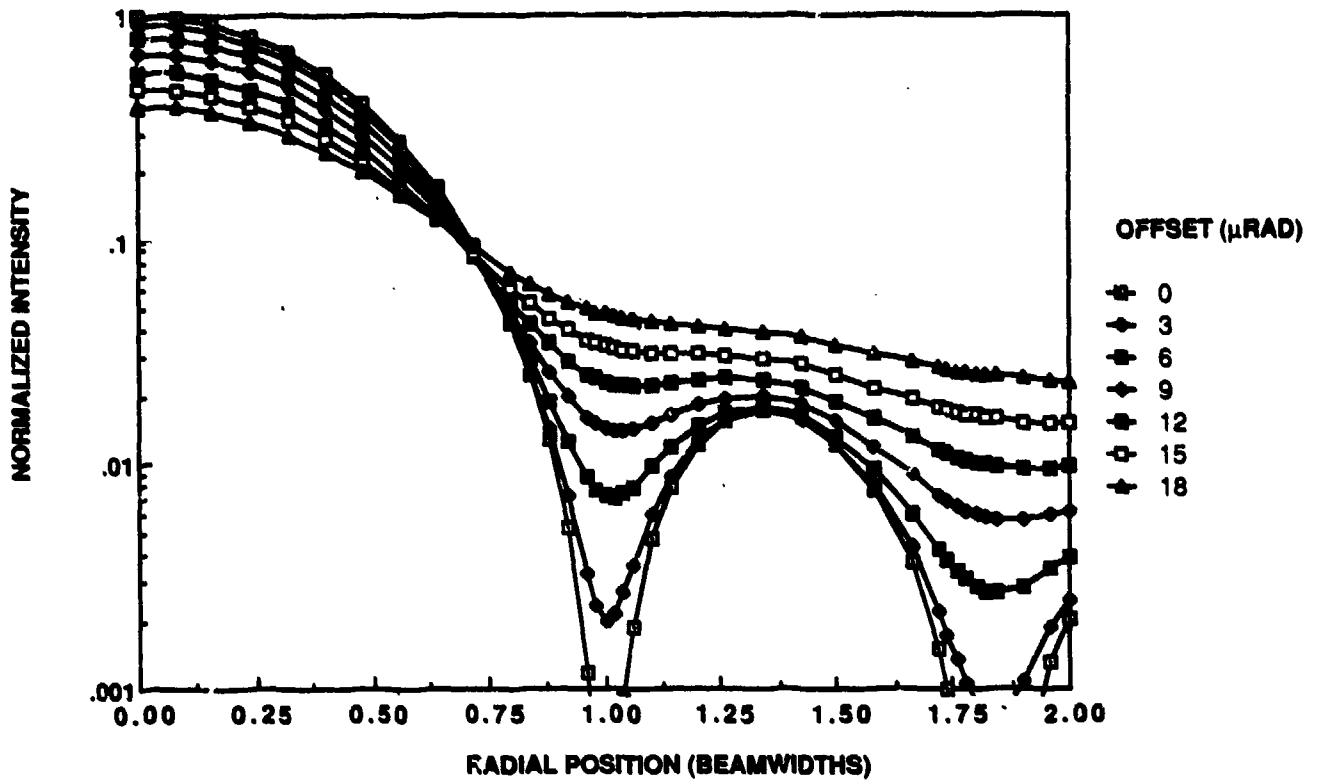
Figure 3-35. Beam shape with anisoplanatism for a 0.6-m aperture at zenith for the SLCSAT day model.
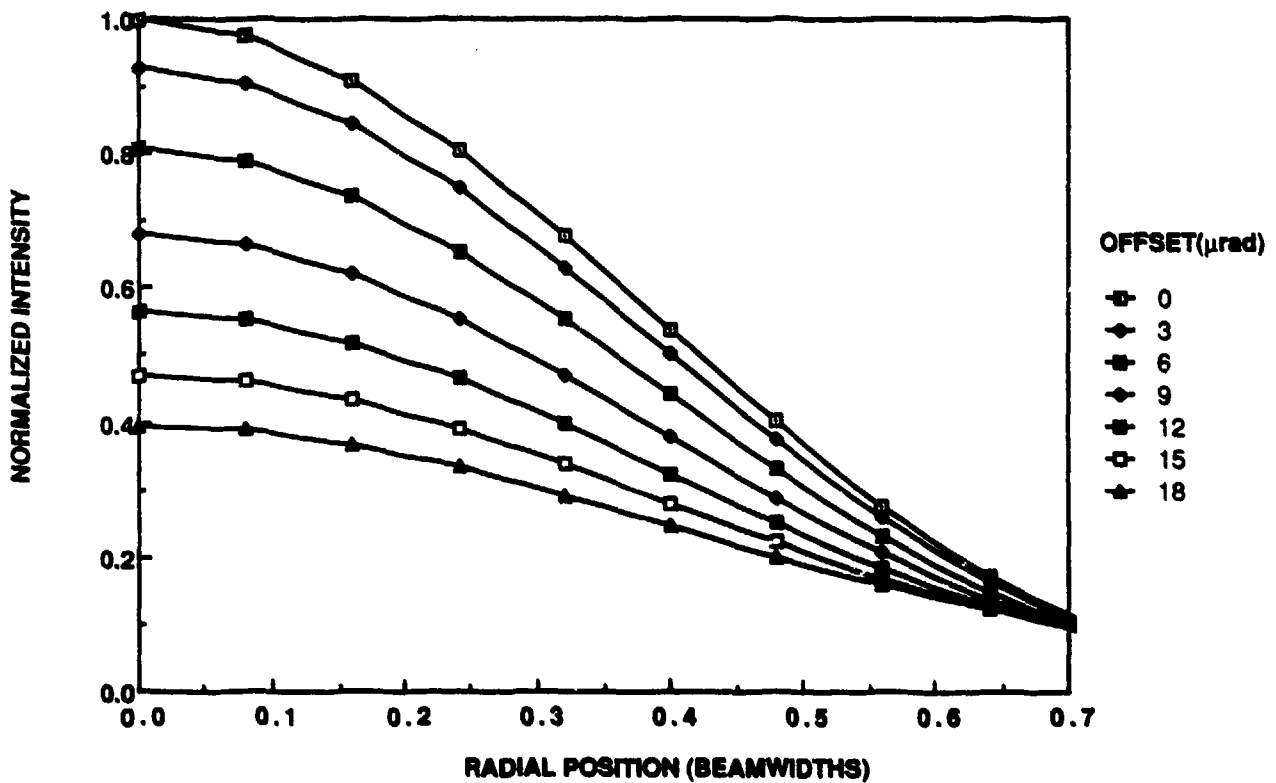

Figure 3-36. Beam shape close to the axis with anisoplanatism for a 0.6-m aperture at zenith for the SLCSAT day model.

201

REFERENCES

1. V. I. Tatarski, *Wave Propagation Is a Turbulent Medium* (Dover, New York, 1961).

2. D. L. Fried, J. Opt. Soc. Am. **72**, No. 1, 52-61 (January 1982).

3. G. A. Tyler, J. Opt. Soc. Am. **1**, No. 3, 251-262 (March 1984).

4. O. I. Marichev, *Integral Transforms of Higher Transcendental Functions* (Ellis Horwood Limited, Chichester, England, 1983).

5. F. Oberhettinger, *Tables of Mellin Transforms*, (Springer–Verlag, Berlin, Germany, 1974).

6. Born and Wolf, *Principles of Optics*, Appendix III (Pergamon Press, New York, 1959).

7. N. Bleistein, and R. A. Hendelsman, *Asymptotic Expansions of Integrals* (Dover, New York 1986).

8. Y. Luke, *The Special Functions and Their Approximations* (Academic Press, New York, 1969).

9. R. M. Range, *Holomorphic Functions and Integral Representations in Several Complex Variables*, p. 8 (Springer-Verlag, Berlin, Germany, 1986).

10. I. S. Gradshteyn and I. M. Ryzhik, *Table of Integrals, Series, and Products* (Academic Press, New York, 1980).

11. E. Jahnke , and F. Emde, *Table Of Functions* (Dover Publications, New York, 1945).

12. R. J. Noll, J. Opt. Soc. Am. **66**, No. 3, 207-211 (March 1976).

13. J. D. Shelton, private communication.

14. J. F. Belsher, and D. Fried, "Chromatic Refraction Induced Pseudo Anisoplanatism," the Optical Sciences Company, Placentia, California, tOSC Report TR-433 (June 1981).

15. J. F. Belsher, "Adaptive-Optics Mirror Fitting Error," the Optical Sciences Company, Placentia, California, tOSC Report TR-521 (June 1983).

16. B. L. Ellerbroek, "The Temporal Dependence of Turbulence-Induced Line-of-Sight Jitter as Measured by a Wavefront Gradient Sensor," the Optical Sciences Company, Placentia, California, tOSC Report No. TR-572 (May 1984).

17. H. T. Yura, and M. T. Travis, J. Opt. Soc. Am. A2, 765 (1985).

18. R. L. Fante, Proc. IEEE 68, No. 11, 1424-1443 (November 1980). This particular result is on page 1431.

19. A. M. Prokhorov, F. V. Bunkin, K. S. Gochelashvily, and V. I. Shishov, Proc. IEEE 63, No. 5, 790-811 (May 1975).

20. G. A. Tyler, "The Magnitude of Angle-of-Arrival Jitter in Ground to Relay Mirror Propagation for Various Turbulence Models," the Optical Sciences Company, Placentia, California, tOSC Report No. TR-673 (November 1985).

21. D. P. Greenwood, J. Opt. Soc. Am. 67, No. 3, 390-393 (March 1977).

22. D. V. Murphy, private communication.

23. B. L. Ellerbroek, and P. H. Roberts, "Turbulence Induced Angular Separation Errors: Expected Values For the SOR-2 Experiment," the Optical Sciences Company, Placentia, California, tOSC Report No. TR-613 (December 1984).

24. D. P. Greenwood, J. Opt. Soc. Am. 67, No. 3, 282-289 (March 1977).

25. V. I. Tatarski, "The Effects of the Turbulent Atmosphere on Wave Propagation," U.S. Dept. of Commerce, Washington, D.C., NTIS T68-50464 (1971).

26. D. P. Greenwood, and D. L. Fried, J. Opt. Soc. Am. 66, No. 3 (March 1976).

27. D. A. Fields, Appl. Opt., 22, No. 5 (March 1983).

28. G. A. Tyler, "The Power Spectrum for G-tilt and Z-tilt," the Optical Sciences Company, Placentia, California, tOSC Report No. TR-700 (March 1986).

29. J. L. Vaughn, "Calculation of the Power Spectra of Z-tilt and G-tilt," the Optical Sciences Company, Placentia, California, tOSC Report No. TR-710 (May 1986).

30. C. B. Hogge, and R. R. Butts, "Frequency Spectra for the Geometric Representation of Wavefront Distortions Due to Atmospheric Turbulence," IEEE Trans. Antennas Propaga., **AP-24**, No. 2 (March 1976).

31. R. R. Butts, "Spectra of Turbulence induced Wavefront Aberrations," AFWL, Report No. AFWL-TR-80-107 (1980).

32. D. L. Fried, J. Opt. Soc. Am. **56**, 1372 (1966).

33. R. F. Lutomirski, W. L. Woodie, and R. G. Buser, Appl. Opt. **16**, 665 (1977).

34. M. T. Travis and H. T. Yura, Appl. Opt. **15**, 2922 (1976).

35. J. Y. Wang and J. K. Marky, J. Opt. Soc. Am. **68**, No. 1, 78-87 (January 1978).

36. J. Y. Wang, Appl. Opt. **17**, No. 16, 2580-2590 (15 August 1978).

37. J. Y. Wang, J. Opt. Soc. Am, **67**, No. 3, 383-393 (March 1977).

APPENDIX A
VALUE OF THE INTEGRAL WITH MULTIPLE POLES

It will be shown in this section that the occurrence of multiple poles, while it requires special treatment, does not pose any conceptual difficulties in calculating power or asymptotic series. Multiple poles can be viewed as the limit as two or more poles coalesce. To evaluate the integral in terms of a power series, the residue at the $1/s$ term must be determined. To find the asymptotic series, the residues must be found and the steepest descent contribution must be evaluated. The residues are found by expanding *all* the functions in the integrand into a Laurent series about the point of the multiple pole, multiplying all the series together, and determining the coefficient of the $1/s$ term. This technique is illustrated with examples of double and triple poles, and then with a physical example encountered in calculating the speckle from a rotating diffuse plate. I have not encountered any problems in turbulence wave propagation that have multiple poles in the complex plane.

A.1 Expansion Of Integrand Functions

As a start in this process, the Taylor series expansion of z^{-s} about the point $s = k$ is easily found to be equal to

$$z^{-s}\Big|_{s=k+\varepsilon} = z^{-k} \sum_{n=0}^{\infty} \frac{(-1)^n}{n!} [\ln(z)]^n \varepsilon^n. \tag{A.1.1}$$

The Gamma function $\Gamma(s + N)$ has poles at $s = -N - k$, and the expansion of this close to a pole can be shown to be equal to

$$\Gamma(s + N)\Big|_{s=-N-k+\varepsilon} = \frac{(-1)^k}{k!} \sum_{n=0}^{\infty} \frac{a_n(N-k)}{\varepsilon} \varepsilon^n. \tag{A.1.2}$$

The expansion of the Gamma function with $-s$ as the argument about a pole is

$$\Gamma(-s + N)\Big|_{s=-N+k+\varepsilon} = -\frac{(-1)^k}{k!} \sum_{n=0}^{\infty} \frac{a_n(-N+k)}{\varepsilon}(-\varepsilon)^n. \tag{A.1.3}$$

207

The first few coefficients of these expansions can be found in Marichev as

$$a_o(s) = 1, \tag{A.1.4}$$

$$a_1(s) = \Psi(1 - s), \tag{A.1.5}$$

$$a_2(s) = \Psi'(1) + [\Psi^2(1 - s) - \Psi'(1 - s)] / 2, \tag{A.1.6}$$

where the logarithmic derivative of the Gamma function is defined as

$$\Psi(z) = \frac{d \ln [\Gamma(z)]}{dz} = \frac{\Gamma'(z)}{\Gamma(z)} . \tag{A.1.7}$$

The value of this function is given in Jahnke and Emde,[11] (page 18), as

$$\Psi(z) = \frac{d \ln [\Gamma(z)]}{dz} = - C + \sum_{n=1}^{\infty} \left[\frac{1}{n} - \frac{1}{z + n - 1} \right], \tag{A.1.8}$$

where C is Euler's constant that is equal to 0.5772. The derivative of the last expression can be taken to obtain

$$\Psi'(z) = \sum_{n=1}^{\infty} \frac{1}{(z + n - 1)^2} . \tag{A.1.9}$$

This can be summed numerically to find the following values, which are all we will need to evaluate the integrals encountered in this appendix: $\Psi(1) = -C = -0.5772$; $\Psi(0.5) = -1.9635$; $\Psi(0.5) = 0.7034$; $\Psi'(1) = 1.645$; and $\Psi'(0.5) = 4.935$.

In addition, one requires the expansion of the Gamma function at a point that is not close to a pole. If s is positive in the argument, the expansion is

$$\Gamma(s + M)\big|_{s = -N - k + \varepsilon} = \Gamma(M - N - k)\{1 + \varepsilon\Psi(M - N - k)$$
$$+ \varepsilon^2 [\Psi(M - N - k) + \Psi(M - N - k)] / 2 + \dots\}. \tag{A.1.10}$$

If s is negative in the argument, the expansion is

$$\Gamma(-s - M)\big|_{s = -n - k + \varepsilon} = \Gamma(-M + N + k)\{1 - \varepsilon\Psi(-M + N + k)$$
$$+ \varepsilon^2 [\Psi'(-M + N + k) + \Psi(-M + N + k)] / 2 + \dots\}. \tag{A.1.11}$$

The above expansions will be used to evaluate integrals with multiple poles.

208

The integrals considered in the following examples are of the form

$$I = \frac{1}{2\pi i}\int F(s)ds.$$ (A.1.12)

where the path of integration goes from $-i\infty$ to $+i\infty$, and the path crosses the real axis with a very small negative real part.

A.2 Example No. 1

Consider the following integrand with a double pole

$$F(s) = \frac{1}{s^2} = \frac{\Gamma(s)\Gamma(s)}{\Gamma(s+1)\Gamma(s+1)} ;$$ (A.2.1)

The path of integration and pole location are shown in Figure A-1. It is obvious that there is no term that varies as $1/s$; therefore, the integral is zero. If the Gamma functions in the numerator are expanded using Equation (A.1.2), the terms with $1/\varepsilon$ cancel. The integral is again zero.
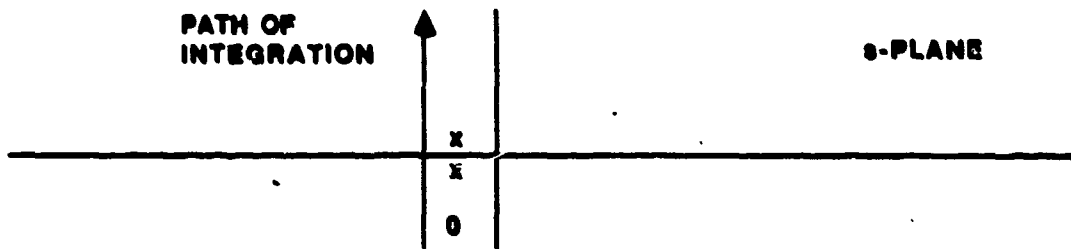
Figure A-1. The path of integration and pole location for Example No. 1.

A.3 Example No. 2

Consider the slightly more complicated integrand

$$F(s) = \frac{z^{-s}}{s^2} = \frac{\Gamma(s)\Gamma(s)z^{-s}}{\Gamma(s+1)\Gamma(s+1)} .$$ (A.3.1)

The path of integration and pole location are the same as in Figure A-1. The value of $\Delta = 0$, and the direction of path closure depends on the magnitude of z. For $z < 0$ the path of integration can be closed in the left-half plane, and the value of the integral is zero. For $z > 1$ the path of integration can be closed in the right-half plane. If the expansions in Equations (A.1.1) and (A.1.2) are used, the $1/\varepsilon$ term comes from the second term of the first equation and the second terms of the second equation. One obtains for the value of the integral

209

$$I = \ln(z)U(z - 1).$$

(A.3.2)

A.4 Example No. 3

Consider the integrand

$$F(s) = \frac{\Gamma(s)}{s} z^{-s} = \frac{\Gamma(s)\Gamma(s)z^{-s}}{\Gamma(s + 1)}.$$

(A.4.1)

The path of integration and pole location are shown in Figure A-2. The poles go off to the left to infinity just as they do in the succeeding examples. For this example, $\Delta = 1$, and the path of integration can be closed to the left for all z. All the enclosed poles are simple since the only double pole at $z = 0$ is on the right side of the path of integration. The integral is equal to

$$I = \sum_{n=1}^{\infty} \frac{(-1)^n}{n!} \frac{z^n}{n}.$$

(A.4.2)
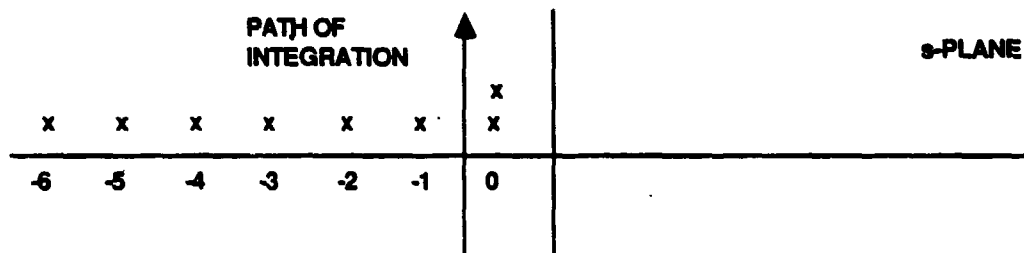
Figure A-2. The path of integration and pole location for Example No. 3.

For large z, an asymptotic series can be found. Since $B = 0$ the steepest descent contribution has exponential decay as given in Equation (2.4.36) and can be neglected. Using Equations (A.1.1) and (A.1.2) for the numerator and Equation (A.1.10) for the denominator, the asymptotic series which only has 3 terms in this case is

$$I = \exp(-z) + \ln(z) + 0.5772.$$

(A.4.3)

The first 20 terms of the power series and the asymptotic series are plotted in Figure A-3, and the difference between the two values is plotted in Figure A-4. Notice the agreement of the two series over a large argument range. Both are accurate in this region of agreement.

210
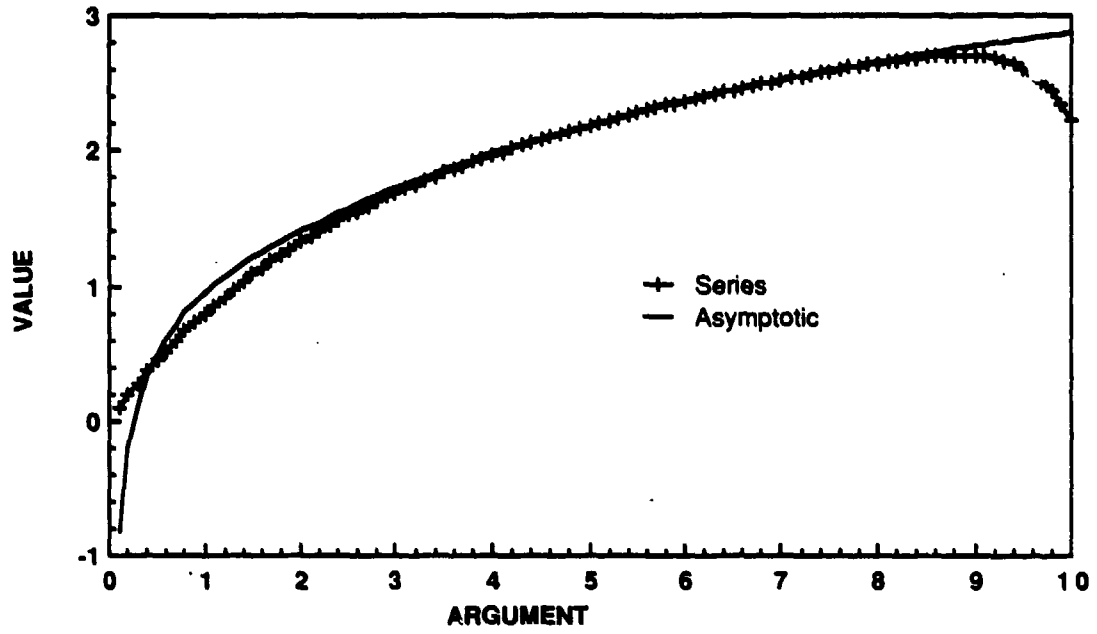
*Figure A-3. Plot of the power and asymptotic series for Example No. 3.*
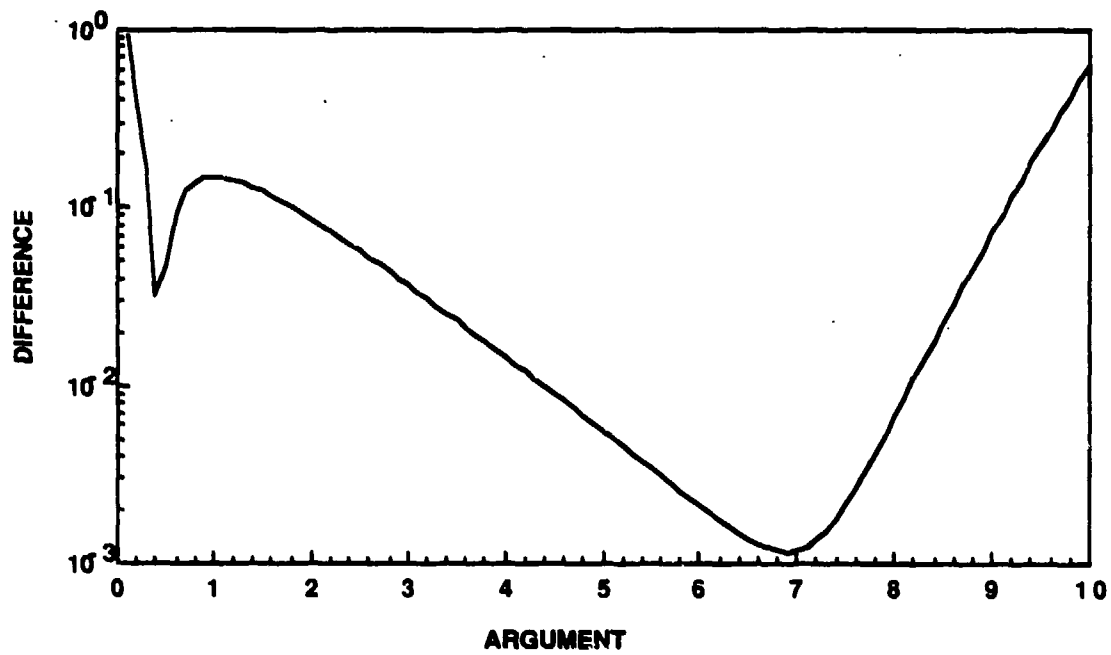
Figure A-4. Difference between the asymptotic and power series for Example No. 3.

211

A.5 Example No. 4

Consider the integrand

$$F(s) = \Gamma(s, -s) z^{-s}. \tag{A.5.1}$$

The path of integration and pole location are shown in Figure A-5. Since $\Delta = \Delta' = 0$, the path of integration can be closed in the left-half plane when $z < 1$, and in the right-half plane when $z > 1$. There is a double pole to the right at $z = 0$ that can be evaluated using Equations (A.1.1), (A.1.2), and (A.1.3), and the solutions are

$$I = \sum_{n=1}^{\infty} \frac{(-z)^n}{n} \qquad z < 1, \tag{A.5.2}$$

and

$$I = \sum_{n=1}^{\infty} \frac{(-z)^{-n}}{n} - \ln(z) \qquad z > 1. \tag{A.5.3}$$
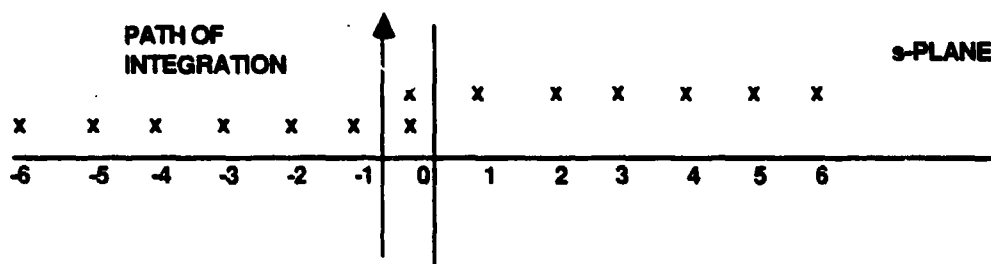
Figure A-5. The path of integration and pole location for Example No. 4.

A.6 Example No. 5

Consider the integrand

$$F(s) = \Gamma(s, -s - N) z^{-s}. \tag{A.6.1}$$

The path of integration and pole location are shown in Figure A-6. The value of $\Delta = \Delta' = 0$, and the direction of path closure depends on the magnitude of z. There is one double pole to the right of the path of integration, and N double poles to the left. The value of the integral is

212

$$I = (-1)^N \sum_{n=1}^{N} \frac{\ln(z) + \Psi(1 + N - n) - \Psi(1 + n)}{n!(N + n)!}$$

$$+ (-z)^{N+1} \sum_{n=0}^{\infty} \frac{n!(-z)^n}{(N + n + 1)!} \qquad z < 1,$$

(A.6.2)

and

$$I = (-1)^N \frac{\Psi(1) - \Psi(1 + N) - \ln(z)}{N!} + (-1)^{N+1} \sum_{n=0}^{\infty} \frac{n!(-z)^n}{(N + n + 1)!} \qquad z > 1.$$

(A.6.3)
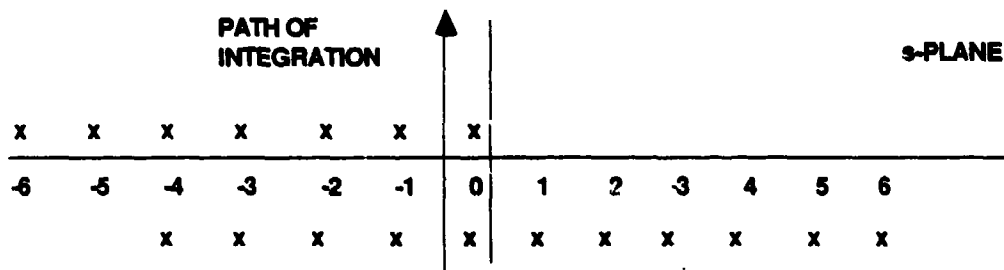
Figure A-6. The path of integration and pole location for Example No. 5 when N = 4.

A.7 Example No. 6

Consider the following integrand that has triple poles

$$F(s) = \Gamma(s, s, -N - s)z^{-s}.$$

(A.7.1)

The path of integration and pole location are shown in Figure A-7. For this case $\Delta = 1$, and there is one triple pole to the right of the path of integration, and N triple poles and an infinity of double poles to the left. Three terms in the expansion of each of the functions must be retained to get the complete residue at each of the triple poles.

Since $\Delta = 1$, the path of integration can be closed in the left-half plane. The residue at a double pole is

$$\text{Residue} = \Gamma(k - N)[2\Psi(1 + k) - \Psi(k - N) - \ln(z)]\frac{z^k}{(k!)^2}.$$

(A.7.2)

213
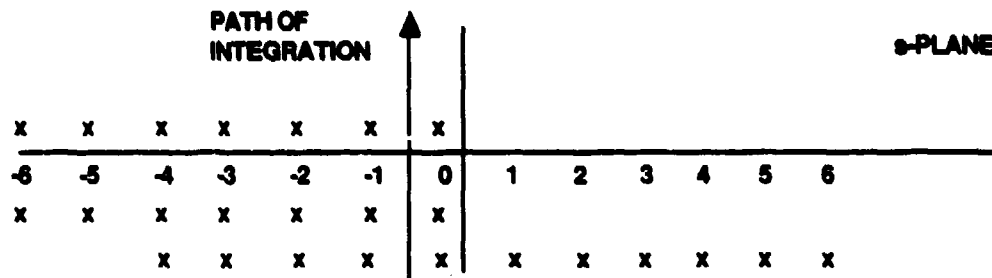
Figure A-7. The path of integration and pole location for Example No. 6.

The residue at a triple pole is

$$\text{Residue} = \left[\frac{\ln^2(z)}{2} + \ln(z)\{\Psi(1 + N - k) - 2\Psi(1 + k)\} + 2\Psi^2(1 + k) + 3\Psi'(1) \right.$$

$$+ \frac{\Psi^2(1 + N - k) - \Psi'(1 + N - k)}{2}$$

$$\left. - \Psi'(1 + k) - 2\Psi(1 + N - k)\Psi(1+ k) \right] \frac{(-1)^{N-k-1} z^k}{(k!)^2(N - k)!} .$$

(A.7.3)

The power series will not be written down explicitly since it is lengthy, and it can easily be evaluated from the residues given above. For large values of z an asymptotic series is wanted. Since condition 1 in Equation (2.4.48) applies, the asymptotic series is equal to the residue of the poles to the right of the path of integration. This contains one triple pole and the single poles. The asymptotic series is equal to

$$I = \sum_{n=1}^{\infty} \frac{(-1)^{N+n+1}\Gamma^2(n)}{(N + n)!} z^{-n} + \frac{z^N}{(N!)^2}\left[\frac{\ln^2(z)}{2} + \ln(z)\{\Psi(1) + \Psi(N + 1)\} \right.$$

$$\left. + 2\Psi^2(1 + N) + \frac{5\Psi'(1)}{2} + \frac{\Psi(1)}{2} - \Psi'(1 + N) - 2\Psi(1)\Psi(1+ N) \right].$$

(A.7.4)

A.8 Speckle From a Rotating Diffuse Plate

The variance in the intensity will be derived for a rotating square plate with side L that is a diffuse reflector. A diffuse reflector has the property that the reflected field is completely

214

uncorrelated from point to point. This property produces the phenomenum of speckle in which there is a variation in intensity from point to point in the received energy from the plate. The intensity variance can be reduced by averaging speckle patterns, and the type of averaging that is considered is produced by a rotation of the diffuse plate. This causes different speckle patterns to sweep across the receiver. If the receiver is incoherent, that is, it averages the instantaneous intensity and not the field, there will be a reduction in the speckle amplitude. That will be calculated here. The reason for considering this problem is that the final result is an integral that can be approximated using the Mellin transforms methods, and the resulting integral in the complex plane has a double pole. The return from a uniformly illuminated diffuse plate can be approximated using the paraxial assumption in Equation (2.2.1). Assume that the plate is rotating about the y axis with rotation rate ω as is shown in Figure A-8.


ROTATION AXIS
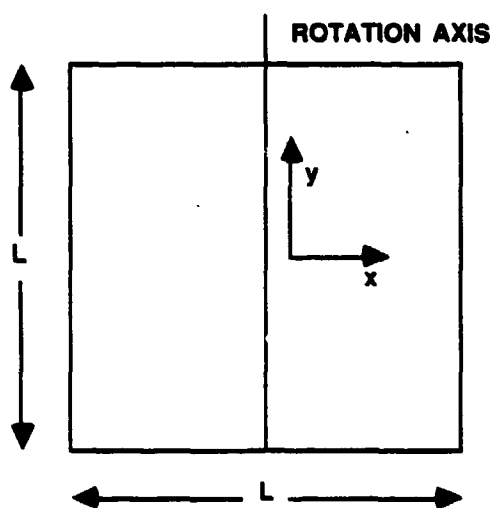
Figure A-8. Geometry of the rotating diffuse plate.

Expressing the return in cartesian coordinates, one obtains for the field as a function of time

$$E(t) = \int_{-L/2}^{L/2} dx \int_{-L/2}^{L/2} dy \, \exp\left\{ i\left[k_o\left(R + r^2(x, y) / 2R + 2x\omega t\right) + \phi(x, y)\right]\right\}, \quad (A.8.1)$$

where $r(x, y)$ is the transverse position of a point in the plate, and $\phi(x, y)$ is the arbitrary phase produced in reflecting from the plate. The factor of 2 arises because the change in round

215

trip distance is twice the distance moved by a point in the plate. The average normalized intensity is found by multiplying this return by its complex conjugate, averaging over a time T, and dividing by both the plate area and the averaging time, to give

$$\langle I \rangle = \frac{1}{TL^2} \int_0^T dt \int_{-L/2}^{L/2} dx_1 \int_{-L/2}^{L/2} dy_1 \int_{-L/2}^{L/2} dx_2 \int_{-L/2}^{L/2} dy_2 \exp\left\{2\,ik_o[\,x_1 - x_2]\omega t\right\}$$

$$\left\langle \exp\left\{ i\left[k_o\left([\,r^2(x_1,\,y_1) - r^2(x_2,\,y_2)]/2R\right) + \phi(x_1,\,y_1) - \phi(x_2,\,y_2)\right]\right\}\right\rangle. \qquad (A.8.2)$$

Because the phase is uncorrelated from point to point there will only be contributions whenever $x_1 = x_2$, and $y_1 = y_2$. For that case, the argument of the exponent is zero, and the average intensity is equal to 1. This produces the physically reasonable result that the average intensity is not affected by speckle. The variance of the intensity will be found from the relation

$$\sigma_I^2 = \left\langle (I - \langle I \rangle)^2\right\rangle = \left\langle I^2\right\rangle - \langle I \rangle^2. \qquad (A.8.3)$$

Introduce the notation that b_n is a point corresponding to x_n and y_n. The average of the intensity squared is equal to

$$\left\langle I^2\right\rangle = \int db_1 \int db_2 \int db_3 \int db_4 \int_0^T dt_1 \int_0^T dt_2$$

$$\times \frac{\exp\left\{ ik_o\left[r^2(b_1) - r^2(b_2) - r^2(b_3) + r^2(b_4)\right]/2R\right\}}{T^2L^4}$$

$$\times \exp\left\{ ik_o[(x_1 - x_2)t_1 - (x_3 - x_4)t_2] + i[\phi(b_1) - \phi(b_2) - \phi(b_3) + \phi(b_4)]\right\}.$$

$$(A.8.4)$$

Once again, because the phase is uncorrelated the integrals over b_3 and b_4 only contribute when the phase terms vanish. This occurs for the two separate cases of

$$b_1 = b_2 \text{ and } b_3 = b_4, \qquad (A.8.5)$$

or

$$b_1 = b_3 \text{ and } b_2 = b_4. \qquad (A.8.6)$$

The first condition produces unity for the value of the integral, and this cancels the second term of Equation (A.8.3). With the second set of conditions inserted, the integrations over the two

216

y coordinates can be performed and the result is that the variance of the intensity is

$$\sigma_I^2 = \frac{1}{T^2 L^4} \int dx_1 \int dx_2 \int_0^T dt_1 \int_0^T dt_2 \exp\left\{ i2\omega k_o[x_1 - x_2][t_1 - t_2] \right\}. \qquad (A.8.7)$$

Each of the integrations over time are the same, and can be performed to give

$$\sigma_I^2 = \frac{1}{T^2 L^4} \int dx_1 \int dx_2 \frac{\sin^2\left(\omega k_o[x_1 - x_2]T\right)}{\left(2\omega k_o[x_1 - x_2]T\right)^2}. \qquad (A.8.8)$$

Make the changes of variables

$$z = \omega k_o TL(x_1 - x_2) = a(x_1 - x_2), \qquad (A.8.9)$$

and

$$z_+ = \frac{\omega k_o TL}{2}(x_1 + x_2) = \frac{a}{2}(x_1 + x_2), \qquad (A.8.10)$$

where

$$a = \omega k_o TL. \qquad (A.8.11)$$

The area of integration has been transformed from the the same one as in Figure 3-3 to the one in Figure 3-4. The resulting expression is

$$\sigma_I^2 = \frac{1}{a^2} \int_0^a dz \frac{\sin^2 z}{z^2} \int_{-(z-a)/2}^{(z-a)/2} dz_+. \qquad (A.8.12)$$

The last integration can be performed to give

$$\sigma_I^2 = \frac{2}{a^2} \int_0^a dz \sin^2(z) \frac{(a-z)}{z^2}. \qquad (A.8.13)$$

This integral can be evaluated by considering the following integral

$$I(r) = \int_0^\infty \frac{dz}{z} U\left[1 - \left(\frac{z}{a}\right)^2\right] z^{-r} \sin^2(z). \qquad (A.8.14)$$

The original integral can be expressed in terms of this new integral as

$$\sigma_I^2 = 2\left[\frac{I(1)}{a} - \frac{I(0)}{a^2}\right]. \qquad (A.8.15)$$

Using the convolution integral, Equation (A.8.14) can be written as

$$I(r) = -\frac{\sqrt{\pi}}{4} \frac{1}{2\pi i} \int \Gamma\begin{bmatrix} -s, \ s - \frac{r}{2}* \\ -s + 1, -s + \frac{r}{2} + \frac{1}{2} \end{bmatrix} a^{-2s} \, ds. \qquad (A.8.16)$$

217

Expressing the integral of interest in terms of this integral gives

$$\sigma_I^2 = -\frac{\sqrt{\pi}}{4a^2}\frac{1}{2\pi i}\int ds \; \Gamma\left[\begin{array}{c} -s, \; s^*, \; s+\frac{1}{2}^* \\ -s+\frac{1}{2}, \; -s+1, \; s+\frac{3}{2} \end{array}\right]a^{-2s}. \qquad (A.8.17)$$

The pole location and path of integration are shown in Figure A-9. Notice the double pole at s = 0. Since Δ = 2, the path of integration can be closed in the left-half plane to give for the value of the integral

PATH OF
INTEGRATION

s-PLANE

x   x   x   x   x   x   x
-6 -5 -4 -3 -2 -1 0

x
-1/2
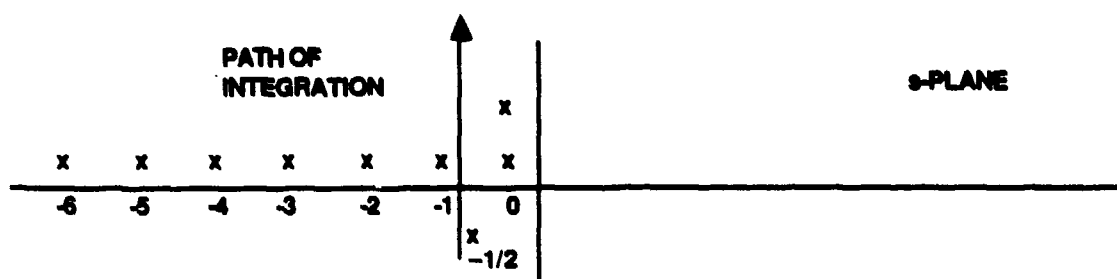
Figure A-9. Path of integration and pole location for the integral in Example 7.

$$\sigma_I^2 = -\frac{\sqrt{\pi}}{4}\sum_{n=1}^{\infty}\frac{(-1)^n}{n!}\frac{a^{2n-2}}{n\left[n-\frac{1}{2}\right]\Gamma\left[n+\frac{1}{2}\right]}. \qquad (A.8.18)$$

The leading terms of this series are

$$\sigma_I^2 = 1 - 0.0556 \; a^2 + 0.00296 \; a^4 - 0.000113 \; a^6 + 0.00000314 \; a^8 + \ldots. \qquad (A.8.19)$$

We are interested in the case in which there is great deal of speckle averaging, a condition that requires large values of a. The asymptotic series is composed of the residue of the poles to the right of the path of integration and the steepest descent contribution. The asymptotic series is

$$\sigma_I^2 = \frac{\pi}{a} - \frac{\ln(a)}{a^2} - \frac{2.27}{a^2} + \frac{\cos(2\,a)}{4\,a^4}. \qquad (A.8.20)$$

The first term comes from the residue at $s = -1/2$, the next 2 come from the residue at $s = 0$. This residue is

$$\text{Residue } (0) = \frac{\sqrt{\pi}}{4\Gamma(3/2)\,a^2}[-3\,\Psi(1) + 2\Psi(0.5) - \Psi(1.5)]. \qquad (A.8.21)$$

218

The power series and the asymptotic series are both plotted in Figure A.10. The difference between the series is plotted in Figure A.11. There is good agreement of the values of the two series over a range of parameter.
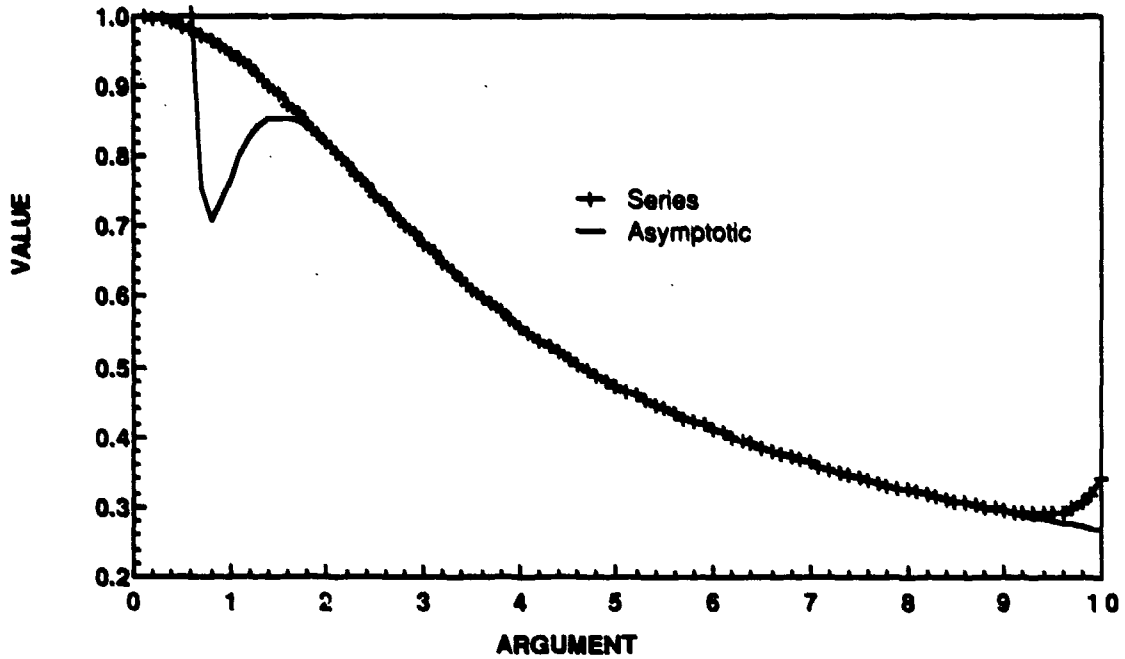

Figure A-10. Power and asymptotic series for the speckle problem.
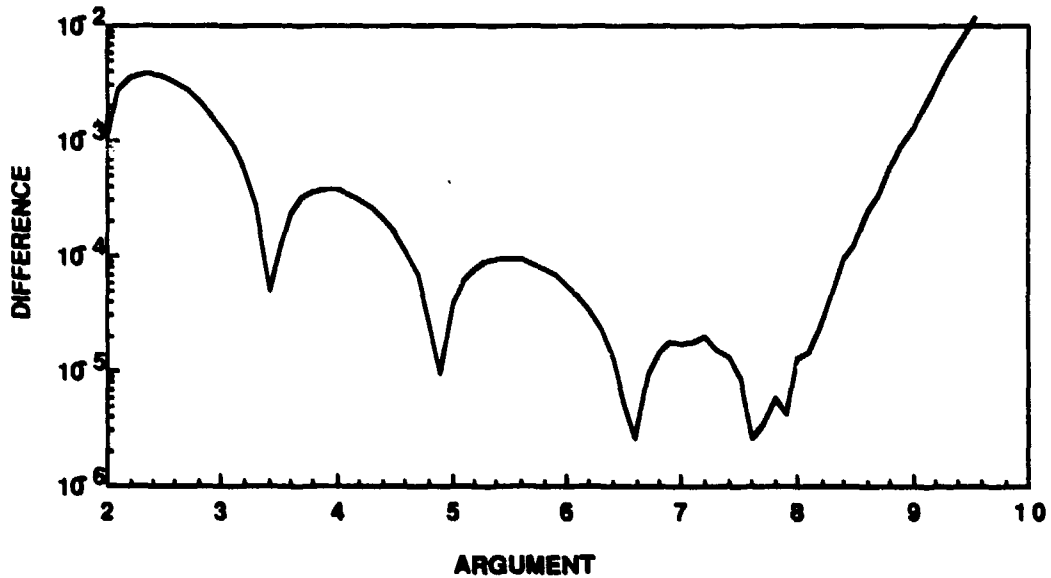
Figure A-11. Difference between the power and asymptotic series for the speckle problem.

219

As a concrete application of these results consider the speckle from a proposed target satellite. This satellite has a retroreflector that is composed of an array of corner cubes that will be approximated here as a square diffuse plate. The array is earth stabilized and the change of the line of sight as the array moves in its circular orbit at 500 km produces an apparent rotation about the line of sight. The geometry of the satellite pass can be approximated by a flat earth geometry as shown in Figure A-12.
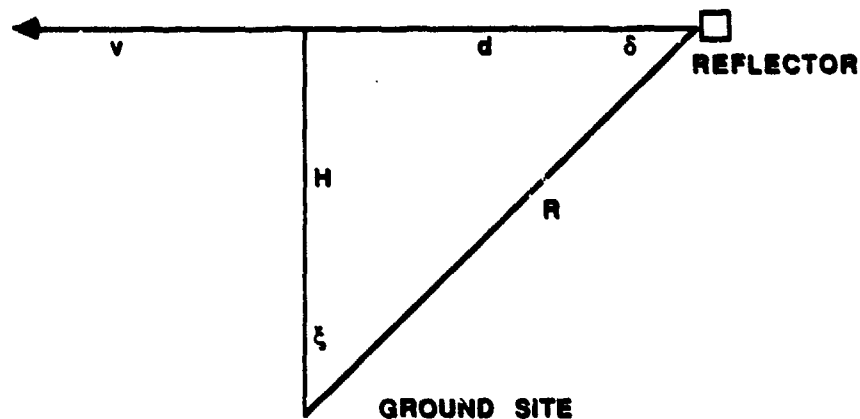

*Figure A-12. Geometry of a satellite pass with a diffuse reflector.*

From this figure one obtains

$$\tan(\xi) = d \ / \ H.$$ (A.8.22)

From this, one can obtain the apparent rotation rate as

$$\omega = \frac{d\delta}{dt} = -\frac{d\xi}{dt} = \frac{v \ \cos^2(\xi)}{H}.$$ (A.8.23)

The reduction of the intensity variance versus normalized averaging time is plotted in Figure A-13. For this satellite, there will be a reduction of the variance by a factor of 16 if the averaging time is 0.4 ms. Remember that the standard deviation decreases as the square root of the plotted decrease.
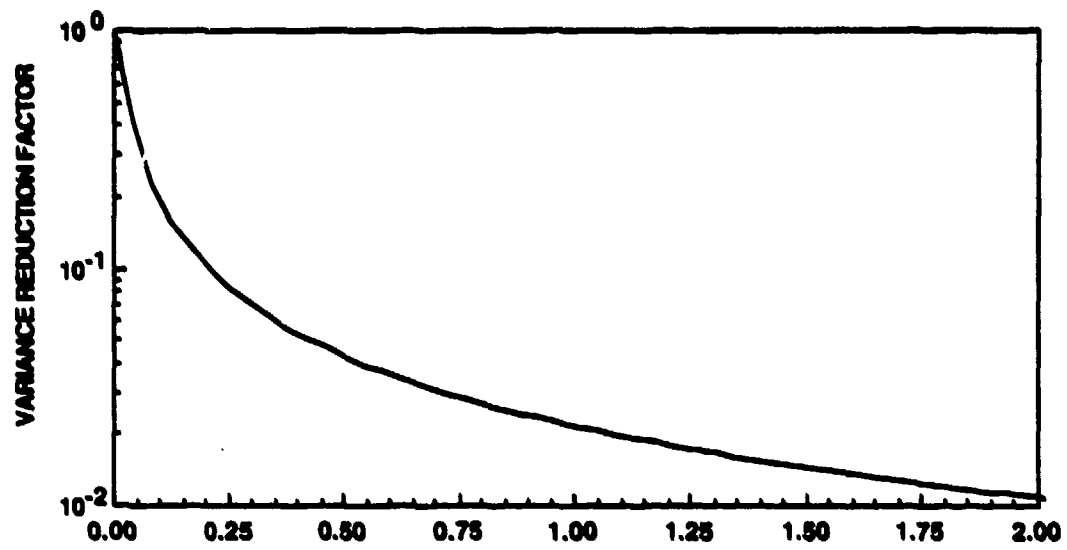
Figure A-13. Speckle reduction for an earth stabilized satellite.

APPENDIX B
ERROR PRODUCED BY
AXIAL APPROXIMATION ON TRACKED TILT

The approximation in which z' z" is replaced by zz is examined for the case of tracked tilt that is analyzed in Section 3.5.6. Similar arguments for other cases show that this is a very good approximation. The exact relation that should be used after the change in variables given in Equation (3.3.34) and (3.3.35) is

$$z' z'' = z^2 - z_-^2 / 4. \tag{B.1.1}$$

The first term gives the result that is calculated with the approximation, and the second term produces an error term. The same approximation previously made, that the integration over the difference coordinate can be extended to infinity, is also made here. Performing the integration over z, the error term is equal to

$$E = \frac{1}{4}\left(\frac{16}{D}\right)^2 \frac{\mu_o}{L^2} \int d\vec{\kappa} \left(\frac{J_2(\kappa D / 2)}{\kappa D / 2}\right)^2 \int_0^\infty dz_- \, z_-^2 E_n(\vec{\kappa}, | z_- |). \tag{B.1.2}$$

Equation (3.3.28) can be used to evaluate the integral over the difference coordinates as

$$I = \int_0^\infty dz_- \, E_n(\vec{\kappa}, | z_- |) \, z_-^2 = -\frac{\partial^2}{\partial \kappa_-^2} \int_0^\infty dz_- \, E_n(\vec{\kappa}, | z_- |) \cos(\kappa_- z_-)\Bigg|_{\kappa_- = 0}. \tag{B.1.3}$$

Assuming the turbulence is isotropic and inner and outer scale effects are negligible, then

$$I = -0.033\pi \frac{\partial^2}{\partial \kappa_-^2}\left(\kappa^2 + \kappa_-^2 \right)^{-11/6}\Bigg|_{\kappa_- = 0} = 0.3801 \kappa^{-17/3}. \tag{B.1.4}$$

Using this result, the error term is

$$E = \frac{7.66 \, D^{5/3} \mu_o}{L^2} \int_0^\infty dx \, x^{-17/3 - 1} J_2^2(x) = \frac{0.239 \, \mu_o D^{5/3}}{L^2}. \tag{B.1.5}$$

223

The ratio of this error term to the approximate answer is

$$\text{Ratio} = \frac{0.0393 \, \mu_0 D^2}{\mu_2}.$$

(B.1.6)

Since the second moment is over six orders of magnitude larger than the zeroth as seen in Table 3-1, this ratio is very small, and the error made in neglecting the correction term is insignificant.

APPENDIX C
ANALYTIC EXPRESSION FOR THE
HUFNAGEL-VALLEY TURBULENCE MOMENTS

The turbulence strength versus height for the Hufnagel-Valley model is

$$C_n^2(h) = 0.00594 \left(\frac{W}{27}\right)^2 (10^{-5} \times h)^{10} \exp\left(\frac{-h}{1000}\right)$$
$$+ 2.7 \times 10^{-16} \exp\left(\frac{-h}{1500}\right) + A \exp\left(\frac{-h}{100}\right). \tag{C.1.1}$$

where W is the pseudo-wind and A is a parameter that is usually set equal to 1.7×10^{-14}. The strength of the turbulence is usually changed by varying the W term. For instance, the HV-21 model has the above value for A, and W is equal to 21. This model is sometimes referred to as the $HV_{5/7}$ model since the coherence diameter is about 5 cm and the isoplanatic angle is 7 µrad for a wavelength of 0.5 micrometers.

The full moments are equal to

$$\mu_n = \int_0^\infty C_n^2(z) z^n \, dz = \sec^{n+1}(\xi) \int_0^\infty C_n^2(h) h^n \, dh, \tag{C.1.2}$$

where ξ is the zenith angle. One finds that the full moments are equal to

$$\mu_n = \int_0^\infty dz \, C_n^2(z) z^n = \sec^{n+1}(\zeta)\left[5.94 \times 10^{-20+3n}\left(\frac{W}{27}\right)^2 \Gamma(n+11)\right.$$
$$\left. + 4.05 \times 10^{-13} \Gamma(n+1)(1500)^n + A \times 100^{n+1} \Gamma(n+1) \right]. \tag{C.1.3}$$

By choosing the proper values of the parameters the same values of the coherence diameter and the isoplanatic angle can be obtained as those from the SLCSAT models. In the Hufnagel-Valley model, a value of A = 1.77E-14 (2.5E-15) and a pseudo wind speed of 11.7 (10.5) gives a coherence diameter of 4.98 (10) cm and an anisoplanatic angle of 11.8 (12.9) µrad, which are the same as the SLCSAT-day (night) models. The Hufnagel-Valley models with

these parameters are called the pseudo SLCSAT-day (night) models. Other definitions could have been used to define the pseudo SLCSAT and night models. Because of the importance of the zeroth, 5/3 and second moments, this definition was chosen because it will give answers that are very close to those derived for the original models.

Define the partial moments in the following way for a distance L, which is at a height H where

$$L = \sec(\xi)H \quad \text{as} \tag{C.1.4}$$

$$\mu_n^+(L) = \int_L^\infty C_n^2(z)\, z^n\, dz = \sec^{n+1}(\xi) \int_H^\infty C_n^2(h)\, h^n\, dh; \tag{C.1.5}$$

and

$$\mu_n^-(L) = \int_0^L C_n^2(z)\, z^n\, dz = \sec^{n+1}(\xi) \int_0^H C_n^2(h)\, h^n\, dh. \tag{C.1.6}$$

The definitions of the incomplete Gamma functions are

$$\gamma(b+1, x) = \int_0^x y^b \exp(-y)\, dy, \tag{C.1.7}$$

and

$$\Gamma(b+1, x) = \int_x^\infty y^b \exp(-y)\, dy. \tag{C.1.8}$$

Using those definitions, one can find the partial moments of the turbulence to be equal to

$$\mu_n^+(L) = \int_L^\infty dz\, C_n^2(z)\, z^n = \sec^{n+1}(\zeta)\left[5.94 \times 10^{-20+3n}\left(\frac{W}{27}\right)^2 \Gamma\left(n+11, \frac{H}{1000}\right)\right.$$
$$\left. + 4.05 \times 10^{-13}\Gamma\left(n+1, \frac{H}{1500}\right)(1500)^n + A \times 100^{n+1}\Gamma\left(n+1, \frac{H}{100}\right)\right]. \tag{C.1.9}$$

and

$$\mu_n^-(L) = \int_0^L dz\, C_n^2(z)\, z^n = \sec^{n+1}(\zeta)\left[5.94 \times 10^{-20+3n}\left(\frac{W}{27}\right)^2 \gamma\left(n+11, \frac{H}{1000}\right)\right.$$
$$\left. + 4.05 \times 10^{-13}\gamma\left(n+1, \frac{H}{1500}\right)(1500)^n + A \times 100^{n+1}\gamma\left(n+1, \frac{H}{100}\right)\right]. \tag{C.1.10}$$

226

REPORT DOCUMENTATION PAGE

1a. REPORT SECURITY CLASSIFICATION	1b. RESTRICTIVE MARKINGS
Unclassified	

2a. SECURITY CLASSIFICATION AUTHORITY	3. DISTRIBUTION/AVAILABILITY OF REPORT
	Approved for public release; distribution unlimited.
2b. DECLASSIFICATION/DOWNGRADING SCHEDULE	

4. PERFORMING ORGANIZATION REPORT NUMBER(S)	5. MONITORING ORGANIZATION REPORT NUMBER(S)
Technical Report 807	ESD-TR-88-136

6a. NAME OF PERFORMING ORGANIZATION	6b. OFFICE SYMBOL (If applicable)	7a. NAME OF MONITORING ORGANIZATION
Lincoln Laboratory, MIT		Electronic Systems Division

6c. ADDRESS (City, State, and Zip Code)	7b. ADDRESS (City, State, and Zip Code)
P.O. Box 73 Lexington, MA 02173-0073	Hanscom AFB, MA 01731

8a. NAME OF FUNDING/SPONSORING ORGANIZATION	8b. OFFICE SYMBOL (If applicable)	9. PROCUREMENT INSTRUMENT IDENTIFICATION NUMBER
Air Force Systems Command	AFSC/USAF	F19628-85-C-0002

8c. ADDRESS (City, State, and Zip Code)	10. SOURCE OF FUNDING NUMBERS			
Andrews AFB Washington, DC 20334	PROGRAM ELEMENT NO. 63221C	PROJECT NO. 33	TASK NO.	WORK UNIT ACCESSION NO.

11. TITLE (Include Security Classification)

A Unified Approach to Electromagnetic Wave Propagation in Turbulence and the Evaluation of Multiparameter Integrals

12. PERSONAL AUTHOR(S)
Richard J. Sasiela

13a. TYPE OF REPORT	13b. TIME COVERED	14. DATE OF REPORT (Year, Month, Day)	15. PAGE COUNT
Technical Report	FROM _____ TO _____	1 July 1988	238

16. SUPPLEMENTARY NOTATION

17. COSATI CODES			18. SUBJECT TERMS (Continue on reverse if necessary and identify by block number)
FIELD	GROUP	SUB-GROUP	turbulence, electromagnetic-wave propagation, integrals, asymptotic series, Rytov approximation, Gegenbauer polynomials, Mellin transforms, multiple complex planes.

19. ABSTRACT (Continue on reverse if necessary and identify by block number)

A powerful method is presented to allow one to quickly set up problems of wave propagation in a turbulent atmosphere and to evaluate the integrals in terms of rapidly converging series. The method allows one to find the phase and log-amplitude variances, the power spectral density, Strehl ratio and beam profiles. The method of setting up the problem uses filter functions to extract Zernike aberrations, and to incorporate anisoplanatism, and the effects of point and distributed sources. These filter functions can often be cascaded to evaluate the quantities of interest when the effects are present simultaneously. The evaluation of the resulting integral expression uses Mellin transform techniques in multiple complex planes. This integration method can be used to evaluate any integral whose integrand can be written as the product of generalized hypergeometric functions.

20. DISTRIBUTION/AVAILABILITY OF ABSTRACT	21. ABSTRACT SECURITY CLASSIFICATION
☐ UNCLASSIFIED/UNLIMITED ☒ SAME AS RPT. ☐ DTIC USERS	Unclassified

22a. NAME OF RESPONSIBLE INDIVIDUAL	22b. TELEPHONE (Include Area Code)	22c. OFFICE SYMBOL
Lt. Col. Hugh L. Southall, USAF	(617) 981-2330	ESD/TML

DD FORM 1473, 84 MAR   83 APR edition may be used until exhausted. All other editions are obsolete.